Reference Copy

FAA-73-36

REPORT NO. FAA-RD-73-203

HORIZONTAL COLLISION AVOIDANCE SYSTEMS STUDY

SYSTEMS CONTROL, INC.

260 SHERIDAN AVE.
PALO ALTO, CA 94306

DECEMBER 1973

FINAL REPORT

PREPARED FOR:

DEPARTMENT OF TRANSPORTATION

FEDERAL AVIATION ADMINISTRATION
SYSTEMS RESEARCH & DEVELOPMENT SERVICE
WASHINGTON, D.C. 20590

Technical Report Documentation Page

1. Report No. FAA-RD-73-203	2. Government Accession No.	3. Recipient's Catalog No.
4. Title and Subtitle Horizontal Collision Avoidance Systems Study		5. Report Date December 1973
		6. Performing Organization Code
7. Author(s) J.A. Sorensen, A.W. Merz, T.B. Cline, J.S. Karmarkar, W. Heine, and M.D. Ciletti		8. Performing Organization Report No. DOT-TSC-73-36
9. Performing Organization Name and Address *Systems Control, Inc. 260 Sheridan Avenue Palo Alto, Ca 94306		10. Work Unit No. (TRAIS) FA 414/R4119
		11. Contract or Grant No. DOT-TSC-535
12. Sponsoring Agency Name and Address Department of Transportation Federal Aviation Administration Systems Research and Development Service Washington, D.C. 20590		13. Type of Report and Period Covered Final Report Dec. 1972 - Nov. 1973
		14. Sponsoring Agency Code
15. Supplementary Notes *Under contract to: Department of Transportation Transportation Systems Center Kendall Square, Cambridge, Ma 02142		

16. Abstract

This report presents the results of an analytical study of the merits and mechanization requirements of horizontal collision avoidance systems (CAS). The horizontal and combined horizontal/vertical maneuvers which provide adequate miss distance with minimum initial range, minimum deviation off track, and acceptable turn rates are found. Horizontal maneuvers are compared with vertical maneuvers and speed control for collision avoidance in terms of initial range requirements, deviation off track and flight path time loss. Requirements for implementing an airborne horizontal CAS are outlined. Digital filtering is analyzed for estimating airspeed and relative heading from noisy range and bearing measurements between aircraft. An algorithm (suitable for airborne mechanization) is developed for computing appropriate collision avoidance maneuvers. The effects of dynamic and measurement errors on the CAS's ability to provide safe miss distance are examined. A digital computer program which simulates encounters between two aircraft with random measurement errors is used for conducting error and sensitivity analyses of various effects. Statistical quantities such as false alarm rate, missed alarm rate, collision rate, incorrect maneuvers, and near miss probability are computed. These data allow specification of sensor accuracy to achieve fixed levels of airspace safety. The results are applicable to both airborne and ground-based mechanizations.

17. Key Words Collision Avoidance Air Traffic Control Aircraft Guidance System Error Analysis		18. Distribution Statement Unlimited. Document is available to the public through the National Technical Information Service, Springfield, Va 22151	
19. Security Classif. (of this report) Unclassified	20. Security Classif. (of this page) Unclassified	21. No. of Pages 262	22. Price

Form DOT F 1700.7 (8-72) Reproduction of completed page authorized

TABLE OF CONTENTS

TABLE OF CONTENTS (Concluded)

LIST OF FIGURES

LIST OF FIGURES (Continued)

LIST OF FIGURES (Continued)

LIST OF FIGURES (Concluded)

PREFACE

The Transportation Systems Center and the Federal Aviation Administration of the United States Department of Transportation are conducting and sponsoring analyses, simulations, and flight tests to develop national standards for aircraft collision avoidance systems. Several methods can be used to decrease midair collisions and near-misses, and many alternate systems are being considered for this purpose. The merits of each of these alternate systems must be determined and compared to enable making a clear decision on further developmental efforts required.

This report presents the results of an analytical study of the merits and mechanization requirements of collision avoidance systems which operate chiefly by commanding horizontal maneuvers. The horizontal maneuvers are determined which provide an appropriate combination of miss distance, off-track deviation, and initial relative range for aircraft with arbitrary turn rate limits and airspeeds. Comparison of horizontal maneuvers to vertical maneuvers and speed control are made with respect to measures of airspace usage. The effects of measurement errors on the statistical performance of a typical horizontal collision avoidance system are numerically computed. The sensitivity of airspace usage, probability of collisions, and probability of false alarms to variations in several system parameters are presented.

The technical monitor for this work was G. A. Gagne of TSC. The project manager at Systems Control, Inc. was J. A. Sorensen. Project engineers were M. D. Ciletti, T. B. Cline, W. Heine, J. S. Karmarkar, and A. W. Merz. Project programmers were M. V. Bullock and G. Fuji. Report preparation and artwork were done by D. A. Buenz.

I. INTRODUCTION

Midair collision avoidance for aircraft has been the subject of intense technical investigation and development since the tragic Grand Canyon collision of 1956. Since that time, air traffic densities have been steadily increasing, and there has been a corresponding increase in the number of midair collisions or near misses. This has led to the study and development of various competitive concepts for reducing the frequency of these incidents. For each of these systems, attention has been focused on the problem of how to measure the relative position and velocity of the nearby "intruder". In comparison, much less attention has been directed toward the simultaneous problem of controlling the two aircraft, as functions of these measurements. Understanding the control problem allows realistic requirements to be set on the measurement accuracies and provides a better understanding of the performance which is achievable from a given system. This study addresses both the measurement and control problems of collision avoidance concepts.

The systems which have been previously studied to various degrees are of three general levels of sophistication. The Pilot Warning Indicator (PWI) merely warns of the presence of an aircraft, but does not evaluate the hazard. The Collision Detection System (CDS) is more complex in that the miss distance is estimated. The Collision Avoidance System (CAS) detects the intruder, evaluates the hazard, and calculates and displays an evasive maneuver. This project studies the latter systems.

Both airborne and ground-based collision avoidance systems are currently under development or being flight tested. Airborne systems include those which can potentially command collision avoidance maneuvers in the vertical plane, the horizontal plane, or a combination of these maneuvers. The systems which command vertical maneuvers are based on measuring range, range rate, and altitude difference between the two aircraft. When the time to conflict becomes less than a threshold value, the higher aircraft climbs, and the lower aircraft dives until the threat is passed.

To compute the best horizontal maneuvers requires additional measurements--namely, the bearing of the threat aircraft, its airspeed, and its heading relative to that of the threatened aircraft. Different questions arise concerning the provision of this horizontal capability: How should the aircraft maneuver in the horizontal plane, based on these additional measurements? How accurate must these measurements be to provide a given level of safety? What extra benefit is provided by horizontal maneuver capability? Finally, what is the additional cost of providing horizontal maneuver capability?

The answers to all of these questions have not previously been determined. The existing literature on hardware systems claim a wide range of measurement accuracies and operational flexibility, with a corresponding range in cost. However, there has been no published effort showing how the general performance of a collision avoidance system (e.g., probability of achieving acceptable miss distance) depends on the quality and type of the input data required for its operation. Instead, the system errors have only been compared to the corresponding errors of competitive systems. But, the maneuver commands and the resulting aircraft motion obviously depend upon the measurements. Furthermore, the measurements depend upon the relative position of the two aircraft, so that the overall performance is a very complex function of measurement errors. The present study represents the first unified treatment of the interaction between aircraft dynamics, measurement errors, and maneuver specification.

This study examined the merits and mechanization requirements of aircraft horizontal collision avoidance systems. The basic objective of the study were the following:

1. Determine the appropriate horizontal and combined horizontal/vertical maneuvers to be taken to avoid midair collisions.

2. Determine the requirements for mechanizing horizontal maneuvers.

The specific mechanization studied was the airborne system. However, the basic results of this study are general, and are applicable to ground-based conflict prediction and resolution systems such as IPC. This is because ground-based systems view potential conflicts projected in the horizontal plane due to radar tracking. Thus, conflict resolution from the ground would also be done primarily in the horizontal plane.

The objective of determining the appropriate evasive maneuvers required taking a systems approach with many interrelated steps. These included:

1. Developing a mathematical model of the relative motion of two aircraft. The effects of arbitrary initial conditions, type of aircraft, control surface deflections, and throttle settings were taken into account.

2. Examining various criteria that could be used to pick the best, or optimum, horizontal collision avoidance maneuvers. This resulted in choosing miss distance as the fundamental criterion which should be used to govern the maneuver strategy.

3. Solving for horizontal maneuvers that produce maximum miss distance, as determined for arbitrary aircraft in arbitrary relative positions, and with bounded turn rate capabilities.

4. Extending the maximum miss distance maneuver strategy results to include the effects of other criteria. The result was a tradeoff analysis between miss distance, turn rate, initial range, and deviation from the nominal flight path.

5. Extending the horizontal maneuver results to include vertical motion for full three-dimensional avoidance maneuvers.

6. Examining and comparing these results with pure vertical maneuvers and speed control which also could be used for collision prevention.

The second objective, that of examining mechanization requirements, accounted for the limitations of CAS systems, including their hardware and software. Again, a number of interrelated steps were taken to determine the mechanization requirements of an airborne system. This included an estimate of the degradation in the system's performance due to dynamic and measurement errors. These steps included:

1. Identifying and defining the overall functions and elements that are part of a horizontal collision avoidance system mechanization.

2. Developing algorithms which can be used in an airborne computer to command simplified versions of the optimum horizontal collision avoidance maneuvers.

3. Studying the feasibility and performance of digital filter algorithms which are used to estimate airspeed and relative heading of the intruder aircraft, if cooperative information is not exchanged between two aircraft.

4. Determining the error characteristics of typical sensors which would be required for mechanizing a horizontal collision avoidance system and determining the effect of these errors.

5. Developing a detailed computer simulation of an encounter between two conflicting aircraft. This simulation included the effects of sensor errors and various time delays. It also contained typical logic for commanding the maneuvers and various program constants which affect system performance.

6. Using the encounter simulation to determine the statistical distribution of miss distance as a function of errors in range, bearing, relative heading, and airspeed measurement. Other effects studied were false alarm rate, missed alarm rate, and collision rate, as functions of these same errors.

This study of the maneuver dynamics and mechanization requirements provides data and conclusions regarding the measurement accuracy required to provide various levels of safety. This appears in the form of performance sensitivity curves as functions of the error magnitudes.

The report is organized into the following chapters:

- Chapter II presents the historical development of aircraft collision avoidance systems and other background material. It presents a survey of previous analytical efforts in studying aircraft systems and a critique of some of the widely quoted sources.

- Chapter III discusses the dynamics of encountering aircraft and the equations of relative motion which are required to analyze maneuver performance.

- Chapter IV is devoted to determining the most appropriate (optimum) horizontal and horizontal/vertical maneuvers for avoiding midair collisions or near misses. Various criteria are examined for choosing the maneuvers, and tradeoff curves are presented showing the relationship between these criteria.

- Chapter V makes basic comparisons of collision avoidance system performance resulting from horizontal maneuvers, vertical maneuvers, and speed control.

- Chapter VI examines the computational and sensor requirements for providing horizontal maneuver commands.

- Chapter VII determines the effect of dynamic and measurement system errors on the performance of a horizontal collision avoidance system. The sensitivity of miss distance to variations in measurement errors and system parameters is presented.

- Chapter VIII presents a summary of the study results, the conclusions that have been reached, and the recommendations for further work.

- Appendices A - G provide technical detail in support of Chapters III - VII.

The reader who wishes to omit the technical detail can refer directly to the summary in Chapter VIII, which is self-contained.

II. BACKGROUND

A brief synopsis of the history of aircraft collision avoidance systems is given here, to provide background material for the succeeding chapters of the report. This is necessary in order to place in perspective the analytical and experimental conclusions of prior research efforts.

2.1 HISTORICAL DEVELOPMENT OF COLLISION AVOIDANCE SYSTEMS

A vast amount of technical literature exists on the collision avoidance problem. Engineering reports, technical papers, and sales brochures all describe some aspect of the problem, but here it is possible to mention only these documents which:

1. Are frequently cited by other authors in the field; or

2. Are recently published and show that the material has drawn heavily on the experience of others; or

3. Are informative and unbiased surveys of the history of the significant developments in this technology.

Several recent publications[1-5] provide extensive lists of references in one or more of the above classifications, and current hardware and test developments are regularly reported in various journals and periodicals.[6-9] The purpose here is to draw on these sources in order to list significant events in the field and to discuss them in historical order when possible. Several published survey articles[10-16] are helpful in directing attention to the important results of the past, and they provide historical perspective in this way.

The Civil Aeronautics Board, following the widely publicized Grand Canyon midair collision in 1956, began to direct attention to the need for collision avoidance systems, and during the intervening 17 years, numerous improvements in air traffic control capabilities have taken place. Separation of enroute air traffic by means of "positive" control[17] methods has become a well-known concept, and many different types of systems have been brought to the hardware stage of development.[18-25]

The first significant step in the analytic study of the collision avoidance problem began with studies by Bendix for the Federal Aviation Agency in the late 1950s.[16,26-28] Bendix studied the "ground bounce" measurement concept of computing estimates of the approximate "time-to-go"; i.e., the ratio of range to closing range rate gives an estimate of time remaining (tau) until a collision. The concept was accurate only when both aircraft followed straight paths to the collision point, but it has retained considerable popularity since that time because of its simplicity. The useful feature of the "tau" concept is that it can be considered as a warning time to the pilots involved. Its simplicity, however, concealed other questions of equal importance. That is, under this principle, two aircraft are defined as threats to each other if the range could reduce to near zero during a specified time interval. The influence of the relative speeds, bearings, headings, or altitudes on this "time-to-go" was acknowledged to exist, but had never been fully explored.[13,16] A more important shortcoming of the concept[29,30] by itself was that the pilots of the aircraft, when provided with a current estimate of tau, were not also provided with an evasive maneuver. They were left with the certainty that something must be done, but their courses of action were left open. A wrong turn by either pilot can quickly reduce the time-to-go to zero, before the system has time to react.

In 1959, the FAA organized its Collision Prevention Advisory Group (COPAG), which was formed of representatives of the military services and civil aviation. This group stirred interest in the development of collision avoidance and proximity warning devices.[31] In 1963, an FAA-funded experimental study by Bendix,[32] of the "ground-bounce" method of measuring range and range-rate, was published. The results of these tests, however, were not encouraging, and the active program to develop collision avoidance equipment was reduced by the FAA to a more passive "monitoring" operation. The COPAG personnel were charged with establishing characteristics of collision avoidance systems that would make them "compatible" with air traffic control systems.

A study begun by Collins Radio in 1963[11] investigated the potential of the various collision avoidance concepts considered feasible at that time, by means of analytical studies and computer simulations. The early work performed under these contracts was principally concerned with the requirements of "air derived separation assurance" systems. The candidate concepts being considered in 1966 were categorized in three distinct groups:

1. "Range-altitude" systems, in which only these two quantities are estimated and exchanged.

2. "Relative position-velocity" systems, which measure and exchange all components of the current relative position and velocity vectors.

3. "Projected hazard prediction" systems, which incorporate turns or other accelerations into the flight paths, so as to include the effect of future maneuvers on the predicted miss distance.

Implementation of any of these concepts requires that range be estimated. These schemes utilized ground-bounce, interrogator-transponder, or time-frequency methods of relative position measurement. The ground-bounce technique[32] required each aircraft to transmit a periodic pulse signal which was coded with its own altitude data. Receiving aircraft measure the difference between the arrival times of the direct and ground-reflected signals, which, with the knowledge of both aircraft altitudes, permits computation of the range between the aircraft. The major restriction on the accuracy of the system was due to the roughness and slope of the terrain between the aircraft. The density of the signals increases linearly with the traffic population which is within signaling range of the protected aircraft.

The interrogator-transponder method[12] permits the determination of relative range and velocity components parallel and normal to the line of sight. An interrogator in the "protected" aircraft transmits a periodic signal by means of an antenna which scans in azimuth. These signals can be coded with altitude data, and are received by the "intruder" aircraft via an omnidirectional antenna. If the altitudes are sufficiently close to indicate a possible collision risk, the transponder on the intruder transmits an omnidirectional reply which may include the altitude difference and the intruder's velocity components. This message is received at the protected aircraft on its directional antenna, which has not moved appreciably in the interim. The time delay and the antenna position then permit computation of the range, the relative velocity, and the time-to-go, so that the urgency of the threat can be evaluated. Each range measurement requires two radio transmissions, however, and the rate at which transmissions must be made increases nearly as the square of the number of aircraft in the area.

The time-frequency method[6,41-44] is accomplished by allowing signal transmissions by each aircraft only at prearranged instants of time. All receiving aircraft note the time of receipt of the signal, which permits the relative range to be measured to an accuracy dependent on the accuracy of the start of the transmission and that of the receiving clock. Each aircraft in the system is assigned a specific periodic time-block, and a transmission occurs at the beginning of each block. The aircraft can also code altitude and velocity data on its signal. The major technical problem in this method is the clock accuracy required, since a microsecond of time error corresponds to a range error of about 1,000 feet.

In the final report[33] by Collins, a recommendation for adoption of the time-frequency method of collision threat detection was made. This report had been preceded by several interim publications and it supported earlier claims that transponders could not effectively operate in high density environments. It appeared that, as the number of aircraft increases, the number of transmissions increases geometrically such that the system becomes saturated. Consequently, the time-frequency concept appeared to be the strongest contender for the collision avoidance system implementation. However, even in 1969, it was recognized that the expense of the system made its acceptance by general aviation extremely unlikely.[16]

Meanwhile, wide distribution was being given to other aspects of the collision avoidance problem.[10-12] McDonnell-Douglas installed experimental systems in military aircraft in 1967, and the Air Transport Association (ATA) established its Collision Avoidance Working Group at this time.[34]

The ATA staff in Washington, as well as individual airline members, frequently expressed their desires to the FAA that the time-frequency method be recognized and implemented, but up to this time the FAA has not formally adopted any system as the basis for the industry's collision avoidance system. Under the auspices of the ATA, theoretical and experimental studies related to time-frequency were performed by many groups, and reported in 1967-70.[35-39] The most recent information regarding the technique[40-44] indicates that hardware and data processing problems have largely been surmounted, and that some progress is being made on the economic difficulties of implementation.

In the past few years, the interrogator-transponder ideas have once again gained favor. In 1968, RCA began development of its SECANT system, and RCA currently claims to have surmounted the saturation problem associated with such systems.[45-48] In 1969, the Army funded the development by Honeywell of proximity warning devices for use by helicopters.[19,49] The basic proximity warning device has the cooperative capacity to activate more sophisticated collision avoidance units carried by other aircraft.

A number of other types of collision avoidance systems and pilot warning indicators have also been developed, usually on a smaller scale, including those designed and built by Instrument Systems Corp. (ISC), Microlab/FXR, Quantronix Corp., and General Aviation Electronics, Inc. The system built by ISC is described[50] as a cooperative system which estimates range, range-rate and bearing, by interrogating nearby aircraft with a stream of unique time-spaced pulses. A transponder in the threat aircraft returns the pulses, which are then correlated to eliminate responses to other interrogators; their delay is used to estimate range. Range-rate is obtained by differencing successive values of range, and coarse bearing information is obtained through the relative delay at two receivers at different locations on the aircraft. An altitude discrimination can also be included by having the responding aircraft code its altitude on the returned pulse train.

The Microlab/FXR system[51] consists of a microwave transmitter and a receiver timed to a harmonic of the transmitted signal; these are both carried by the commercial aircraft. The system requires cooperation by the general aviation aircraft, which carries a low-cost arrangement of diode targets. These diodes receive the signal, generate harmoics of it and re-radiate them in the direction of the received signal. This response signal is modulated with altitude information, and range, range-rate, and bearing are extracted from it. Since the system provides no information to the general aviation pilot, any evasive maneuvers must be accomplished solely by the commercial aircraft.

Quantronix Corp.[52] has developed a system based on using an optical reflector on the passively cooperative intruder aircraft, and a rotating laser diode on the protected aircraft. The system can estimate range and range-rate, and discriminates on altitude as well. It is also intended for use in the encounters between commercial and general aviation aircraft.

The General Aviation Electronics System[53] is a PWI unit which has been marketed since May, 1970. The system requires a cooperative transponder on the intruder, and includes a variation of range gates from 3 miles to 1 mile. In these respects, this system is similar to other low-cost PWI units[54-56] which are at various levels of development. Typically, only range information is provided by these PWI systems, although bearing and altitude can also be provided by some of them.

In the 1957-1970 time interval, the theoretical aspects of the maritime ship collision problem received considerable attention in the literature.[57-64] Here, however, the emphasis was on the specification of avoidance maneuvers, while in the airborne application, the topic of principal interest was the measurement of relative range. Several efforts were also made to determine the link between these obviously related problems.[26,57,65] Unfortunately, these studies rarely provided more than an intuitive approach to the problem of evasive maneuver determination. The analogy between the two applications has, therefore, never been fully exploited, although certain recent publications[66,67] have shown how horizontal evasive maneuvers can be determined for both aeronautical and maritime applications.

2.2 PRIOR ANALYSIS OF COLLISION AVOIDANCE MANEUVERS

In the past, attempts have been made to determine collision avoidance maneuvers analytically or to develop a collision hazard criterion. Representative studies of this kind are those of Morrel,[26,27,68] Bolie[69] and Holt and Marner[33], and all of these sources considered short-term maneuvers modeled without instantaneous changes in heading or speed. Many other references[12,29,57-61] during the past 15 years have treated the maneuver problem but only by ignoring the transient effects completely. The works of Morrel and Bolie are concerned specifically with the effects of collision avoidance maneuvers in an encounter where only one aircraft maneuvers to avoid the collision. The work of Holt and Marner is concerned with the hazard potential, or the possibility of collision in a given fixed time interval.

Morrel mentions briefly the systems in which both aircraft maneuver but their presentation involves unusual complexity in determining general results and presenting them in a tractable manner. Both Morrel and Bolie performed the analysis on a geometric basis, with the numerical parameters specialized to particular speeds, ranges, and times. The specific methods used lead to limitations in providing general results.

Morrel, however, was able to provide definite contributions to the collision avoidance problem. Most noteworty of these was the predicted time-to-collision criterion, commonly referred to as the tau (τ) criterion.[27] This criterion is satisfactory provided the aircraft are on or near a collision course, following straight-line paths. Morrel was able to indicate also those collision geometries for which a lateral turn in the wrong direction merely delayed the collision by a small time. Bolie pursued this further and determined analytically those collision geometries for which "turn away from the hazard" maneuvers were actually futile. These results have been quoted out of context to suggest that lateral turns are sometimes dangerous and, hence, only vertical maneuvers should be implemented.[16]

In his discussion of the physical aspects of collision avoidance, Morrel dismissed speed control maneuvers as inapplicable to the collision avoidance problem. This was based on an assumption of negligible speed-change capabilities of an aircraft. However, analysis of aircraft capability indicates that in some cases speed control is actually a practical and attractive type of maneuver, since there is no off-track deviation required and the time loss due to the maneuvers is small.

A set of "rules-of-the-road" were deduced from Morrel's gemetric approach to the horizontal collision avoidance maneuver problem. Other sets of horizontal maneuvers for avoiding collison have been described in recent publications [70-71] but they have always been based on intuitive approaches. As a result, they are often contradictory, and all of the rules fail under some geometric or operational conditions.

A major aspect of a collision avoidance system is the accuracy of the warning capability. It is necesary to have acceptably few false alarms while achieving no missed alarms. Morrel indicated certain information requirements for non-cooperative systems. Holt and Marner [33] defined hazard regions based on the τ-criterion and range, range-rate and relative velocity information assuming no maneuvers. Given range and range-rate only, the hazard regions are necessarily (because of lack of information) conservative. The dimensions of the regions increase with measurement uncertainties, but decrease with additional information, such as relative heading.

Until recently, [66] all published studies of aircraft collision-avoidance maneuvers have been based on showing the effects of an assumed set of evasive maneuvers. For encounters involving only vertical maneuvers, it is sufficient to command the higher aircraft to evade by climbing, and the lower aircraft to dive, in order to increase the miss distance. This simple intuitive "rule-of-thumb" is an effective vertical maneuver in the majority of reasonable encounter geometries. A corresponding simple rule for horizontal maneuvers cannot be stated, however, because the transient aircraft dynamics are of much greater significance.

Complex horizontal dynamics have had the effect of discouraging thorough studies of such maneuvers. Consequently, the major portion of past research and development efforts in aircraft collision avoidance has been concerned only with the measurement problem. This is the problem of measuring relative aircraft position and velocity (range, range-rate, bearing, etc.). Very little has been learned about the associated "control" problem, which is the determination of the maneuvers that should be performed by the aircraft. The maneuvers obviously depend on the relative geometry, so the measurement and control problems are not independent. This report fills the need for a unified study of both problems.

III. DYNAMICS OF ENCOUNTERING AIRCRAFT

In this chapter, attention is focused on modeling the dynamics of relative motion resulting from applying available controls to each of two aircraft in a typical encounter situation. The initial purpose is to develop a set of equations of motion for an arbitrary aircraft. These coupled, nonlinear equations provide a quantitatively accurate means of computing the aircraft trajectory, or time history of position and orientation, in response to the available control inputs. This motion is characterized and used to develop simpler equations of relative motion between two aircraft. A general discussion is presented on the use of these equations for generating maneuvers for collision avoidance.

3.1 RESPONSE OF A SINGLE AIRCRAFT TO CONTROL INPUTS

The equations of motion for a representative aircraft must include the effects of the control inputs--rudder, aileron, and elevator deflections from trim--as well as variations in thrust from the equilibrium value. To simulate a typical maneuver by integration of these equations requires that the typical pilot's control inputs be specified as functions of the errors in the aircraft state (position, attitude, and their rates of change). The coupled, nonlinear equations required for such a simulation are given in general form in Appendix A. A digital computer program was generated from these equations and utilized to study the complex response of an aircraft to various control inputs.

The controls introduced by the pilot were specified by assuming that he acts to control a simplified dynamic model of the aircraft. That is, lower-ordered dynamic models were used to approximate both the horizontal and the vertical motion of the aircraft. The feedback gains representing the pilot's behavior were determined by analysis of the simplified models and the resulting controls were applied to the actual system (which was represented by the more complex nonlinear equations). Various simple nonlinearities (saturation and/or dead-zone) were also included, to provide a more realistic representation of the pilot-control system characteristics. The resultant pilot-induced control (pilot model) was found to generate a satisfactorily realistic representation of the motion of the entire system.

Individual pilots obviously differ in their manner of controlling an air plane, so there is no unique representation of this component of the system. Therefore, the gains in the "pilot" model were assumed to be adequate when the associated step response of the aircraft/pilot system (to a turn rate or climb-rate command, for example) was both prompt and well-damped.

A typical desired change in the aircraft flight condition can be considered as a change in magnitude and direction of the velocity vector. The errors in the azimuth (heading) and elevation (flight path) angles were used to generate control deflections in the simulation according to the following logic:

1. Azimuth correction: The aileron deflection is proportional to the error in yaw rate or roll angle, subject to saturation constraints. The rudder deflection is proportional to the sideslip angle, which should always be small, such that the turn is "coordinated".

2. Elevation correction: The elevator is deflected in proportion to the pitch angular error, and the thrust is increased for a climb maneuver or decreased for a dive maneuver. The amount of thrust change is arbitrary but "reasonable", since it is introduced only to keep the airspeed within acceptable bounds. The maximum available thrust level is usually known at each flight condition.

An aircraft's total maneuver over a short period of time can most easily be interpreted in terms of the horizontal turn-rate maneuver, and the vertical climb-rate maneuver. A change in steady horizontal turn-rate requires that the roll angle be changed by a nearly proportional amount. The time required to orient the aircraft in roll is a measure of the roll transient, and the resulting turn-rate transient has the qualitative form of Fig. 3.1. Similarly, the climb-rate is typically controlled by elevator and thrust, and has a time variation such as shown in Fig. 3.2.

Physical limits exist on the allowable roll rate and the climb and dive rates. The large maneuvers required for collision avoidance may cause the aircraft to reach these control limits. If saturation of the controls does occur,

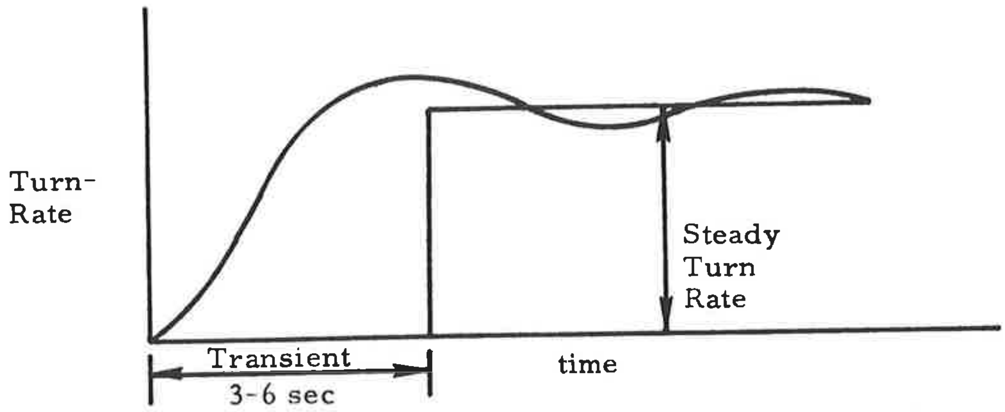

Figure 3.1 Horizontal Turn Maneuver Transient

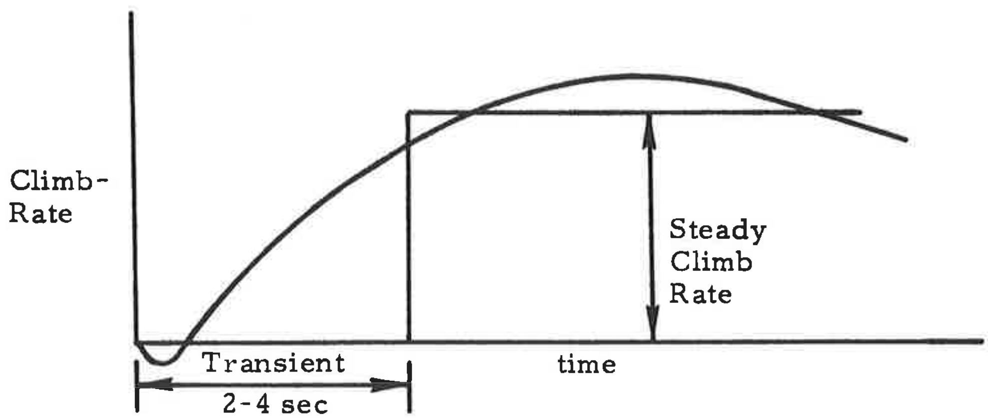

Figure 3.2 Vertical Climb Maneuver Transient

the horizontal maneuver transient time is nearly proportional to the final roll angle. This type of nonlinear behavior is also present for the vertical maneuver, for which the transient time is dependent on the magnitude of the final rate of climb or dive.

The magnitude of the maneuvers depends on the aircraft involved, the airspeed, and the degree of hazard felt by the pilots. For example, a high-performance combat aircraft is easily able to turn at much higher rates than those of typical light aircraft or commercial jets. In many circumstances, the pilot of a combat jet might roll the aircraft to 45^{o} or more, without danger of structural failure due to the high accelerations involved. The turn rates can easily approach 10^{o}/sec in such cases. On the other hand, passenger comfort and safety are more important considerations for commercial jet aircraft, and relatively slow turns are preferred in these cases. The "standard" turn rate of 3^{o}/sec is a typical value in a terminal area, in which case the aircraft can be rolled up to 30^{o}.

Equivalent statements hold for the magnitudes of the steady climb rates which are possible for various aircraft. The throttle and elevator are both available for controlling climb and dive maneuvers, although the throttle is typically changed in an open-loop, step input manner.

The aircraft of interest in the simulation study were the general aviation and commercial jet types. Any of a large number of existing aircraft could have been chosen as representative; those selected for detailed numerical study were the Cessna 172 and the Boeing 727. The inertial, aerodynamic and operational data required for simulation of their maneuvers were obtained from the manufacturers' sources.[72,73] The data received from these sources permitted a detailed study of transient response characteristics in various flight conditions.

The dynamic approximations which have been discussed can be readily illustrated using these aircraft. The simulated trajectories of the aircraft were found by numerical integration of the nonlinear equations of motion, and these time variations were compared with approximate maneuvers which resulted from ignoring the transients. These approximations are illustrated in Fig. 3.3 for the Cessna 172, and in Fig. 3.4 for the Boeing 727 aircraft. In these figures, the dots represent simulated position and the solid line illustrates the approximation. The maneuver transients result from deflecting the aerodynamic control surfaces in proportion to the errors in aircraft attitude, as described in Appendix A. It can be seen that the resulting motion in the horizontal plane can be accurately represented by a circular arc. Similarly, motion in the vertical plane can be sufficiently well approximated by a sloping straight line. The vertical maneuvers are typical, but the indicated dive and

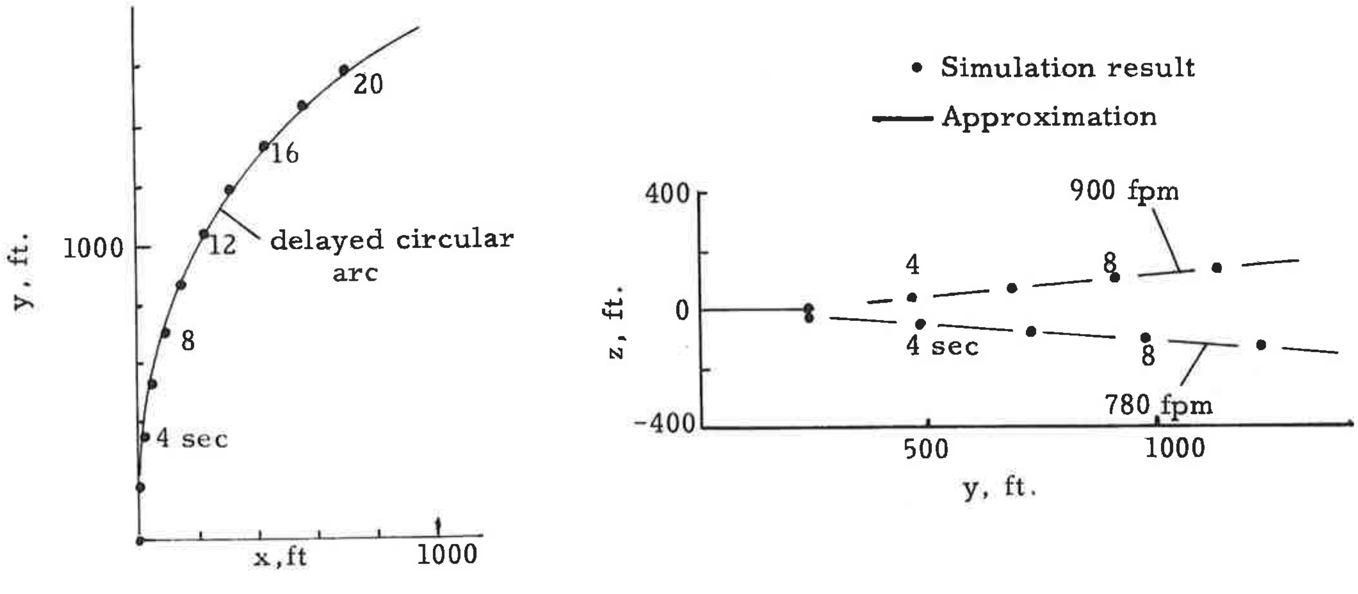

a) Horizontal Maneuver

b) Vertical Maneuver

Figure 3.3 Exact and Approximate Responses for the Cessna 172

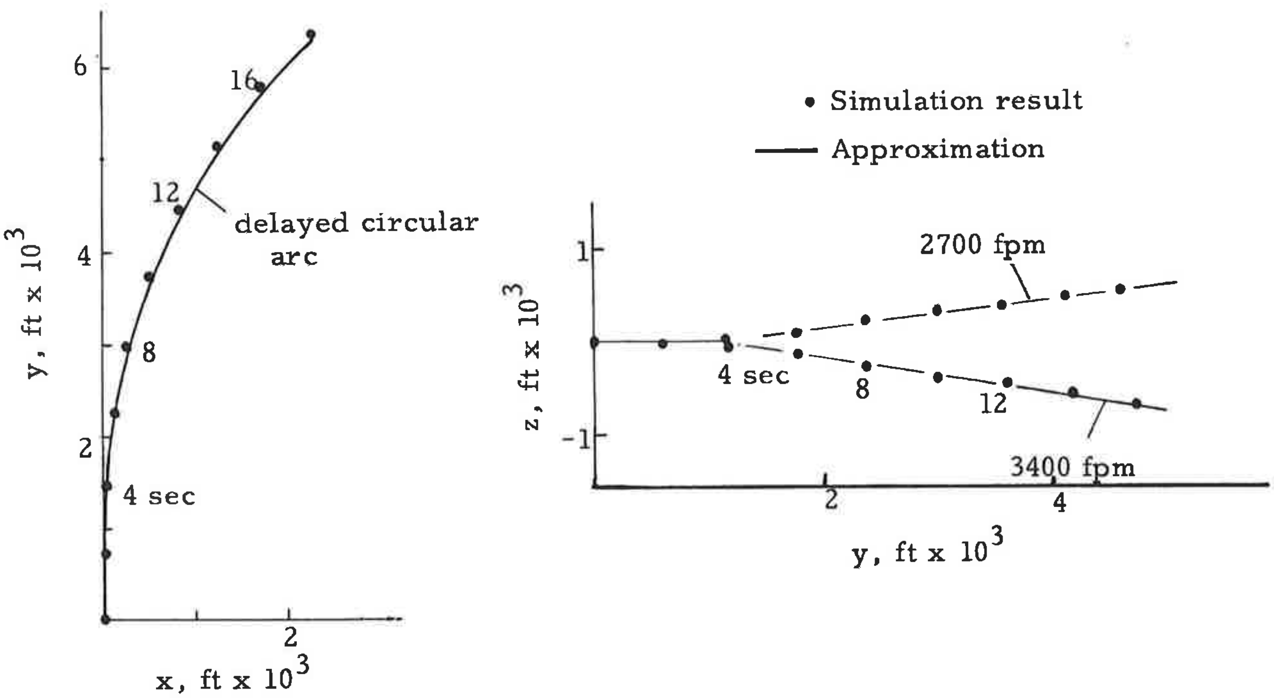

a) Horizontal Maneuver

b) Vertical Maneuver

Figure 3.4 Exact and Approximate Responses for the Boeing 727 climb rates are not meant to be extreme values for the two aircraft. The transient time interval, separating the initial and final steady-state conditions, has the effect of translating these simple geometric figures in the directions of the initial velocity. Therefore, the horizontal motion corresponding to a steady-turn input can be approximated by a delayed circular arc. The vertical motion corresponding to a steady climb or dive input can be approximated by a delayed straight-line segment.

3.2 RELATIVE MOTION OF AIRCRAFT DURING MANEUVERS

For simulating an encounter between two aircraft, aerodynamic data (stability and control derivatives) should be consistent with the range of both aircraft altitudes and airspeeds. Since this type of data is not usually available, an adequate approximation resulted by using the following assumptions:

1. The stability derivatives are constant with respect to small variations in airspeed.

2. The initial flight conditions of the aircraft are steady flight paths, and the angles-of-attack required for equilibrium are known functions of gross weight, altitude, and airspeed.

These assumptions permitted calculation of the initial equilibrium angle-of-attack and thrust for each of two aircraft in a potential collision situation.

Simulation of the aircraft motion in the typical encounter also required assigning the evasive maneuvers, based on the relative position, airspeeds, and available turn rates of the aircraft. The maneuvers could include both horizontal and vertical components, e.g., a typical maneuver might follow from the instructions "turn right and climb".

The relative motion between the two encountering aircraft was simulated by numerical integration of the equations of motion for each aircraft. The results were then presented in either an inertially fixed or relative axis system. In the latter case, the integration was followed by algebraic differencing of the positions and reorientation of the axis system.

In the inertial axis system, the turn and climb maneuvers are more readily understood, but two trajectories are required in order to describe the resulting motion. Generally, all coordinates of both aircraft change with time, so that a three-view drawing of the two paths is required for a general set of initial conditions. An example of this type of representation of motion between two aircraft is illustrated in Fig. 3.5.

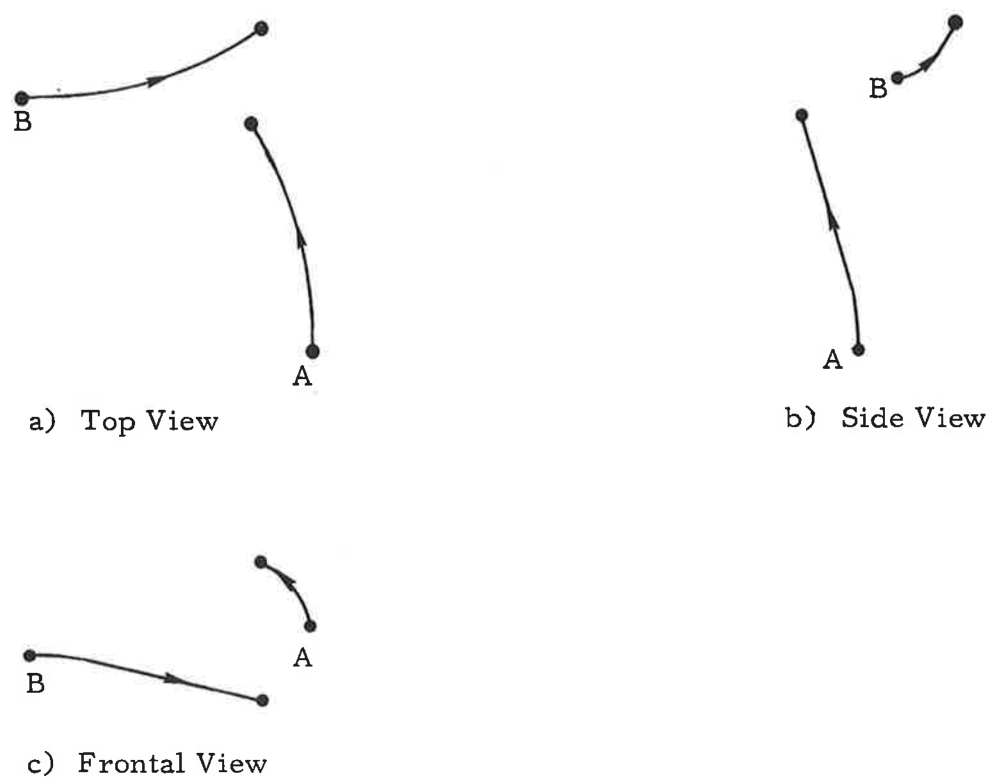

Figure 3.5 Real (Inertial) Space Representation of Aircraft Motion

The same dynamic problem is more conveniently shown in a relative axis system which has its origin centered at one of the aircraft. In such an axis system, the motion of the second aircraft appears as it would to the pilot of the first aircraft. Because only the relative motion is measured, only half as many variables are required to illustrate the maneuver. This implies a lower-ordered model of the system dynamics, and a more efficient and direct method of solution to the fundamental aspects of the collision avoidance problem.

Based on the approximations which can be used to characterize horizontal and vertical motion of individual aircraft (discussed in Section 3.1), much simpler equations can be used to describe the relative motion between the aircraft. This simplified dynamic model of the relative motion makes use of the fact that the time interval of interest for the approximation is large enough so that the maneuver transients can be ignored. For the collision avoidance problem, this means that the aircraft begin to maneuver when the range is large enough so that extreme violent maneuvers are unnecessary, and that most of the motion can be described as steady-state. When initial transients are ignored, the horizontal and vertical relative motion of two aircraft is governed by the following dynamic equations:

$$
\begin{aligned}
\dot{x} &= -\omega_A y + V_B \sin\theta & \qquad |\omega_A| &\le \omega_{A_{max}} \\
\dot{y} &= -V_A + \omega_A x + V_B \cos\theta & \qquad |\omega_B| &\le \omega_{B_{max}} \\
\dot{\theta} &= -\omega_A + \omega_B & \qquad |\delta_A| &\le \delta_{A_{max}} \\
\dot{z} &= -\delta_A + \delta_B & \qquad |\delta_B| &\le \delta_{B_{max}}
\end{aligned}
\qquad (3.1)
$$

These equations are derived in Appendix A. Here, the subscript A refers to the aircraft at the origin of the relative coordinate system, and B is the other aircraft. V_A and V_B are A and B's horizontal airspeeds which are assumed to be constant over the duration of the collision avoidance maneuvers. The turn rates ω_A and ω_B, and the climb rates δ_A and δ_B, are the control inputs to this system of equations. When the rates ω_A and ω_B are set to constant values, both aircraft describe circular arcs at constant velocity in the horizontal plane. The climb rates δ_A and δ_B are the corresponding controls in the vertical equation, and when they are set to constant values, the slope of each flight path is changed proportionally. The relative position and heading (x, y, z, and θ) of aircraft B with respect to aircraft A are defined in Fig. 3.6. Equations (3.1) describe the relative motion with an accuracy suitable for the collision-avoidance analysis purpose.

Figure 3.6 is also used to define the range r and the bearing angle β of aircraft B's horizontal position relative to the velocity vector of A. These

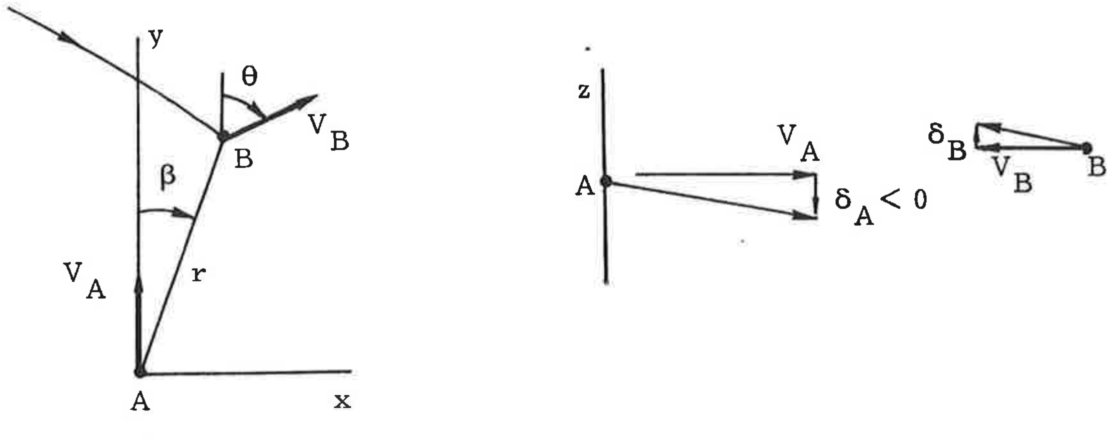

a) Horizontal Motion Viewed from Above

b) Vertical Motion Viewed from the Side

Figure 3.6 Relative Motion Coordinates for Encountering Aircraft

two quantities are normally measured as part of a horizontal collision avoidance system. Also illustrated in Fig. 3.6 are the climb and dive rates which govern vertical motion.

Equations (3.1) are used as the basis for determining the appropriate collision avoidance maneuvers of the aircraft in Chapter IV. The principal features of this model of the relative motion are summarized as follows:

1. Each aircraft can maneuver horizontally by turning to the right or left, at rates which are bounded between symmetrical limits ($\omega_{A_{max}}$, $\omega_{B_{max}}$). Horizontal trajectories are, therefore, approximated by circular arcs.

2. Each aircraft can maneuver vertically by choosing a vertical velocity which is bounded above and below, corresponding to steady climb and dive rates ($\delta_{A_{max}}$, $\delta_{B_{max}}$). Vertical trajectories are, therefore, approximated by straight-line segments.

3. The relative motion of the two aircraft depends upon both climb rates (δ_A and δ_B) and both turn rates (ω_A and ω_B). These controls

and the associated maneuvers are obtained in Chapter IV with respect to the collision avoidance problem.

Extensive comparison was made of the relative motion of the aircraft, as governed by Eqs. (3.1) and by the more exact nonlinear equations of both aircraft via the computer simulation. In all cases, excellent agreement was found. Further discussion of this comparison and a typical numerical example are presented in Section 4.6.

IV. OPTIMUM COLLISION AVOIDANCE MANEUVERS

The analysis of horizontal collision avoidance systems must begin by first attempting to answer the following question: How should either or both aircraft maneuver in the horizontal plane in order to best avoid a detected conflict? This chapter presents the results of a systematic approach to answering this question.

First, it was necessary to select a criterion with which to choose the maneuver characteristics. The rationale is presented in this chapter for selecting miss distance as the basic quantity to be maximized by the maneuvers, subject to bank angle constraints.

With the objective of choosing maneuvers which maximize miss distance, the maneuver strategies were determined for conflicting aircraft having arbitrary relative initial conditions. These strategies are presented in a series of charts which indicate how each aircraft should turn as a function of relative range, bearing, and heading.

There are several airspace usage problems that are associated with avoiding collisions by always turning in the direction which maximizes miss distance. These include interference between the two aircraft when returning to the initial track after the maneuver is completed and interference with a third aircraft before minimum range is reached. The complexity of these problems is discussed to indicate the need for considering other criteria for selecting the maneuvers, in addition to miss distance.

With the motive of reducing airspace usage, the interrelationships between aircraft miss distance, deviation off track, bank angle during the turns, and (initial) range separation when the maneuvers must begin were examined. Initial range and deviation off track can be reduced at the cost of increased bank angles and/or decreased miss distance. Tradeoff curves are presented which show quantitatively the relationship between these criteria.

The tradeoff curves can be used with the maneuver charts to answer the question of what maneuvers to use for horizontal collision avoidance. The maneuver charts and tradeoff curves together form the basis for deriving the perfect horizontal collision avoidance command logic for an ideal CAS. These results are necessary to measure the performance degradation due to measurement equipment errors and dynamic effects. The results also serve as a standard for evaluating the adequacy of the collision avoidance command logic of any existing system.

This chapter is concluded with an analysis of combined horizontal/vertical maneuvers for collision avoidance. It is shown that adding the vertical component does not significantly increase the miss distance capability of a horizontal collision avoidance system.

In this chapter, it is assumed that perfect measurements are available for determining the required maneuvers. Furthermore, it is assumed that adequate computation facilities exist for processing the data and for computing these maneuvers. The limitations on the system's performance which are due to computer characteristics and measurement errors are addressed in Chapters VI and VII. This chapter determines how an ideal CAS should function based on considering only the dynamics of the encountering aircraft.

4.1 CHOICE OF CRITERION

It is first necessary to determine the appropriate horizontal maneuvers for two aircraft which encounter each other when both are flying at the same constant altitude. The maneuvers must be based on consideration of various interrelated characteristics which describe a pair of evasive maneuvers. Examples of such characteristics are the following:

1. Miss distance, or separation at minimum range.

2. Distance off the nominal track or flight path for each aircraft.

3. Turn rate, or normal acceleration, of the aircraft.

4. Initial range at which maneuvers begin.

These elements can be used as criteria with which to judge the maneuvers. Each criterion is now discussed.

The miss distance has a fundamental importance to air safety. When the maneuver begins at close range, miss distance should be maximized. If the initial range is sufficiently large, on the other hand, it is preferable to execute maneuvers which meet a specific acceptable miss distance, by requiring each aircraft to maneuver just enough to meet this condition at the point of minimum separation. The most important feature of an operational collision avoidance system, under this reasoning, would be to guarantee that two aircraft could never be separated by less than a specified distance.

The distance off the nominal track is a rough measure of the aircraft's use of surrounding airspace. Such deviations from a scheduled flight path should be controlled to reasonable levels, to minimize interference with adjacent air traffic, and to maintain the nominal trajectory as long as the separation constraints are not violated.

Turn rate is an indication of the severity of the horizontal maneuver, and must be kept within bounds that are acceptable both to the structure of the aircraft and to the comfort of passengers and crew. Very rapid horizontal turns must be performed at large roll angles, and the resulting normal accelerations are undesirable. The horizontal maneuver severity must, therefore, be limited in the steady-turn accelerations.

The initial range at which the maneuvers must begin should also be kept to reasonable levels. It is intuitively clear that necessary maneuver severity decreases as the initial range increases, but that relative position measurements become less accurate at large range. Furthermore, the magnitude of the air traffic control problem for each aircraft increases with the "protection" range, since more adjacent aircraft can be considered as potential threats.

These four criteria can be used collectively to measure the basic performance of the collision avoidance system. These components of the system's performance are not independent, and have levels of relative importance which depend on the circumstances of the initial flight condition or relative geometry. Because of the interdependence of the components, the system's performance can be examined in a "trade-off" fashion. That is, one or two criteria can be fixed to enable obtaining the relationship among the remaining components. The trade-off study then can answer such questions as the following:

1. How does the distance off-track vary with the turn rate, when the miss distance is fixed?

2. For a given turn rate and miss distance, at what initial range must the maneuvers begin?

3. How does the distance off-track depend on the directions of the turn maneuvers?

A number of different maneuver pairs can be used to avoid a collision, when the potential conflict is detected with sufficient time for action. These maneuvers can be compared by computing a performance measure of relative "goodness", and it should be emphasized that a control input and the system's resulting performance can be optimal only with respect to a specific criterion. Thus, for example, a maximum miss distance optimal path can be quite different from a minimum airspace usage optimal path, because these two criteria usually have opposite effects on the controls applied to each aircraft. Careful consideration was made of the potential components of a performance criterion, because the criterion determines both the maneuvers and the difficulty in implementing the actual system.

When more than one maneuver pair yields a miss which is greater than the acceptable value, then the turn rates of each maneuver can be adjusted in such a way that all maneuvers considered yield the same miss distance. There are two reasons for first determining the maneuvers which maximize the miss distance. These are:

1. For sufficiently small initial separation, only maneuvers in the optimal direction produce a satisfactory miss distance.

2. For larger initial separation, the turn directions which maximize the miss distance are also the directions which will produce a given acceptable miss with the smallest turn rates.

Thus, maneuvers were first determined which produced maximum miss distance, and the miss distance was initially chosen as the performance criterion.

It must be understood that this portion of the study, based on a simplified version of the two-aircraft encounter, does not answer questions related to measurement errors, or to constraints (e.g., multiple aircraft flight patterns) which would exist under operational conditions. This part of the study is based on the belief that a complete understanding of the approximate system model given in Eqs. (3.1) is much more useful than a fragmentary knowledge of a more exact and detailed system model. It is also found that maneuver determination based on even this simple model of the relative motion entails a considerable amount of numerical computation. Increasing the accuracy of the model beyond this level is not justified on the basis of current or forseeable instrumentation and data accuracies.

4.2 SOLUTION TO THE MAXIMUM MISS-DISTANCE PROBLEM

The solution to the problem of determining how the aircraft should maneuver to achieve maximum miss distance requires the following: (a) suitable equations describing the controlled motion of the two aircraft, (b) an optimization procedure, and (c) a method for presenting the results in a compact, general form. The equations of motion for this problem are derived in Appendix A and discussed in Chapter III. The optimization procedure which uses these equations to determine how the aircraft should maneuver is presented in Appendix B. This section explains how the results are presented in maneuver chart form and elaborates on how these charts are to be interpreted.

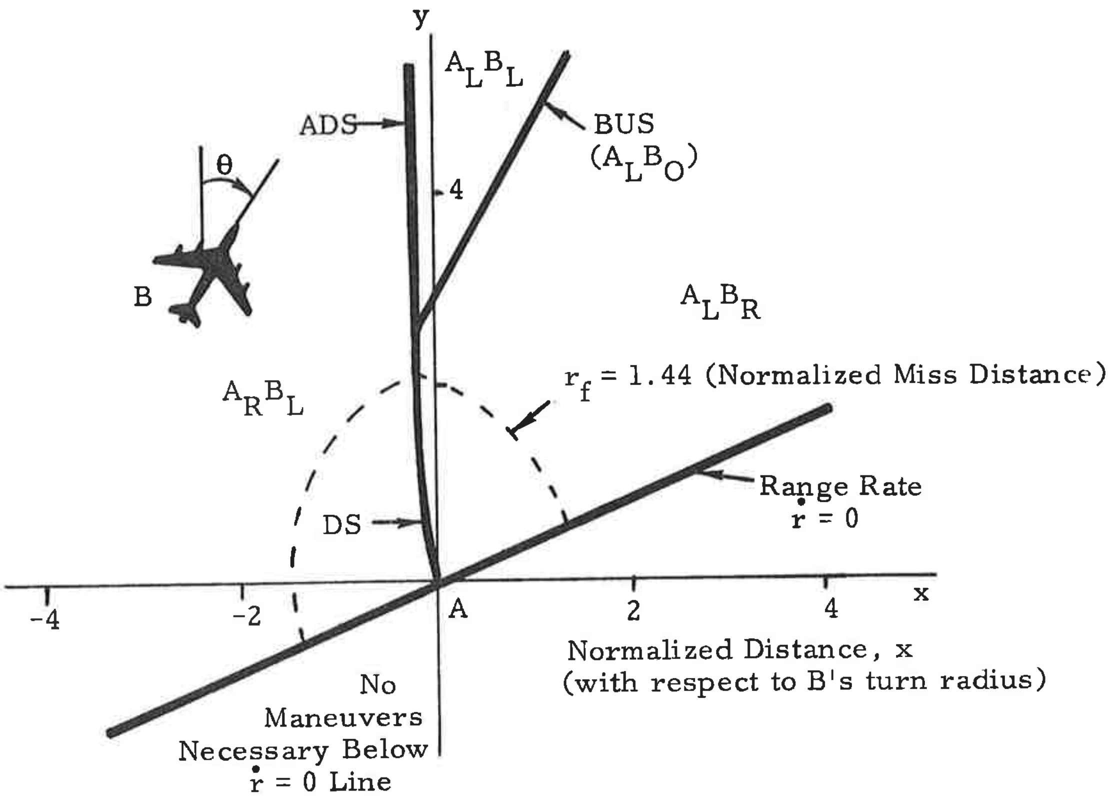

(a) $\theta = 30^{o}$

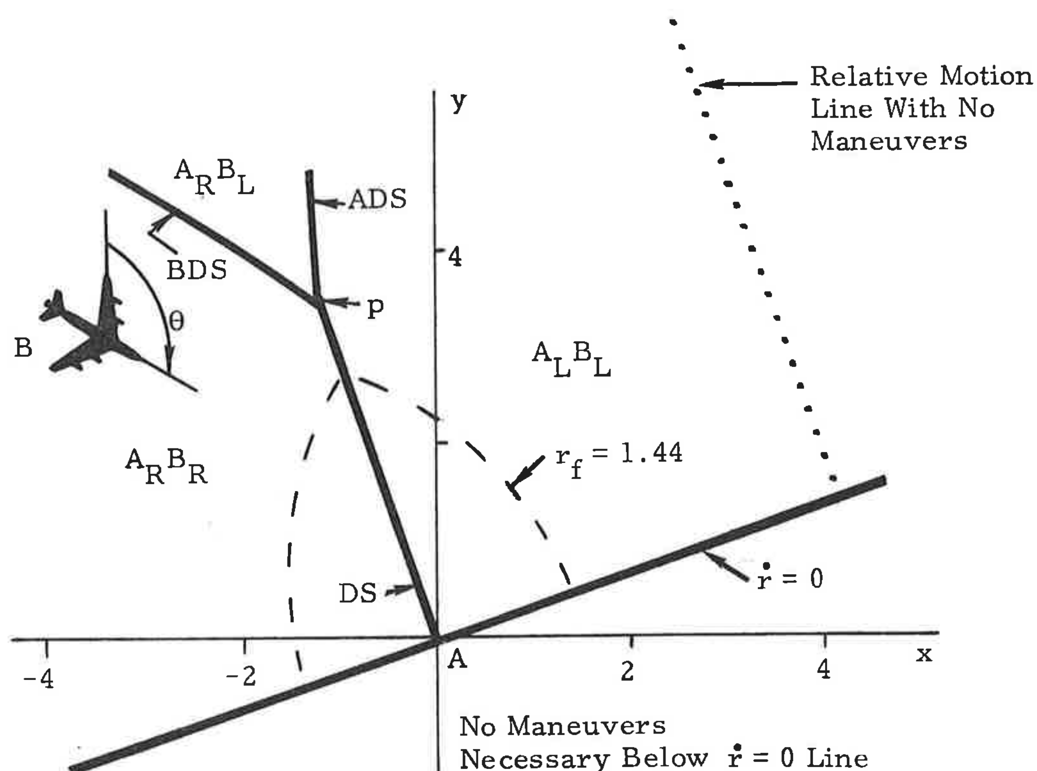

(b) $\theta = 120^{o}$

Figure 4.2 Normalized Optimal Collision Avoidance Maneuver Strategy Charts for the Ratios $V_B/V_A = 0.5$ and $\omega_B/\omega_A = 2.0$

of allowing a single chart to present the maneuver strategies for an infinite number of aircraft pairs with the same speed and turn rate ratios. For example, any pair of aircraft with speed ratio $V_B/V_A = 0.5$, turn rate ratio $\omega_B/\omega_A = 2$, and $\theta = 30^o$ can use the chart in Fig. 4.2(a).

3. The diagonal line through the origin (passing through the first and third quadrants) divides the x-y plane into two regions, corresponding to points where the range rate is negative or positive. Above this line, the range rate is negative. The turn maneuvers are indicated only for this region with negative rate ($\dot{r} < 0$), when the aircraft are approaching one another. Along this diagonal line, the range rate is zero, and when aircraft B is on this line, it is at the point of minimum range. Below this line, the aircraft are moving away from each other. Before the turning maneuvers begin, the relative motion of B with respect to A is perpendicular to this line and parallel to the indicated dotted line.

4. The region where range rate is negative is divided into smaller regions separated by the heavy lines, as depicted in Fig. 4.2. Each of these smaller regions has a different maneuver strategy, as indicated, which produces maximum miss distance. The notation used in each region of the charts indicates the optimal turn directions (R, L or O) for both aircraft (A and B). For example, $A_R B_L$ means that A turns right and B turns left, when B is in this region (x,y) relative to A, in order to maximize the miss distance.

5. The different maneuver regions are separated by lines, along which the maneuver strategy is not unique. For example, along the line separating the $A_R B_L$ region from the $A_L B_L$ region in Fig. 4.2(a), aircraft A can either turn right or left, and the resulting miss distance will be the same. A line across which aircraft A's or B's maneuver changes from "turn right" to "turn left" is known as "A's or B's dispersal surface" [74] and is indicated by ADS or BDS. The line

across which the turn directions of both A and B change is termed a "dispersal surface" and is indicated by DS. The combinations of position and heading for which B's maneuver should be to fly straight is known as "B's universal surface" and is indicated by BUS. Aircraft B can initially be in the $A_L B_L$ or $A_L B_R$ regions and as θ changes, end up on the $A_L B_O$ line (BUS). This would be true for aircraft B executing a two-part maneuver. The point p in Fig. 4.2(b) is where three maneuver strategy regions meet, and all three maneuvers produce equivalent miss distance. The presence of the dispersal surfaces with ambiguous strategies implies that it is essential that the two aircraft communicate which strategy is to be used. Otherwise, incorrect maneuvers can result causing a dangerous situation.

6. When both aircraft continue to fly straight, the relative motion is along a straight line which is perpendicular to the line $\dot{r} = 0$. For this case, the relative heading θ remains constant. An example of this motion is illustrated by the dotted line in Fig. 4.2(b). A special case of this type is the "collision" line which passes through aircraft A, at the origin. This line denotes those relative positions for which a collision will occur if neither aircraft turns. The bearing rate is zero on this rectilinear collision course.

7. The loci of points where a maneuver must begin to achieve a specified miss distance can also be shown on these charts. For example, the loci of initial positions which produce a normalized miss distance of $r_f = 1.44$ (if the optimal maneuver strategy is used) are shown by the dashed lines in Figs. 4.2(a)-(b).

The derivation of the lines on the charts is presented in Appendix B, where the associated computational details are described. The use of the charts for a representative example is illustrated by the discussion in the following paragraphs.

Suppose the two conflicting aircraft have speeds of $V_A = 400$ fps and $V_B = 200$ fps, so that the speed ratio is $\gamma = .5$. If it is further assumed that the aircraft perform coordinated turns at the same bank angle of $\varphi = 20^\circ$, the individual turn rates will be

$$\omega_A = (g/V_A) \tan \varphi = 1.68 \text{ deg/sec.}$$

$$\omega_B = (g/V_B) \tan \varphi = 3.36 \text{ deg/sec.}$$

The corresponding turn rate ratio is $\omega = \omega_B/\omega_A = 2.0$. The steady turn radii will then be

$$R_A = V_A/\omega_A = 13750 \text{ ft.}$$

$$R_B = V_B/\omega_B = 3440 \text{ ft.}$$

The unit of distance in the charts is, therefore, the turn radius of aircraft B (3440 ft), which is less than that of aircraft A.

If a desired miss distance due to optimum maneuvers is 5000 ft., the normalized miss distance r_f is obtained by dividing the desired miss distance by the turn radius R_B, or

$$r_f = 5000/3440 \cong 1.44.$$

As mentioned before, contours corresponding to initial points which produce this dimensionless value of miss distance are illustrated by the dashed lines on the charts of Fig. 4.2. These contours represent the loci of initial conditions for which immediate (optimal) turns in the indicated directions and at the given bank angle, will yield a final miss distance of 5000 ft. Turns in the wrong directions or with smaller bank angle by either aircraft will result in a smaller miss distance.

In order to be able to include essentially all realistic combinations of aircraft performance, one must examine variations of the dimensionless miss distance over the approximate range, $0 \leq r_f \leq 4$. Larger values of r_f occur when the slower aircraft has a high turn rate, because in this case, the desired miss distance can be several times greater than the corresponding minimum turn radius.

4.3 OPTIMIZATION RESULTS FOR VARIOUS AIRCRAFT

Figure 4.2 is an illustration of the maneuver strategies in chart form for the particular speed ratio of γ of 0.5, turn rate ratio ω of 2.0, and relative heading θ of 30° and 120°. The complete solution would require an infinite number of charts for the various values of (γ, ω, θ). Specific sets of these parameters were selected, and the corresponding optimal maneuvers were solved and depicted in chart form. These specific sets were chosen: (1) to provide representative solutions, (2) to illustrate the changing characteristics of the maneuver region boundaries, and (3) to provide enough information to allow study of the performance of a system which commands optimal maneuvers but is subject to measurement errors. This section discusses the charts that were obtained.

The optimum horizontal maneuvers (which maximize miss distance) can be determined by using the method of Appendix B, for any combination of aircraft speed ratio γ and turn rate ratio ω. Since results can be obtained only by numerical computation, the values of these parameters must be specified before the maneuver regions can be computed. The speed ratio (γ) of two aircraft flying at the same altitude can vary from about .3 to 1.0, while the ratio of turn rates (ω) can take any positive value. Specific values of these two parameters chosen for this study are shown by the dots in Fig. 4.3. The optimal maneuvers for these sets of parameters were determined, and they are presented in chart form in Appendix C. The cooperative optimal maneuvers, as found for each specific set of these parameters, are presented as functions of the relative position and heading of the two aircraft.

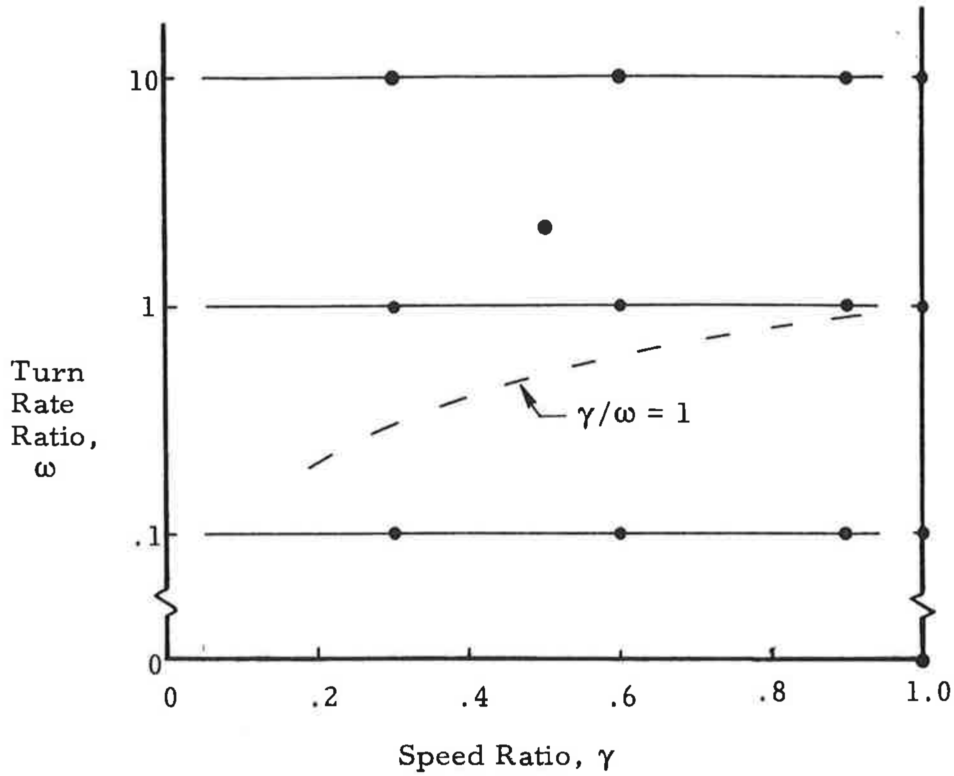

Figure 4.3 Parameters Chosen for Horizontal Maneuver Study

A more complete set of maneuver charts is illustrated in Fig. 4.4, for the parameters $\gamma = .5$ and $\omega = 2.0$. Here, as in Section 4.2, the slower aircraft is assumed to have half the speed but twice the turn rate of the faster aircraft. Notice that, for these parameters, the minimum turn radius of the slower aircraft B is only .25 as large as that of aircraft A, and, therefore, the unit of distance in the charts is B's minimum turn radius. For a typical case, as discussed in Section 4.2, this might correspond to a distance of 3440 ft. The locus of initial points which produce miss distances of 2 turn radii is indicated by the dashed contour in each maneuver chart.

Certain details of the optimal maneuver regions of Fig. 4.4 require discussion. In Fig. 4.4, most of the maneuver regions are separated by dispersal surfaces and that the universal surface appears only for $\theta = 30^{\circ}$. This universal surface (points where aircraft B should fly straight) is actually present at all relative headings between -60° and $+60^{\circ} = \cos^{-1}(\gamma)$. This surface changes its

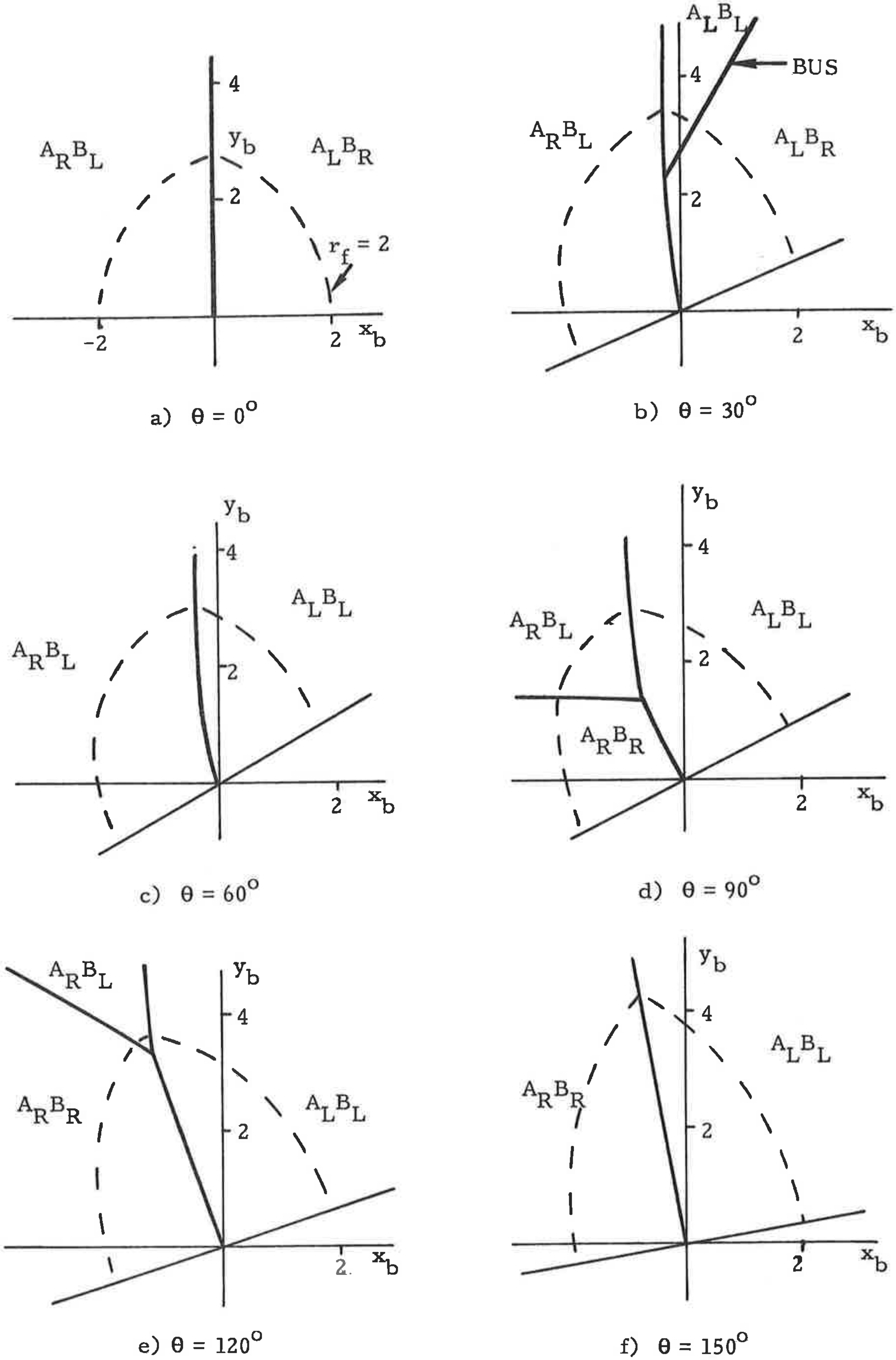

Figure 4.4 Optimum Maneuver Charts for a Speed Ratio $\gamma = .5$ and a Turn Rate Ratio $\omega = 2$.

position as a function of θ more sharply than do the other maneuver region boundaries. A more detailed illustration of the manner in which the universal surface changes with the relative heading is shown in Fig. 4.5.

An optimum "two-stage" evasive maneuver which illustrates the effect of the universal surface's presence in real space is shown in Fig. 4.6. As both aircraft turn, the value of θ changes, and B's position with respect to A eventually falls on the universal surface. At that point in time, B transitions from turning

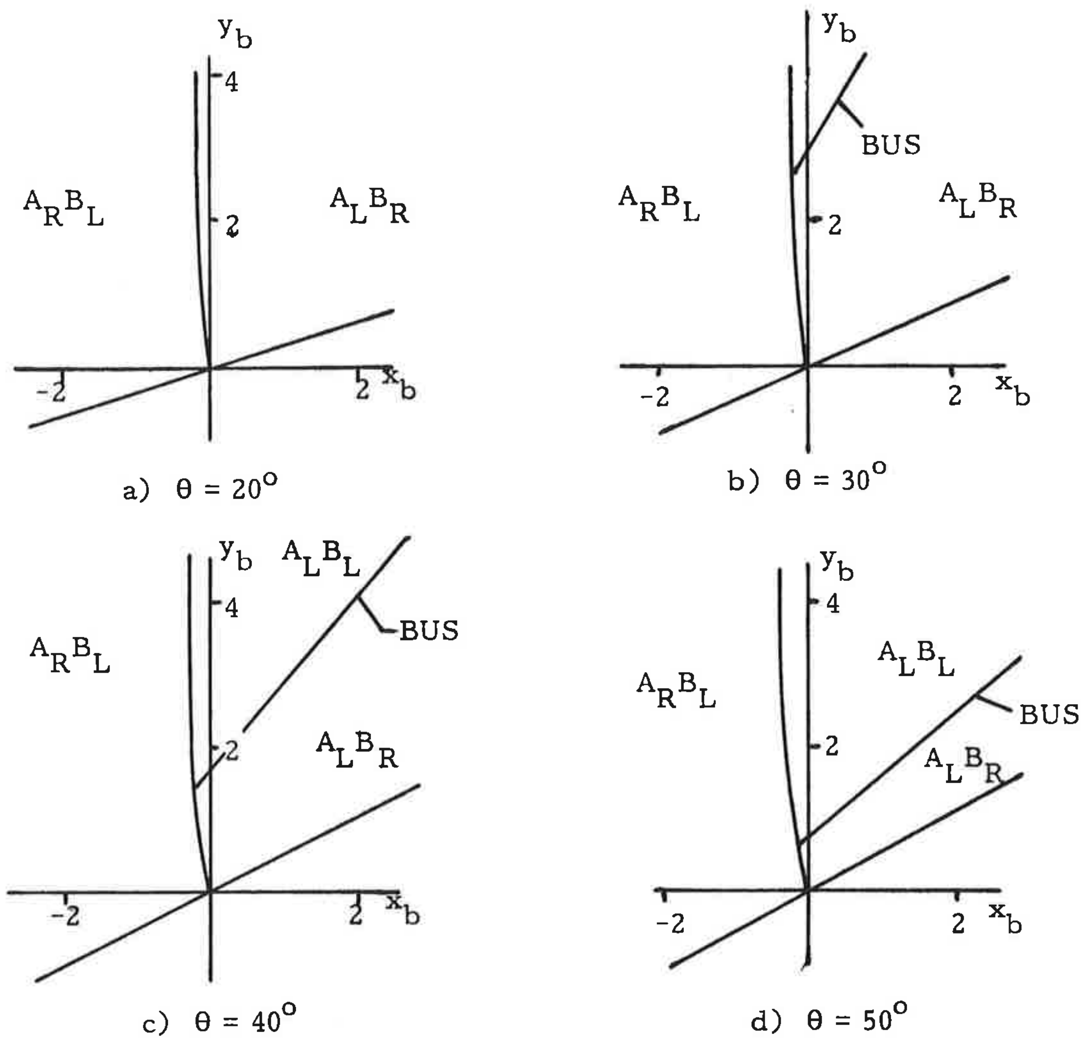

Figure 4.5 The Movement of B's Universal Surface as a Function of θ for $\gamma = .5$, $\omega = 2$.

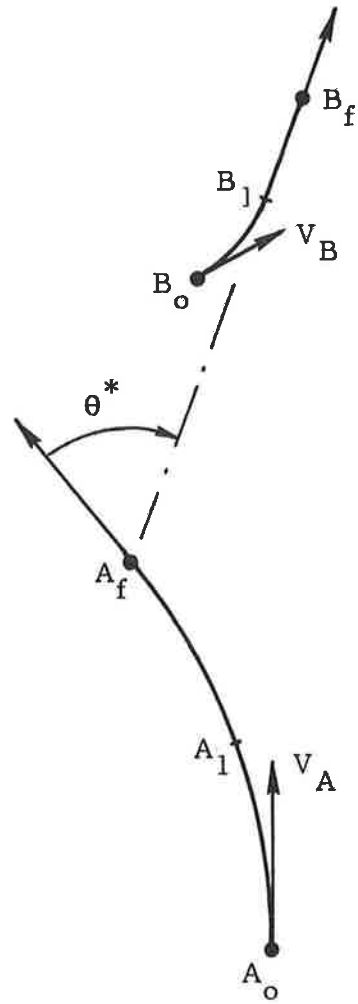

A_o, B_o = initial positions

A_1, B_1 = positions where B begins to fly straight

A_f, B_f = positions at minimum range

$\theta^* = \cos^{-1} \gamma = 60^o$

Figure 4.6 Two Stage Maneuver in Real (Inertial) Space

to flying straight. This is held until the point of minimum range. It is seen that at the time of minimum range, the aircraft B is headed directly away from aircraft A.

Generally, it is found that two-stage maneuvers can make an appreciable difference in the miss distance, compared to that which results from using one-stage maneuvers. This effect is most pronounced when the slower aircraft has a relatively large turn rate ($\omega >> 1$), for in this case, rapid heading changes are followed by a straight path for the remaining time until the range is a minimum.

The effect of "cooperation" on the optimal maneuver regions and the resulting miss distances can also be examined using these charts. Here, cooperation is used to mean that both aircraft actively maneuver to avoid the collision. Degree of cooperation is indicated by the value assigned to the turn-rate ratio, ω. That is, when $\omega = 0$, the slower aircraft does not turn, and when $\omega = \infty$, the faster aircraft does not turn. If the speed ratio is fixed (e.g., $\gamma = 1$) and the initial relative heading is fixed (e.g., $\theta = 90^{\circ}$), the variations in the boundaries of each aircraft's maneuver regions can be found as functions of ω. Such variations in A's boundaries are shown in Fig. 4.7, when both aircraft have the same airspeed. Also shown are the miss distance loci for $r_f = 1$ when

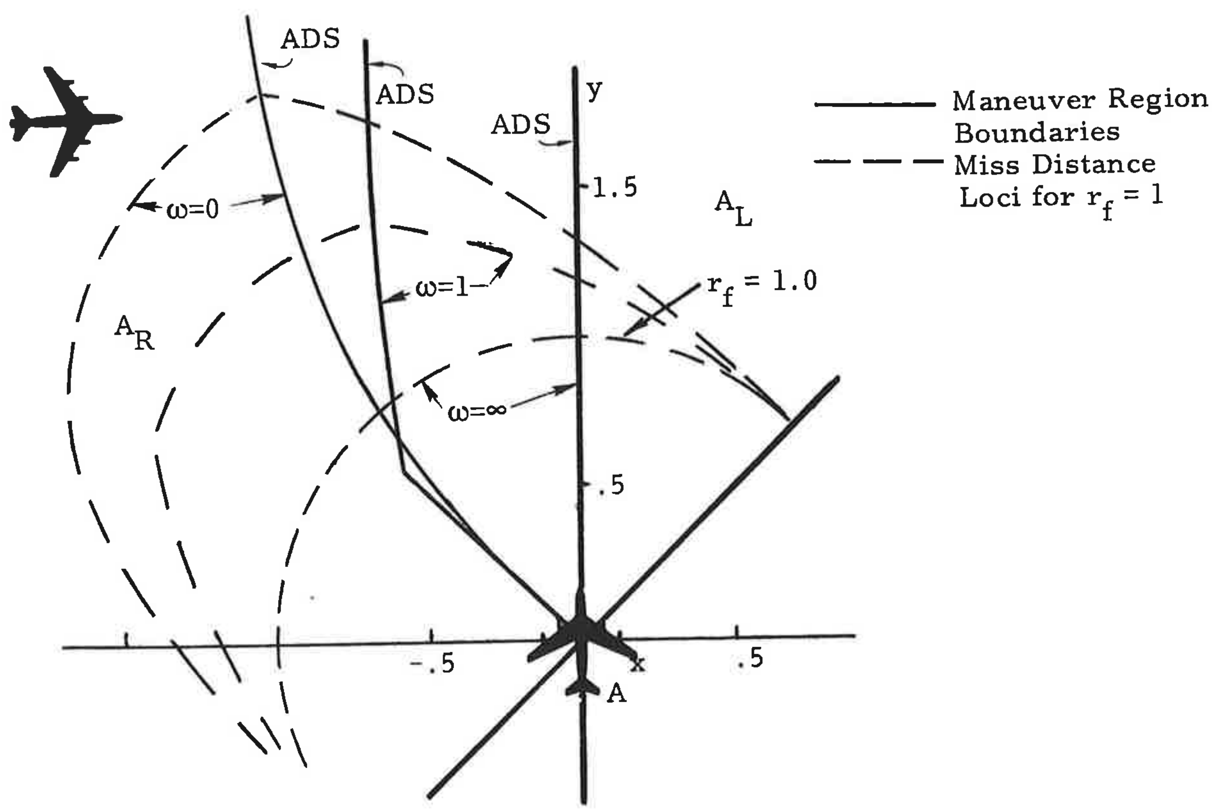

Figure 4.7 Effect of Cooperation (Turn Rate Ratio) on Aircraft A's Maneuver Region Boundaries and the Resulting Miss Distance for $\theta = 90^{\circ}$

$\omega = 0$, 1, and ∞. The unit of distance in this figure is A's turn radius in all cases. It is seen that the miss distance achievable from a given initial condition increases with ω. This is exactly as expected, since this ratio is a measure of the total available control level of the system.

Another physical interpretation which can be gained form Fig. 4.7 is the amount of "lead" which is necessary to maximize the miss-distance. That is, as shown in Fig. 4.7, aircraft A should turn left toward aircraft B's present position, when B is located between the y-axis and the ADS dispersal line. The region containing such initial conditions is largest when $\omega = 0$. This means that the noncooperative case (B does not maneuver) requires the largest amount of "lead compensation". At the other extreme, when ω is very large ($\omega \to \infty$, and B maneuvers instantly), A's dispersal line approaches the y-axis. The optimal maneuver for A when B is anywhere to the left of this line is to turn right, away from B's initial position. Intermediate levels of available control cause the location of A's dispersal line to fall between these two extreme cases.

It is interesting to examine the appearance of the maneuver regions in an axis system attached to the slower aircraft B. Such a diagram contains no more information than is available in the figures which have already been discussed, but the change in axis system does introduce some new features. In Fig. 4.8, the maneuver regions are shown for the parameter values $\gamma = .5$, $\omega = 2$, which were presented for A at the origin in Fig. 4.4. In the present case, however, the relative position and heading are measured with respect to the slower aircraft, in the (x_b, y_b, θ_b) coordinates.

Notice in Fig. 4.8 that, when $90^\circ < |\theta| < 180^\circ$ (near head-on encounters), the qualitative form of the maneuver regions is quite similar to those of Fig. 4.4. But, when the initial velocities are nearly aligned, and $|\theta|$ is small, the maneuver regions in B's axis system are very different from those in A's axis system. Figure 4.8 thus shows the importance of knowing the relative speeds, particularly for near parallel encounters. That is, when $|\theta| \cong 0$, the faster aircraft (A) need not maneuver if the second aircraft is located behind A, since $\dot{r} > 0$ in all such cases. But, when $|\theta|$ is small, the slower aircraft must obviously

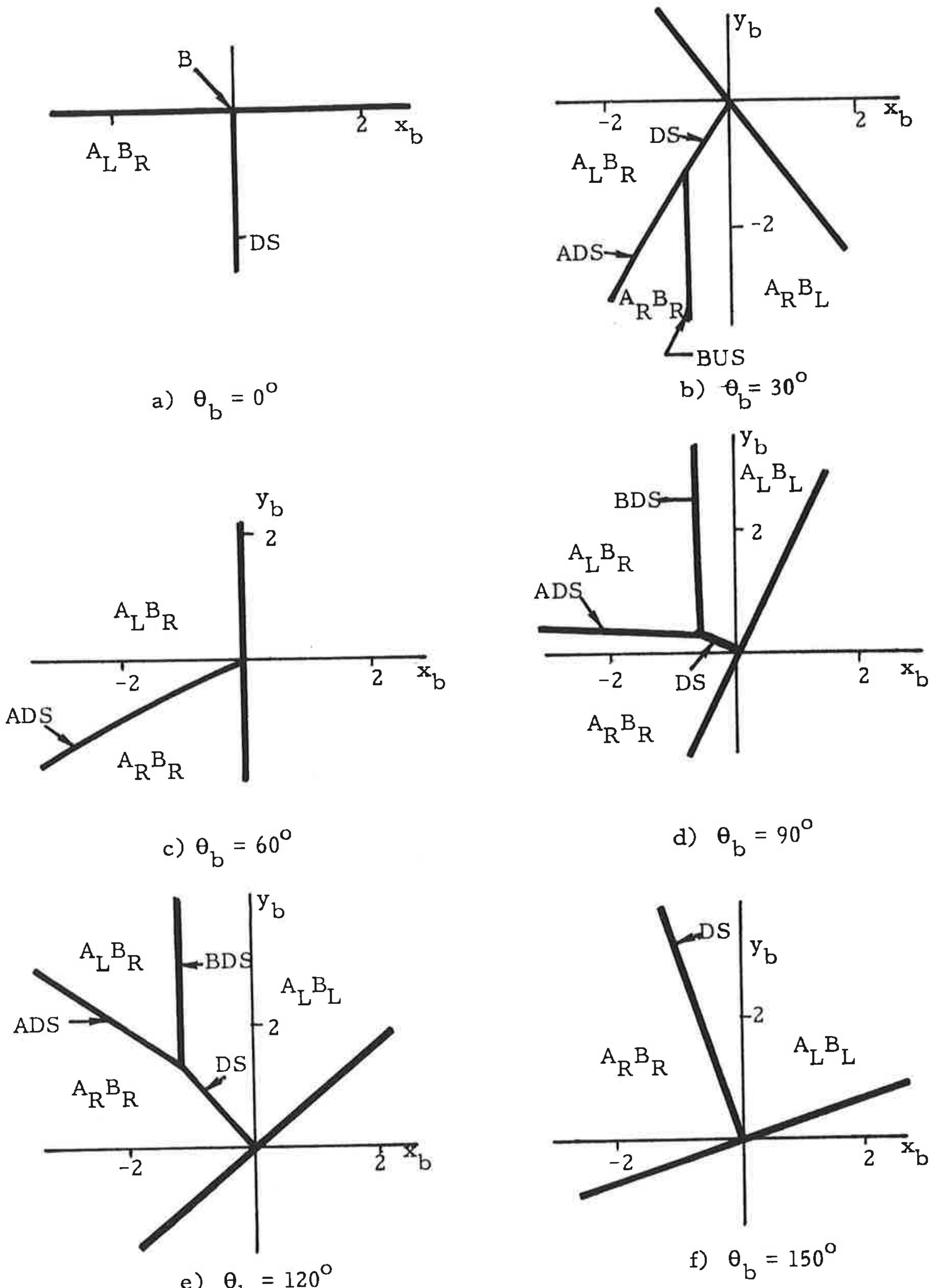

Figure 4.8 Maneuver Regions as Seen by Slower Aircraft (B) for $\gamma = .5$, $\omega = 2.0$

guard against being overtaken from the rear by a faster aircraft. This figure thus illustrates and emphasizes the need for full angular coverage in the region surrounding each aircraft.

According to published statistical data,[13] a very large proportion of midair collisions in the interval 1964-1968 occurred for crossing angles between -30° and 30°. A partial explanation for this phenomenon may be that the faster aircraft is out of sight of the slower, who is, therefore, unaware of being overtaken. Nevertheless, it appears plausible to conjecture that since the evasive turn directions depend strongly on the speeds of both aircraft, uncertainty as to these speeds could explain the large number of collisions which occur for near-parallel encounters.

The maneuver charts of Fig. 4.4 and Appendix C have been prepared for relative headings in the range 0° to 180°. That is, the slower aircraft (B) is generally to the left of the faster aircraft (A), with their paths converging. For negative headings, when θ is between 0° and -180°, the geometry and maneuvers would be reversed. Straightforward symmetry considerations then show that these maneuver charts would be the "mirror image" of the charts given in this report for the same positive values of heading. That is, for negative headings, the lines in the maneuver chart would be reflected about the y-axis, and "right" and "left" turns are interchanged for both aircraft.

The maneuver charts represent a summary, in compact normalized form, of the turn strategies that should be used to maximize miss distance. They are valid for any aircraft with arbitrary speed and turn rate ratios and having arbitrary relative initial conditions. With bank angle limits specified, these charts can be used to determine what miss distance is available from any starting conditions. Likewise, these charts can be used to determine when two conflicting aircraft should begin to maneuver to achieve a given miss distance.

4.4 AIRSPACE USAGE PROBLEMS

Maximizing the miss-distance has been described earlier as a fundamental purpose of a collision avoidance system. When the initial range is extremely small, the miss-distance obviously far outweighs any other performance consideration. But, when the initial range is sufficiently large (i.e., when the CAS is operating correctly so that small initial ranges do not occur), other performance criteria are more important.

Interference with the nominal path of a third aircraft, by either of two aircraft performing evasive maneuvers, must be minimized to prevent the so-called "domino" effect from becoming significant. This means that other considerations must be introduced when determining the appropriate collision avoidance system's commanded maneuvers. As described in Section 4.1, airspace usage is an important characteristic, and it is conveniently measured in the present context by the maximum distance off-track of the maneuvering aircraft. To a smaller extent, the initial range at which a maneuver begins is also a measure of airspace usage, but this quantity is more appropriate in specifying the range requirements of sensors, which is discussed later.

Certain characteristics of the maneuvers are more easily understood by examining the real-space trajectories of the aircraft. Comparisons with the relative-space paths also help to clarify these characteristics. In Fig. 4.9 is shown a representative "crossing" encounter between two aircraft, for which the initial heading is greater than 90^o. The aircraft both turn right, and the point of closest approach occurs as shown in the figure, where the quantities r_o, r_f, D_A and D_B are defined. The relative motion is also shown as it appears to the pilot of aircraft A. It is assumed that the same turn rates are used to return to track as to avoid the collision. Thus, the total deviations off track (D_A, D_B) of both aircraft are twice the amounts which occurs at the point of minimum range for same turn maneuvers.

A similar pair of illustrations can be prepared for a typical "overtaking" encounter, as shown in Fig. 4.10. Here, the turns can be regulated so that the range is kept constant for a short time, while the faster aircraft moves ahead

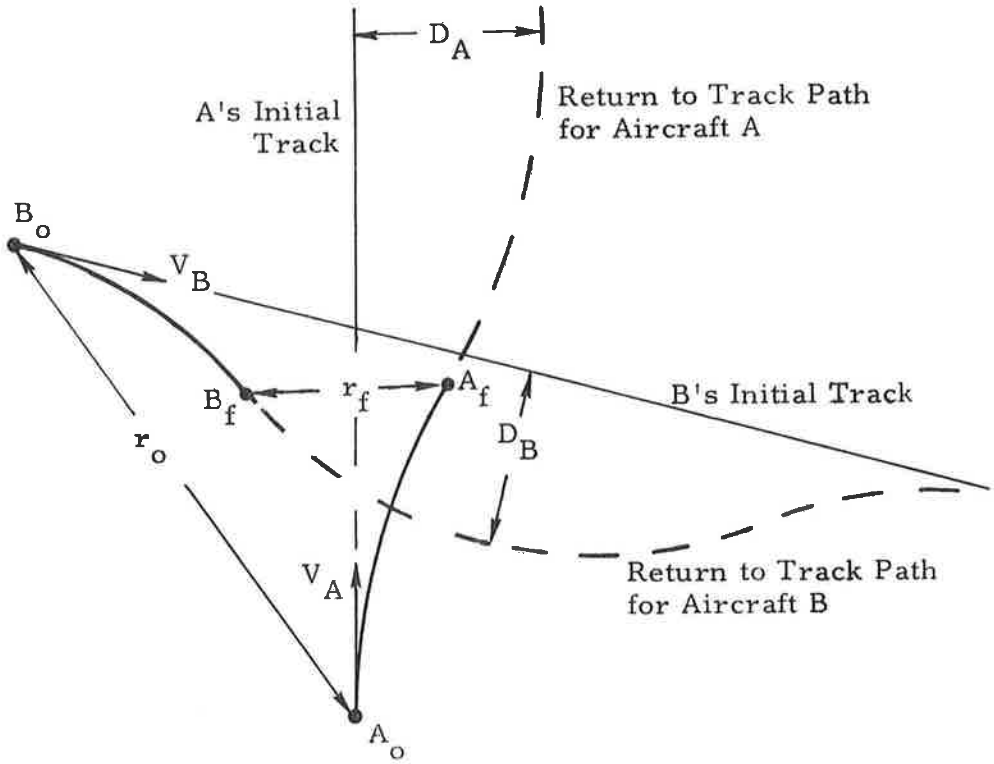

a) Real (Inertial) Space Motion of Typical Maneuvers Illustrating Initial Range r_o and Deviation Off Track D_A and D_B

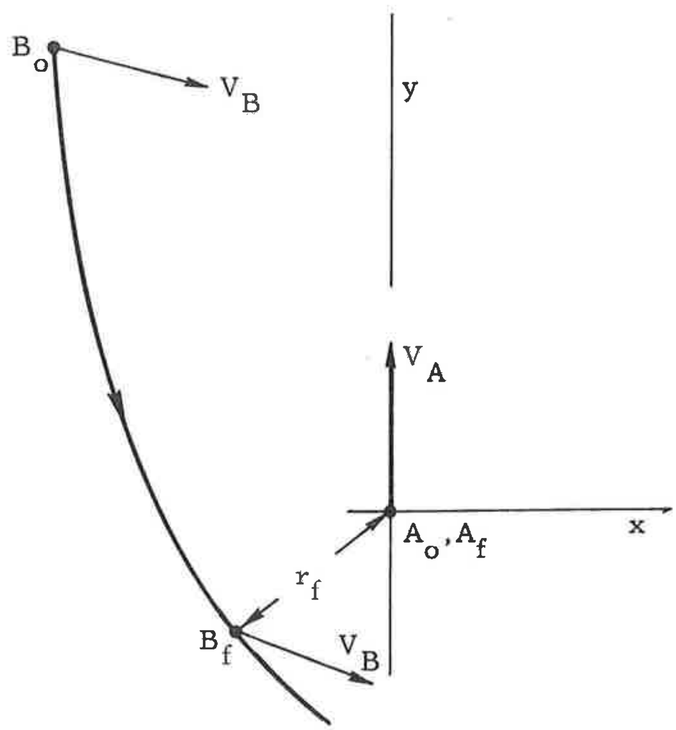

b) Relative Space Motion for the Same Typical Maneuvers

Figure 4.9 Geometry for "Crossing" Maneuvers

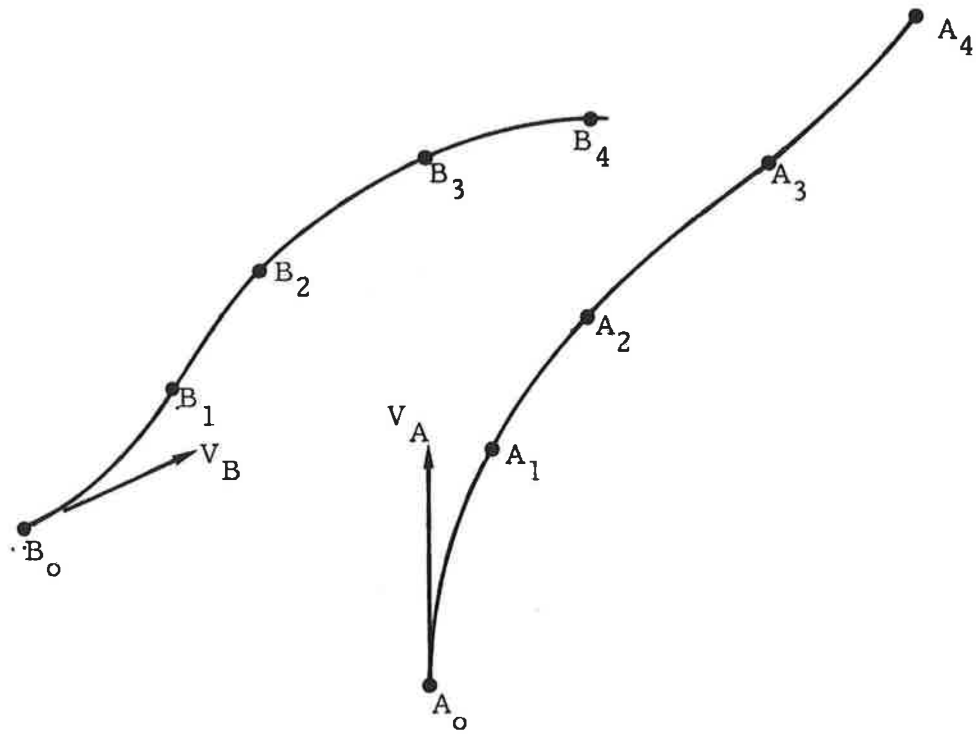

a) Real Space Motion

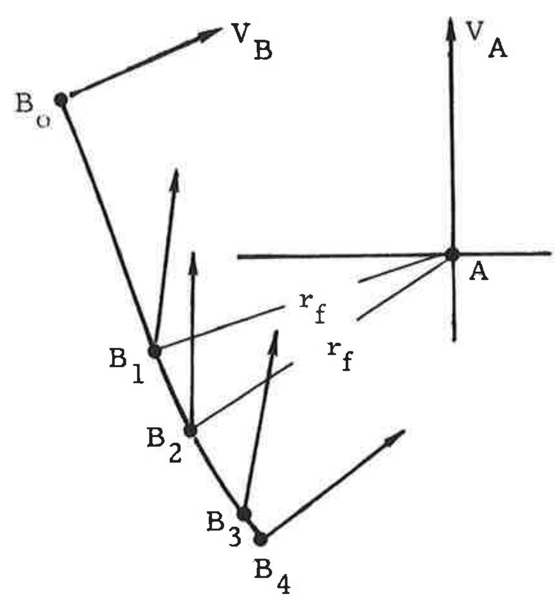

b) Relative Space Motion for the Same Maneuvers

Figure 4.10 Geometry for "Overtaking" Maneuvers of the slower. Subsequently, the range increases as the tracks cross, and the ensuing turns are related only to the return-to-track portion of the maneuver.

The problem of returning the aircraft to their original tracks is also encountered when two aircraft of nearly equal speeds turn away from each other (using opposite turns). After minimum range is reached, the aircraft cannot reverse their turn directions without causing the range to decrease again. Therefore, assuming altitude changes cannot be implemented, either a small speed difference must be generated and used to separate the aircraft longitudinally, or one of the aircraft must turn through 360°, before returning to its original track, as shown in Fig. 4.11. In either case, at least one of the aircraft deviates considerably from its nominal track.

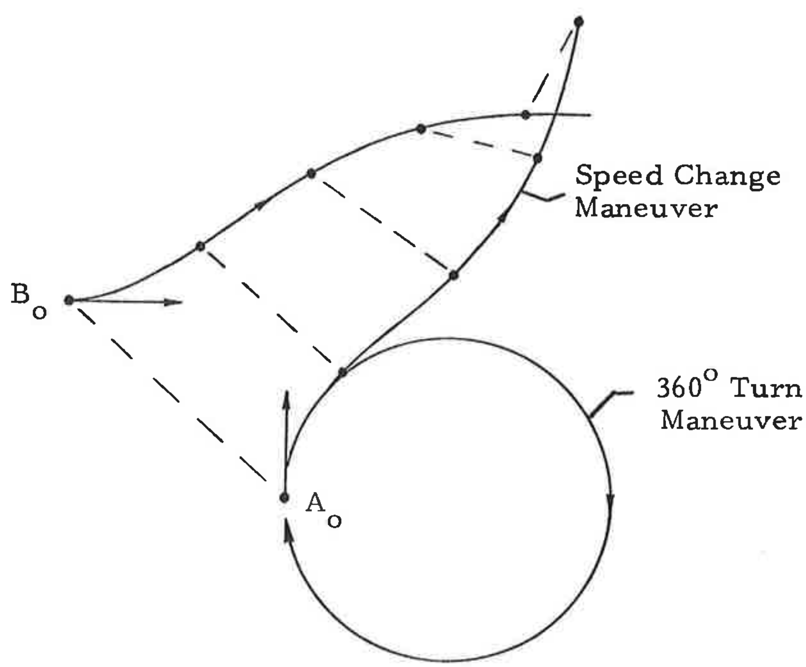

Figure 4.11 Possible Methods of Returning to Track When Initial Turns in Opposite Directions are Required

The general opposite-turn encounter can be further complicated by including a straight-path portion (i.e., a universal surface) in the evasive maneuver of the slower vehicle. This makes the computation and presentation of the maneuvers both difficult and time-consuming. Implementation of such multistage maneuvers is correspondingly difficult, because of the need to return each aircraft to its nominal track without violating the minimum separation requirement. The time-varying turn rates of both aircraft during the interval when the range is constant can be found only when additional constraints or criteria are imposed on the problem. Because of these features, the study of opposite-turn maneuvers has been restricted to the determination of the motion only up to the time of minimum range.

Another aspect of the airspace usage problem is related to the influence of the turn-rates on the initial range. It is found that a given miss distance can be achieved for same-turn maneuvers, by turning at a low rate for a long time, or by turning more sharply for a shorter time. In Fig. 4.12 are shown in inertial space the paths of aircraft A and B which result from starting the maneuvers at two points; they yield the same miss distance. Both aircraft are assumed to turn to the right with identical rates. The initial range and distances off the nominal tracks vary inversely with the magnitude of the turn rates.

4.5 TRADEOFF STUDIES BETWEEN MANEUVER PERFORMANCE CRITERIA

The principal criteria governing the maneuvers in the horizontal collision avoidance problem have been defined and discussed in Section 4.1. An objective study must allow for varying points of view with respect to the importance of each of these criteria. For example, in some circumstances, the distance off-track may be considered to be more important than the miss distance, provided that sufficient safety is guaranteed. Because such components of the performance can be compared only subjectively, it is necessary to see just how these parameters depend on each other.

The quantities of primary interest in such a tradeoff study are listed in Table 4.1. These variables are interrelated in a highly nonlinear way, and these quantities can each take values over a wide range. Consequently, a great deal

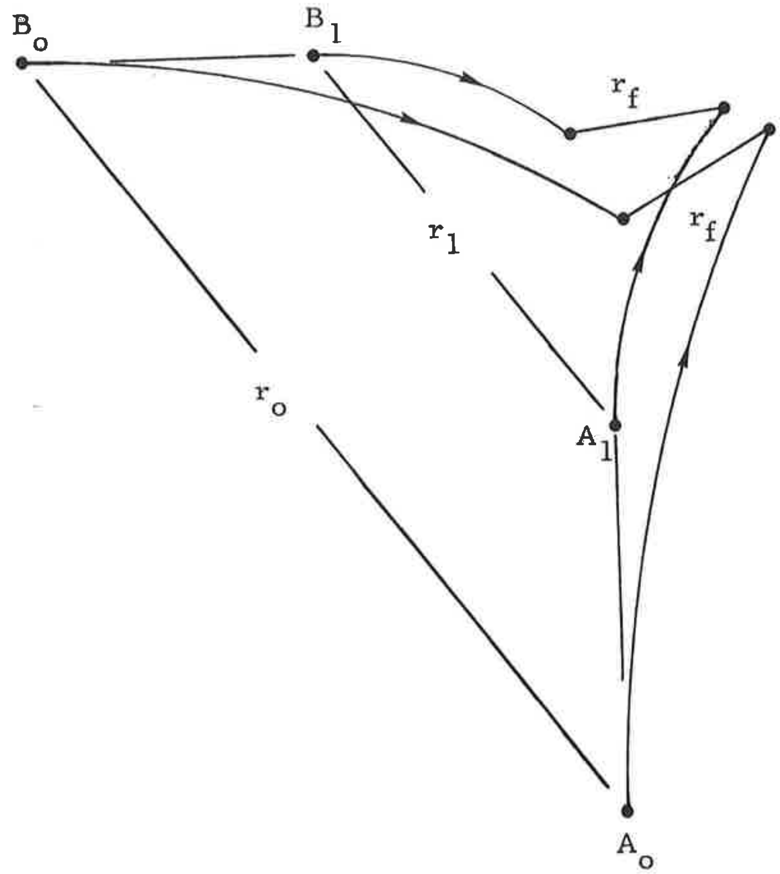

Figure 4.12 Turn Rate Variation With Initial Range Required to Produce a Fixed Miss Distance (Seen in Real Space)

TABLE 4.1

Parameters Affecting Maneuvers for Horizontal Collision Avoidance

Aircraft Speeds, V_A and V_B
Available Turn Rates, ω_A and ω_B
Relative Final Position and Heading, (x_f, y_f, θ_f)
Relative Initial Position and Heading, (x_o, y_o, θ_o)
Initial Range at Which Maneuvers Begin, r_o
Distances Off Nominal Tracks, D_A and D_B

of numerical comparison is possible, and the interpretation of the results is difficult. General trends of a useful nature, however, can be established by the following specializations:

1. Restrict initial conditions to combinations of position and heading which would lead to collision if neither aircraft turned.

2. Consider only "worst-case" encounters, for which at least one aircraft has the maximum allowable terminal speed of 250 kts = 425 ft/sec.[75]

3. Assume the bank angles of the aircraft A and B are equal ($\varphi_A = \varphi_B$) and the resulting turn rate is $\omega_i = (g/V_i) \tan \varphi_i$ (i = A or B).

4. Restrict attention to turns in the same direction, or to opposite turn maneuvers only up to the time of minimum range.

The interaction between various performance criteria is shown in the tradeoff curves of Figs. 4.13 and 4.14. These have been prepared according to the specializations given above, for a range of relative heading angles, θ.

When the aircraft have the same maximum airspeed (250 kts), and turn in the same sense, it is shown in Fig. 4.13 that decreasing the distance off-track (D_A) is more easily accomplished by decreasing the miss-distance (r_f) than by increasing the bank angle (φ). On the other hand, the range at which the maneuver begins (r_o) can be considerably reduced by increasing the bank angle for a fixed miss-distance. This figure also shows that the distance off-track is less for the head-on case ($\theta = 180^o$) than for other relative heading angles. However, initial range required is greater for $\theta = 180^o$. Furthermore, it is seen that the initial range r_o corresponding to the 2000 ft. miss-distance can be kept below 10,000 ft. only by implementing sharp turns at nearly 30^o bank angles.

Both same-turn (right-right) and opposite-turn (right-left) tradeoff curves are illustrated in Fig. 4.14 for aircraft having different speeds. The

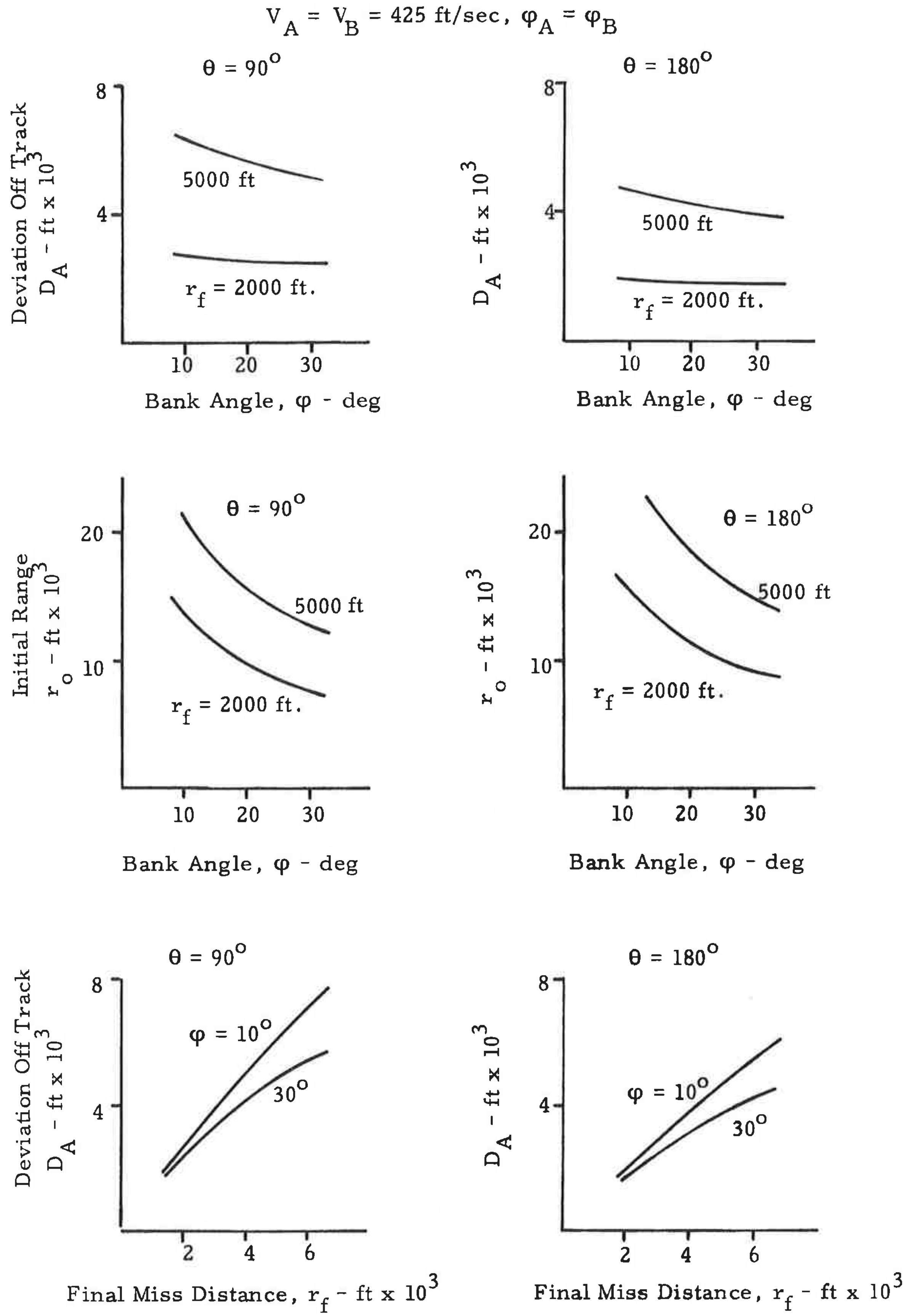

Figure 4.13 Tradeoff Curves Showing Relationship Between Miss Distance (r_f), Deviation Off Track (D_A), Initial Range (r_o), and Bank Angle (φ).

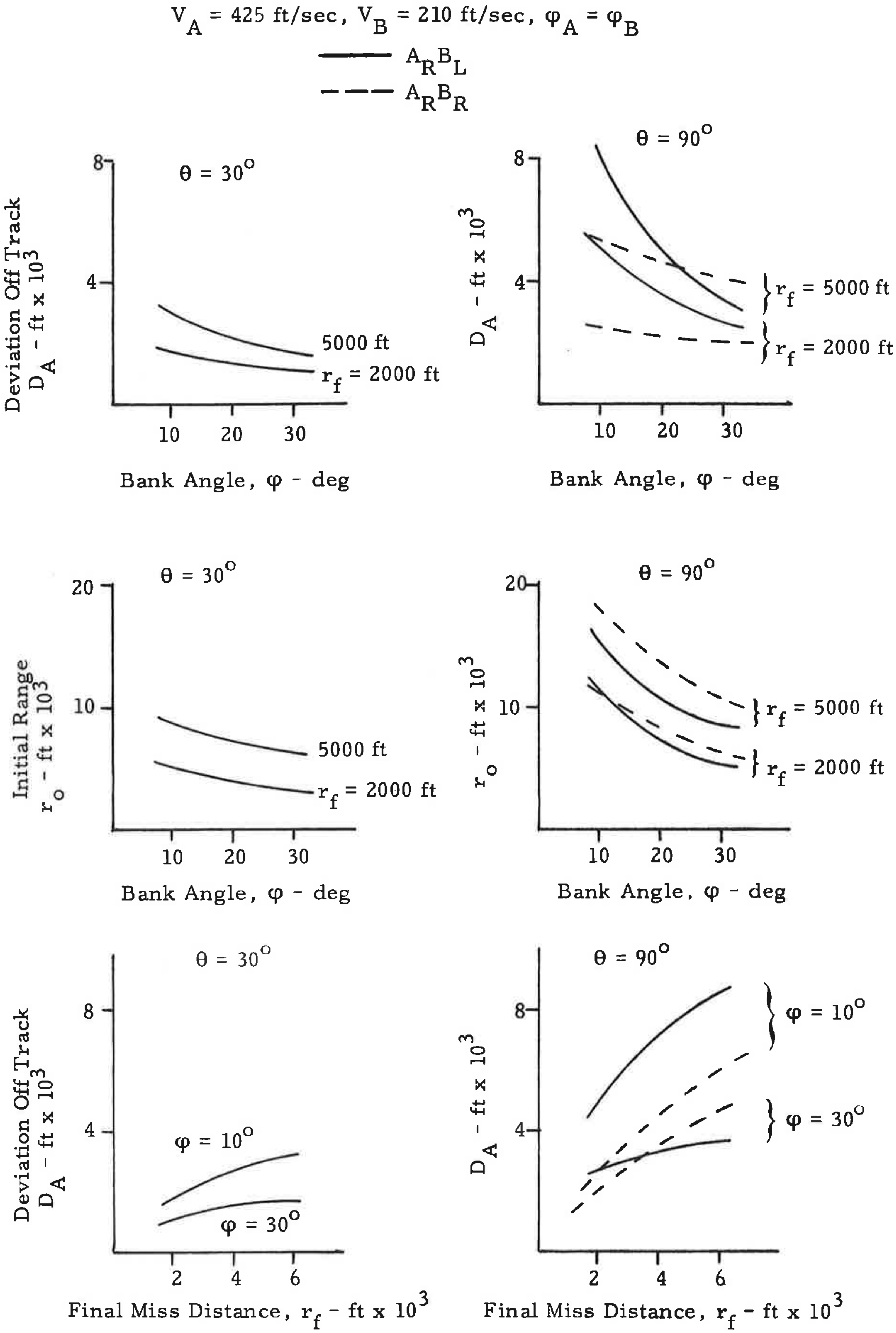

Figure 4.14 Tradeoff Curves for Unequal Airspeeds and Both Same and Opposite Turn Directions

speeds assumed here are 250 kts and 125 kts, and the relative heading angles have been taken to be 30° and 90°, for illustration. Suppose that it is desirable to achieve a 2000 ft. miss-distance with bank angles of 20°. From the $\theta = 90^{\circ}$ curves, it can be seen that the initial separation required when the maneuver begins is greater for the same turn maneuvers than for opposite turns (increased from 7000 ft. to 8500 ft.). However, the deviation off-track is considerably decreased (reduced from 3600 ft. to 2200 ft.) by turning in the same direction. By comparing the $\theta = 90^{\circ}$ curves in Figs. 4.13 and 4.14, one can see that as V_B is reduced by one-half, the required initial range is decreased by about 2000 ft. and the deviation off-track is reduced by about 500 ft.

These tradeoff curves, together with the maneuver charts, summarize the solution to the problem of determining what maneuvers are to be used for horizontal collision avoidance. The tradeoff data allow the selection of maneuver parameters which obtain the best combination of airspace usage (deviation off track), alarm volume size and alarm rate (initial range), passenger comfort (bank angle limit), and airspace safety (miss distance). The maneuver charts and tradeoff data can be used with sensor accuracy and error analysis data (Chapter VII) to provide avionics standards for collision avoidance software and hardware. Comparison of horizontal collision avoidance maneuvers to pure vertical maneuvers and speed control is made in Chapter V, with respect to initial range, deviation off track, and flight path time loss.

4.6 OPTIMUM HORIZONTAL/VERTICAL MANEUVERS

The solutions to the problem of achieving maximum miss distance in the horizontal plane are presented in Sections 4.2 and 4.3 and Appendices B and C. The results can be extended to the combined horizontal/vertical maneuver case in a rather simple way, which is described in this section.

For the combined maneuver problem, the following additional assumptions are made:

1. The vertical speeds of the individual aircraft are small, compared to the horizontal speeds, and are bounded between known limits.

Maximum rate of climb varies with altitude and airspeed, and maximum rate of dive is assumed to be limited by this same value.

2. Any desired climb rate within these specified limits can be immediately obtained.

3. The horizontal component of the velocity remains constant during a combined maneuver.

The first assumption coupled with thrust control is necessary to justify the third assumption. The second assumption is essentially valid for small general aviation aircraft as is shown in Section 3.1. However, the climb-rate transient is longer for large commercial aircraft, and its validity is more difficult to establish. However, studies of such aircraft, as summarized in Chapter III, indicate it to be a reasonable assumption for the time intervals of interest in the collision avoidance problem.

Implicit in these assumptions are the mechanization and operational constraints that no last-resort severe maneuvers are allowed, that the avoidance maneuver strategies be simple and open-loop, and that sensor and instrumentation requirements (and hence, cost) be minimized.

Given the above assumptions and constraints, an appropriate model for the combined horizontal/vertical maneuver problem consists of Eqs. (3.1). The equation governing relative vertical motion is

$$\dot{z} = -\delta_A + \delta_B \tag{4.1}$$

Here, z denotes the altitude difference between the two aircraft and δ_A and δ_B are the respective climb rates which are assumed to be constrained by

$$|\delta_i| \leq \delta_{i_{max}} \quad , \quad i = A,B \tag{4.2}$$

Note that the dynamics for the vertical motion are thus decoupled from the dynamics for the horizontal motion.

As is shown in Appendix B, the choice of vertical maneuver is determined by the initial altitude difference between the aircraft. If aircraft B is above aircraft A at the initiation of maneuvers, then B climbs at maximum rate and A dives at maximum rate. Conversely, if A is above B, then A climbs and B dives. If they are at the same altitude, the choice is not unique and a random choice of maneuvers is indicated. Of course, this strategy satisfies one's intuitive feeling for what the vertical maneuvers should be.

In summary, the combined maneuver strategy is to determine turns in the same manner as the horizontal only case and determine the vertical maneuvers based on the relative altitudes at the beginning of the maneuvers. Computer simulations of encounters of aircraft representing two performance classes were performed to confirm the validity of the above analysis. General aviation aircraft were represented by the Cessna 172 and commercial jets were represented by the Boeing 727. The simulation program is described in Appendix A, and this program has been used to model many typical encounters.

The accuracy of the dynamic approximations which have been used depends partly on the relative time-durations of the turn-rate and climb-rate transients, compared to the time spent in the steady turn or climb conditions. Under conditions of maximum maneuverability, for example, and for certain relative geometries, the entire maneuver may require only a few seconds. That is, maneuvers can still be in the transient phase at the time of minimum range, and maneuvers of this type are very poorly represented by the dynamic model that has been described here. However, these maneuvers are not appropriate for normal collision avoidance system operation.

It has also been implicitly assumed that the time duration of the maneuver is sufficiently large that the horizontal displacement of each aircraft considerably exceeds the vertical displacement. This assumption is necessary to the specification of horizontal strategies, which are independent of the relative vertical motion. There is actually a slight dependence, however. This condition of larger horizontal displacement can usually be met for maneuver times greater than 10 sec., if the bank angle exceeds 15^{o} and the rate of climb is under 2000 fpm.

A representative two-aircraft encounter can be used to illustrate the accuracy obtained by use of the fourth order dynamic model of the relative motion used in this study. Aircraft relative position, speeds, and maneuver severities are chosen such that the conditions described above are not particularly well satisfied. That is, bank angles in the present example are only 10^{o}, and the nominal time to collision is only 17.5 sec. The aircraft involved in the encounter are the Boeing 727 (aircraft A) and the Cessna 172 (aircraft B), which have speeds of 210 kts and 105 kts, respectively (360 fps and 180 fps, and, therefore, $\gamma = .5$). The aircraft are initially at 5000 ft. altitude, and the nominal flight paths cross at 90^{o}, with the 172 initially ahead and to the left of the 727. The steady turn rates corresponding to the 10^{o} bank angle are found to be $\omega_A = .90^{o}/\text{sec}$ and $\omega_B = 1.80^{o}/\text{sec}$, the ratio being $\omega = 2.0$.

When the turn-maneuvers begin, the 172 simultaneously implements its maximum steady climb rate of approximately 800 fpm [72], while the 727 reduces throttle and soon achieves a steady rate of descent of about 1300 fpm. [73]

The maneuver chart of Fig. 4.4 can be used with the given relative geometry to deduce the turn maneuvers. In the present case, the optimum horizontal maneuvers associated with the given initial conditions are right turns for both aircraft. At the same time, the elevator and thrust are controlled to give the steady climb and dive maneuvers described above. The equations of motion presented in Appendix A are then integrated numerically for both aircraft, using the known controls, with the results shown in Figure 4.15. Notice that the horizontal turns closely resemble circular arcs, while the vertical maneuvers are practically straight lines, following the brief initial transients. At the time of minimum range ($t_f = 15.2$ sec), the speeds have changed to 406 fps and 168 fps, respectively. The horizontal and vertical miss distance components are $r_h = 1175$ ft. and $z_f = 544$ ft.; the total miss is then 1295 ft.

The approximate motion of the aircraft is found by replacing the actual turn-rate and climb-rate variations of both aircraft with delayed step functions. These two quantities represent the essential features of the horizontal and vertical maneuvers, respectively, and the "steady-state" values reached are sufficiently accurate measures of the maneuver severity. For maneuvers of

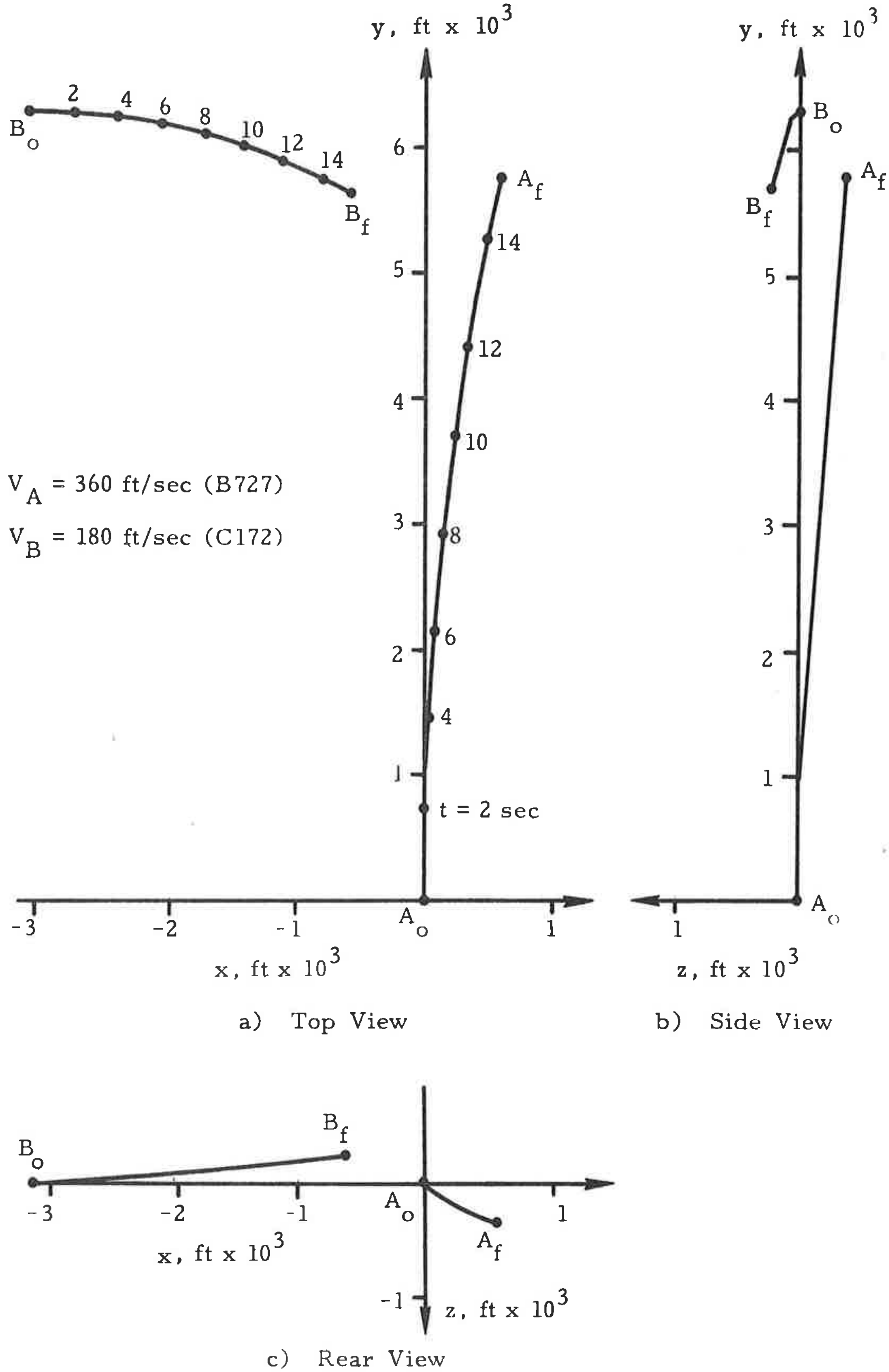

Figure 4.15 Example Collision Avoidance Trajectories for a Boeing 727 (Aircraft A) and a Cessna 172 (Aircraft B)

this level of severity, the transients of both aircraft can be adequately modeled by a time-delay of 2 sec., as suggested by Figs. 3.1 and 3.2. That is, in the approximation, both aircraft continue straight flight for this time interval. At the resulting relative position, the horizontal turn maneuvers are found from Fig. 4.4 to be right turns for both aircraft. The maneuver chart can also be used to give the approximate terminal miss in the horizontal plane, equal to r_h = 1100 ft., and this occurs at the estimated time of t_f = 14.1 sec. In this same time interval (which includes the 2 sec delay cited above) the vertical separation is estimated to be

$$z_f = (\delta_a + \delta_b)(t_f - 2) = 423 \text{ ft.}$$

Thus, the total miss as estimated by the simple dynamic model of the relative motion is r_f = 1180 ft. A numerical comparison of the exact and approximate results obtained in this example is shown in Table 4.2.

TABLE 4.2

Numerical Example, Boeing 727 and Cessna 172 at $\theta_o = 90^o$

PARAMETER	EXACT	APPROXIMATE
Terminal time, sec.	15.2	14.1
Horizontal miss, ft.	1175	1100
Vertical miss, ft.	544	423
Total miss, ft.	1295	1180
Final speeds, ft/sec.	406, 168	360, 180

The errors found in the present extreme example are seen to be well within acceptable limits. It appears reasonable to conclude that the approximate dynamic model of the turn-climb maneuver gives excellent results providing only that an appropriate delay time be included in the turn rate and climb rate responses. It is emphasized again that the quantity of interest in the collision avoidance problem is the relative position of the aircraft, and that the kinematic integration of the approximate acceleration has the effect of "smoothing" these errors. The result is that fairly large approximation errors in acceleration produce relatively small approximation errors in position.

The example also illustrates a general characteristics of the horizontal and vertical maneuvers, which has been pointed out earlier. That is, the vertical maneuver approaches straight line motion, while the horizontal maneuver approaches circular arc motion. Therefore, for very short maneuver times (of the order of 5 sec), the aircraft's vertical displacement can exceed its horizontal displacement. Over larger time intervals, however, the horizontal displacement is much greater. These conclusions hold for maximum available climb rates (e.g., 2000 fpm) and turn rates (e.g., corresponding to a 30° bank angle) and are practically independent of the airplane or its flight condition. Furthermore, the example indicates that the contributions to total miss distance by the vertical component is minor for a 15 sec maneuver. Thus, adding vertical capability to a horizontal CAS must be questioned from the point of view that it adds increased miss distance.

4.7 SUMMARY

This chapter has presented the systematic approach which was taken to determine the optimal horizontal collision avoidance maneuvers. These maneuvers are unique functions of the aircraft speed ratio; the turn rate ratio; the initial range, relative bearing, and relative heading; and the bank angle limits. A series of optimal maneuver charts was generated for various sets of these parameters; these charts present the maneuver strategy (turn directions) which yields maximum miss distance.

The maneuver charts were extended by way of a tradeoff analysis to show the interrelationships between initial range to begin the maneuver, bank angle limit, miss distance, and resulting deviation off track. This tradeoff data can be used to balance airspace usage with desired safety as governed by miss distance. The maneuver charts and tradeoff curves together represent the solution to the question of how aircraft should maneuver in the horizontal plane in order to avoid a collision.

These results represent the ideal solution to horizontal collision avoidance maneuvers, and they have not been obtained elsewhere before. The results represent the strategy which should be used for best airspace usage and maximum safety. Any other maneuver logic that is used would represent a deterioration in the degree of safety provided. Therefore, these optimization results represent a standard by which any other suboptimal logic can be judged. Furthermore, the results of this chapter can be used to derive maneuver logic to compliment any given measurement system. This includes both airborne and ground-based (IPC) collision avoidance systems.

V. COMPARISON OF DIFFERENT TYPES OF COLLISION AVOIDANCE MANEUVERS

The primary purpose of this chapter is to compare different types of aircraft maneuvers with respect to their attributes for midair collision avoidance. The maneuvers referred to are those which result from horizontal (lateral), vertical, and longitudinal acceleration (speed control) of one or both aircraft from their steady flight paths. If only one aircraft acts to change its flight path, the maneuver is termed "uncooperative". Likewise, if both aircraft maneuver, it is referred to as "cooperative". The results of this chapter can be used quantitatively to make a judgment as to which type of maneuver offers the most promise for future implementation.

A secondary purpose of this chapter is to examine in detail the conclusions of prior analytical studies regarding choice of collision avoidance maneuvers. This examination was felt to be necessary because this previous work is frequently referenced and often misinterpreted. The previous work regarding horizontal maneuvers is first shown to be a highly specialized subset of results of Chapter IV. The misleading or incorrect conclusions which appear in the literature are then noted and corrected.

5.1 COLLISION AVOIDANCE MANEUVER ALTERNATIVES

As cited above, there are three types of collision avoidance maneuvers, resulting from either lateral, vertical, or longitudinal acceleration/deceleration of the aircraft. Each of these types of maneuvers is discussed further in this section. Past research and development work on maneuver specification has been principally directed to the subject of vertical maneuvers. This is because the appropriate strategy for these maneuvers is the easiest to comprehend and mechanize. This strategy is referred to in Section 4.6 and explained in more detail here. Vertical maneuvers result from acceleration of the aircraft until a steady climb or dive limit is reached. The change in the velocity vector can be thought of as an abrupt change in flight path angle and rate of climb.

For speed control, the aircraft accelerates or decelerates for some period of time, until a new steady speed is reached. The aircraft cruises at the new speed until the point of closest approach is passed. Since each aircraft changes only the magnitude of its velocity, the aircraft remain on their nominal tracks, and thus the traffic interference problem is minimized.

5.1.1 Previous Horizontal Maneuver Analysis Nomenclature and Specification

In his original work, Morrel[27] referred to two types of horizontal maneuvers--"turn-to-parallel course" and "turn-to-cross course". These have different meanings depending upon whether one or both aircraft are maneuvering. Because Morrel's study of these maneuvers is referred to later in this chapter, each of these terms is now defined.

For the uncooperative case (only one aircraft maneuver), the turn-to-parallel maneuver is depicted in Fig. 5.1. Here, the maneuvering aircraft A turns so that its velocity vector would be either parallel or anti-parallel to the velocity of the non-maneuvering aircraft B. This parallelism would be achieved if aircraft A is turned through an arc of less than 90^{o}. As can be determined by the methods of Chapter IV, this amount of turning is in general not necessary, since minimum range occurs before the tracks are parallel. This case is considered further in Section 5.3.

The turn-to-cross maneuver describes turns in the opposite direction of those depicted in Figure 5.1 for the noncooperative case. The arc of the turn would exceed 90^{o} to achieve the parallel/anti-parallel headings.

For cooperative collision avoidance, a turn-to-parallel maneuver results when the aircraft turn in the opposite sense. That is, one aircraft turns right and the other aircraft turns left. In this manner, the aircraft headings become nearly parallel at the time of minimum range. For aircraft with equal airspeeds, the final headings are in fact parallel. This turn-to-parallel maneuver is shown in Fig. 5.2(a). The turn-to-crossing cooperative maneuver results when both aircraft turn in the same sense (right or left). This is illustrated in Fig. 5.2(b).

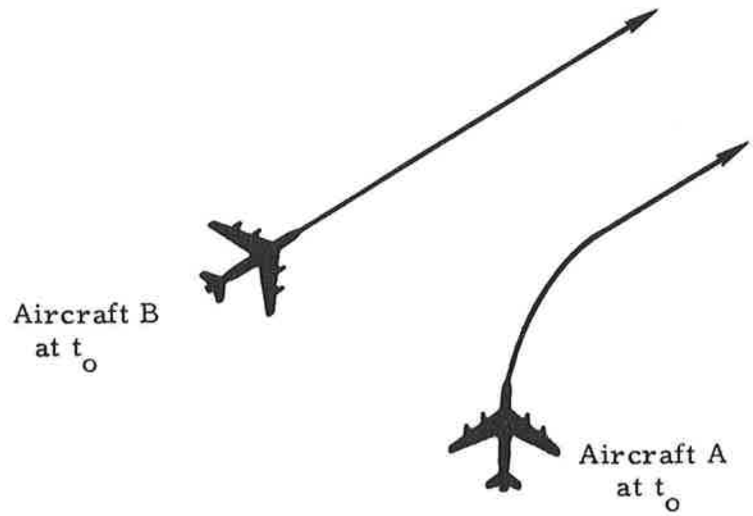

a) Initial Relative Heading Less Than 90^o

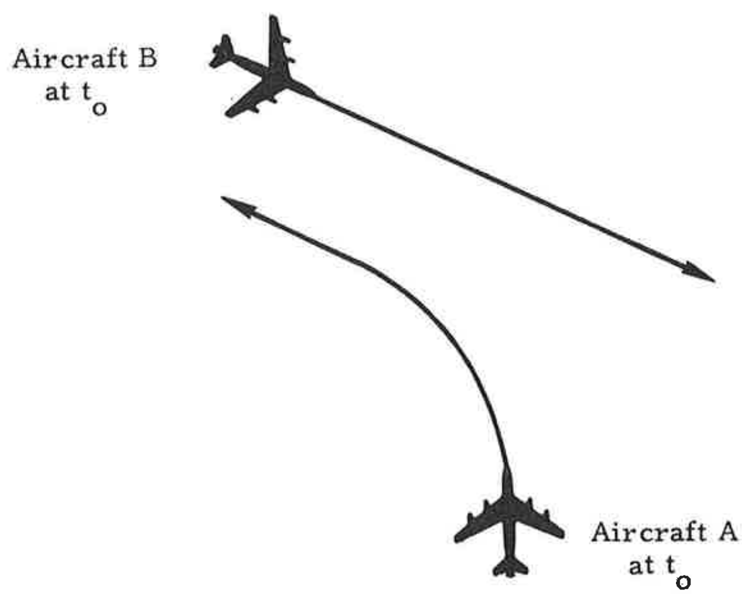

b) Initial Heading Greater Than 90^o

Figure 5.1 Turn-To-Parallel Turn Geometry for Noncooperative Collision Avoidance

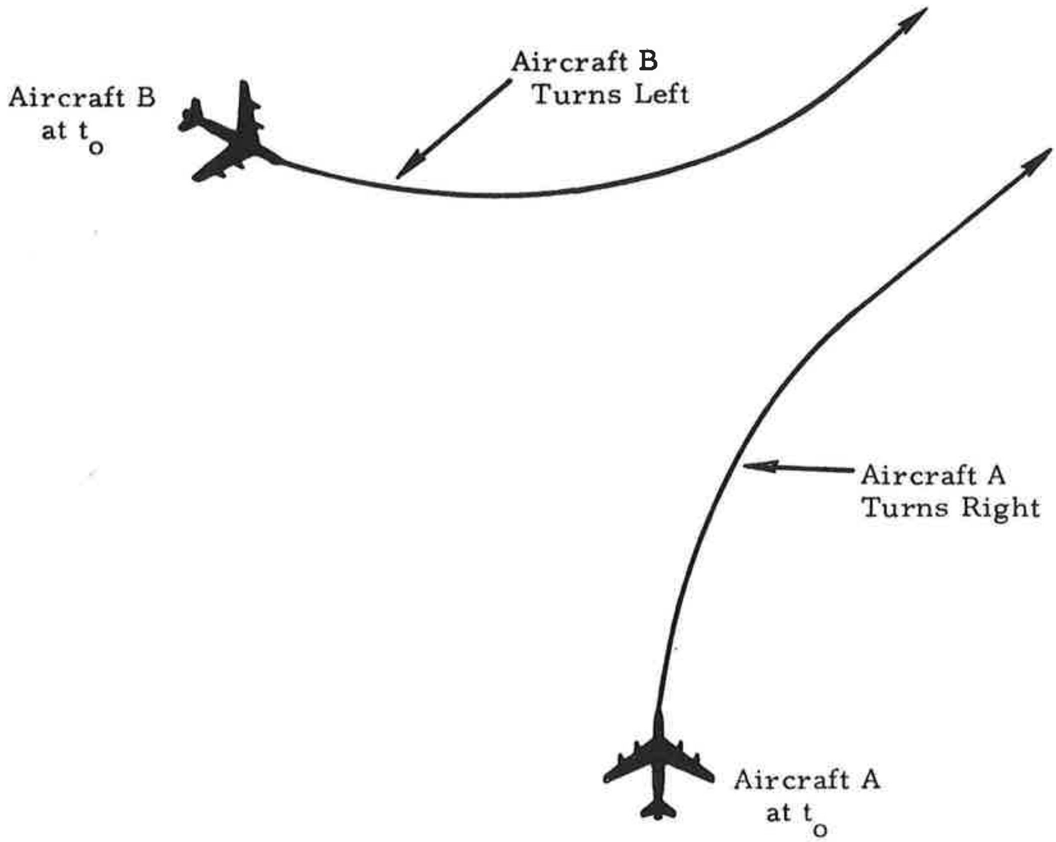

a) Turn-to-Parallel Geometry

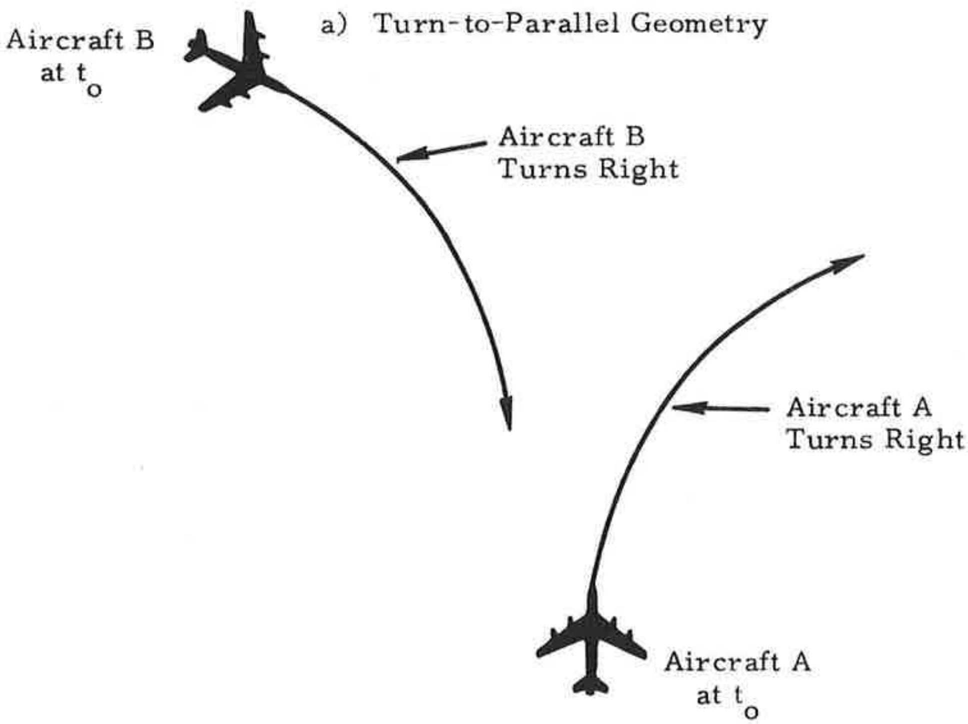

b) Turn-to-Cross Geometry

Figure 5.2 Turn-to-Parallel and Turn-to-Cross Geometry for Cooperative Collision Avoidance

The appropriate choice of turn directions for both aircraft is dependent upon the initial geometry and the airspeeds and turn rates of both aircraft, as explained in Chapter IV.

The maximum horizontal turn rates are determined by the structural and passenger comfort load limits. A detailed analysis of the forces felt by a passenger during a turn would be complex. However, the major effect can be obtained by considering the total magnitude of the acceleration during a steady-turn maneuver, as sensed by a passenger located at the center of mass of the aircraft.

The geometry of the coordinated turn is shown in Fig. 5.3. For a given bank angle, φ, the differential acceleration (load factor) felt by the passenger is seen to be

$$a_p = a_z - g = g\,(\sec\varphi - 1) \quad . \tag{5.1}$$

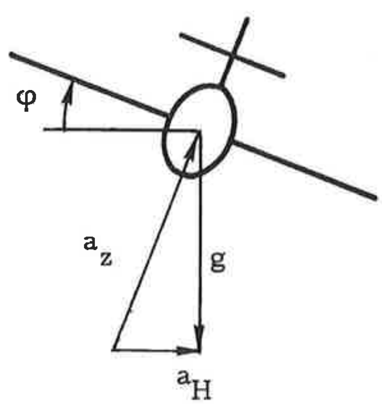

Figure 5.3 Acceleration Vectors for a Coordinated Turn

Here, the bank angle is given by

$$\tan \varphi = V^2/gR = V\omega/g \tag{5.2}$$

where V is the aircraft speed, R the turn radius, and ω the horizontal turn rate. If the bank angle is 30°, the load factor a_p is 0.15g, but the turn acceleration a_H is about 0.57g. This shows that the horizontal acceleration resulting from a steady bank angle can be much larger than the associated load factor felt by the passenger. That is, the passenger in a coordinated 30° turn is actually accelerating horizontally at about 18 ft/sec^2. However, the additional acceleration physically sensed by the passenger is less than 5 ft/sec^2. The horizontal acceleration is thus more efficient than the vertical acceleration, in that relatively large, long-term accelerations can be applied without causing undue passenger discomfort and/or anxiety.

5.1.2 Vertical Maneuvers

Generally, vertical collision avoidance maneuvers are limited by the maximum dive and climb rate achievable by the aircraft. The fact that the aircraft cannot accelerate vertically for any appreciable length of time (only long enough to achieve the maximum rate of climb or descent), limits the achievable vertical displacement in a specified time. For example, an aircraft maneuvering laterally with an acceleration of $\frac{1}{2}$ g can achieve a turn displacement of approximately 3200 feet in 20 seconds. An aircraft with a maximum climb rate of 2400 feet per minute (typical of commercial jet transports) can attain a vertical displacement of only 800 feet in the same time period. The important qualitative difference is that altitude changes are linear with time, while horizontal turns are approximate circular arcs. In a combined maneuver, the vertical displacement typically is larger than the horizontal displacement only for short maneuver time periods of 10 sec or less.

For vertical maneuvers, the time required to achieve a given vertical separation can be found by analogy with the horizontal maneuver parameter τ. This is defined as the ratio of range to range-rate, or the time when a collision would occur if no maneuver were enacted. For vertical maneuvers, the ratio of vertical displacement z_f to relative vertical velocity gives the required maneuver time. Figure 5.4 is a plot of τ_z as a function of the relative vertical separation rate with the desired miss distance as a parameter. These curves assume that the horizontal components of velocity remain constant. When an aircraft with a climb rate of 1000 ft/min attempts to avoid an aircraft with a dive rate of 1500 ft/min, the relative vertical separation rate is the sum of the two, or 2500 ft/min. For a desired vertical miss distance of 2000 ft, the corresponding τ is found to be 48 sec. The plotted τ does not reflect any transient time delays which need to be added. The initial separation required to achieve a desired miss distance for vertical maneuvers is discussed in more detail in Section 5.2. Morrel[26] refers to vertical collision avoidance as "turn out of the collision plane" maneuvers.

5.1.3 Speed Control Maneuvers

Although it has been stated that speed control provides insufficient maneuver capability,[27] highly desirable advantages of this type of escape maneuver motivate further investigation. One advantage is that the aircraft need not leave its track, so that interference with adjacent aircraft is avoided. The chief disadvantage is the small longitudinal acceleration/deceleration capability to provide rapid separation. Also, this maneuver is ineffective for head-on or overtaking encounters. However, analysis indicates that this type of maneuver can be feasible for other geometries. This subsection indicates the conditions under which this maneuver is feasible. The tradeoff between the required warning time and the achievable miss distance obtainable for collision course initial conditions is also presented.

Two aircraft are assumed to be flying at fixed speed on intersecting straight-line flight paths. The aircraft are in conflict if at some time the distance between them is less than a specified separation standard or desired miss-distance, r_a. The speed-control technique requires one of the aircraft to reduce speed by a specified amount while the other aircraft maintains speed.* The reduced speed is maintained for a certain length of time, and

*An alternate scheme in which one aircraft slows down while the other speeds up may be treated in the same manner as given here.

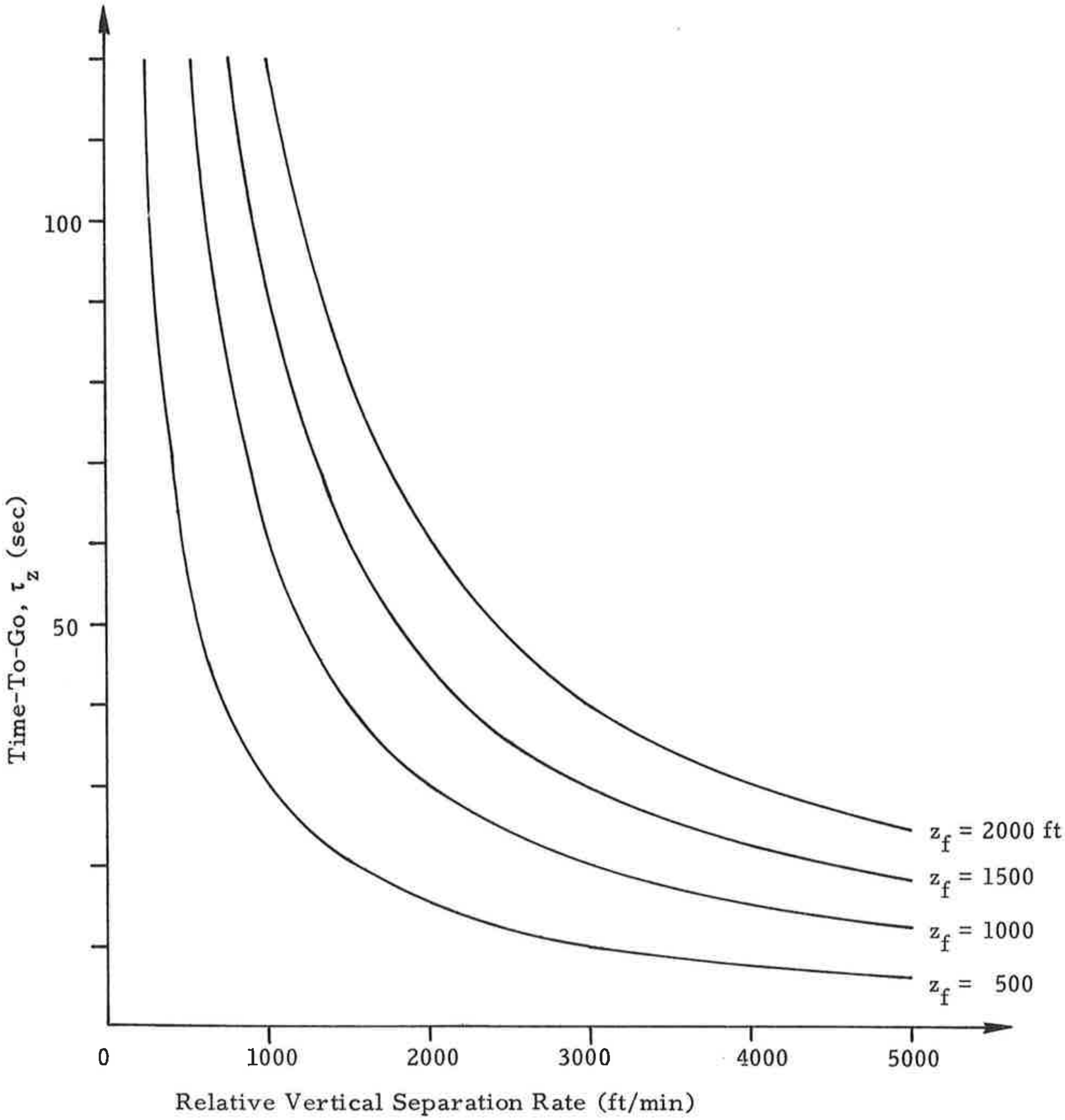

Figure 5.4 Time-To-Go Requirements for Varying Relative Vertical Separation Rates

then the original speed is resumed. No deviations from flight paths are required. The amount of time spent flying at reduced speed is determined by the available speed change and the desired miss distance.

A method is presented in Appendix D for computing the time at which the slow-down maneuver should begin. This time is found as a function of the aircraft speeds, encounter geometry, and deceleration capability. It is assumed that one aircraft decelerates at a constant rate until a fixed lower speed is achieved. This reduced speed is then maintained until the point of minimum range. At that time, the aircraft accelerates at the same longitudinal rate until the nominal speed is again reached. The second aircraft is assumed to fly continuously at constant speed.

Figures 5.5 and 5.6 indicate typical results obtained from the algorithms presented in Appendix D. These results are found for a relative heading of 90° and a speed reduction of 10%. Figure 5.5 shows the normalized time-to-go, τ_g, as a function of the parameters ρ and γ. These parameters are defined as follows:

V_B = constant speed of non-decelerating aircraft

V_A = initial speed of decelerating aircraft

γ = V_A/V_B

r_f = normal miss distance (=0 for a collision, <0 if A normally passes behind B, and >0 if A normally passes in front of B)

r_a = desired miss distance

t_g = normal time to closest approach based on the lower speed of the decelerating aircraft

τ_g = normalized time-to-go, $V_B t_g/r_a$

ρ = normalized miss distance, r_f/r_a

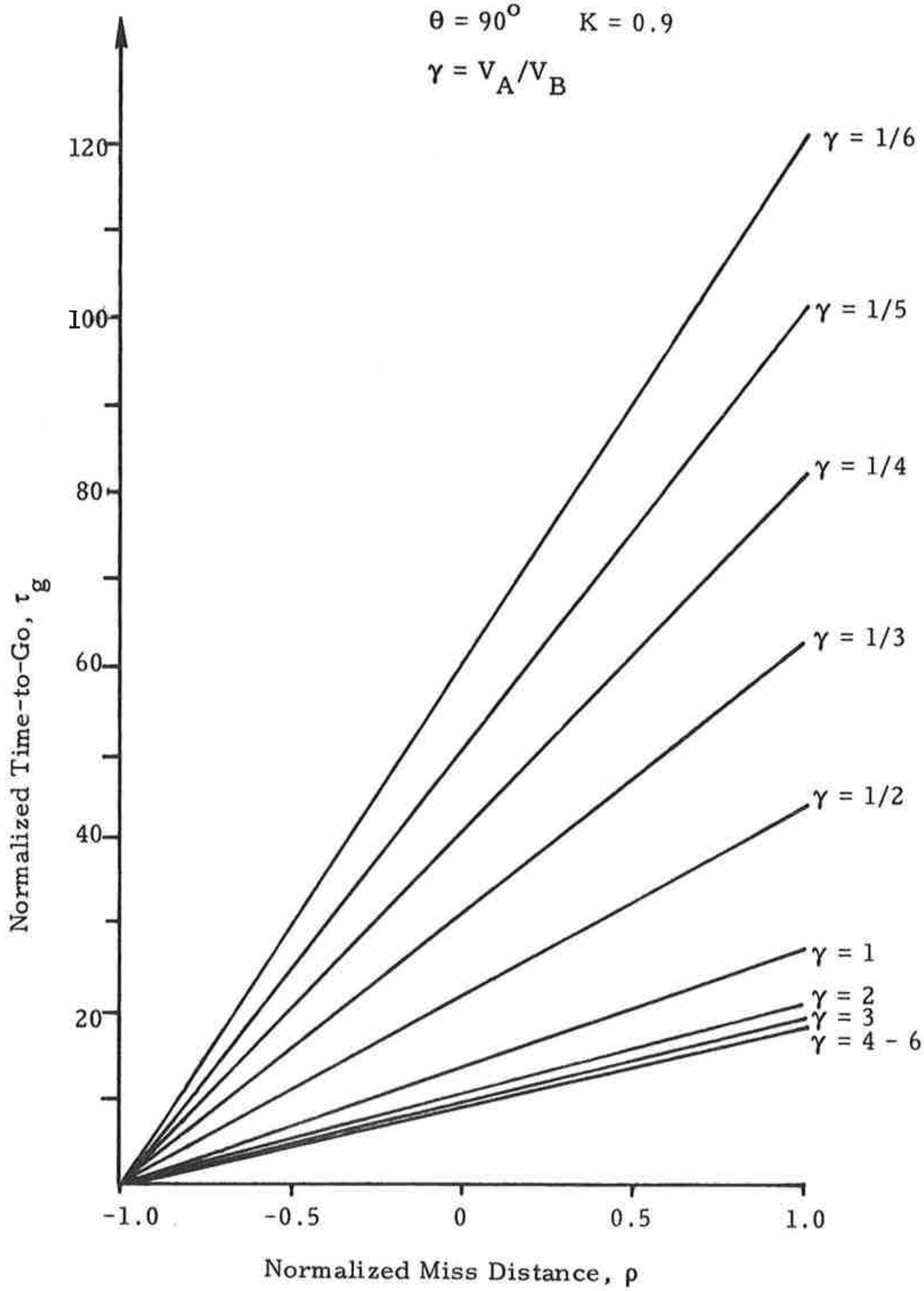

Figure 5.5 Time-To-Go for Varying Miss Distance and Several Speed Ratios

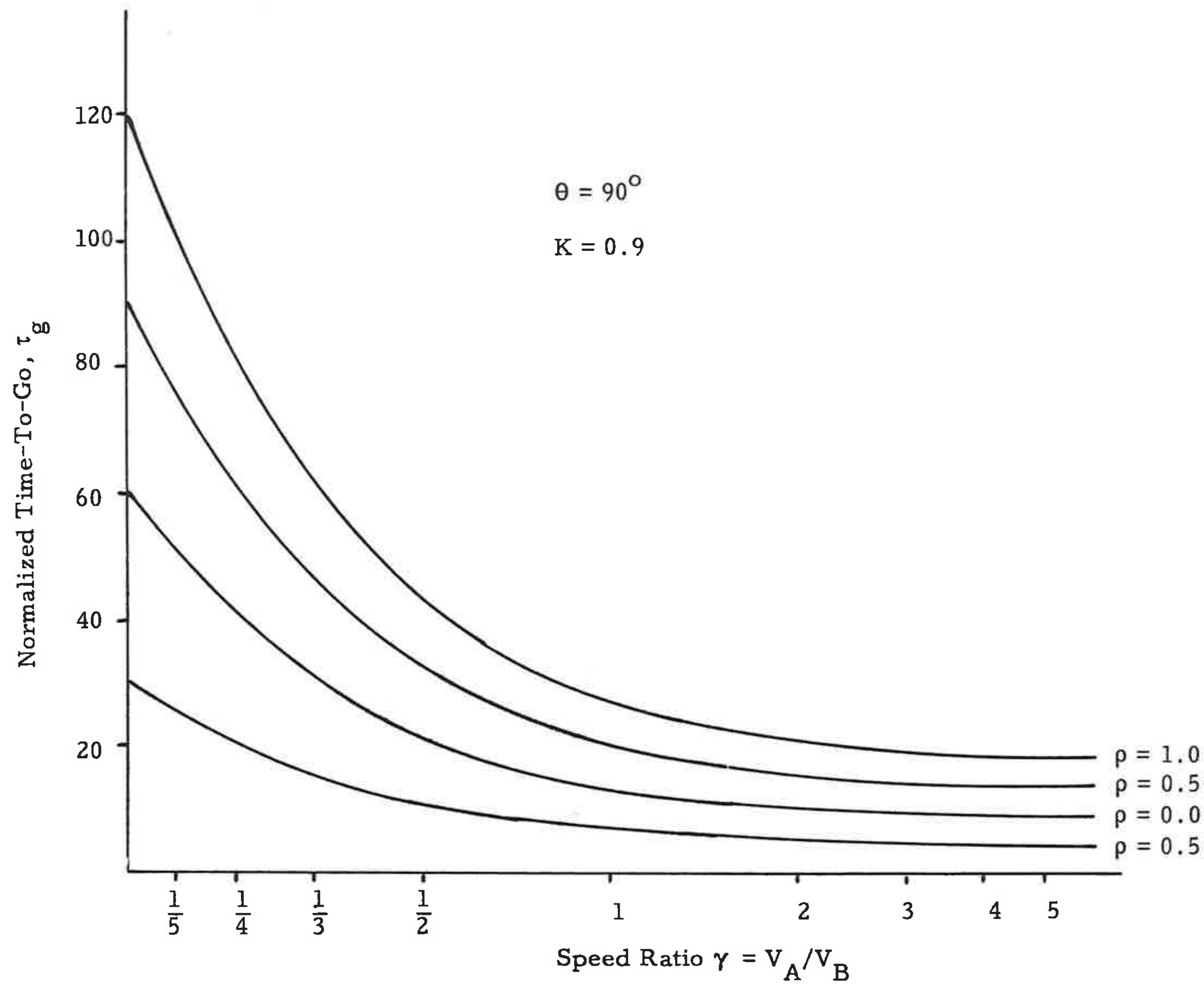

Figure 5.6 Time-To-Go for Varying Speed Ratios and Several Normalized Miss Distances

Thus, the quantity τ_g represents the time expired during the period that the decelerated aircraft A has the speed KV_A (where K is some constant). Figure 5.6 illustrates the same results with τ_g as a function of the initial velocity ratio γ and the initial miss distance ρ treated as a parameter.

To evaluate the total time required for a speed control maneuver, the transient time to reduce the aircraft speed must be included. If an aircraft is assumed to accelerate and decelerate at a constant value a, then the rate of velocity change can be expressed as

$$\dot{V} = a \tag{5.3}$$

where V is the aircraft speed. If aircraft A's speed is reduced from V_A to KV_A, then the time required for this is

$$t = \frac{(K-1)V_A}{a} \tag{5.4}$$

Figure 5.7 indicates a plot of t/V_A (=t') for several values of K and as a function of a. For example, to obtain the time to decelerate 10% (K=.9) using $a = -0.1g$, Fig. 5.7 indicates a value of t' of .031. If V_A = 300 ft/sec, the transient time is 9.3 sec.

The potential results of using speed control as a collision avoidance maneuver are indicated in Fig. 5.8. In this figure, the desired miss distance is taken to be 2000 feet and the relative heading angle θ is 90^o. In the first case, the aircraft are nominally on a course with a 1000 ft miss distance. Initial speed ratios (γ) of 0.67, 1.0, and 1.5 are considered. The plot represents the total maneuver time necessary to achieve the desired miss distance as a function of the nonmaneuvering aircraft's speed. In each case, it is assumed that one aircraft slows down by 10% using a 0.1g deceleration rate. For the cooperative case, the other aircraft speeds up 10% using 0.1g acceleration.

As speeds increase, the warning time decreases initially, because larger speed changes reduce the time required to achieve a given miss. At

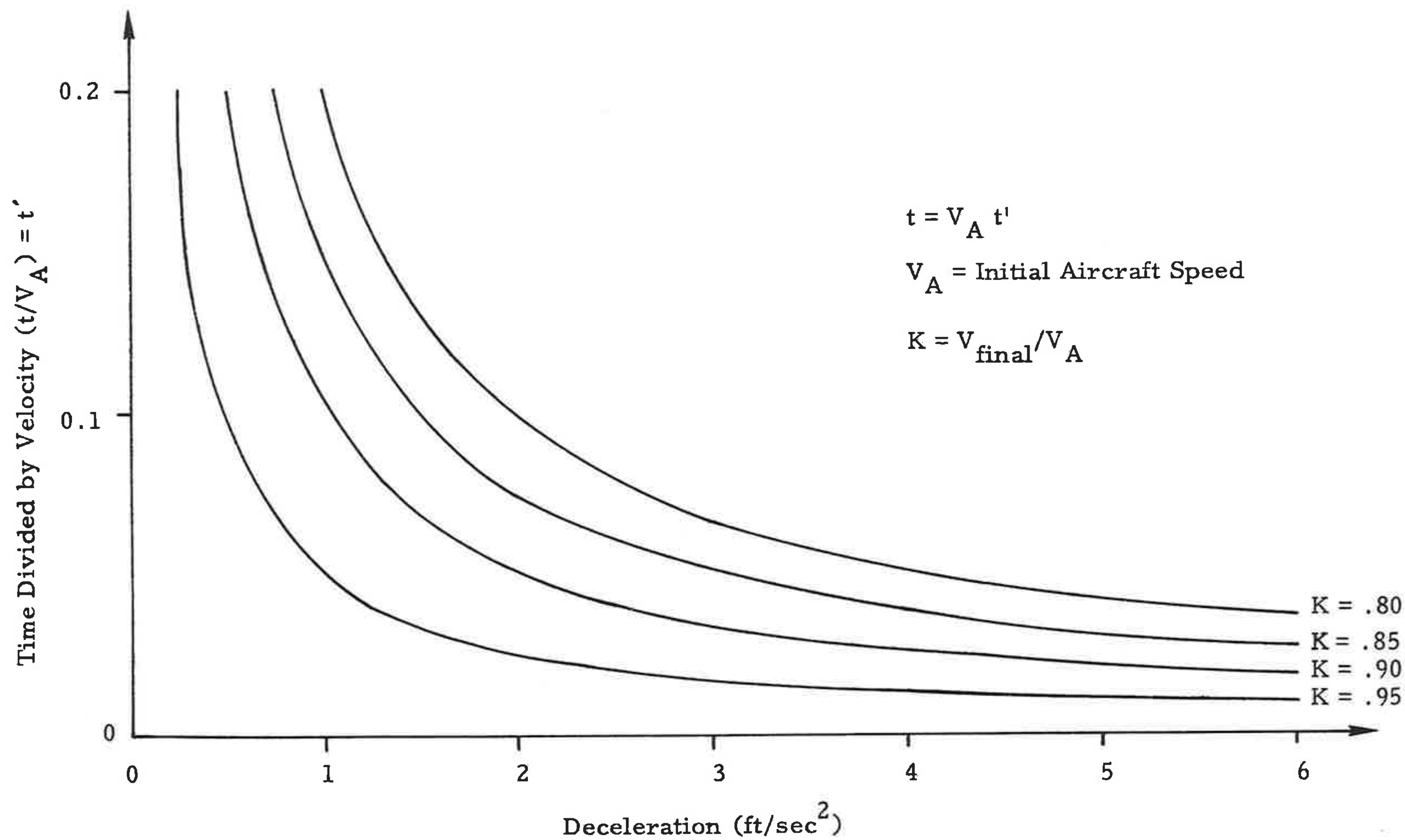

Figure 5.7 Time to Reduce Speed for Various Deceleration Rates

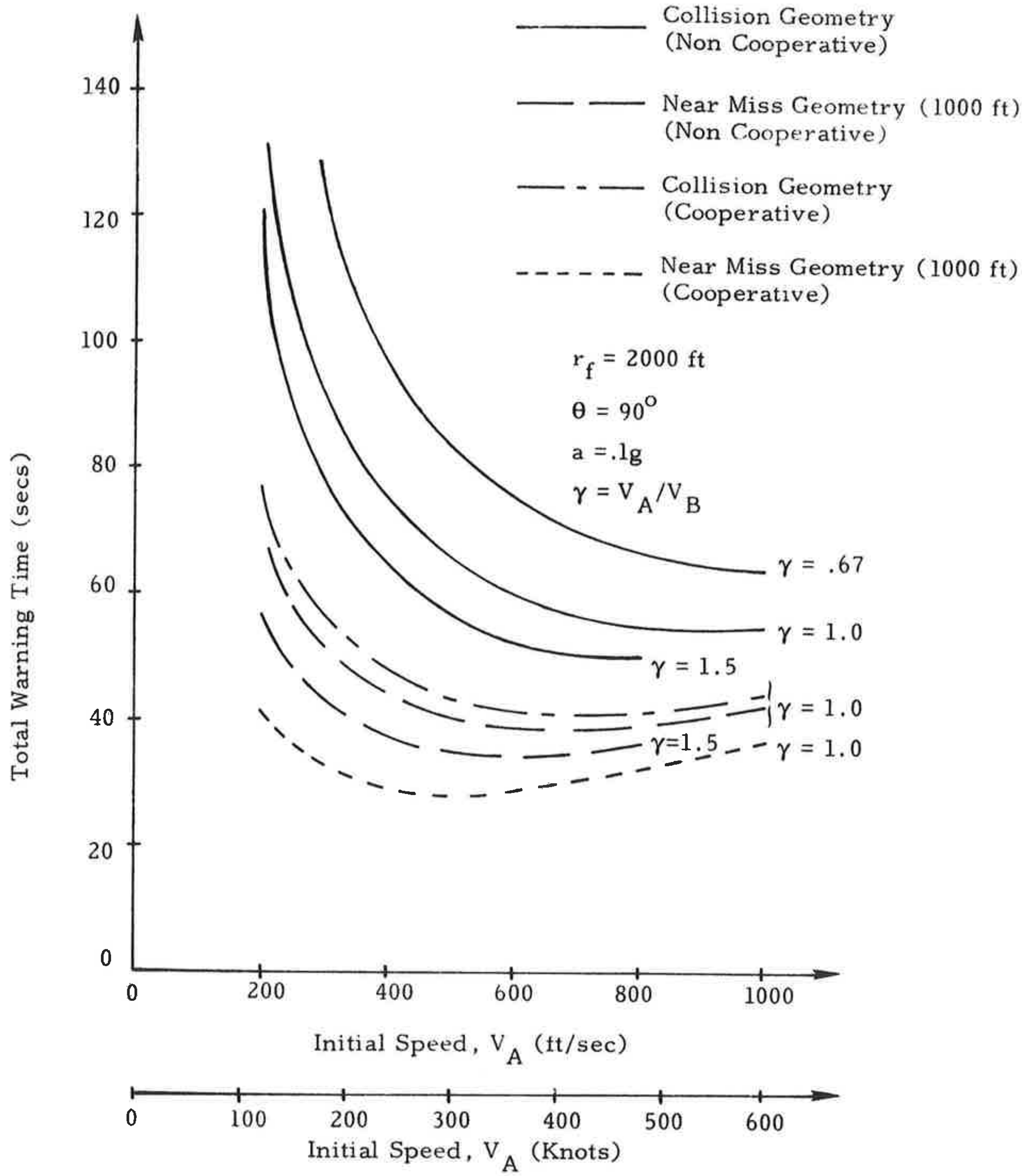

Figure 5.8 Total Warning Time Required for Speed Control Maneuvers

larger velocities, the time of the speed change transient becomes more prominent and the total time increases. It can be seen that even for the collision geometry, the total warning times are not excessively large. Tradeoffs exist between the benefits to be gained by speed control (zero deviation from flight path and small in-track delay) and the total warning time required. The derivation of the speed control algorithm is discussed in more detail in Appendix D.

Another observation made from Fig. 5.8 is that the faster aircraft should slow down as demonstrated by comparing the total maneuver times associated with γ of 0.67 and of 1.5. A γ of 0.67 implies the slower aircraft slows down, and a γ of 1.5 implies the faster aircraft slows down. Two curves are also plotted in Fig. 5.8 to indicate the required cooperative maneuver times when one aircraft slows down and the other speeds up. For these curves, it is assumed that they both initially travel at the same speed.

5.2 COMPARISON OF MANEUVERS

Each maneuver type has certain inherent disadvantages. Vertical maneuvers are restricted by their climb and dive rates, lateral maneuvers are limited by turn rates or the passenger load factor, and longitudinal maneuvers are restricted by the thrust and drag characteristics of the aircraft. The disadvantages displayed by the various maneuver types become more apparent in the following results.

A comparison can be made of the effectiveness, relative to several criteria, of lateral, longitudinal, and vertical collision avoidance maneuvers. This comparison is based on three criteria:

- Initial separation requirements for meeting a given safe miss-distance;
- Maximum deviation off-track incurred while attempting to avoid the other aircraft;
- In-track time delay incurred as a result of the collision avoidance maneuver.

The initial separation at which a maneuver must begin for attaining a given miss distance directly affects such quantities as airspace usage and threat alarm rates. The alarm rate also governs the false alarm rate. For a comparison of the initial separation required for vertical, lateral and longitudinal maneuvers, the case where the two aircraft begin on a collision course is examined. The airspeeds used are representative of near terminal area speeds of commercial jet aircraft.

In Fig. 5.9, initial separation requirements are plotted as a function of required miss-distance and initial relative heading with both aircraft maneuvering. The vertical climb/dive rate is restricted to 2000 ft/min, the lateral turn is restricted to a load factor of .15g (this corresponds approximately to a bank angle of 30^{o}) and speed changes of 10% are assumed using an acceleration/deceleration of 0.1g. Except for miss-distances less than 100 ft, horizontal maneuvers require less initial separation to meet a given miss-distance, independent of the initial geometry of the encounter. It is of interest to note that the initial separation requirements for speed control maneuvers are comparable to the initial separation requirements for vertical maneuvers.

An additional point to be mentioned here is the effect of combined horizontal/vertical maneuvers. For these maneuvers, the initial separation requirements very nearly duplicate the initial separation requirements for the horizontal maneuver only. This result implies that for combined maneuvers, the initial separation requirements for the horizontal maneuver contribution dominate with very little additional effect due to vertical maneuver contribution.

The second principal criterion for comparing the various maneuver types is the off-track deviation required by a given miss-distance. In Fig. 5.10, the off-track deviation is shown as a function of the desired miss-distance and initial geometry. From this plot, it can be noted that the vertical maneuvers require less off-track deviation than horizontal maneuvers, independent of geometry. The aircraft flight path direction is changed considerably more for horizontal maneuvers than for vertical maneuvers. For example, an aircraft climbing at 2000 ft/min and moving horizontally with a speed of 360 ft/sec has

$V_A = V_B = 360$ ft/sec

Vertical Climb Rate = 2000 ft/min

Bank Angle = 30^o

Longitudinal Deceleration = .1g

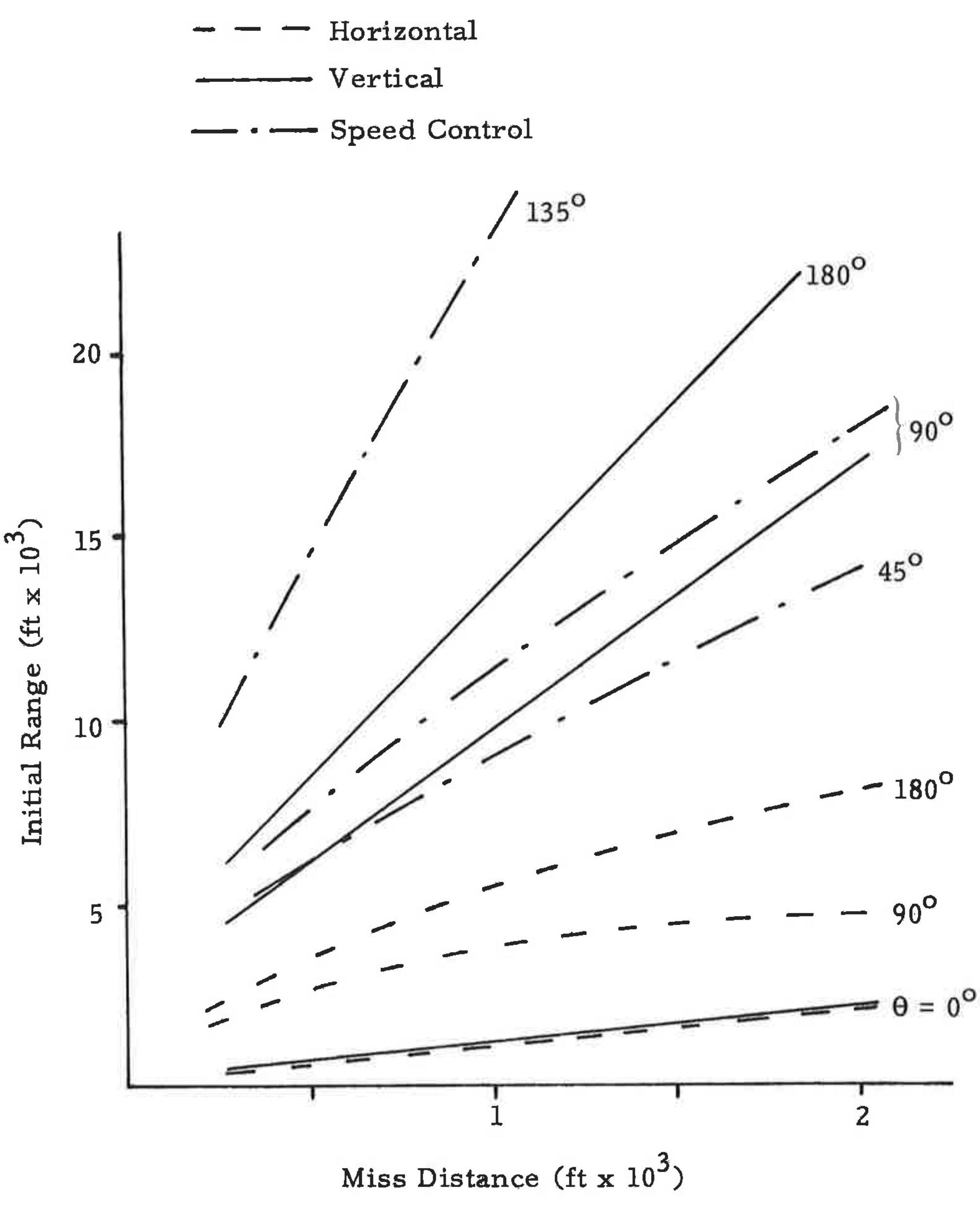

Figure 5.9 Initial Separation Requirements for Different Collision Avoidance Maneuver Concepts

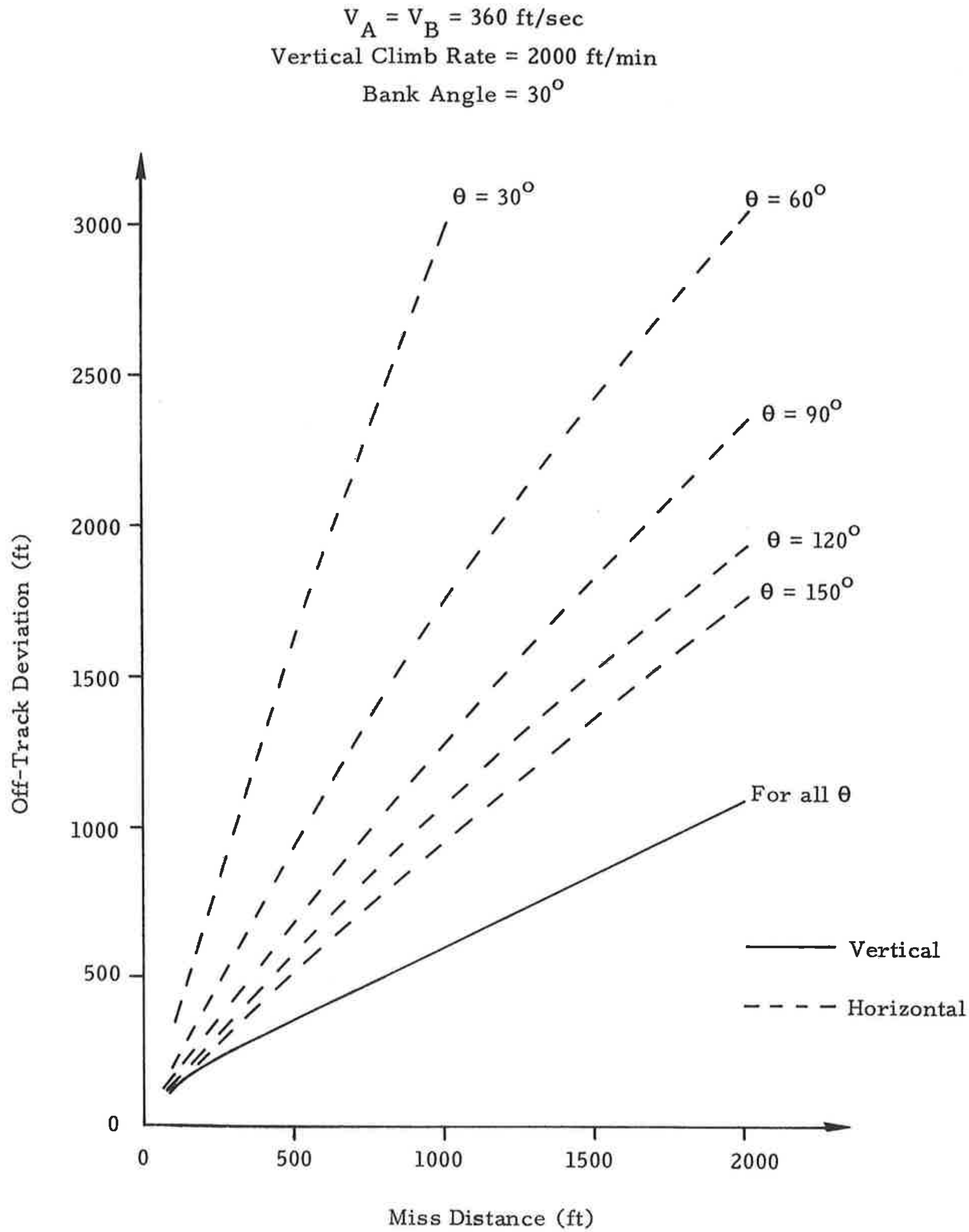

Figure 5.10 Off-Track Deviation Comparison with Varying Geometry

a flight path angle of approximately 5.5°. This compares to heading changes which can approach 90° for lateral turns. It is significant to note that the speed control maneuver requires no deviation from track at all. However, speed control's applicability is dependent on the encounter geometry and the time available.

The third criterion that was examined is the in-track time delay incurred as a result of the collision avoidance maneuver. For vertical maneuvers, the in-track time delay is essentially zero since the additional path length for an aircraft to change altitude by 1000 ft and return to the original altitude is negligible. This assumes no change in the horizontal component of each aircraft's velocity. Hence, the traverse times of both paths will be the same.

For the horizontal maneuvers, the path length while executing the maneuver may be significantly larger than the straight-line path. Consider the maneuver geometry in Fig. 5.11. Here, the aircraft is assumed to have reached minimum range after subtending an angle α. To return to track requires an additional turn in the opposite direction through an angle 2α and then a turn in the original direction through another angle α. The aircraft has effectively turned through a total angle equal to 4α. This, of course, assumes that the roll transient of the aircraft is negligible and that the aircraft applies the same turn rate for the return maneuver as for the avoidance maneuver.

From Fig. 5.11, the total time to traverse the avoidance maneuver flight path can be expressed as

$$t_1 = \frac{4R\alpha}{V} \tag{5.5}$$

Here, R is the turn radius, V is the aircraft speed, and α is the turn angle required by the avoidance maneuver. The equivalent time to traverse the straight-line path is given by

$$t_2 = \frac{4R \sin \alpha}{V} \tag{5.6}$$

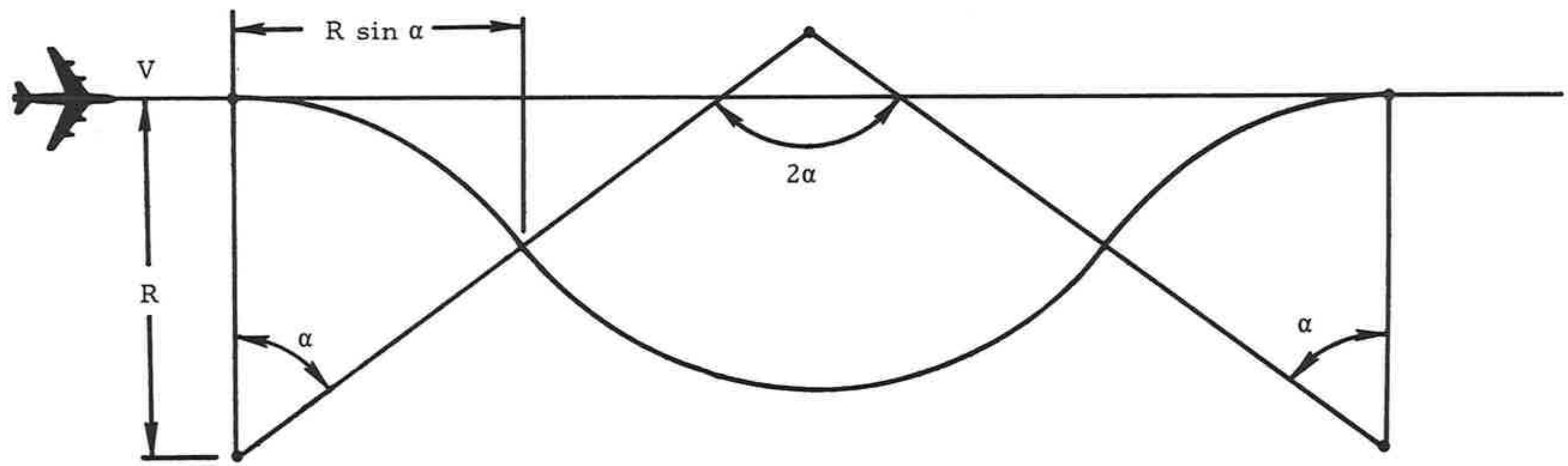

Figure 5.11 Lateral Return-to-Track Maneuver Geometry

The in-track time delay incurred by the lateral maneuver is given by

$$\Delta t = t_1 - t_2 = \frac{4R}{V} (\alpha - \sin \alpha) \tag{5.7}$$

The in-track time delay as a result of speed change maneuvers is more complicated, and the analysis is given in Appendix D. Results of the speed control time delay are presented in Fig. 5.12, together with the horizontal maneuver time delays. It is observed that the speed control time delay is generally less than the horizontal time delay. The actual time delay (ideally) is small for miss distances under 2000 ft. Thus, time delay is probably a secondary performance criterion.

In conclusion, using the three criteria discussed previously, and for the encounter geometries studied, the three maneuver types can be ranked in order of preference. This is done in Table 5.1.

TABLE 5.1

Maneuver Preference With Respect to Different Performance Measures

PERFORMANCE MEASURE	TYPE MANEUVER		
	LATERAL (TURN)	VERTICAL (CLIMB/DIVE)	LONGITUDINAL (SPEED CONTROL)
Initial Separation	1	2	3
Distance Off-Track	3	2	1
In-Track Time Loss	2	1	2

This comparison is not general and is based on certain specialized assumptions. To provide conclusive comparisons requires further study and a decision regarding the relative importance of these and other performance measures.

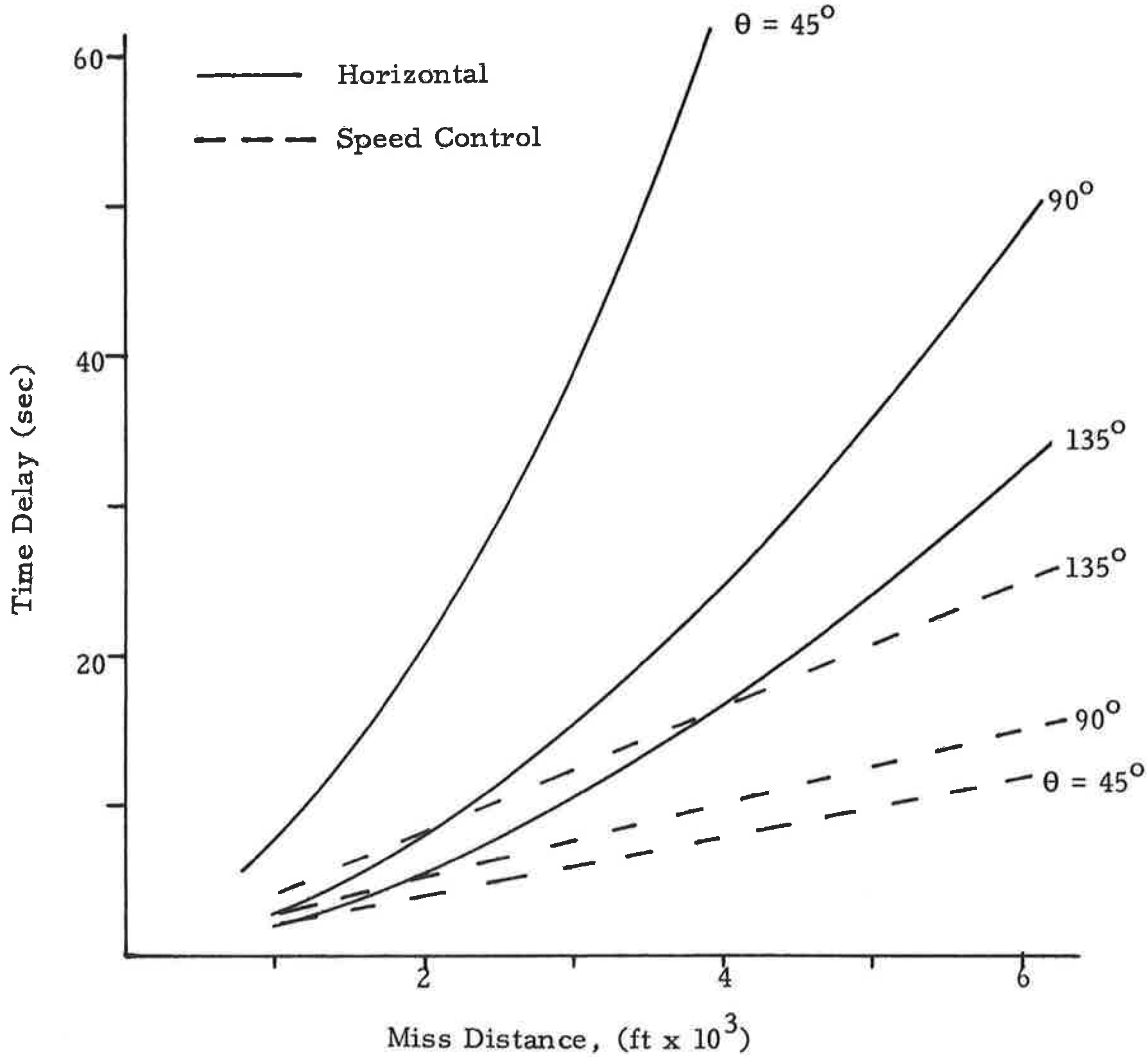

Figure 5.12 Delay Time Comparison for Varying Geometry

5.3 RELATIONSHIP OF RESULTS TO PREVIOUS WORK

It is felt by the authors that this special section of the report is necessary to relate in detail this work to that of previous investigators. The reasons for this are the following:

1. This work, although somewhat limited in detail by the time spent on the effort, is much more general and complete regarding the merits and physical characteristics of horizontal collision avoidance maneuvers than were previous efforts.

2. Previous work contains a number of misleading and incorrect conclusions. These conclusions have been widely quoted[14,16] and it is important for the purposes of this study that any discrepancies be examined and that physical reality be established.

3. Previous work has been incorrectly interpreted, or statements have been taken out of context.

Previous work has concentrated on the maneuvers in the horizontal plane of a single aircraft (which is usually referred to as the uncooperative maneuver case). Attention is first directed to these uncooperative maneuvers. Cooperative maneuvers are then studied, and an examination is made of several other points mentioned in the literature regarding collision avoidance maneuvers.

5.3.1 Non-Cooperative Maneuvers

For non-cooperative collision avoidance systems, it is assumed that only one aircraft maneuvers while the other aircraft remains on its original flight path, and that the original flight paths of each aircraft are straight lines. Morrel[27] obtained relative motion plots for given collision geometries and escape times. A typical plot is shown in Fig. 5.13. The parameters characterizing this plot are airspeed of the maneuvering aircraft of 500 ft/sec, relative range-rate of 600 ft/sec at the time of the alarm, maneuvering acceleration of .5g, and maneuver delay time of 5 sec. The parameter associated with the

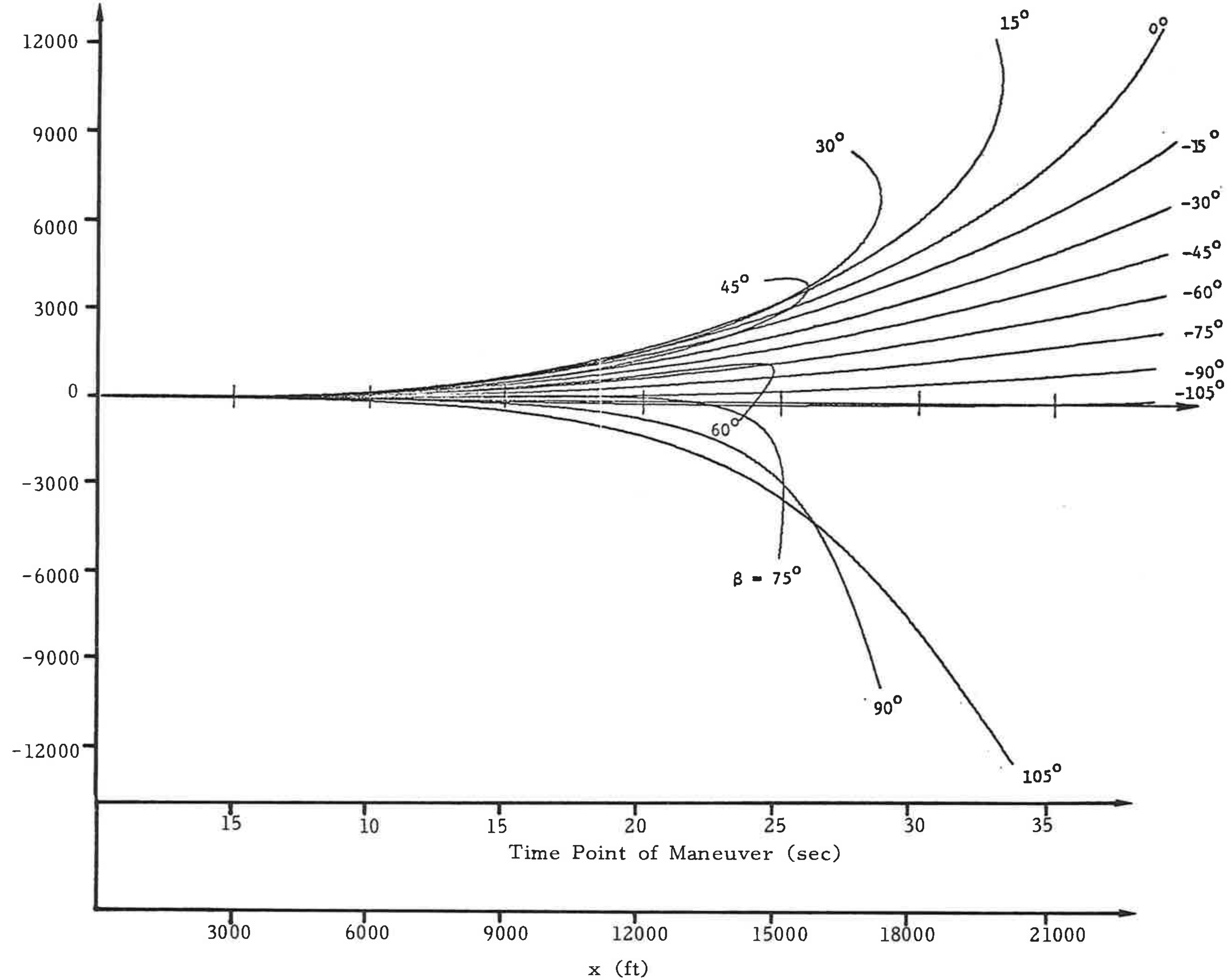

Figure 5.13 Relative Escape Paths for Conflict Geometry Which Would Produce a Collision in Thirty Seconds

family of curves is the relative bearing at the time of collision warning. The sign convention on the bearing was used by Morrel to denote the evasive maneuvers. That is, a positive bearing implies a turn away from the threat and a negative bearing implies a turn towards the threat. The intruding aircraft speed was bounded by 900 ft/sec. From such a relative motion chart, Morrel obtained conclusions influencing the choice of horizontal maneuver strategies. The charts, however, also yield incorrect results if care is not taken in their interpretation. This occurs because the dynamic model never allowed a maneuver to change, and the turn maneuver continues even after a point of minimum range is reached.

The curves of Fig. 5.13 represent the relative motion of the maneuvering aircraft A. The x-axis indicates time-to-go (or "escape time") to collision if no maneuver is made. For example, for an escape time of 30 seconds, the nonmaneuvering aircraft B remains stationary at that point on the x-axis. The maneuvering aircraft moves along one of the curves relative to the nonmaneuvering aircraft.

The incorrect results occur in the form of delayed collisions despite maneuvering. For example, the curve corresponding to an initial relative bearing of 60° indicates, for an escape time of approximately 24 seconds, that despite maneuvering to avoid a collision, a later collision occurs. This delayed collision is explained more clearly in Fig. 5.14, which is a plot of both horizontal trajectories in real-space. This real-space plot corresponds to the curve labelled $\beta = 60^{\circ}$ in Fig. 5.13. The nominal minimum miss distance is indicated. For this geometry, the maneuvering aircraft should cease its turn at the approximate time $t = 34$ sec.

To avoid this misleading interpretation of Morrel's relative space curves, the following use of the curves should be made. Minimum range occurs when the motion of the maneuvering aircraft relative to the nonmaneuvering aircraft is perpendicular to a line joining the two aircraft. (This geometry is indicated in Fig. 5.15). This represents the point at which the relative position vector is perpendicular to the relative velocity vector. At this point, the collision avoidance problem is complete, and the remainder of the relative motion curve can be ignored as other maneuvers are then initiated to return to track.

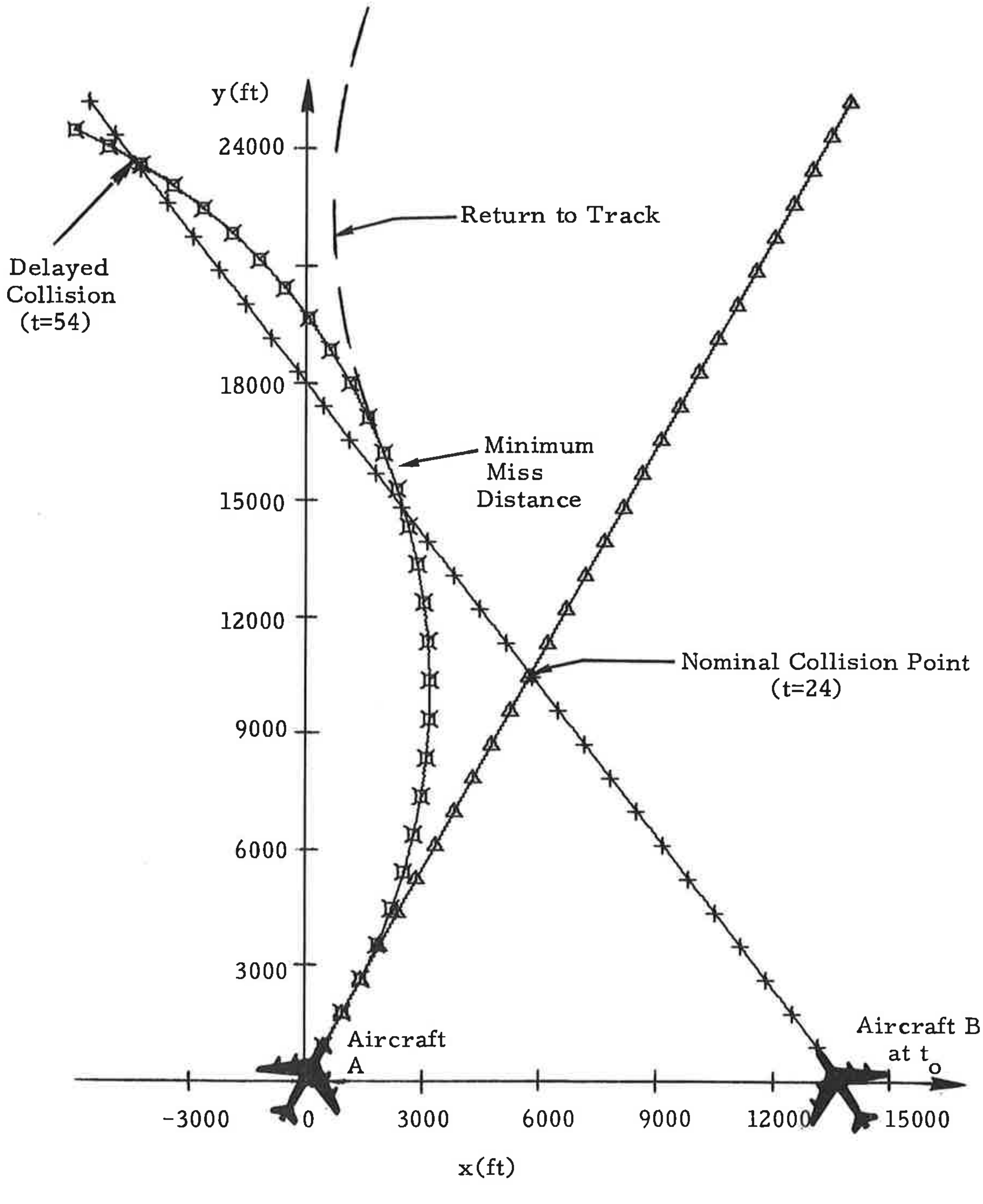

Figure 5.14 Collision Geometry for Initial Relative Bearing of 60^o

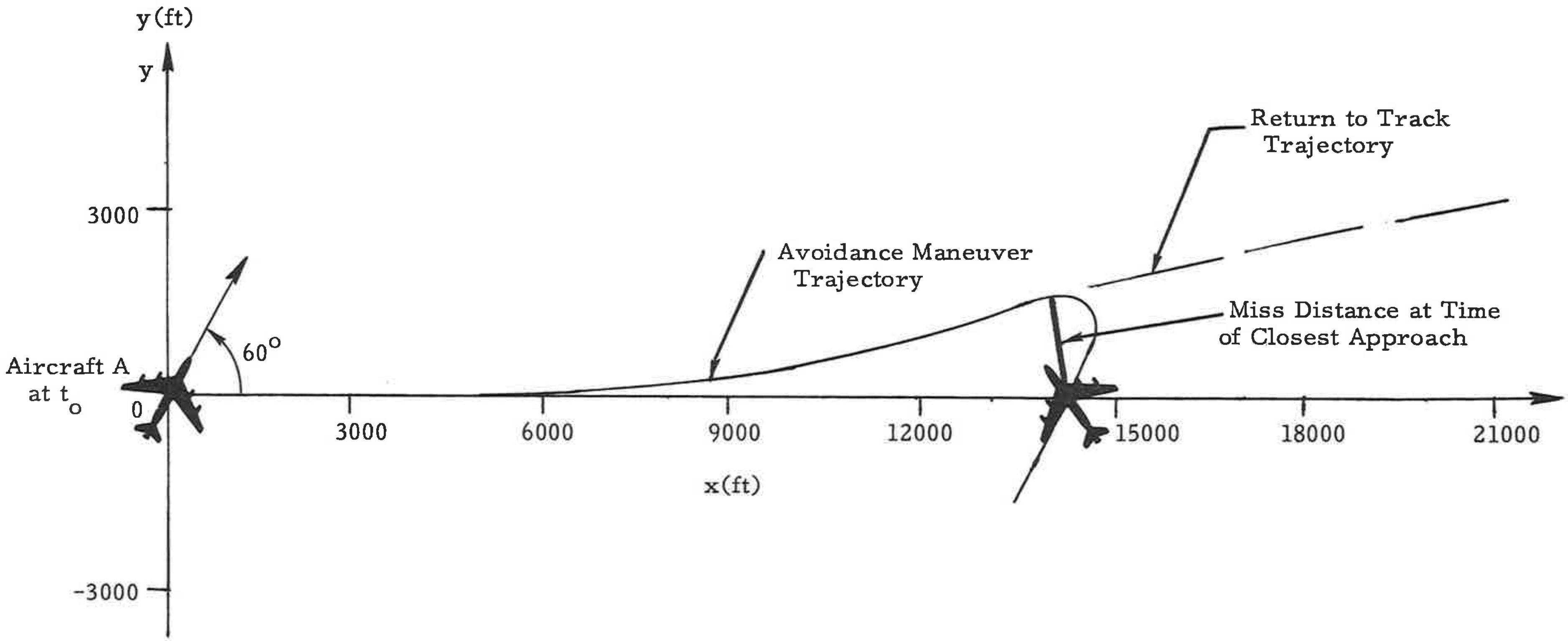

Figure 5.15 Effect of Return to Track Maneuver

For some of the relative motion curves, however, a collision occurs ($r = 0$) before the range-rate is zero ($\dot{r} = 0$). This can be seen in Fig. 5.13 for the relative motion curve labelled by 75^o. This type of condition corresponds to Bolie's[83] definition of a "futile" escape maneuver. The delayed collision appears to occur for an escape time of 22 seconds and the real motion is observed to occur as shown in Fig. 5.16. The collision is seen to occur at a delayed point rather than the nominal collision point. The corresponding turn toward the hazard maneuver is shown in Fig. 5.17. This turn maneuver yields a larger miss distance. That is, Fig. 5.13 shows that, for the 22 sec. escape time, miss distance for the turn toward maneuver (the curve labelled $\beta = -75^o$) is much greater than the miss distance for the turn away maneuver (the curve labelled $\beta = 75^o$).

A similar situation is indicated in Figs. 5.18 and 5.19 for an initial relative bearing of 105^o. Here, however, the turn-away maneuver yields a larger miss distance. This can be observed from Fig. 5.13 for $t = 35$ sec, where the turn-toward maneuver (the curve labelled $\beta = -105^o$) provides a much smaller miss distance than the turn-away maneuver (the curve corresponding to 105^o).

In an effort to explain these charts, Morrel constructed additional charts corresponding to a particular escape time. An example is shown in Fig. 5.20, for an escape time of 22 secs and the collision geometry parameters corresponding to Fig. 5.13. Here, it is seen that for an initial bearing of approximately 75^o, the turn-toward maneuver provides the greater miss distance, and for an initial bearing of approximately 105^o, the opposite is true.

Charts of the type shown in Fig. 5.20 are useful in that they determine the direction in which the maneuvering aircraft should turn in order to achieve the larger of two miss distances. These charts, however, are limited by the fact that they represent aircraft only in collision geometry situations and only at specific escape times. It is clearly desirable to have more general charts which indicate the optimal avoidance maneuvers, not only for collision geometries and specific escape times, but also for hazardous near-miss geometries and for any escape time.

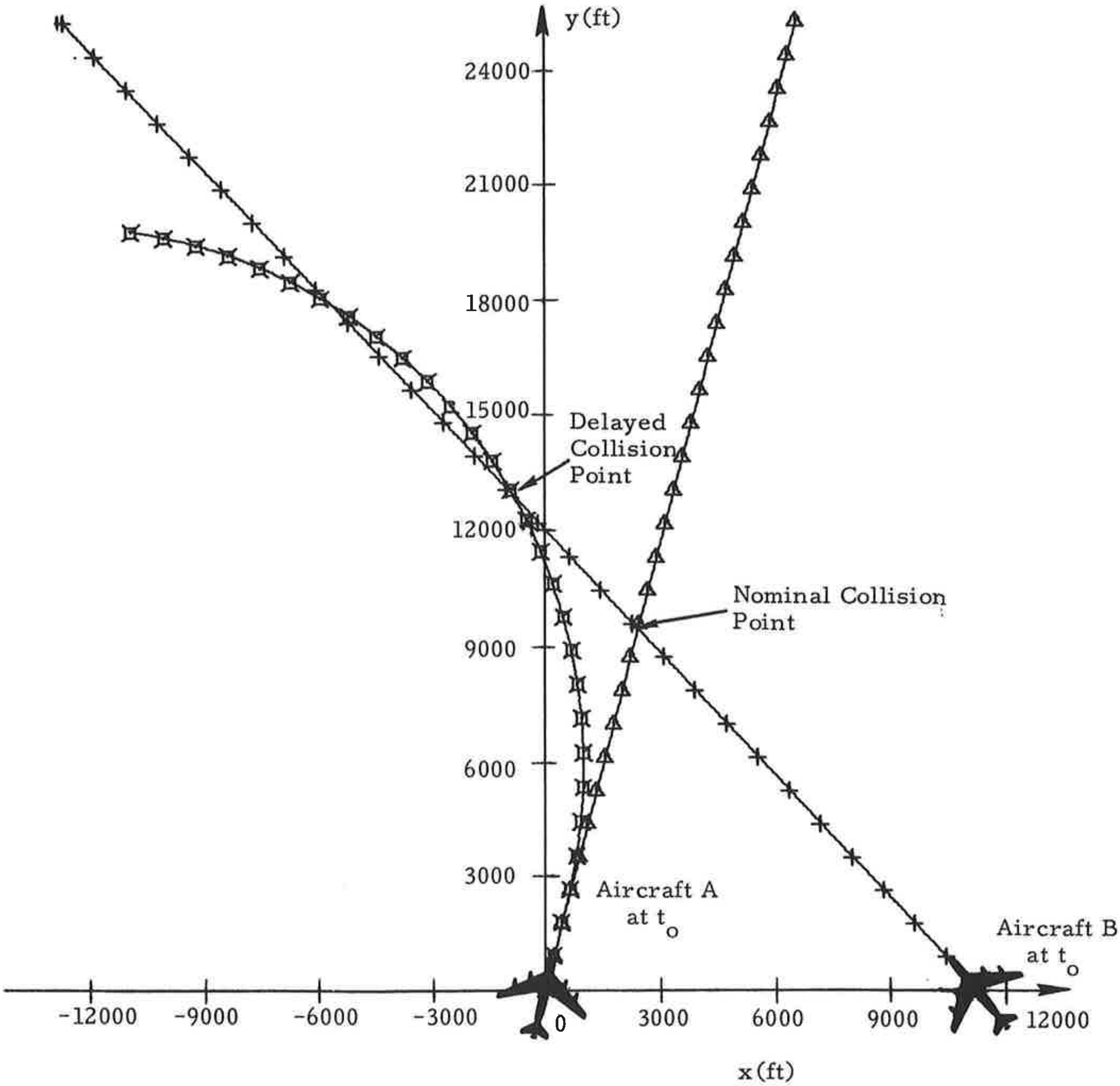

Figure 5.16 Turn Away Maneuver for Initial Relative Bearing of 75°

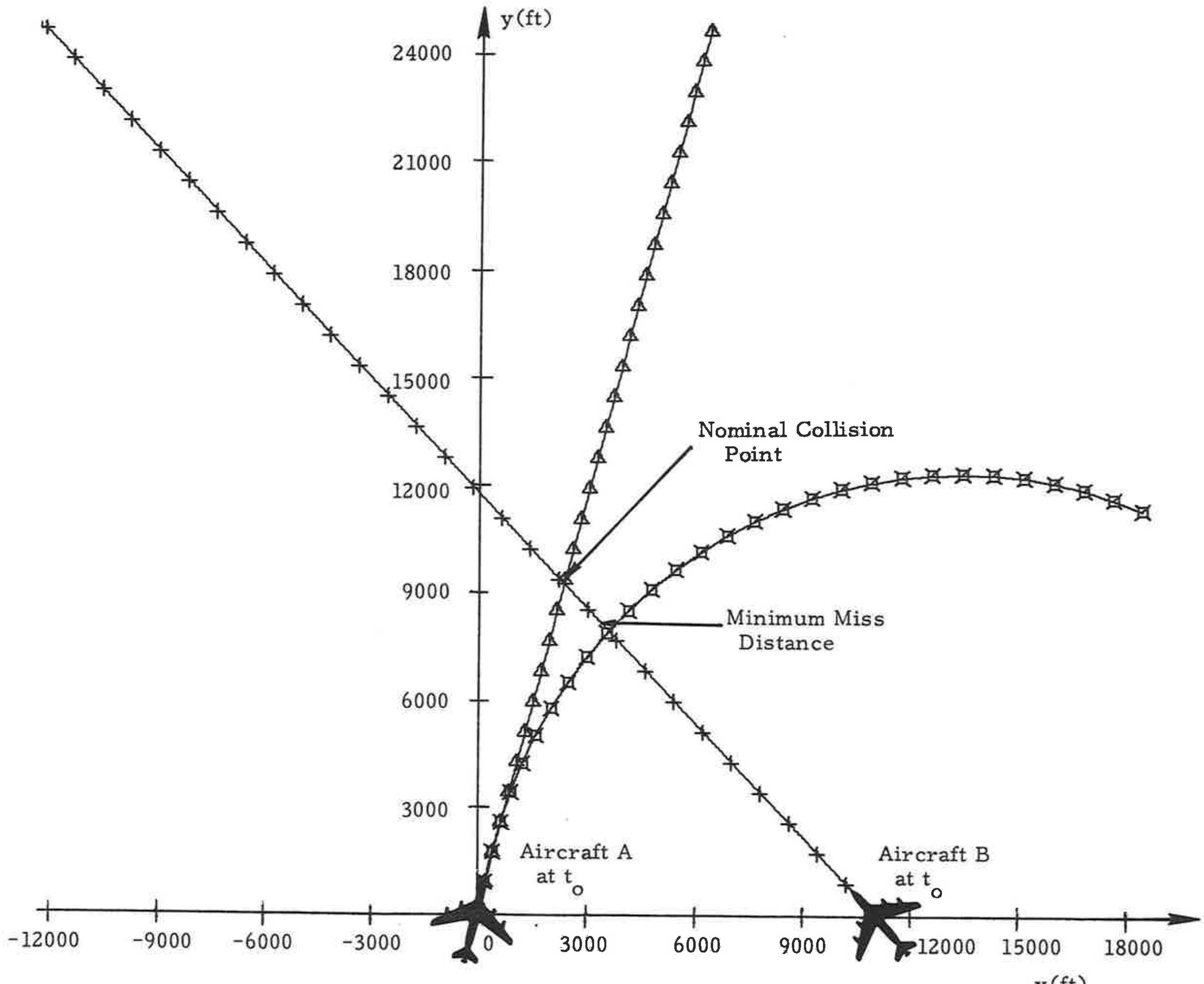

Figure 5.17 Turn Towards Maneuver for Initial Relative Bearing of 75°

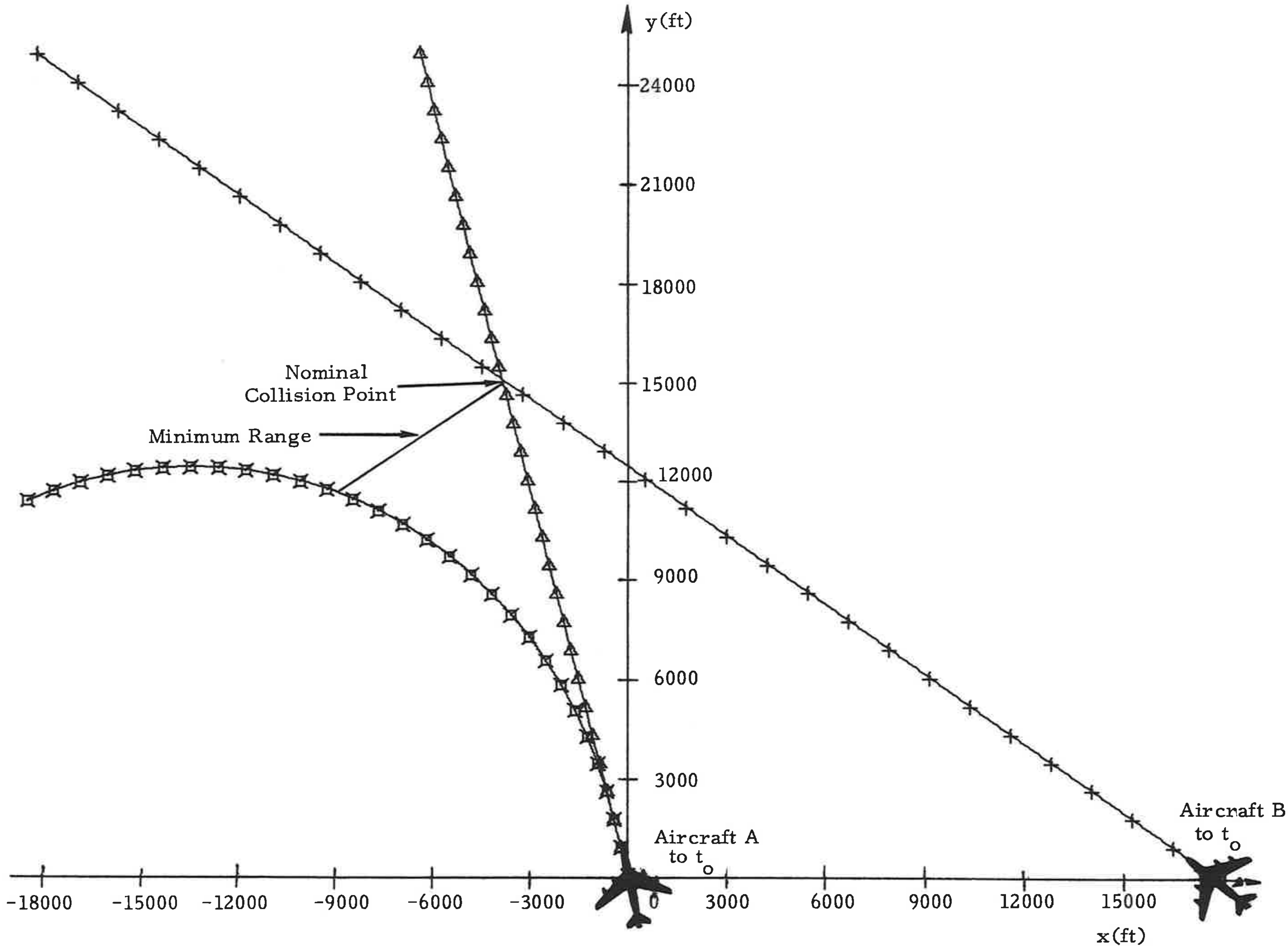

Figure 5.18 Turn Away Maneuver for Initial Relative Bearing of 105°

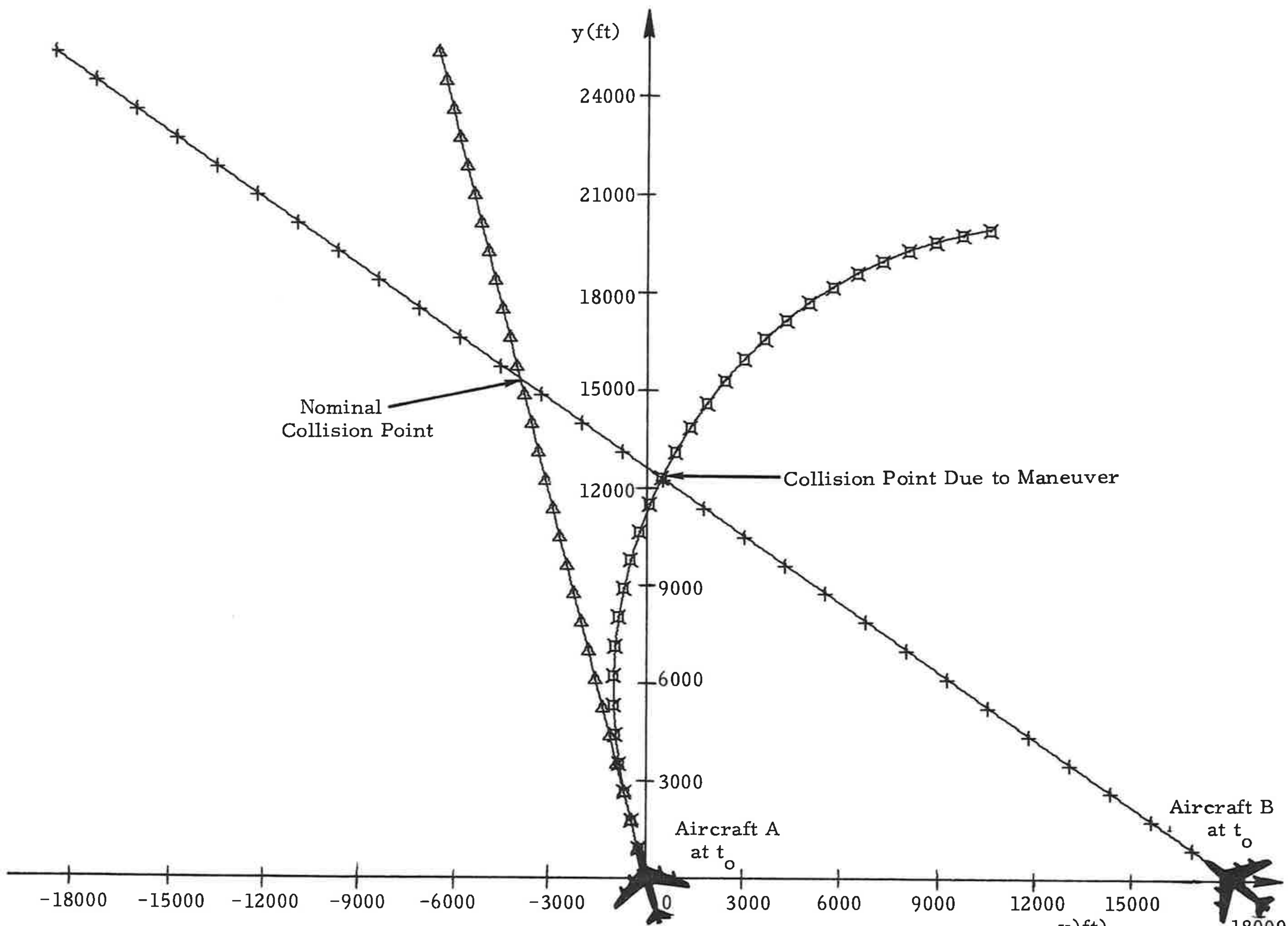

Figure 5.19 Turn Towards Maneuver for Initial Relative Bearing of 105^o

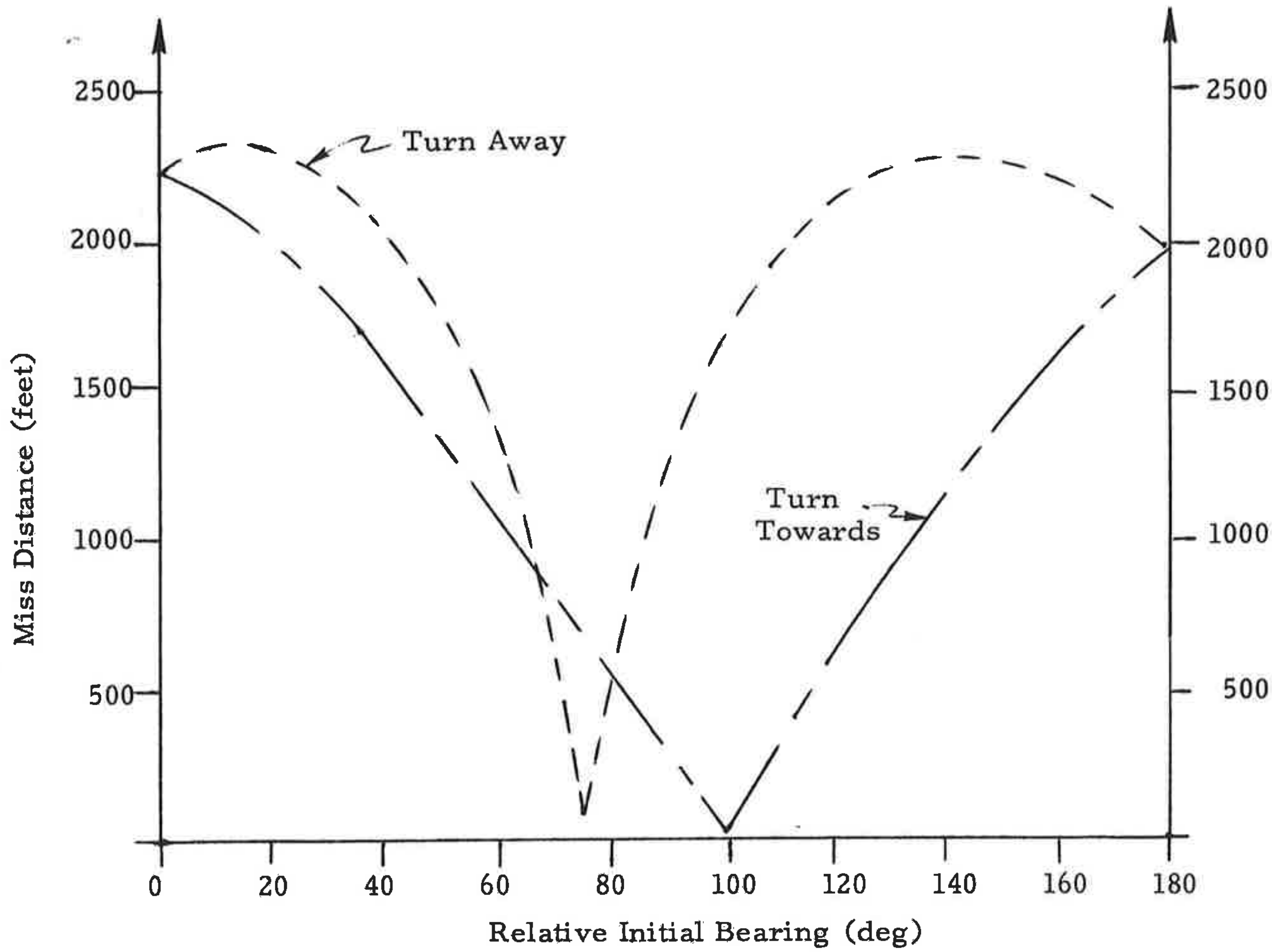

Figure 5.20 Miss Distance as a Function of Collision Geometry for Turn Away and Turn Toward Maneuvers for a Maneuver Time of 22 Seconds and Collision Geometries as Shown in Fig. 5.13

The present horizontal collision avoidance study has provided a method of constructing such charts. To indicate the relationship of these charts to the curves drawn in Fig. 5.20, the geometries associated with Fig. 5.13 are examined. The method used by this study is presented in Appendix B and discussed in Chapter IV.

For the non-cooperative situation, consider the maneuvering aircraft to be located at the origin. This implies that the turn rate ratio ω is zero and γ represents the ratio of the nonmaneuvering aircraft speed to the maneuvering aircraft speed. For the initial relative bearings indicated in Fig. 5.13, the corresponding values of γ and θ for the collision geometries are given in Table 5.2. The maneuver charts for these values are shown in Figs. 5.21(a)-(j).

TABLE 5.2

Maneuver Chart Parameters for Encounters of Fig. 5.13

INITIAL RELATIVE BEARING, β	INITIAL RELATIVE HEADING, θ	SPEED RATIO, γ
0°	180°	.2
20°	104°	.43
40°	84°	.76
60°	69°	1.11
80°	56°	1.42
100°	44°	1.69
120°	32°	1.93
140°	21°	2.07
160°	11°	2.17
180°	0°	2.20

The charts are depicted in a normalized form providing flexibility in their use. The normalization is performed such that the unit of length is represented by the turn radius of the maneuvering aircraft, which is located at the origin

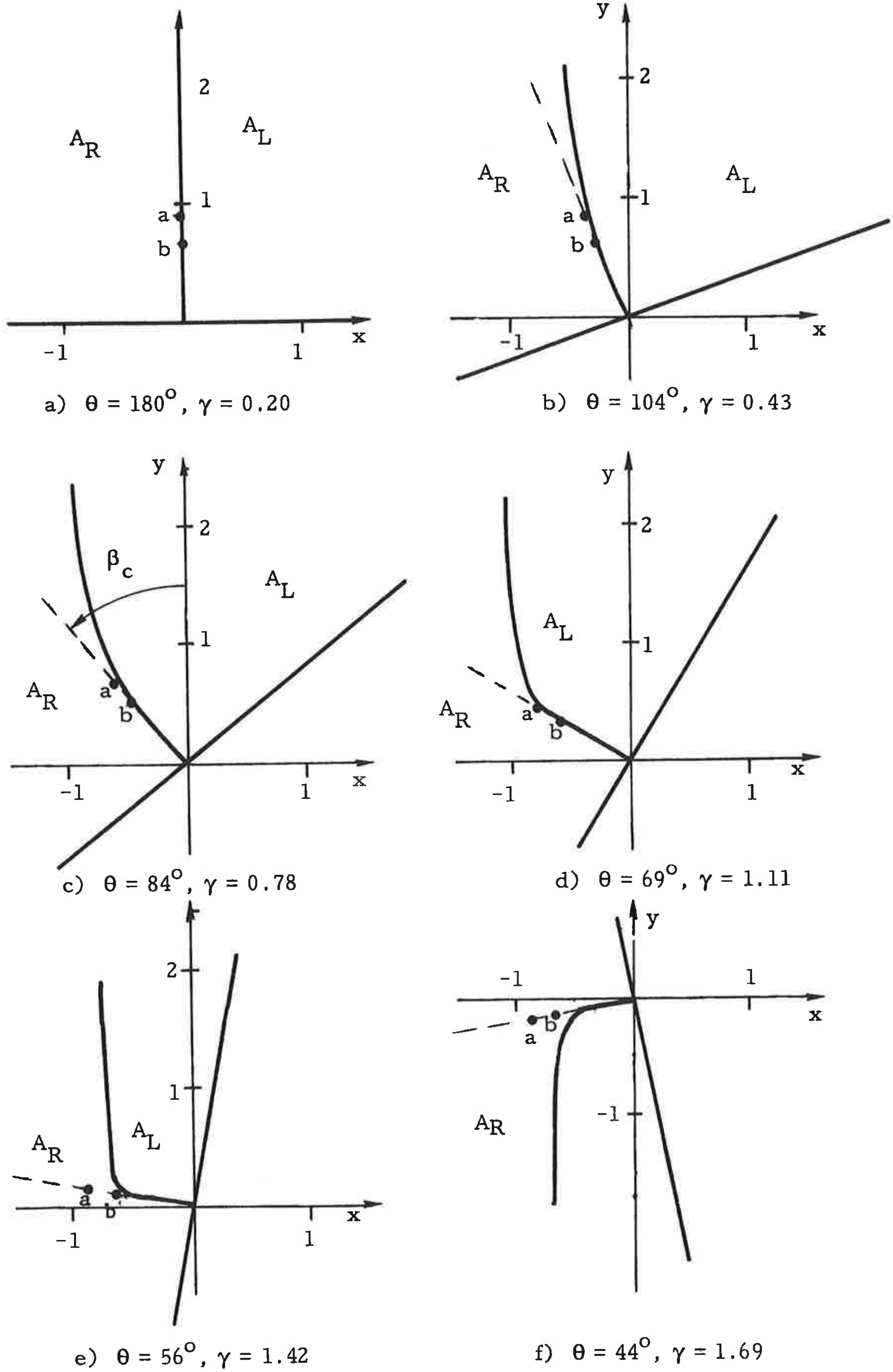

Figure 5.21 Noncooperative Maneuver Charts for Encounters of Fig. 5.13

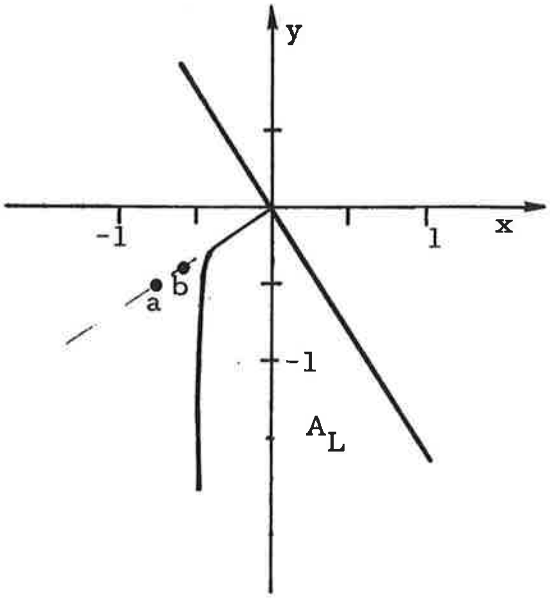

g) $\theta = 32^o$, $\gamma = 1.93$

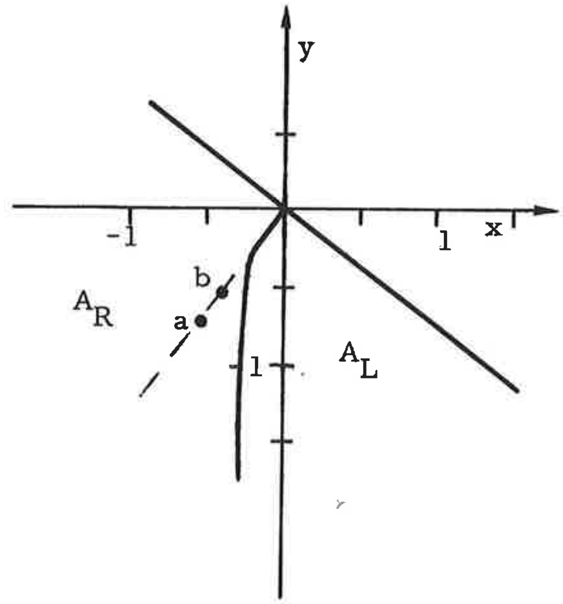

h) $\theta = 21^o$, $\gamma = 2.07$

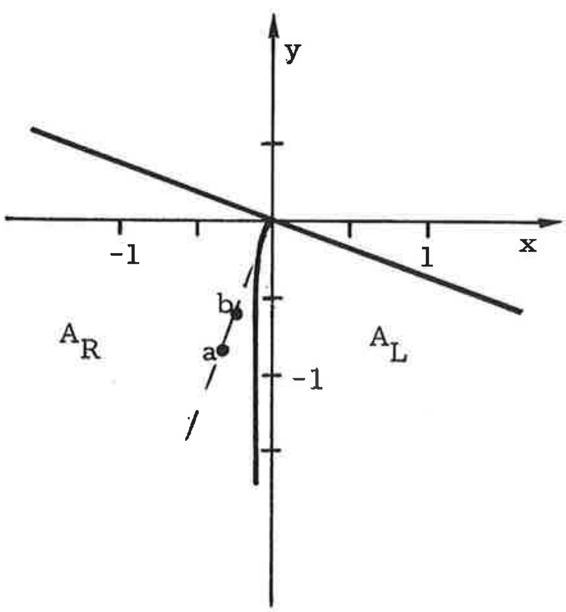

i) $\theta = 11^o$, $\gamma = 2.17$

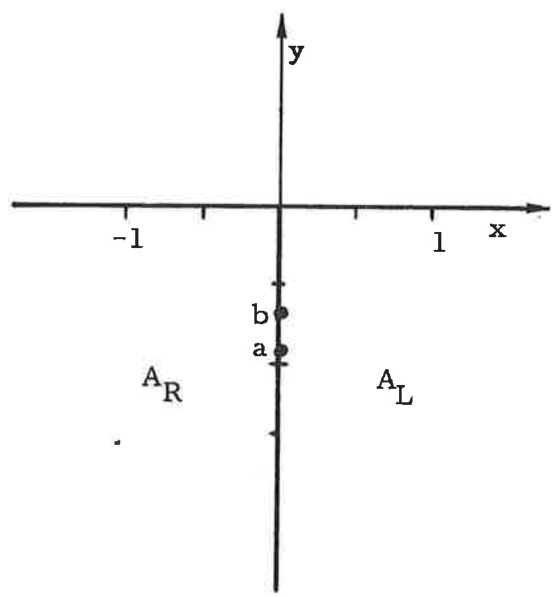

j) $\theta = 0^o$, $\gamma = 2.20$

Figure 5.21 (Continued)

of this axis system. For the specified speed of 500 ft/sec and the turn acceleration of 15 ft/sec^2, this distance is found to be 15,600 ft. Hence, a coordinate value of 1.0 on either axis corresponds to 15,600 ft. For the 22 second escape time considered in the example for Fig. 5.17, the relative distance at the collision warning time, for a relative range rate of 600 ft/sec, is found to be 13,200 feet or, in terms of the normalized units, 0.845. After the assumed 5 second maneuver delay, the relative range is 10,200 feet, or in normalized units, .655.

In the charts, the collision geometries are represented by the locus of relative positions having the relative bearing

$$\beta_c = \tan^{-1}\left[\frac{-1 + \gamma \cos \theta}{\gamma \sin \theta}\right] \tag{5.8}$$

where θ is the initial relative heading and γ is the speed ratio. This angle is indicated in Fig. 5.21(c). The two points, corresponding to maneuver initiation and the delay after maneuver initiation, are marked on each of the charts as points a and b, respectively.

The interpretation of the maneuver charts is simplified by examining their relationship to the collision geometries considered in Fig. 5.13. For any initial relative bearing, the optimum noncooperative maneuver is to turn away from the hazard. From the maneuver charts, it can be seen that each of the points lies in the region denoted as a right turn (away from the hazard) for the maneuvering aircraft, in agreement with Fig. 5.13.

As the time to escape decreases, the relative position translates toward the origin. Hence, the maneuver charts can be used for any escape time. That is, collision geometries are indicated on the maneuver charts by the initial condition along the line given by Eq. (5.8). Initial points which are close to this line represent geometries which lead to a near miss encounter. As explained in Chapter IV, it is possible from these charts to determine the optimal evasive maneuver which maximizes the miss distance. Thus, it is seen that turning toward the threat (A_L) yields maximum terminal miss distance only for relative initial positions between the switch curve and the y-axis (A's velocity direction) as shown in Fig. 5.21(a, b, c, d).

Morrel[27] also discusses the computation of the time required to achieve a parallel course. This "escape time", whether one or both aircraft turn, was expressed by Morrel as

$$t_e = t_o + \frac{r_a}{v} \csc \theta + \frac{v\theta}{a} \tag{5.9}$$

In this equation,

t_o = reaction or delay time,

a = turning acceleration,

v = airspeed,

r_a = required minimum distance if only one aircraft turns (half of this if both turn),

θ = angle between the aircraft tracks, or initial heading difference if only one aircraft turns (half of this if both turn).

The relationship of these quantities is shown in Fig. 5.22. The time given by Eq. (5.9) represents the total effective maneuver time required to allow the aircraft to maneuver to a parallel track offset by a distance r_a. Furthermore, the parallel offset track is such that the aircraft flight paths do not intersect.

To indicate the misleading label attached to this quantity, defined by Morrel as "escape time", consider the following example, shown in Fig. 5.23. Aircraft A, which maneuvers, is flying at 500 ft/sec and aircraft B, which does not maneuver, flies at 215 ft/sec. Their initial relative heading is assumed to be 104^o. Hence, they have a closing speed of 600 ft/sec. Aircraft A is assumed to have a turning acceleration of .5g, and the required minimum miss distance is 2000 feet. From Eq. (5.9), with an 8 sec delay time, t_e is found to be

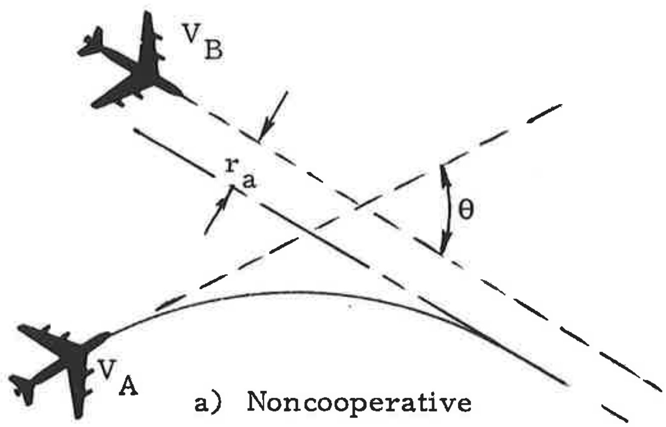

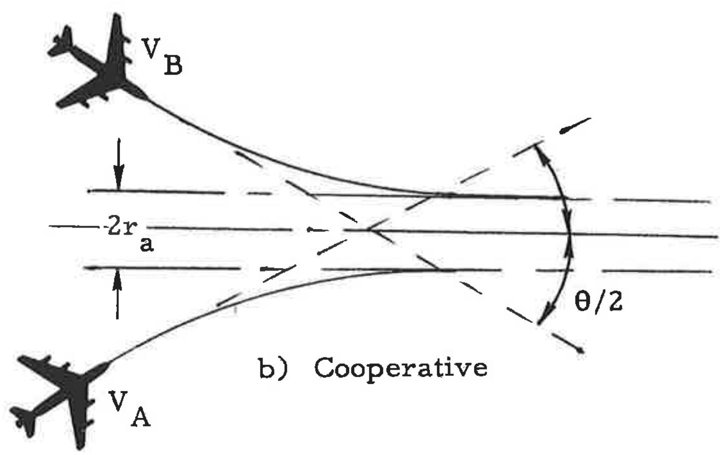

Figure 5.22 Geometry for Morrel's "Escape Time" Computation

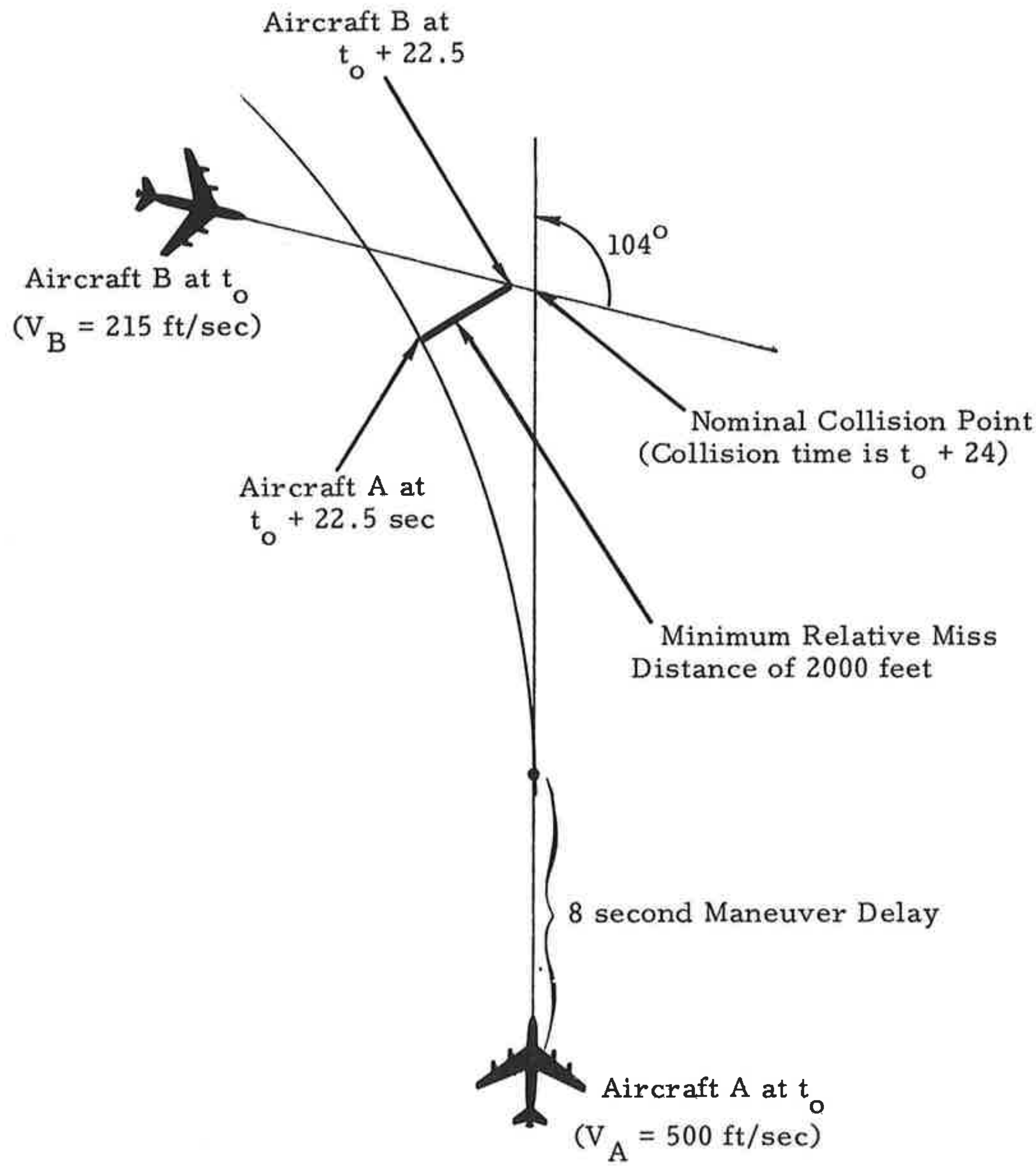

Figure 5.23 Illustration of Fact That Aircraft A Does Not Have to Turn to a Parallel Offset Track to Achieve 2000 ft Miss

$$t_e = 8 + 4.13 + 41.4 = 53.53 \text{ secs}$$

If aircraft A were to wait until a 0.5g maneuver is just sufficient to provide the required 2000 ft miss distance, the "escape time" is much smaller, as indicated by Fig. 5.23. Again, with no maneuver and the 8 sec delay time, the time to collision is 24 secs. A minimum miss distance of 2000 feet is achieved 22.5 secs after the maneuver begins. The two maneuvers are directly compared in Fig. 5.24, which clearly indicates the large time and space difference.

Although the time computed in Eq. (5.9) is sufficient to provide a parallel track separation of r_a, it does not represent a minimum escape time to just provide the minimum aircraft separation of r_a. Generally, the actual minimum escape time will be less since the second and third terms in Eq. (5.9) are unrelated to the requirements. The second term is the time required to traverse the "danger zone" in straight flight, and need not be computed. The third term is also somewhat larger than absolutely necessary. That is, the maneuvering aircraft need not avoid the entire trajectory of the other, and therefore it is not necessary to align the velocities in order to achieve the desired minimum miss distance.

The actual miss distance achievable using the time given by Eq. (5.9) is indicated more clearly in Fig. 5.25. If the collisioin is to occur at position 1, using the same example cited above, then for aircraft A to maneuver to the parallel offset track it must be at position 2 at the beginning of the maneuver, and aircraft B must be at position 3 (this assumes an 8 second delay time). This geometry indicates a time of approximately 36.6 seconds prior to collision. This time more accurately represents the warning time for aircraft A to maneuver to the parallel offset. The actual minimum miss distance occurs approximately 31.4 secs after the escape maneuver initiation. This time is more accurately the escape time. It is of interest to note that the actual miss distance using the left turn maneuver is approximately 5000 feet in comparison to the desired 2000 feet separation. The discrepancy occurs because Eq. (5.9) is based on requiring that the aircraft trajectories never become closer than 2000 ft, while the maneuver charts derived in this study are used to require that the aircraft never become closer than this distance.

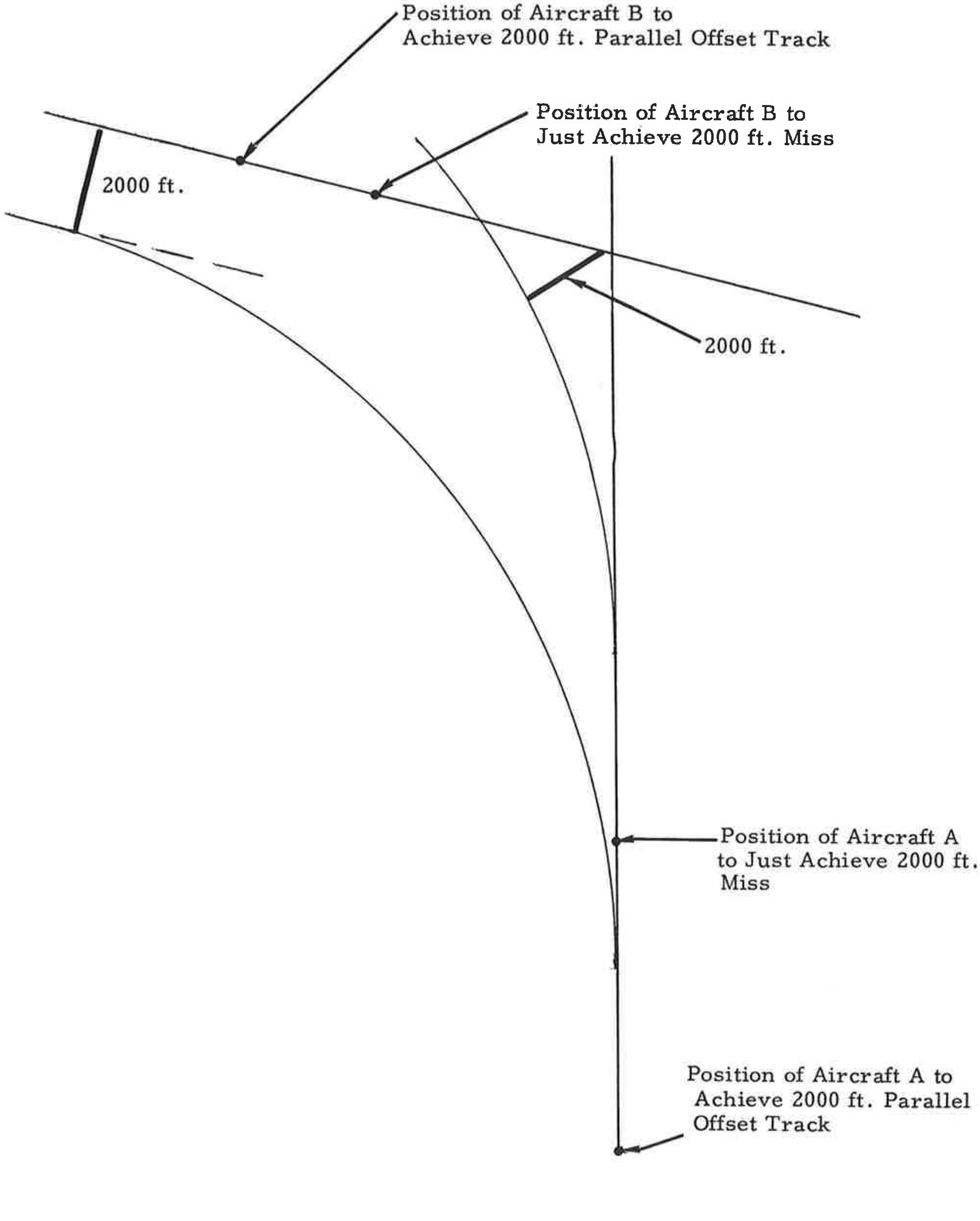

Figure 5.24 Aircraft Initial Positions to Achieve a 2000 Ft. Miss Distance and a 2000 Ft. Parallel Offset Track

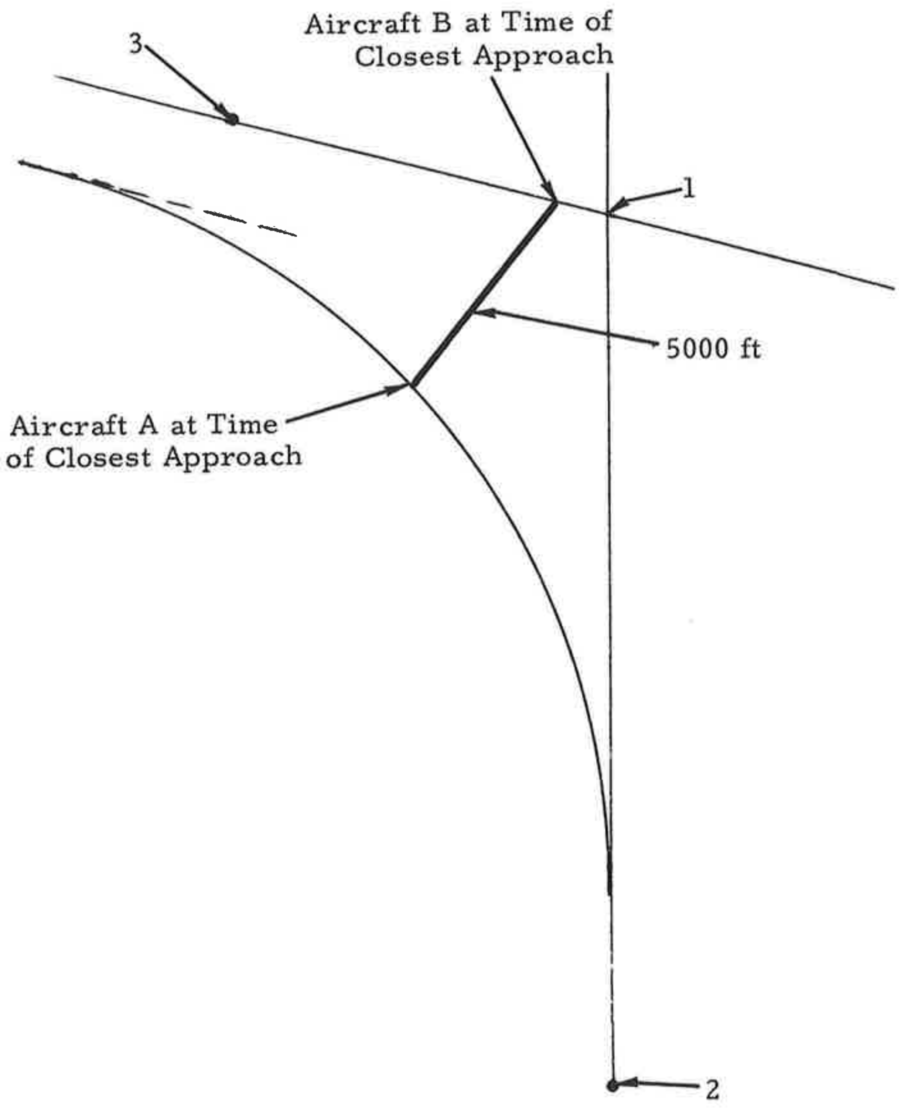

Figure 5.25 Relationship of Maneuver Time and Escape Time

In his paper, Bolie[69] defines a horizontal escape maneuver for the threatened aircraft as a constant acceleration lateral turn away from the initial location of the hazard. For certain geometries and speeds, the effect of this type of a maneuver is merely to delay the collision which occurs at a later time, as is pointed out previously. Bolie's study leaves the distinct impression that this type of maneuver is the only maneuver available for lateral turns to avoid collision. Consider the collision geometry in Fig. 5.26. The parameters for this example were selected to satisfy the equations Bolie developed. Here, the maneuvering aircraft is assumed to have a speed of 600 ft/sec (356 knots) and a turn acceleration of 0.5g. With no maneuvers, the collision is assumed to occur in 20 secs, and the delayed collision, as a result of the turn-to-parallel maneuver, occurs at 30 secs. The relative heading θ is 58.5°, the speed of the nonmaneuvering aircraft is 800 ft/sec (474 knots), and the relative bearing at the initiation of the maneuver is computed to be $\beta = 74.9^{\circ}$.

Maneuvering the aircraft toward the hazard actually maximizes the miss distance. The miss equals 1000 feet and occurs at a time of 17 seconds after the initiation of the maneuver. This is a turn-to-crossing maneuver, and is the optimal, horizontal maneuver for this geometry. An attempt by the maneuvering aircraft to achieve this same miss distance in the vertical plane would require an extremely high climb rate capability of 3000 feet/minute. Here, both the horizontal and vertical maneuvers are assumed to begin at 20 seconds prior to the predicted collision point.

5.3.2 Cooperative Encounters

Morrel[27] acknowledged the added difficulty of cooperative maneuver analysis due to the additional degree of freedom introduced by the maneuverability of both vehicles. The numerical method used by Morrel required specializing the geometry to the collision condition, and tabulating the miss distance resulting from certain assumed turning maneuvers. This did not lead to a compact and general way of presenting the results. It also did not account for the possibility of two-part maneuvers for the slower aircraft, as discussed in Chapter IV.

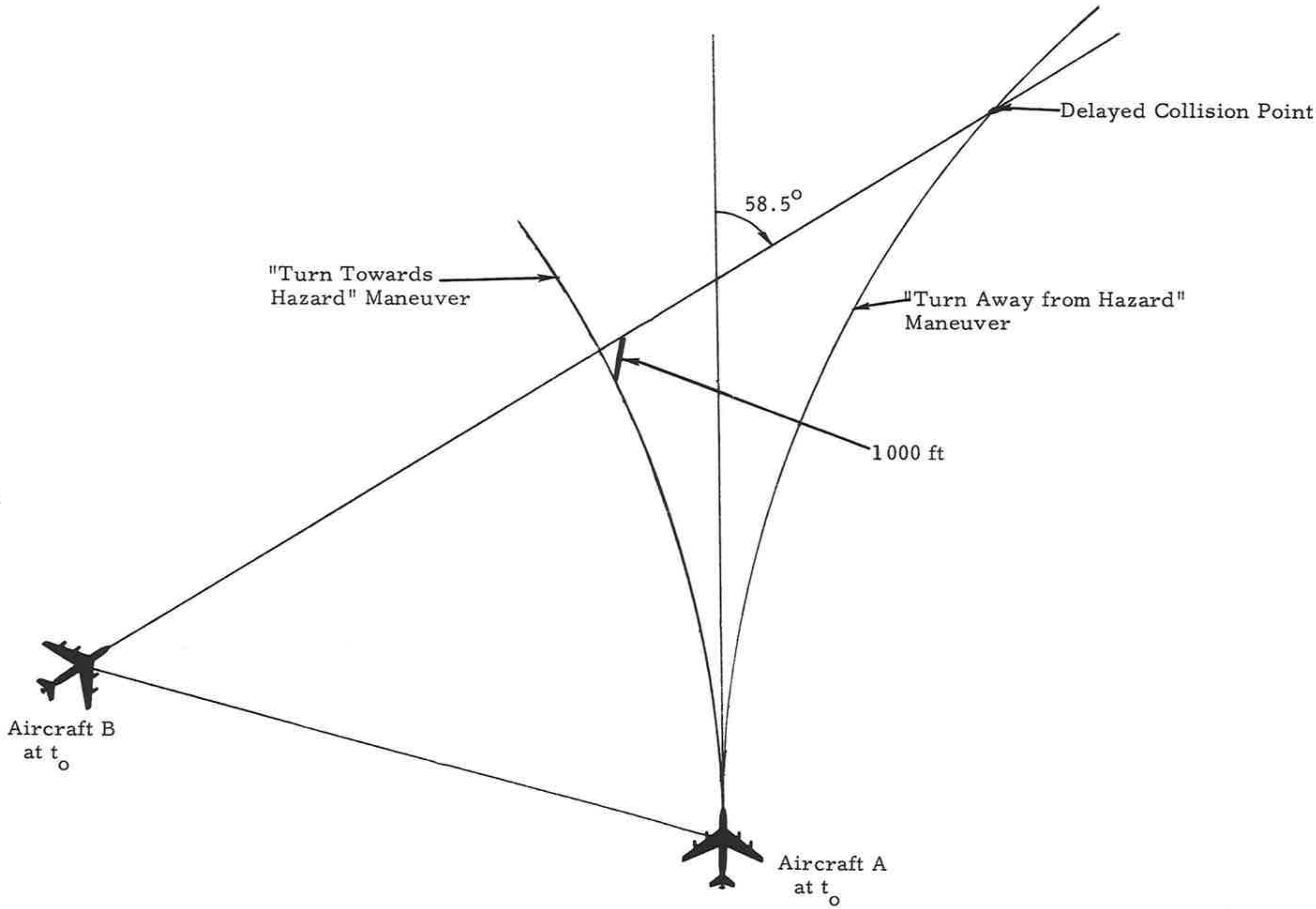

Figure 5.26 Comparison of "Turn Towards" and "Turn Away" from Hazard Collision Avoidance Maneuvers

Morrel presented a relative space chart indicating the motion of one aircraft relative to the other aircraft when both are maneuvering. Figure 5.27 indicates the achievable miss distances using various cooperative maneuver strategies for the collision geometries depicted in Fig. 5.13. For comparison purposes, the uncooperative maneuver miss distances are also included. Note that for the collision geometries considered here, the initial range is large enough so that it is almost always better for the aircraft to turn away from each other, in opposite directions.

Now consider the maneuver charts in Appendix C corresponding to $\omega = 1$, for which the turn rates are equal. For a speed ratio $\gamma = .3$, the collision geometry corresponds to an initial relative bearing of 12^{o} and initial relative heading equal to 124^{o}. For this speed ratio, the most appropriate available maneuver chart is that corresponding to a relative heading, θ, of 120^{o}, shown in Fig. 5.28. The collision point corresponding to the 22 second escape time is observed to be close to the dispersal point (the point at which the terminal miss distance can be achieved using three different maneuver pairs). From Fig. 5.28, for an initial relative bearing of 12^{o}, it is seen that the miss distance is almost identical for the three maneuver pairs, with the strategy $A_R B_R$ providing the largest miss. This result is in agreement with the corresponding maneuver chart.

The purpose of this example is to show that Morrel's curves are a subset of the results contained in the charts of this study. That is, in Morrel's study, a representative choice of collision-course initial conditions (range, bearing, and heading) is associated with a particular set of optimal maneuvers. This initial condition is only <u>one</u> point on a maneuver chart of the type in Chapter IV, which shows the proper maneuvers for <u>all</u> initial conditions.

The collision triangle formed by the components of the relative velocity can be used to derive other conclusions related to the nonmaneuvering motion. As shown in Fig. 5.29, for example, the miss-distance r_f is related to the initial range r in the same way that normal relative velocity V_θ is related to the total relative velocity, $V = |\underline{V}_B - \underline{V}_A|$. That is, similar triangle arguments show that the miss distance in unaccelerated flight is

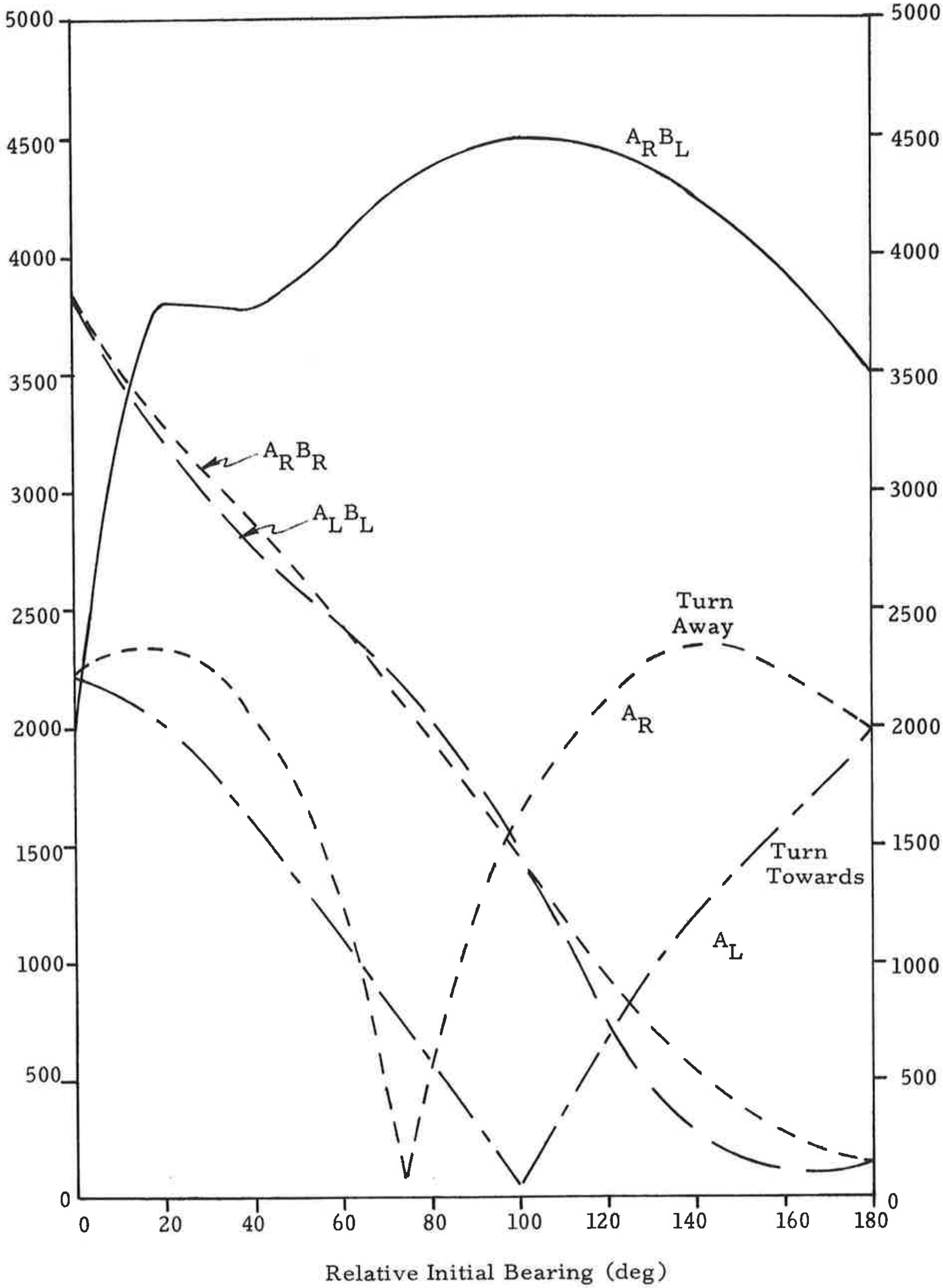

Figure 5.27 Miss Distance as a Function of Collision Geometry for Cooperative and Uncooperative Systems for a Maneuver Time of 22 Seconds for the Collision Geometries Shown in Fig. 5.13

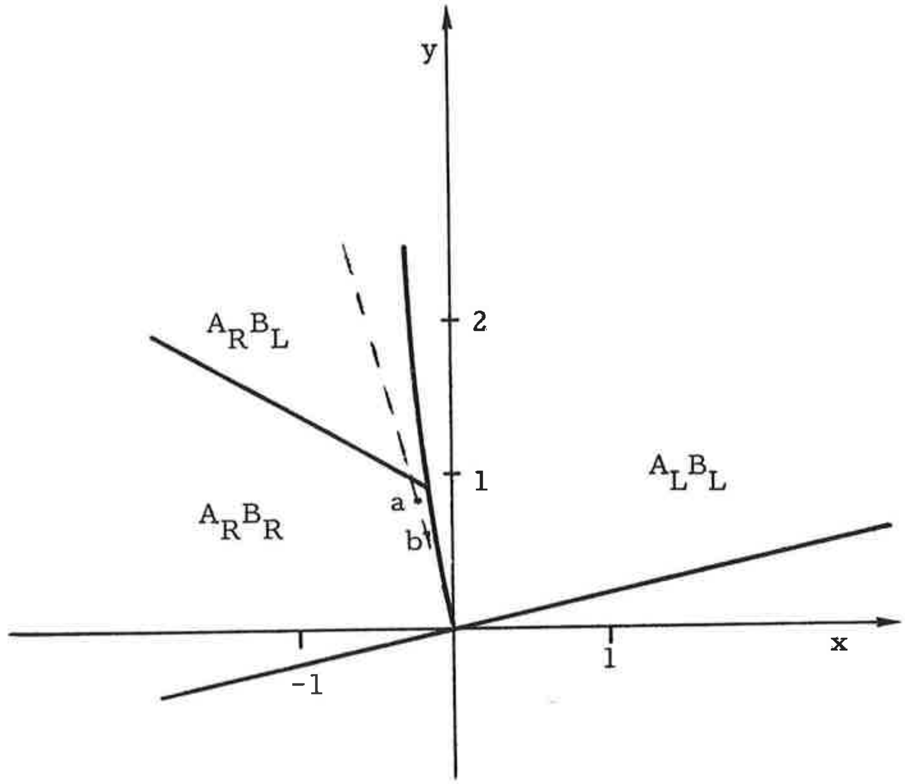

Figure 5.28 Cooperative Maneuver Chart for $\omega = 1.0$, $\gamma = 0.3$, and $\theta = 120^{\circ}$

$$r_f = r(V_\theta / V)\,. \tag{5.10}$$

The time-to-minimum range for rectilinear motion of both aircraft is then derivable in terms of the range and velocity components. This has been shown by Morrel to be

$$t_f = r\, V_r / V^2 \tag{5.11}$$

The ratio of range to range-rate, however, is defined as "Tau", [10,11] and, therefore,

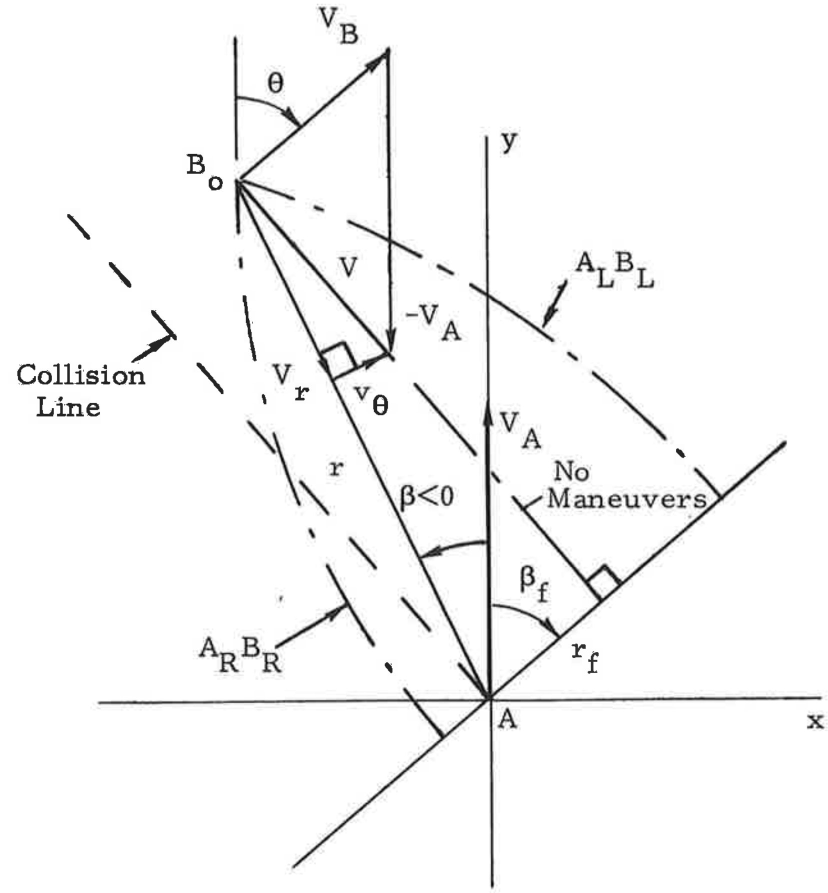

Figure 5.29 Relative Motion When $\omega_A = \omega_B$

$$\tau = r/V_r = t_f(V/V_r)^2 \geq t_f \tag{5.12}$$

This inequality shows that the "Tau" estimate of the time-to-go is actually optimistic, and that minimum range for no maneuvers actually occurs <u>before</u> the time $\tau = r/V_r$.

It is frequently stated[3,13] that horizontal maneuvers are impractical because of the inaccuracy in estimates of the normal velocity, V_θ. The miss distance in unaccelerated flight is related to the current range according to Eq. (5.10). This equation is not sufficiently accurate in practice, because the normal relative velocity V_θ is extremely small when the range r is extremely large. In other words, V_θ and r_f are accurately known only when the range r is so small that a collision is imminent. If the encounter is assumed to be cooperative, however, such that speed and heading information is exchanged, the miss distance can also be computed from the equation

$$r_f = r \cos(\beta_f - \beta) \tag{5.13}$$

where the final bearing can be computed in terms of the speeds and the initial heading, i.e.,

$$\cos \beta_f = \frac{V_B \sin \theta}{\sqrt{V_A^2 + V_B^2 - 2V_A V_B \cos \theta}}$$

Thus, in place of using the inaccurate time-derivative $V_\theta = r\dot{\beta}$ to compute the miss distance, according to Eq. (5.10), this distance can be found in terms of the current values of range, bearing, and relative heading, using Eq. (5.13).

Horizontal collision avoidance maneuvers have been analyzed and discussed in many sources.[12,27,68,71,76] The turn-maneuvers in most of these sources are specified on an intuitive basis, as functions of the relative bearing alone.[12,27,37] This is because the angular location of a potential threat is the most natural relevant data for this purpose. On the other hand, other sources[2] give suggested avoidance maneuvers as functions of relative heading alone.

Typical recommended evasive maneuvers are the following:

1. Opposite turns when $|\theta| < 90^\circ$, same turns when $|\theta| > 90^\circ$.[2]

2. Maximize bearing rate.[12,57] This means turning toward the threat when the threat is to pass in front, and turning away otherwise.

3. Maximize $r/\dot{r}$ = Tau.[37,60,61] This means turning away from the current position of the threat, and it is optimal only if the threat is at rest.

4. Turn right when the threat is in front, $|\beta| < 90^{o}$, and left when $|\beta| > 90^{o}$.[27]

5. Turn to cause a counter clockwise rotation of the sight line.[57,63]

All of these recommended maneuvers give acceptable miss distances under <u>some</u> geometric and kinematic conditions, but all of them fail to do so under other conditions, as well.

Evasive maneuvers should depend in some way upon the relative range. Various examples can be used to show that the maneuvers must also vary with the speed and maneuver capability of the other aircraft. These physical arguments, including the effects of cooperation, have been unified in the results given in this study. It has been proven, using simplified but realistic dynamic models of the relative motion, that "rules of the road" <u>cannot</u> be expressed in terms of only one or two variables. Attempts to do so have been based on unrealistic assumptions concerning available acceleration magnitudes.

In summary, previous work has attempted to determine the general horizontal maneuvers required to avoid midair collisions. These previous results are difficult to understand, treat only very specific pairs of initial conditions, and often have resulted in incorrect conclusions. Also, many of these results are not at all applicable to deriving workable CAS maneuver algorithms. For these reasons, the general results of Chapter IV represent absolutely essential information for further development and analysis of conflict resolution and collision avoidance systems.

VI. MECHANIZATION REQUIREMENTS

Several interdependent factors must be considered in order to derive the mechanization requirements for a CAS. These include whether the system is to be airborne or ground based, the interface with ground controllers and the air traffic control system (ATC), the quality of the measurement system and the associated data update rates, and whether the system is capable of handling several threats simultaneously.

The requirements and algorithms discussed in the following sections are based on a specific scenario constructed from combinations of the above mentioned factors. It is assumed that the algorithms are to be implemented in an airborne system--or more specifically, in a transport plane or large business aircraft. More sophisticated versions of these algorithms can be implemented if the system is to be ground-based, owing to less stringent cost, weight, and power constraints. For noninterfering operation with the air traffic control (ATC) system using either ground controllers or the proposed intermittent positive control (IPC) system, it is necessary that the airborne system detect only those threats that are within the relevant airspace's separation standard and have not been adequately dealt with by the ATC system. On the other hand, the coverage zone must be adjustable for adequate protection in all phases of the flight. This requirement poses a difficult measurement problem.

The general hardware and software requirements of the airborne computer are first detailed. Then, two specific algorithms--a digital filter for estimating relative heading and speed and an algorithm for computing the maneuvers--are examined. Finally, overall hardware requirements are summarized. In this chapter, the airborne algorithms that are investigated are adequate only for two-plane encounters in non-restricted airspace, although straightforward extensions allow several planes to be handled. These examined algorithms, though typical, assume a specific scenario and take advantage of some of the features peculiar to that scenario.

6.1 COMPUTER REQUIREMENTS - HARDWARE/SOFTWARE

In order to specify onboard computer requirements for implementing a horizontal CAS, several factors must be considered. Some of the more important are:

a) Input interface specification in terms of data rates and signal characteristics.

b) Output interface and display subsystem specification.

c) Main software algorithms described in terms of function, core space, accuracy, computation time, and sampling time.

d) Support software available for the system selected in terms of ease of programming, debugging, and other program development tasks.

e) Computer architecture requirements, e.g., microprocessor or miniprocessor.

f) Adequate instruction set.

g) Memory size, page size, and addressing modes.

h) Cost/power/weight and volume tradeoffs.

Selection of a specific computer system for airborne collision avoidance would entail a detailed comparative analysis of the present "state-of-the-art" in terms of the above mentioned factors. Such an analysis is beyond the scope of the present study. Nonetheless, certain general statements regarding these factors can be made as the first step of a comparative analysis.

6.1.1 Input Interface

Appropriate interfaces must be designed to efficiently transfer range, bearing, and other data pertaining to all the threat aircraft to the computer memory in a convenient format. Important considerations are input buffer word length and size, data sampling rate and synchronization signals, automatic (vectored) priority interrupt capability, and direct memory access at sufficiently high data rates.

On activation of certain control lines, it should be possible to sample data buffers containing data transmitted from a particular threat aircraft such as static pressure (to determine relative altitude), pitot pressure (to determine relative airspeed), and other data such as heading and bank angle, if these are to be exchanged rather than estimated. Appropriate decoding and synchronization logic, together with analog-to-digital converters, will also be required for this interface.

Finally, interface slots must be set up to input own aircraft's speed (or pitot pressure), heading, and altitude (or static pressure), Depending on the type of instrumentation onboard and sampling requirements, additional analog-to-digital interfaces and control lines may be necessary.

6.1.2 Output Interface/Display System

After determining the appropriate maneuver for a given threat, the manner in which this information can be effectively displayed to the pilot must be considered. The first choice to be made is whether the display should be expandable to represent maneuvers for more than one consecutive threat. The display options on an electromechanical display are fixed, whereas an electronic (programmable) display (e.g., alphanumeric/graphic, CRT) is quite flexible. Also, the output interface for an electronics display is generally cheaper due to compatible voltage/current levels, and "high power" display drivers are not required. Human factor considerations include legibility of display, refresh rates for a steady image, and brightness control. Depending on the type of display, output data buffers, control/sychronization lines, and digital-to-analog converters may or may not be required.

6.1.3 Main Software Algorithms

The collision avoidance software can be partitioned into several main algorithms. These include: (a) speed-ratio computation, (b) altitude computation, (c) bearing and range data smoothing, (d) speed ratio and heading estimation (necessary if data is not exchanged), (e) threat priority ordering, (f) avoidance maneuver generation, (g) maneuver performance monitoring, (h) return-to-track command generation, and (i) display message generation and driver program. Algorithms and computer requirements for the estimation of speed ratio and heading based on smoothed bearing and range measurements and for the generation and monitoring of avoidance maneuvers between two aircraft are of particular interest to the present study and are considered in Sections 6.2 and 6.3, respectively. The remaining algorithms are discussed in this section.

The pressure at various places on the aircraft's skin is slightly lower (or higher) than the free-stream pressure by an amount called the static defect s_D which depends on sensor location, speed, altitude, and angle-of-attack. If the pitot pressure p_p, static pressure p_s, and static defect s_D are digitized and transmitted, then the speed ratio of aircraft A and B can be determined from the equation

$$\left(\frac{V_B}{V_A}\right) = \left[\left\{\left(\frac{p_{pB}}{p_{sB} s_{DB}}\right)^{1/3.5} - 1\right\} \Big/ \left\{\left(\frac{p_{pA}}{p_{sA} s_{DA}}\right)^{1/3.5} - 1\right\}\right]^{1/2} \qquad (6.1)$$

Interestingly enough, the speed ratio is independent of standard day temperature T_o, pressure p_o, and temperature lapse rate k. Consequently, the ratio can be determined to within 1%. Because the range over which the ratio may vary is quite limited, digitization errors should be negligible.

Altitude of the threat aircraft can be determined from a transmitted digitized pressure transducer readout. Diaphragm, piezoelectric, and semiconductor transducers (compatible with solid state A/D converters) are readily available. Pressure altitude h can be determined from the equation

$$h = \frac{T_o}{k} \left[1 - \left(\frac{p_s s_D}{p_o} \right) \right]^{Rk} \tag{6.2}$$

where T_o and p_o are standard day sea level temperature and pressure, k is the temperature lapse rate (3.5°F/1000 ft.), and R = 53.3 ft/°F. From Eq. (6.2), it is apparent that errors arise because of nonstandard day conditions, variations in lapse rate k and approximations in static defect s_D.

When more than one aircraft poses a threat, it is necessary to have a criterion for arranging these threats on a priority basis. In the past, this has generally been done using the Tau criterion[11,27] which is given by the ratio of range to range rate, but it is exact only for a collision geometry. Another priority ordering criterion, having the advantage of being exact, can also be used; several threats would be ordered on the basis of "time-to-minimum-range". The major disadvantage of this criterion would be increased computational load.

After the threats have been ordered on a priority basis and the maneuver algorithm has determined a sequence of maneuvers such that no future conflicts are generated, an appropriate sequence of messages must be generated for display to the pilot. Several logic tests must be performed prior to driving the display to check for contradictions or inconsistency in the mesage sequence. This is mainly due to the fact that some of the commands are positive (e.g., turn right) while others may be negative (e.g., don't turn left).

Notable for their absence in the above description were important parameters such as core space, accuracy, computation time, and sampling time. These parameters are highly dependent on the actual hardware system and are beyond the scope of the present study.

6.1.4 Hardware Features

The first hardware decision to be made is architectural--is a microprocessor or a miniprocessor more suitable for airborne collision avoidance with regard to cost, computation time, core space, and instruction set?[77-82] Essentially, the microprocessor is a one, four, or eight bit machine with a weaker instruction set. Consequently, it uses approximately four to eight times as much memory and is about four to ten times slower than a sixteen bit miniprocessor. A preliminary technical evaluation in terms of the above mentioned factors indicates that for airborne collision avoidance, a miniprocessor would be more appropriate.

Hardware features considered essential for the present application are fixed point hardware multiply/divide instruction, two's complement arithmetic, minimum 1024 word page, parity, memory protect, sixteen bit instruction/data bus, vectored priority interrupts, real time clock, direct memory access, A/D interface, hardware index registers, automatic restart and standby power, modular construction for easy maintenance, add time less than 4 μsec, and multiply time less than 24 μsec.

Hardware features considered optional but useful from an upgrading and programming viewpoint are floating point hardware multiply/divide, all memory directly addressable, memory expandable to 32K, stack architecture, and a micro-programmable control unit. Other hardware considerations are power, weight, volume, and ruggedness.

6.1.5 Instruction Set and Software Considerations

Most of the hardware features outlined in the previous section can be interpreted in terms of the versatility of the instruction set. The instruction set of any computer can be categorized into the following classes: (a) load, store and transfer; (b) arithmetic; (c) logical; (d) shift; (e) bit/byte manipulation; (f) branch; (g) interrupt; and (h) input/output. If the instruction repertoire is partitioned into these categories, the number of instructions in each group is indicative of the richness of the instruction set. Transfer, shift, bit manipulation and input/output instructions are particularly important for the collision avoidance application.

Besides the instruction set, the quality of the support software must also be considered. Some of the main packages that must be available are assemblers (generally two pass), utility programs/editors, debugging aids, loaders, and executive programs. Other packages that speed up the programming effort but are not essential include cross assemblers, compilers, standard math routine packages and a real time executive.

The availability of higher level language compilers does not imply their unqualified use, even with the potential reduction in program development time. Compiler-generated code is generally inefficient except for stack architecture machines. Assembly language remains the best approach for producing tightly-coded tasks.

6.2 DIGITAL FILTERING FOR STATE ESTIMATION

The information requirements of a horizontal collision avoidance system, based on the results of Chapter IV, are measurements of relative position, airspeed, and heading of the two encountering aircraft. In an encounter for which only one aircraft is equipped with a collision avoidance system and no communication link connects the two, direct measurements are not available of the airspeed and heading of the threatening aircraft. Such a situation could arise in a conflict between a commercial aircraft and a general aviation aircraft.

When airspeed and relative heading are not directly available, it is possible that they can be estimated from range and bearing measurements using digital filtering based on estimation theory techniques. This may be desirable even if direct measurements of all the required parameters are available (using, say, transponder techniques) because the measurements will be in error by some amount due to inaccuracies in the measurement sensors, the signal processing instrumentation, and the signal propagation characteristics of the atmosphere. The accuracy of these estimates is dependent upon the quality and characteristics of the range and bearing measurements.

This section describes the results of a preliminary investigation which was made of the application of estimation techniques to the signal processing problem. The purpose was to determine how well the estimation techniques can be expected to work and how their performance degrades with increased measurement errors.

Two possible estimators (filters) were studied based on the following assumptions:

1. The motion of the two aircraft is in the horizontal plane;

2. The aircraft do not maneuver during the tracking period;

3. Both aircraft maintain constant airspeed;

4. Independent measurements are available to the tracking aircraft of the relative range and bearing of the other aircraft;

5. The sampling rate at which the measurements are obtained is constant;

6. The tracking data was corrupted by white noise having Gaussian statistics.

More complex models of the measurement process, including measurement bias, quantization error, and correlated noise, are certainly possible as are more realistic representations of the signal characteristics. The possibility that the tracked aircraft might be turning could also be accounted for in the filters. However, a compromise must be made between the resulting filter complexity and an adequate representation of the physical processes being modeled. It was felt that the more important characteristics of the measurement errors are included in the white noise assumption. The essential features of the estimation problem are still retained without being obscured by the additional complexity dictated by a more refined measurement model. The intent here was to examine the basic feasibility of digital filtering to obtain relative heading and airspeed estimates. These are obtained from a discrete-time sequence of noisy measurements of the intruding aircraft's range and relative bearing.

There are several approaches which can be taken to solve this problem. In order to get a feel for the complexity and performance that can be expected, only two of the simpler approaches were investigated in detail. Conditioned on this experience, other more promising approaches can be proposed and studied.

Because the relative motion of the two nonmaneuvering aircraft is a straight line, a very simple estimator (filter) can be obtained by fitting a line using the least-squares criterion to the noisy range and bearing measurements in either line-of-sight or Cartesian coordinates. Estimates of relative position, airspeed, and heading can then be computed from the parameters specifying the line. This filter is called the least-squares smoothing (LSS) filter. It is similar to a linear regression filter which has been proposed for radar tracking of manned targets.[83] A similar algorithm was used in a study of the Discrete Address Beacon System.[84] As the LSS filter requires only the solution of a set of four linear equations followed by a nonlinear transformation for each time point that an estimate is desired, its principal advantage is simplicity and low computational requirements. Both the LSS filter and the filter described next are discussed in more detail in Appendix E.

At another level of complexity, linearization of the dynamics and measurements and application of the well-known linear theory[85] results in the so-called extended Kalman (EK) filter. Under certain conditions, quite good performance can be expected from this filter; however, it is extremely sensitive to initial condition and modeling/linearization errors which in many applications result in so-called filter divergence. In general, improved performance and better ability to track a slowly maneuvering aircraft can be expected from the EK filter over the LSS filter. This improvement is at the expense of additional complexity and increased computational load.

To evaluate the performance of the two filters, a Monte Carlo simulation of the encounter dynamics and the filters was exercised for a variety of encounter geometries, sampling rates, speed ratios, and instrument qualities (noise statistics). Both collision and noncollision courses were examined. A sample size of 50 was used, not large enough to allow confident statements of statistical inference, but large enough to permit preliminary conclusions to be reached. The LSS filter was used for a period of five seconds to initialize the EK filter.

The ranges of parameter values which were used in the simulation are listed in Table 6.1. The measurement errors were assumed to be white noise with zero means and Gaussian statistics. The values of σ_r and σ_β correspond to a range of very good to moderately poor measurement subsystems. Values quoted by manufacturers of proposed collision avoidance systems lie in these ranges. The airspeed range reflects the speeds to be found in the near terminal area and in the enroute cruise condition for both general aviation aircraft and commercial jets.

TABLE 6.1

Parameter Values Used for Filter Analysis

PARAMETER	VALUE
Measurement Sample Period, Δt	0.1 - 1.0 sec
Airspeed of Own Aircraft, V_A / Airspeed of Intruding Aircraft, V_B	180 - 840 fps
Standard Deviation of Range Error, σ_r	50 - 200 ft
Standard Deviation of Bearing Error, σ_β	0.75 - 3.00 deg

Although both collision and non-collision courses were simulated for a wide variety of encounter geometries, a single encounter geometry was used for studying the sensitivity of the filter's performance to parameter variations. For this encounter geometry (see Fig. 6.1), the initial conditions were $x_o = -10800$ ft., $y_o = 21600$ ft., and $\theta = 90^o$, which corresponds to a course with 60 sec. to collision for $V_A = 360$ ft/sec and $V_B = 180$ ft/sec (an encounter between a commercial jet and a general aviation aircraft in the near terminal area).

In the following tables, the entries are the steady-state absolute values of the sample mean of the estimation error and the sample standard deviation of the estimation error of the appropriate quantities. The entries are in the form of ordered pairs (mean, standard deviation). The term steady-state is interpreted as the value of the indicated quantity 15 seconds after the initial time in the simulation experiment. The entries for position error are a composite figure reflecting the error in both the x and y coordinates.

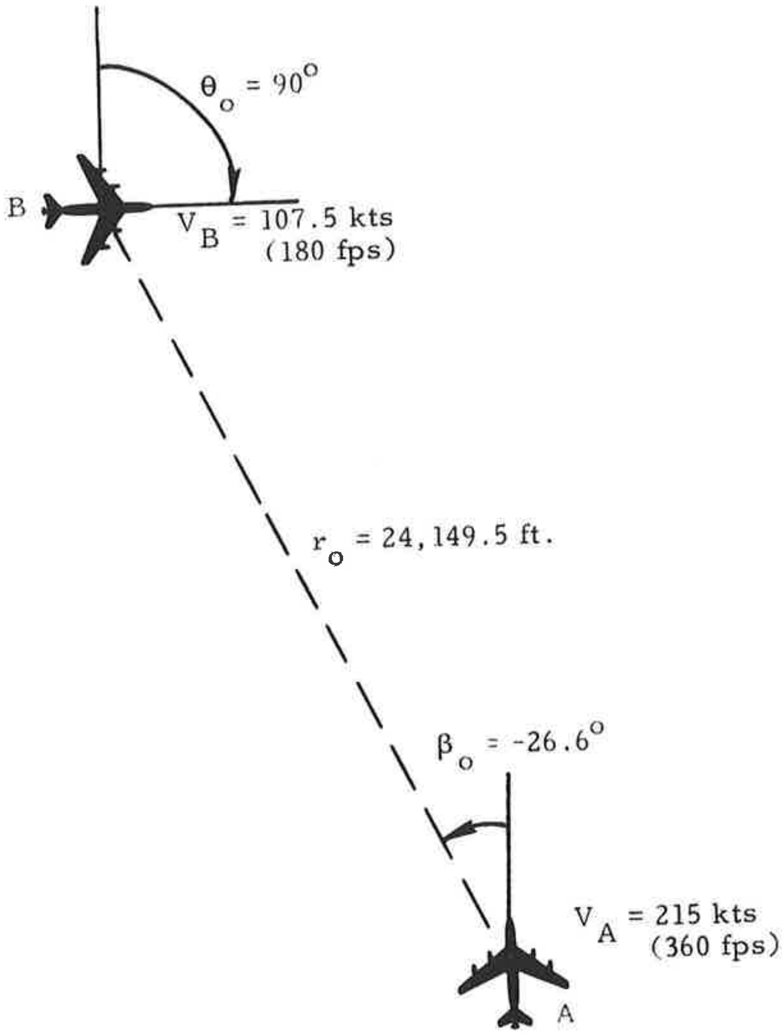

Figure 6.1 Encounter Geometry for Study of the Effects of Parameter Variations

Plots are shown for the sample statistics of the estimation errors for both filters in Figures 6.2 and 6.3. The encounter geometry is that of Fig. 6.1. For the EK filter (Fig. 6.3), the sample mean of the appropriate diagonal element of the P-matrix (which indicates how the filter weights succeeding measurements (see Appendix E)) along with the sample variance, is plotted.

In Table 6.2, variations in LSS filter performance with variations in sampling rate are shown. EK filter performance variations are listed in Table

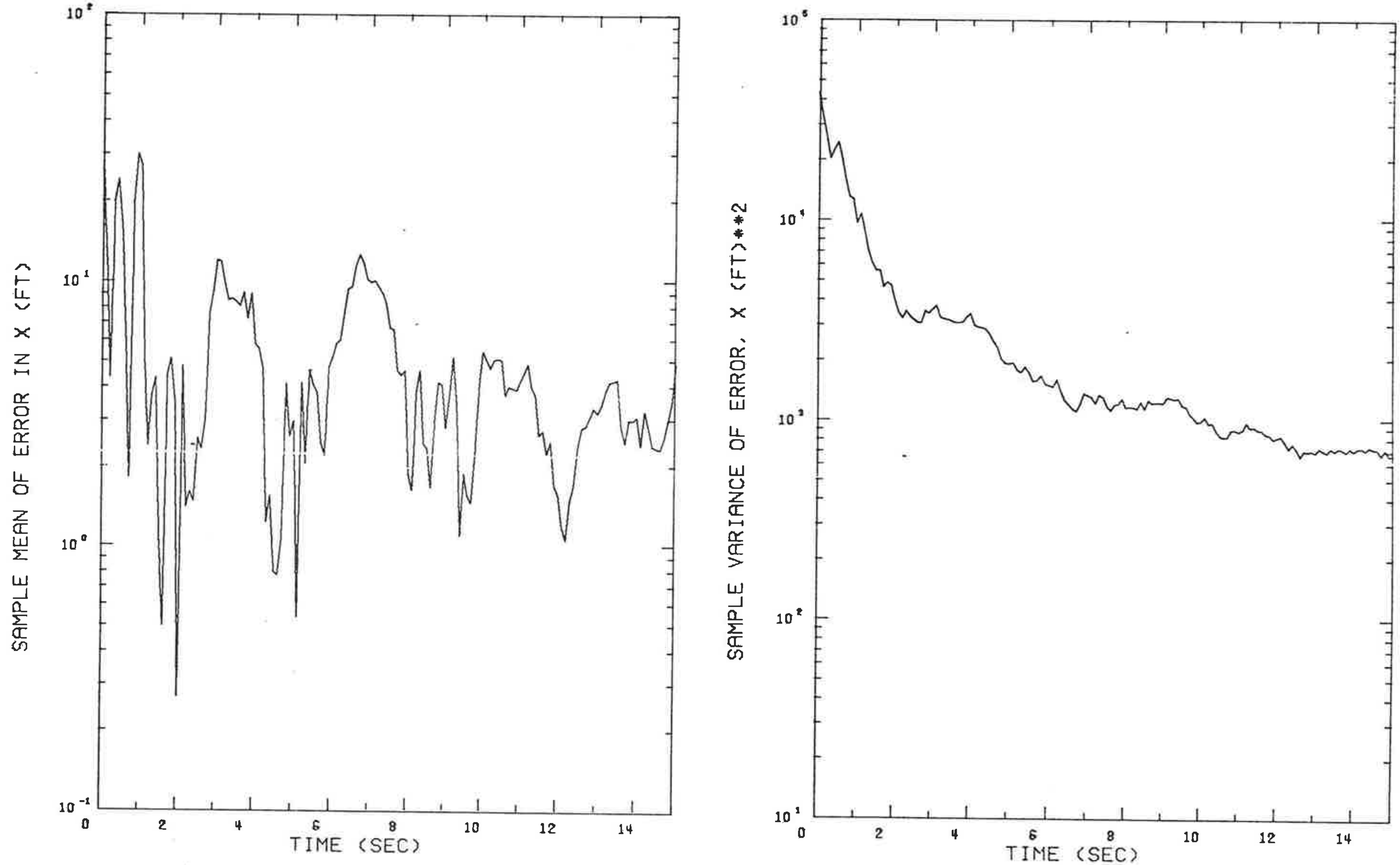

(a) Position Error

(b) Position Error

Figure 6.2 Error Plots for Linear Least-Squares Filter

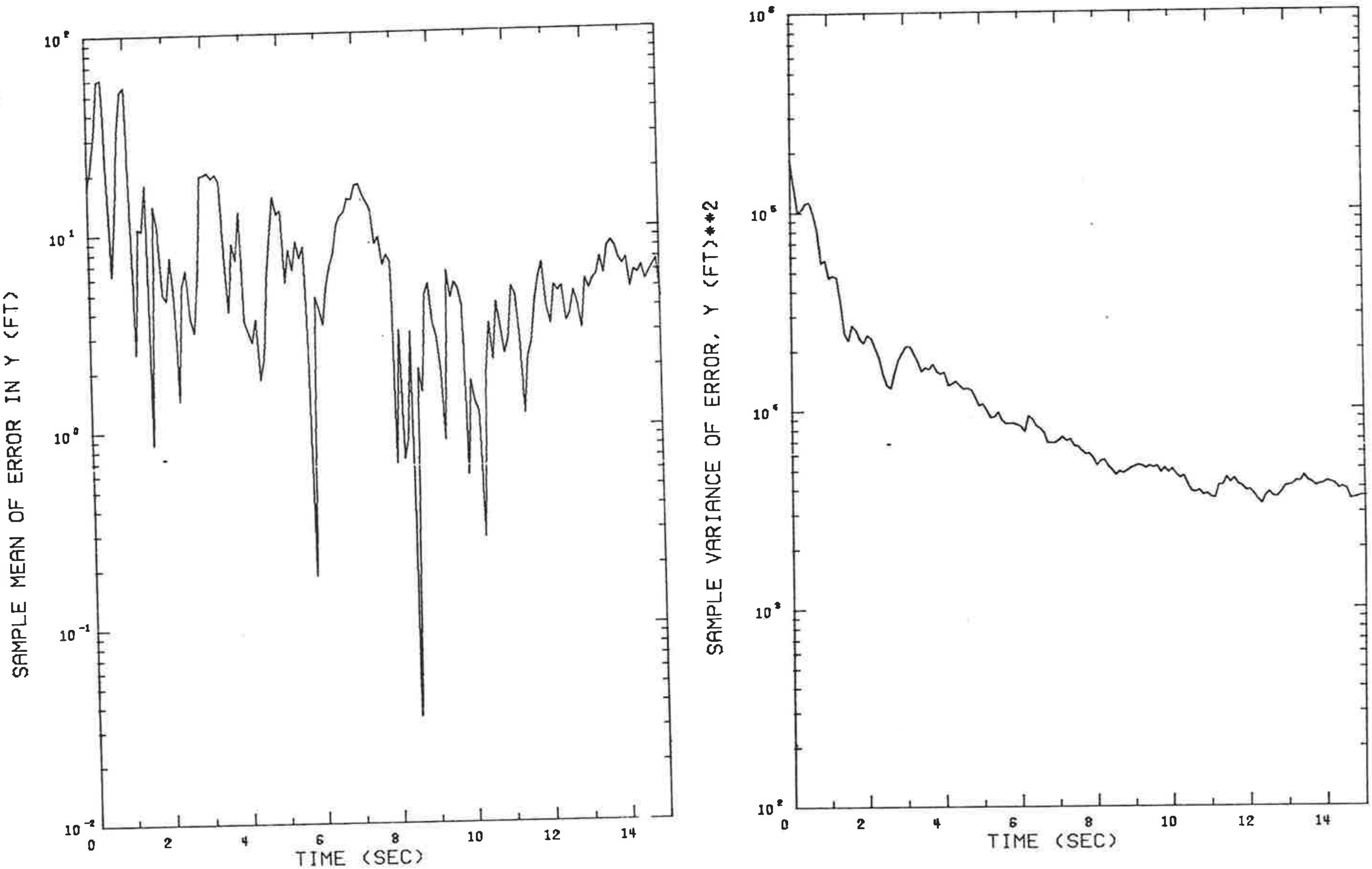

(c) Position Error

(d) Position Error

Figure 6.2 (Cont'd) Error Plots for Linear Least-Squares Filter

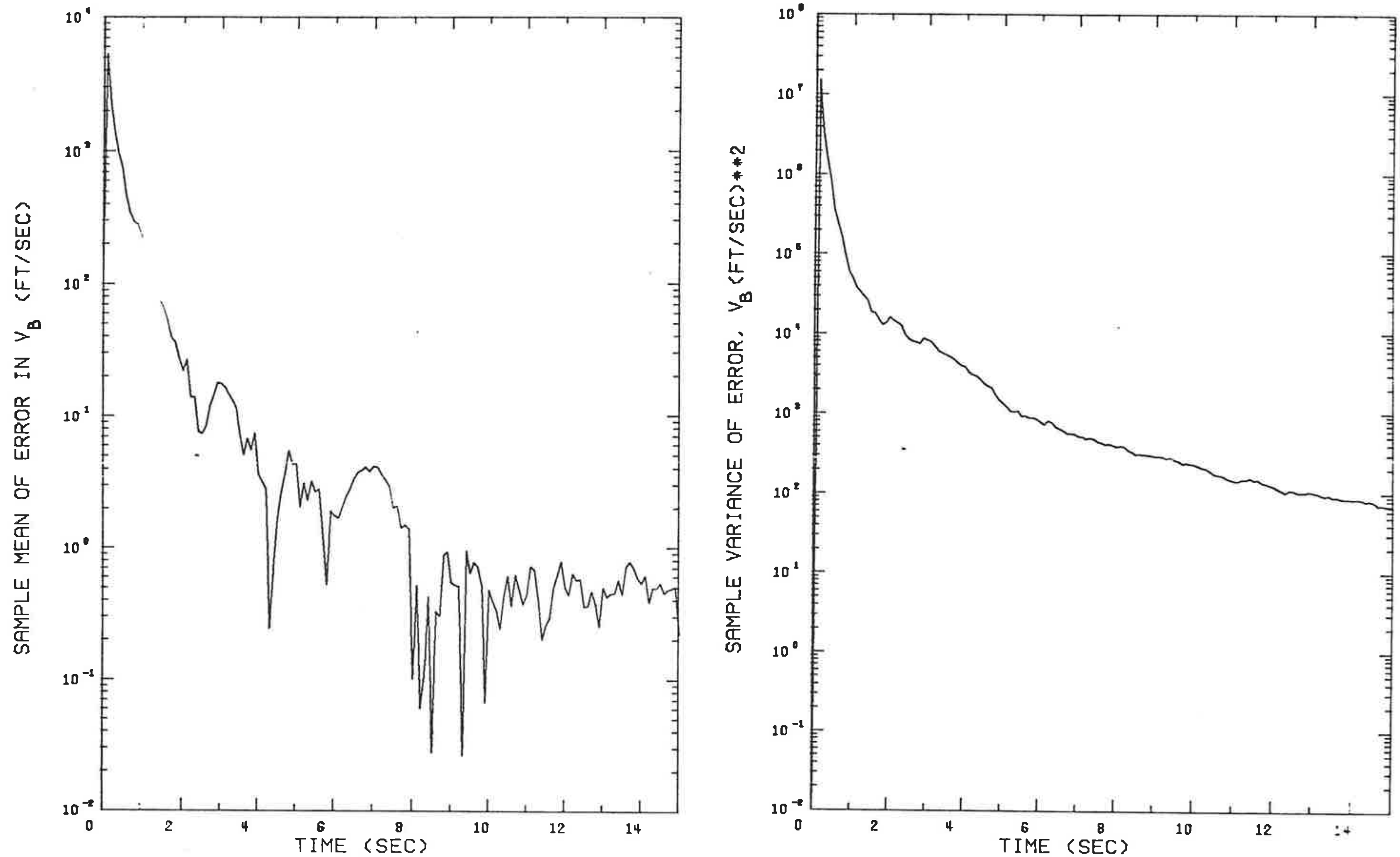

(e) Airspeed Error

(f) Airspeed Error

Figure 6.2 (Cont'd) Error Plots for Linear Least-Squares Filter

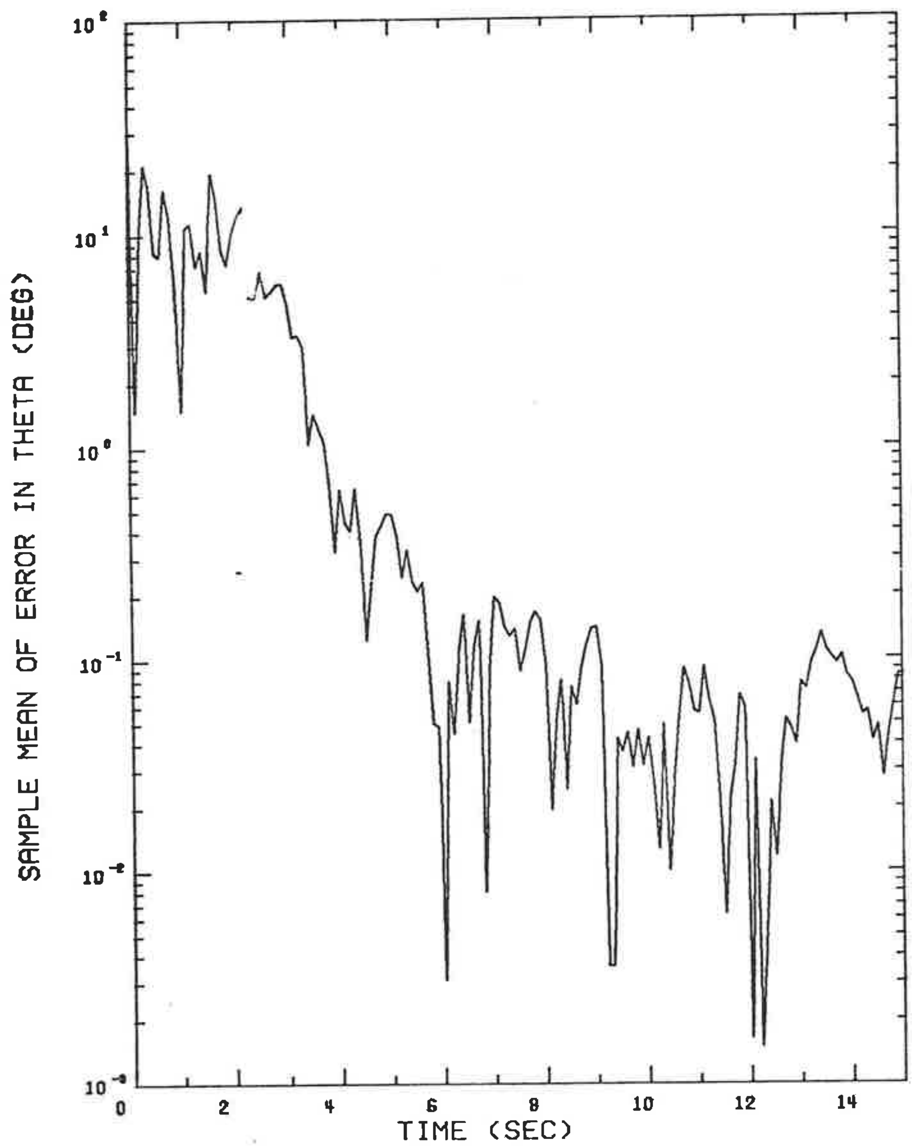

(g) Heading Error

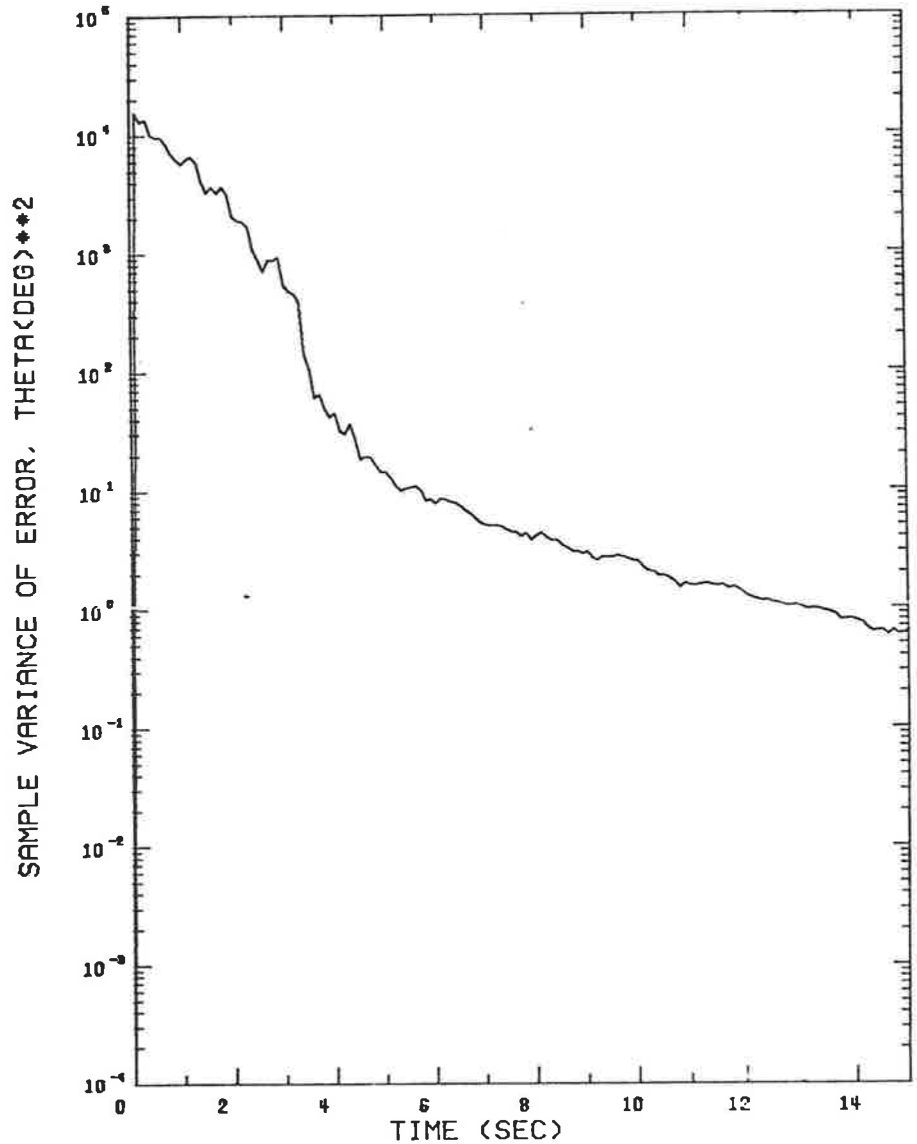

(h) Heading Error

Figure 6.2 (Cont'd) Error Plots for Linear Least-Squares Filter

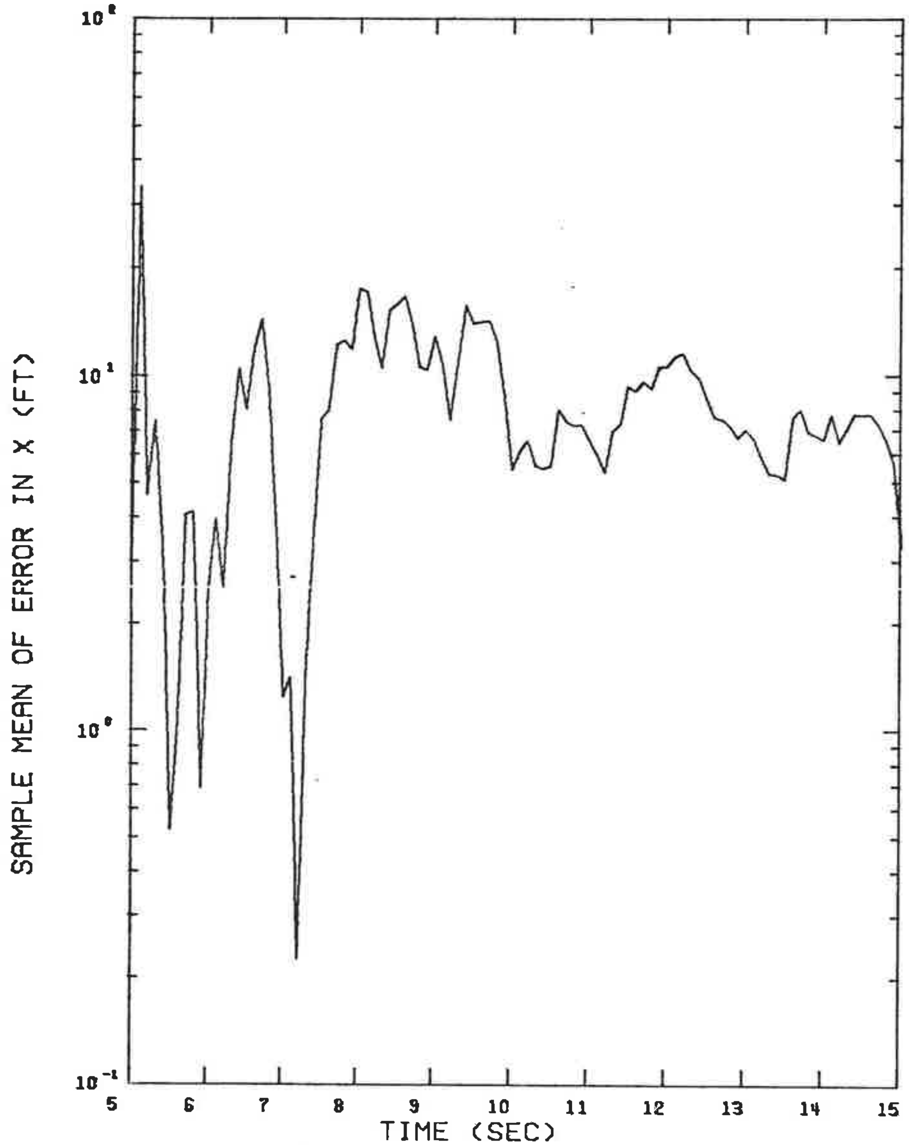

(a) Position Error

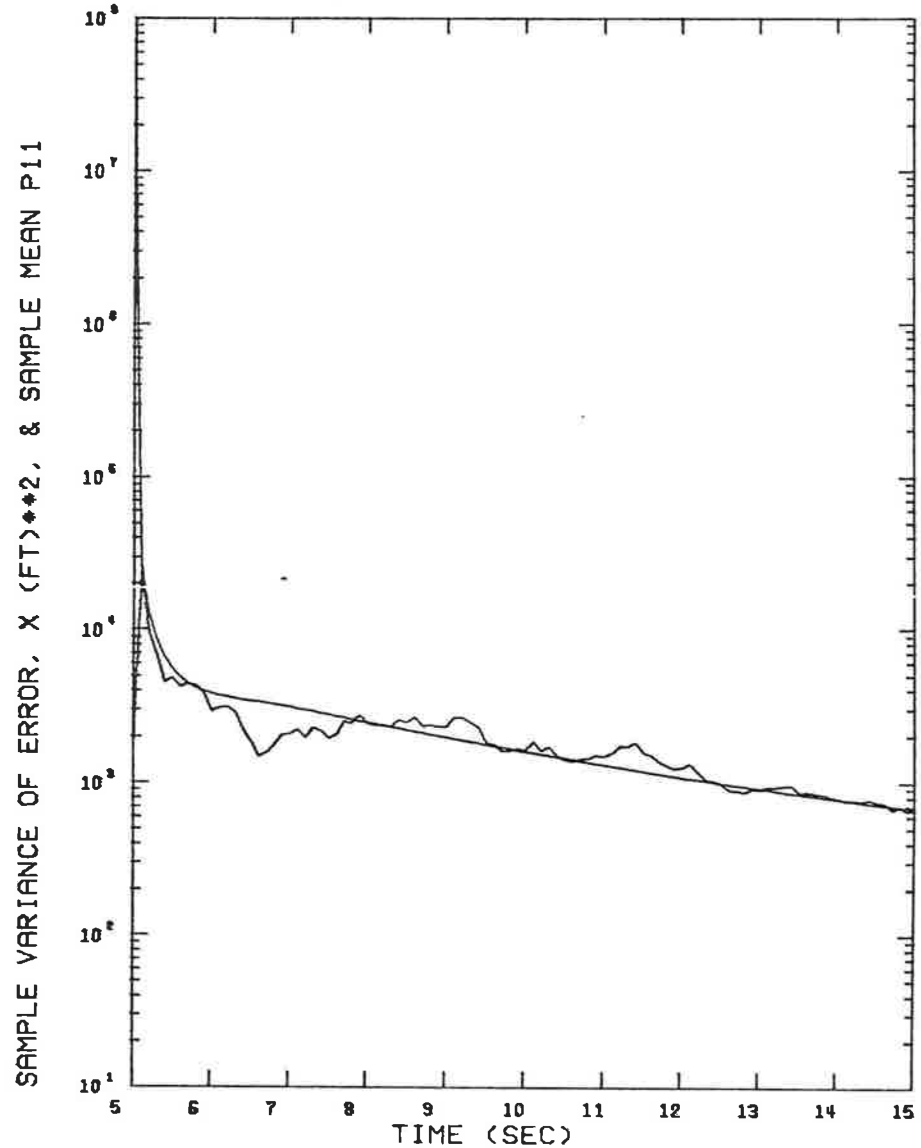

(b) Position Error

Figure 6.3 Error Plots for Extended Kalman Filter

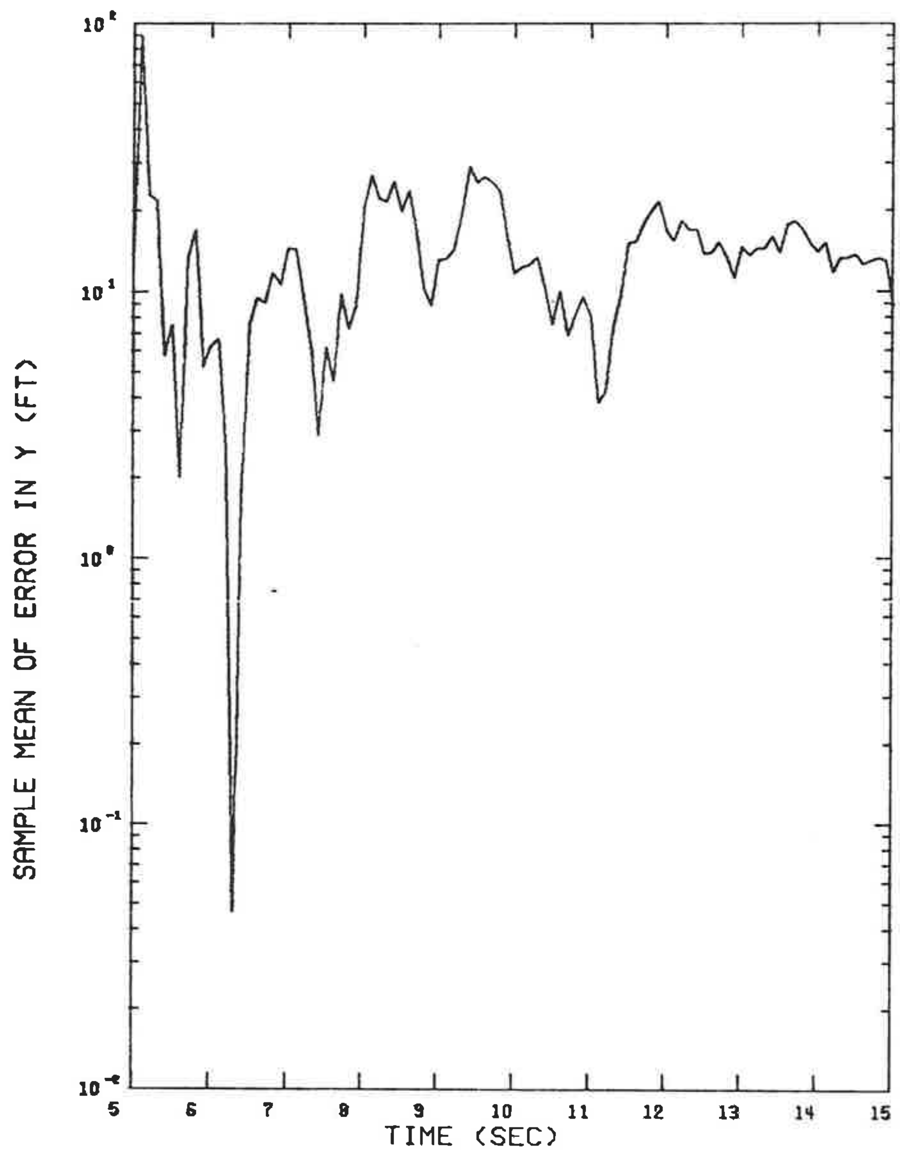

(c) Position Error

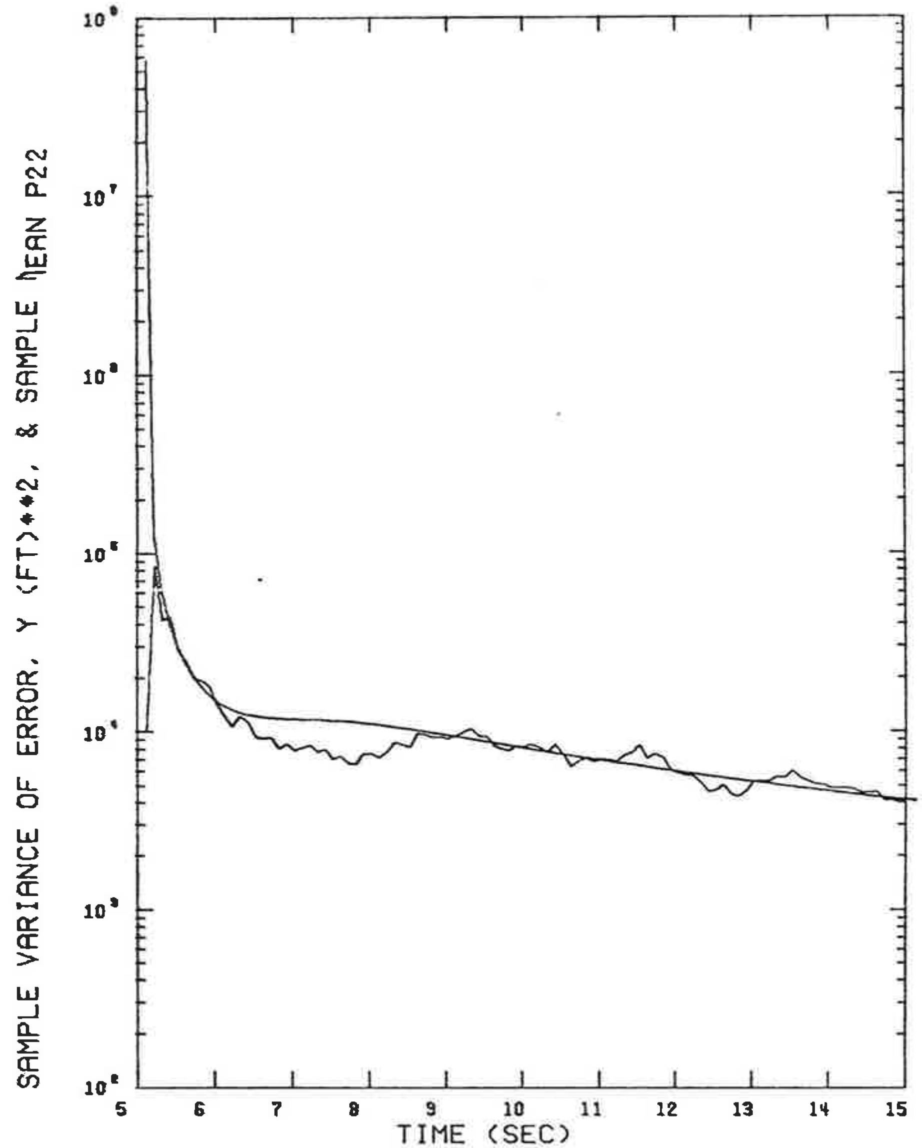

(d) Position Error

Figure 6.3 (Cont'd) Error Plots for Extended Kalman Filter

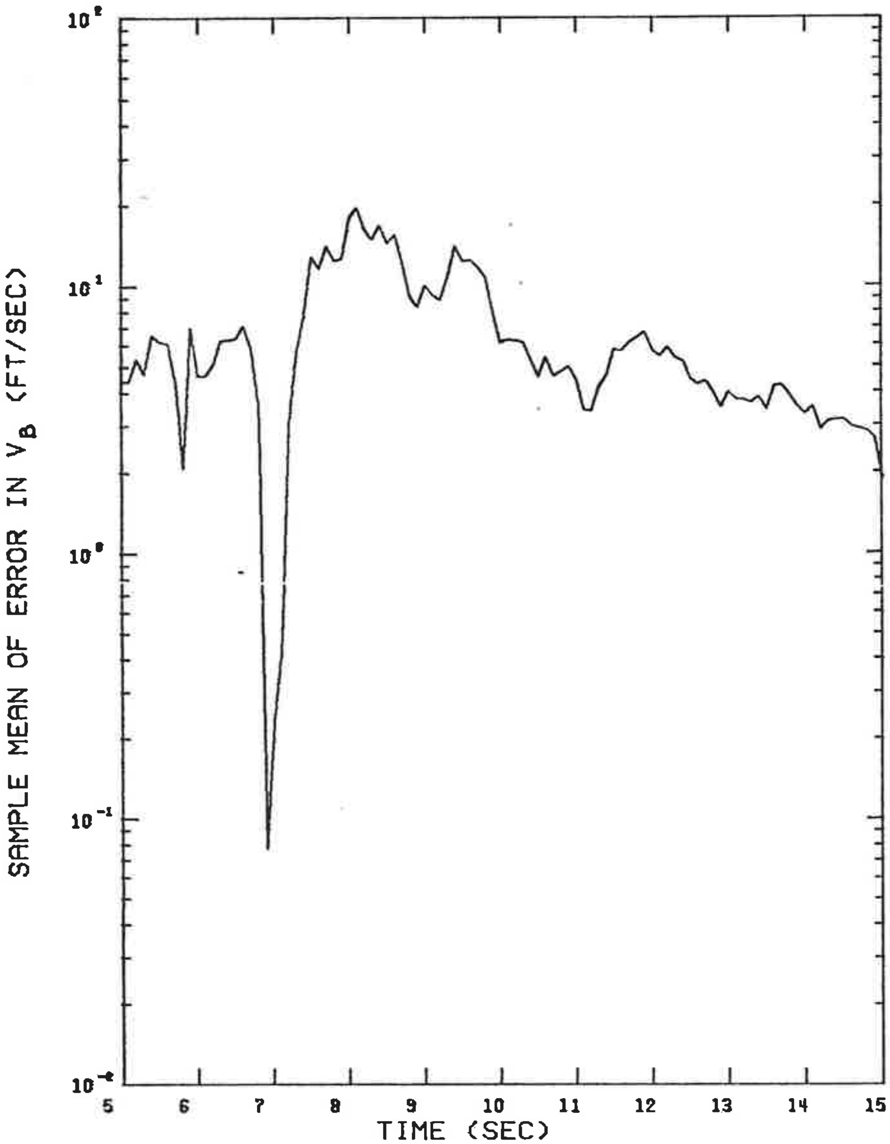

(e) Airspeed Error

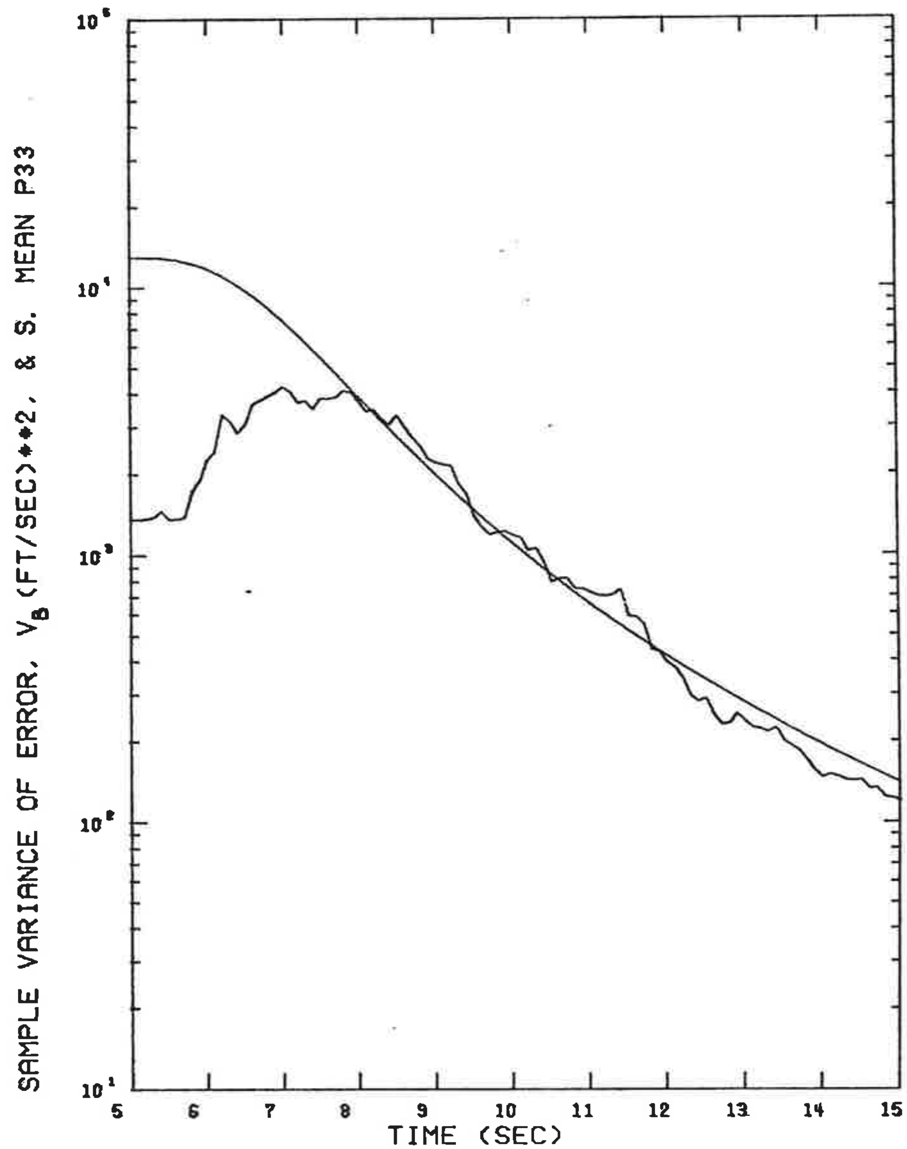

(f) Airspeed Error

Figure 6.3 (Cont'd) Error Plots for Extended Kalman Filter

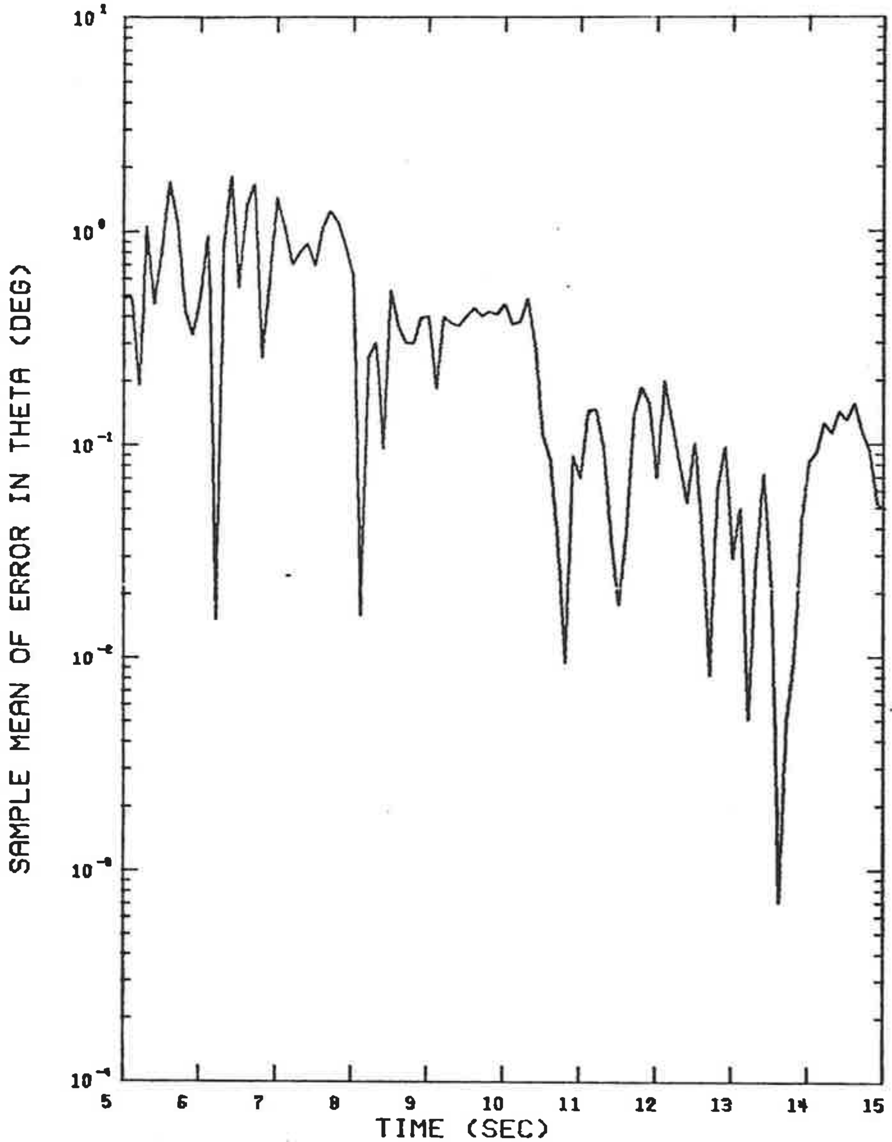

(g) Heading Error

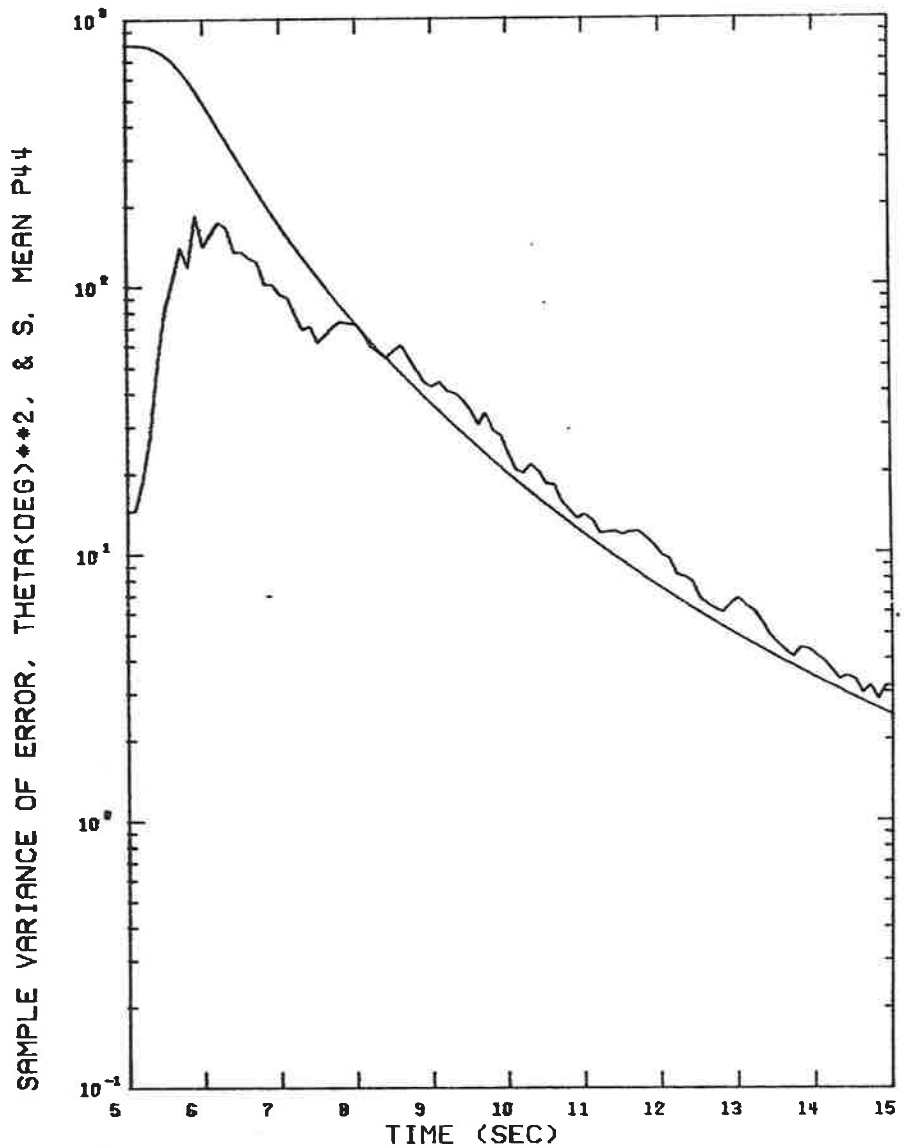

(h) Heading Error

Figure 6.3 (Cont'd) Error Plots for Extended Kalman Filter

6.3. As expected, the filters' performances degrade for slower sample rates, since less information about the track is accumulated in a fixed amount of time. Although the filters converged in all cases, convergence is slower for slower sampling rates.

The variation in the two filters' performances for different quality range measurements for fixed σ_β is tabulated in Tables 6.4 and 6.5. The filters are relatively insensitive to the magnitude of the noise in the range measurements. In Tables 6.6 and 6.7, the variation in filter performance with variations in the magnitude of bearing error σ_β is shown for fixed σ_r. For both filters, degradation of performance occurs as σ_β is increased, with convergence being slower. The LSS filter appears to be a little less affected than the EK filter. Tables 6.8, 6.9, 6.10, and 6.11 exhibit the variation in airspeed and heading estimation errors for a larger number of combinations of range and bearing error magnitudes. Again, the conclusion is that the filters are more dependent on good bearing measurements than good range measurements for better estimation of the intruding aircraft's airspeed and relative heading.

The effect of different airspeed combinations on the estimation of intruder's airspeed and relative heading is tabulated in Tables 6.12 - 6.15. The filters were relatively insensitive to the airspeeds of the encountering aircraft, with performance slightly better at higher speed. This could be expected since the range and bearing rates are higher in these cases, enabling the filters to converge more quickly to the relative velocity of the two aircraft.

Based on sample statistics compiled during the simulations, bounds on the performance of the filters in the collision avoidance context can be indicated. These bounds are based on limited results, so they should be considered in that light. In other words, care must be taken in drawing general conclusions about the suitability of estimation theory techniques to the collision avoidance signal processing problem. A complete study of all the possibilities has not yet been performed.

For the range of measurement errors considered, position estimation errors can be expected to have an absolute mean value less than 50 ft. for the LSS

TABLE 6.2

Variation of Estimation Error with Δt for LSS Filter
σ_r = 100 ft, σ_β = 1.5^o

Δt (sec)	Position (feet)	Airspeed (feet/sec)	Heading (degrees)
0.10	(10, 85.6)	(0.37, 12.5)	(0.23, 2.2)
0.50	(27, 381.0)	(1.4, 22.6)	(0.88, 4.2)
0.75	(29, 338.0)	(1.1, 24.7)	(0.80, 4.5)
1.00	(60, 596.0)	(5.5, 27.4)	(1.7, 5.8)

TABLE 6.3

Variation of Estimation Error with Δt for EK Filter
σ_r = 100 ft, σ_β = 1.5^o

Δt (sec)	Position (feet)	Airspeed (feet/sec)	Heading (degrees)
0.10	(32, 133)	(6.4, 19.9)	(0.12, 4.45)
0.50	(112, 707)	(18.5, 40.8)	(5.8, 17.7)
0.75	(63, 571)	(10.3, 43.8)	(3.2, 14.9)
1.00	(142, 979)	(24.2, 55.6)	(11.0, 26.8)

TABLE 6.4

Variation of Estimation Errors with σ_r for LSS Filter
σ_β = 1.5^o

σ_r (sec)	Position (feet)	Airspeed (feet/sec)	Heading (degrees)
50	(37, 156)	(6.9, 22.7)	(0.84, 5.48)
100	(32, 133)	(6.4, 19.9)	(0.12, 4.45)
150	(28, 128)	(5.8, 18.9)	(0.20, 4.17)
200	(26, 133)	(5.5, 18.3)	(0.33, 4.29)

TABLE 6.5

Variation of Estimation Error with σ_r for EK Filter
$\sigma_\beta = 1.5^o$

σ_r (sec)	Position (feet)	Airspeed (feet/sec)	Heading (degrees)
50	(37, 156)	(6.9, 22.7)	(0.84, 5.48)
100	(32, 133)	(6.4, 19.9)	(0.12, 4.45)
150	(28, 128)	(5.8, 18.9)	(0.20, 4.17)
200	(26, 133)	(5.5, 18.3)	(0.33, 4.29)

TABLE 6.6

Variation of Estimation Errors with σ_β for LSS Filter
σ_r = 100 ft.

σ_β (sec)	Position (feet)	Airspeed (feet/sec)	Heading (degrees)
0.75	(3, 19.6)	(0.13, 5.6)	(0.10, 1.1)
1.50	(10, 85.6)	(0.37, 12.5)	(0.23, 2.2)
2.25	(16, 164.0)	(0.51, 16.7)	(0.34, 2.9)
3.00	(27, 84.9)	(0.66, 22.3)	(0.52, 4.0)

TABLE 6.7

Variation of Estimation Error with σ_β for EK Filter
σ_r = 100 ft.

σ_β (sec)	Position (feet)	Airspeed (feet/sec)	Heading (degrees)
0.75	(75, 203)	(1.7, 7.1)	(0.27, 1.86)
1.50	(32, 133)	(6.4, 19.9)	(0.12, 4.45)
2.25	(52, 276)	(9.6, 27.2)	(1.29, 8.24)
3.00	(78, 618)	(12.2, 39.7)	(3.25, 39.2)

TABLE 6.8

Variation of Airspeed Estimation Error with σ_r and σ_β for LSS Filter

σ_β \ σ_r	50	100	150	200
0.75	(0.17, 5.6)	(0.13, 5.6)	(0.08, 5.7)	(0.03, 5.8)
1.50	(0.37, 11.2)	(0.37, 12.5)	(0.32, 12.5)	(0.27, 12.5)
2.25	(0.55, 16.8)	(0.51, 16.7)	(0.46, 16.7)	(0.41, 16.8)
3.00	(0.70, 22.0)	(0.66, 22.3)	(0.62, 22.0)	(0.56, 22.3)

TABLE 6.9

Variation of Airspeed Estimation Error with σ_r and σ_β for EK Filter

σ_β \ σ_r	50	100	150	200
0.75	(1.9, 7.5)	(1.7, 7.1)	(1.9, 7.3)	(2.1, 7.5)
1.50	(6.9, 22.7)	(6.4, 19.9)	(5.8, 18.9)	(5.5, 18.3)
2.25	(8.5, 11.25)	(9.6, 27.2)	(9.3, 25.6)	(8.9, 25.4)
3.00	(8.1, 48.1)	(12.2, 39.7)	(13.7, 37.6)	(14.0, 36.4)

TABLE 6.10

Variation of Heading Estimation Error with σ_r and σ_β for LSS Filter

σ_β \ σ_r	50	100	150	200
0.75	(0.08, 0.97)	(0.10, 1.1)	(0.12, 1.3)	(0.15, 1.5)
1.50	(0.17, 2.9)	(0.23, 2.2)	(0.25, 2.3)	(0.27, 2.4)
2.25	(0.31, 2.9)	(0.34, 2.9)	(0.36, 3.0)	(0.39, 3.1)
3.00	(0.50, 3.9)	(0.52, 4.0)	(0.55, 4.1)	(0.57, 4.2)

TABLE 6.11

Variation of Heading Estimation Error with σ_r and σ_β for EK Filter

σ_β \ σ_r	50	100	150	200
0.75	(0.28, 1.47)	(0.27, 1.86)	(0.14, 2.25)	(0.07, 2.58)
1.50	(0.84, 5.48)	(0.12, 4.45)	(0.20, 4.17)	(0.33, 4.29)
2.25	(2.49, 11.25)	(1.29, 8.24)	(0.58, 6.86)	(0.17, 6.36)
3.00	(5.56, 17.9)	(3.25, 39.2)	(2.99, 13.42)	(4.89, 41.0)

TABLE 6.12

Variation of Airspeed Estimation Error with V_A and V_B for LSS Filter

$V_B \setminus V_A$	180	360	843
180	(0.44, 13.3)	(0.37, 12.5)	(0.18, 10.6)
360	(0.62, 13.3)	(0.55, 12.5)	(0.35, 10.7)
843	(0.92, 13.3)	(0.85, 12.5)	(0.69, 10.7)

TABLE 6.13

Variation of Airspeed Estimation Error with V_A and V_B for EK Filter
$\sigma_r = 100$ ft, $\sigma_\beta = 1.5^o$

$V_A \setminus V_B$	180	360	843
180	(7.8, 21.9)	(6.4, 19.9)	(2.6, 14.1)
360	(5.7, 16.3)	(4.7, 14.9)	(1.8, 11.1)
843	(4.6, 14.5)	(4.1, 13.2)	(2.7, 9.7)

TABLE 6.14

Variation of Heading Estimation Error with V_A and V_B for LSS Filter

$V_B \setminus V_A$	180	360	843
180	(0.26, 2.2)	(0.23, 2.2)	(0.13, 2.15)
360	(0.079, 0.978)	(0.064, 0.98)	(0.023, 0.97)
843	(0.012, 0.349)	(0.066, 0.346)	(0.0084, 0.35)

TABLE 6.15

Variation of Heading Estimation Error with V_A and V_B for EK Filter
$\sigma_r = 100$ ft, $\sigma_\beta = 1.5^o$

$V_B \setminus V_A$	180	360	843
180	(0.34, 4.62)	(0.12, 4.45)	(0.72, 3.83)
360	(0.024, 1.26)	(0.066, 1.27)	(0.25, 1.30)
843	(0.0042, 0.31)	(0.0067, 0.31)	(0.015, 0.31)

filter and less than 100 ft. for the EK filter, both with a standard deviation of 100 ft. Airspeed estimation errors can be expected to have an absolute mean of less than 1 fps for the LSS filter and 15 fps for the EK filter, with a standard deviation of 25 fps and 50 fps, respectively. Heading estimation errors can be expected to have an absolute mean value of less than 1^o for the LSS filter and 6^o for the EK filter, with standard deviations of 5^o and 10^o, respectively. These values are based on measurement errors with $\sigma_r \leq 200$ ft. and $\sigma_\beta \leq 3^o$.

In the cases which were examined, the LSS filter performed slightly better than the EK filter. These results are consistent with those obtained for similar linear regression type filters in vehicle tracking applications.[83] It also has the advantage of requiring less computational capability to mechanize. However, no effort was made to fine tune the EK filter via the choice of the initial covariance matrix P. It may be possible to find an initial P which produces better performance on the part of this filter. Also, the EK filter can be expected to adapt better to the maneuvering aircraft situation.

To illustrate the preceding discussion, Figs. 6.5 and 6.6 show the average time response of the two filters for a high speed head-on collision encounter for airspeed and heading estimation. The encounter geometry is shown in Fig. 6.4. These figures are plots of the true values of the intruder's airspeed and relative heading and the estimated values as a function of time. Similar results were obtained for other airspeeds and other encounter geometries, such as head-on parallel track (no collision) and nearly head-on ($\theta = 175^o$) encounters.

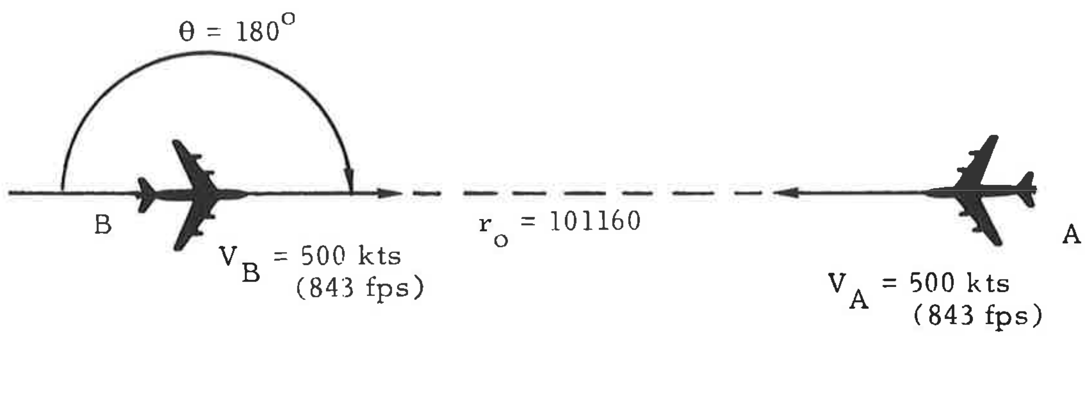

Figure 6.4 Encounter Geometry for Head-On Collision Example

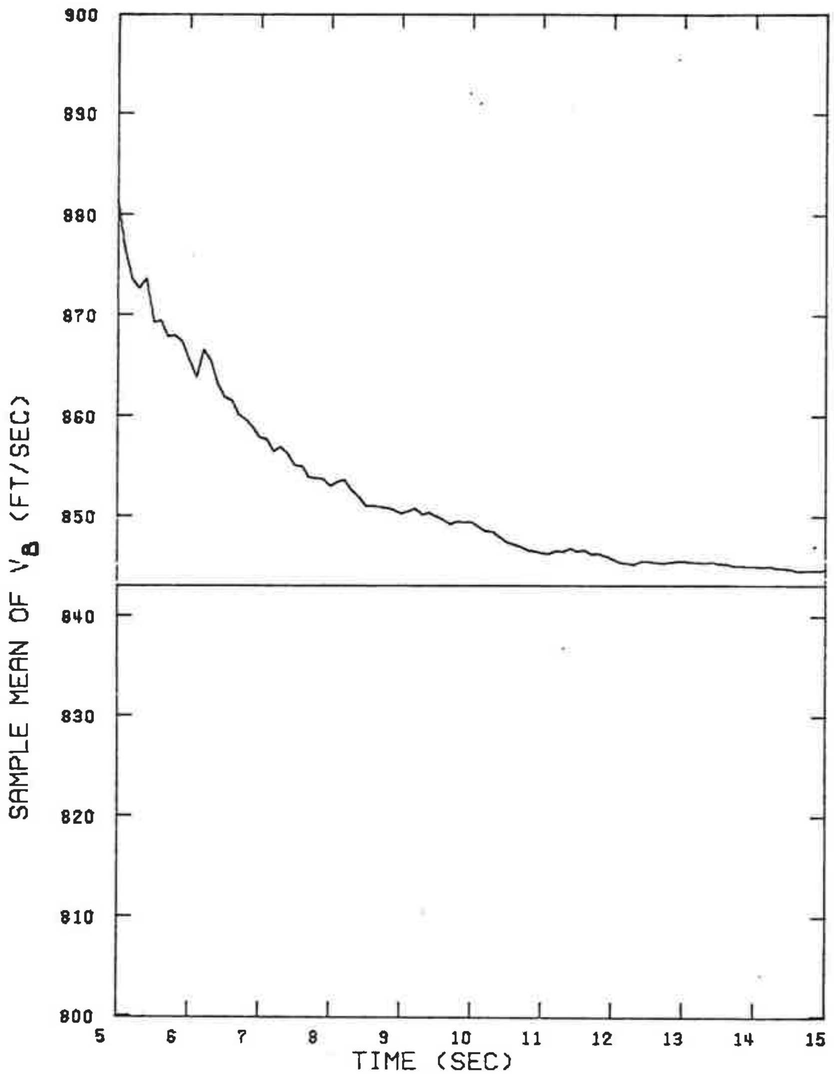

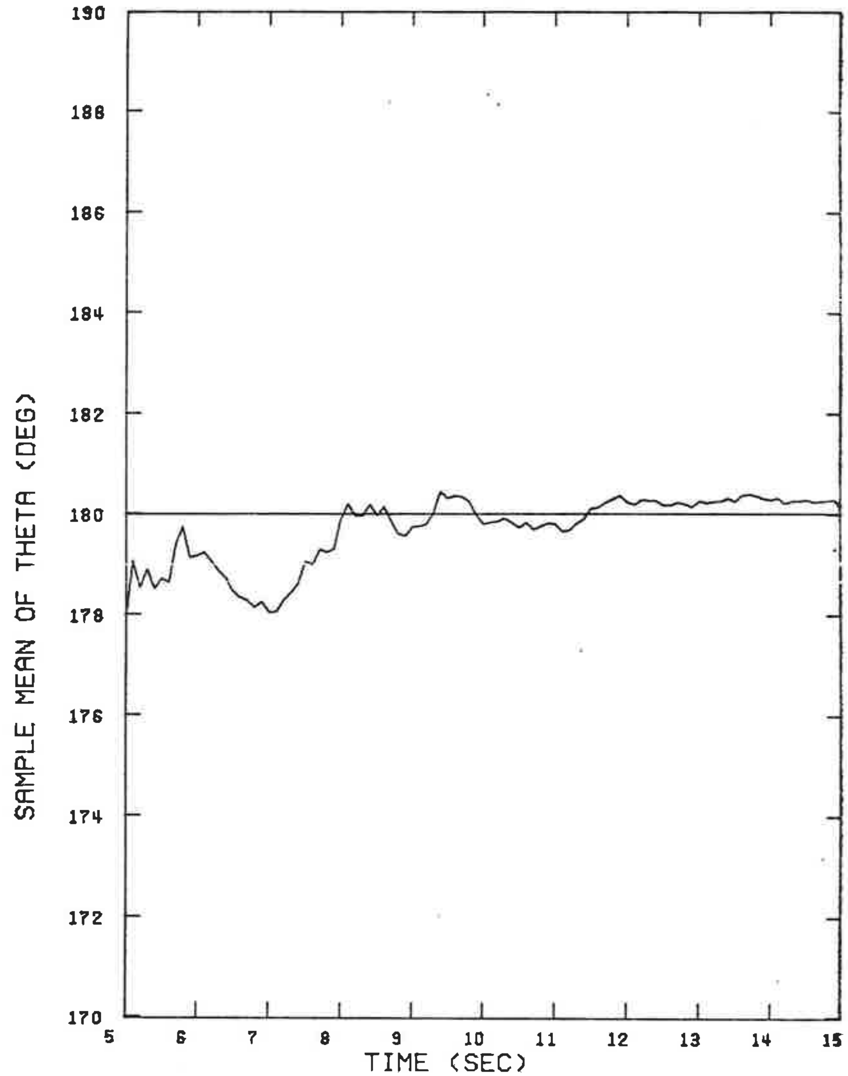

Figure 6.5 Average Time Response of Linear Least Squares Filter

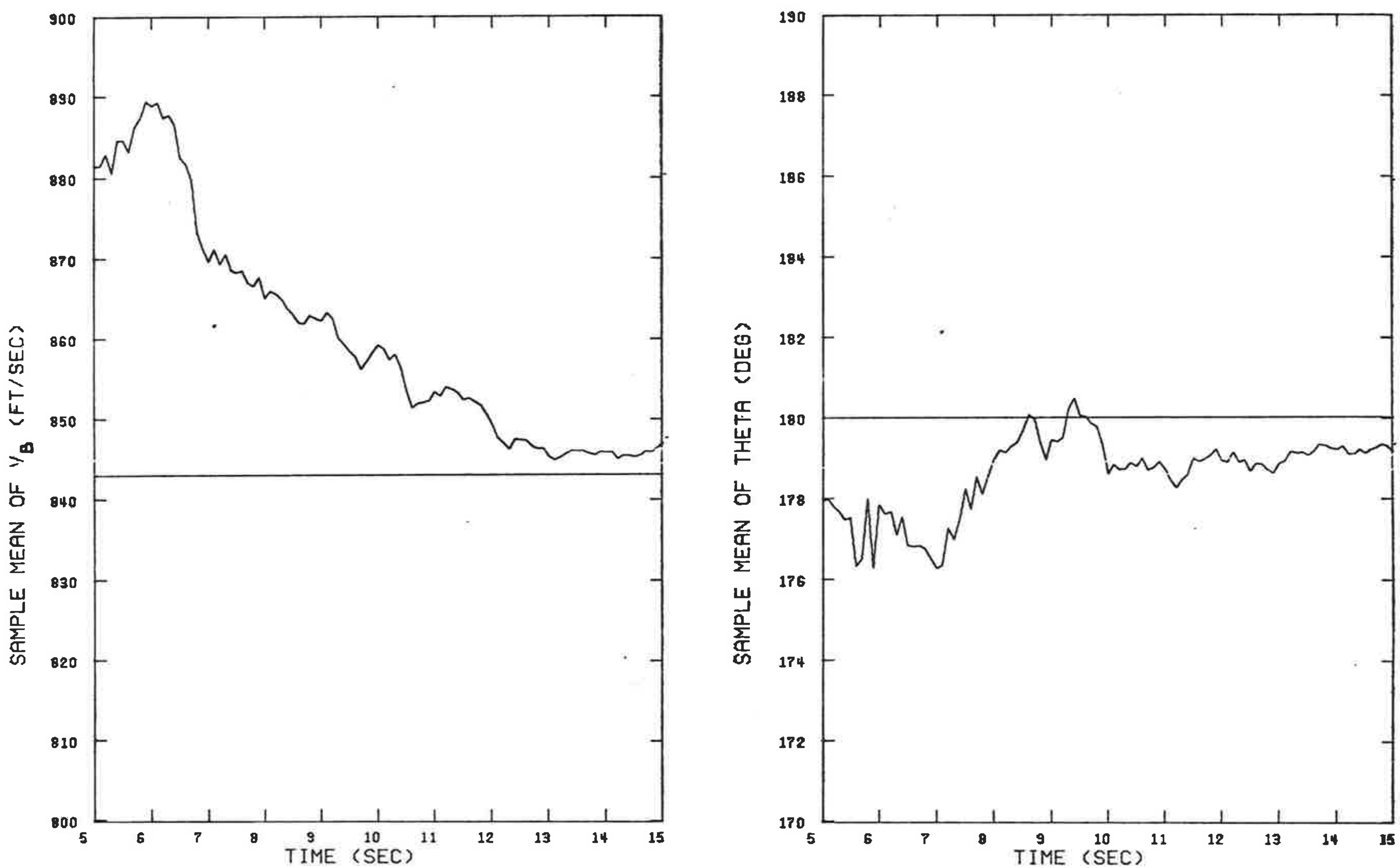

Figure 6.6 Average Time Response of Extended Kalman Filter

As a result of this preliminary investigation of the horizontal collision avoidance signal processing problem, it can be stated that the algorithms discussed here appear to be feasible. The accuracies which are achievable are adequate for purposes of avoidance maneuver determination. The computer requirements of the EK filter, estimated to be 350-500 word memory and 7.5 - 11 msec cycle time, are moderate and the requirements of the LSS filter are much less.

A number of refinements in the present formulation of the filtering algorithms are suggested by the above described simulation study. By increasing the filter complexity, B's turn rate can be estimated and the effect of measurement bias errors can be included. If one's own aircraft is maneuvering, this fact can be accounted for by suitable modification of the model of the dynamics used in the filter.

In the present study, it was assumed that the designer of the EK filter knows exactly the statistics of the measurement noise (i.e., the matrix R). However, R is usually known only approximately. The effect of using an incorrect R matrix and other modeling errors can be studied in a systematic fashion.[86] Such a study is necessary before hardware design decisions are made.

Divergence control mechanisms can be built into the EK filter algorithms to enhance its ability to perform with poor a priori information and to track a maneuvering target.[86] A computationally more efficient and accurate version of the EK filter algorithm is available,[87] which is important for the implementation question, and should be studied in the collision avoidance context. Finally, several other types of filters should be examined for their applicability to this problem, especially if extension to the maneuvering case is desired.[88-90]

6.3 SUBOPTIMAL MANEUVER LOGIC

The purposes in this study of developing maneuver logic for a typical airborne horizontal collision avoidance system were:

1. To assess what the computer requirements would be for implementation.

2. To provide a means of conducting analysis of effects due to dynamic and measurement errors, as discussed in Chapter VII.

A simplified form of the sequence of logic taken by the assumed maneuver mechanization is shown in Fig. 6.7. Here, the protected aircraft A is centered at the origin, and the position and relative velocity of a potential threat aircraft B are determined. Based on these estimates, the following logic sequence is taken:

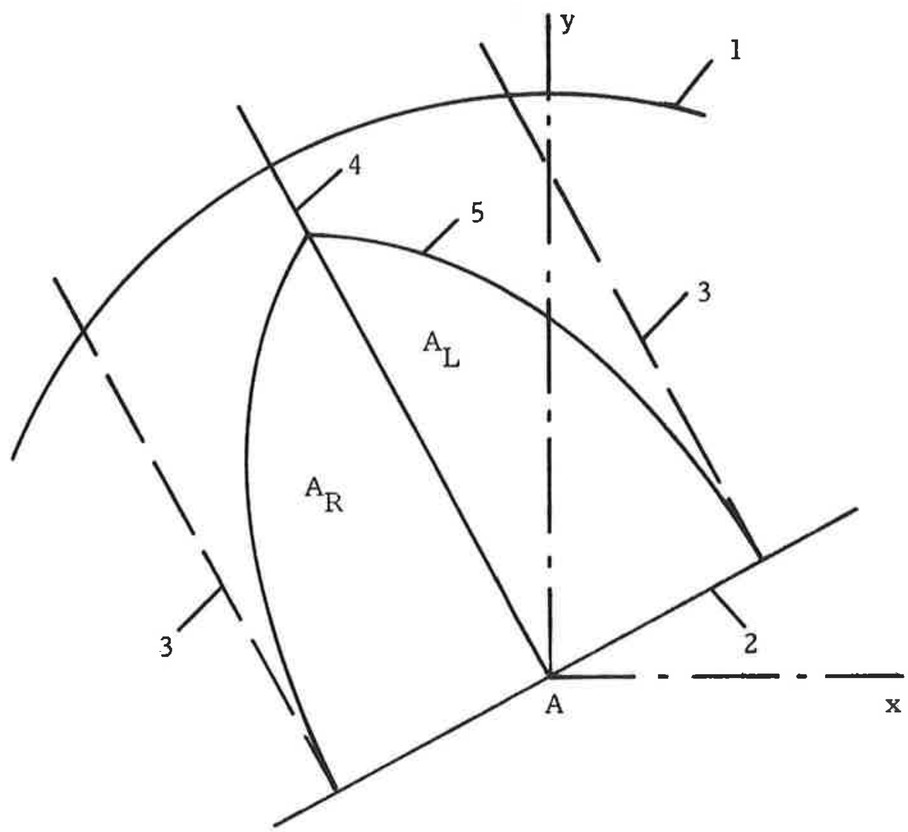

LOGIC SEQUENCE

1. Determine if intruder within alarm radius.
2. Determine if intruder moving away.
3. Determine if miss distance acceptable.
4. Determine turn direction.
5. Determine if time to turn is reached.

Figure 6.7 Illustration of Maneuver Mechanization Logic for Aircraft A

1. Is the threat aircraft inside some circular boundary defined by the radius r_p? If not, ignore the threat.

2. Is the threat aircraft moving away from A? (This is determined by which side of the maneuver chart baseline that B is on.) If so, ignore the threat.

3. Is the miss distance obtained with no maneuver acceptable? (This is determined if the path normal to the baseline governed by the relative velocity vector of B with respect to A is outside the acceptable miss distance r_a.) If so, ignore the threat.

4. Determine the optimum turn direction based on B's location with respect to the maneuver region boundaries.

5. Determine if the time-to-turn is reached which will produce the desired miss distance r_a.

6. After turn initiation, monitor the performance to ensure sufficient miss.

7. After minimum range is reached, issue the return-to-track command.

The maneuver charts discussed in Section 4.3 and Appendix C were used to determine steps (4) and (5) of the above logic sequence. In order to simplify the implementation problem for this study, two conditions were imposed which result in suboptimal maneuver strategies:

1. If both aircraft turn, then the avoidance maneuvers are executed at equal turn rates ($\omega = 1$).

2. Two part maneuvers are not used.

These assumptions allowed for the construction of a workable collision avoidance algorithm which would use a reasonable amount of core space, and yet retain the essential features of the optimum maneuvers, as depicted by the charts. A detailed analysis of the loss of performance, as determined by the reduction in miss distance, due to these assumptions remains to be conducted.

This maneuver algorithm utilized here can readily be augmented to accommodate the situation wherein the planes are not flying level. Finite pilot delay and roll rate were accounted for by building in a sufficient amount of lead time into the algorithm. The relative location of the aircraft is predicted several seconds ahead, and then the algorithm is applied to these predicted positions. This point is dealt with in greater detail in Section 7.1.1.

6.3.1 Maneuver Logic Implementation

The logic for determining optimum turn direction and whether time-to-turn has been reached was implemented by curve fitting the maneuver charts of Appendix C for discrete values of speed ratio γ and relative heading θ. Time-to-turn is determined by continually assessing the terminal miss r_f when the appropriate maneuver is made. The maneuver is initiated when the miss distance falls below a certain threashold (acceptable miss distance r_a).

The dispersal lines or boundaries separating the strategy regions of the maneuver charts were fitted using straight-line approximations. Curves of equal miss distance were approximated by circular arcs. These approximations are illustrated presently. For each value of γ between .2 and 1 (increments of .2; total 5), there is a set of relative heading θ values between 0^o and 180^o (increments of 15^o; total 13). The maneuver charts for $-\theta$ are mirror images of those for θ. For each of these 65 (γ, θ) pairs, four numbers specify the maneuver regions. For r_f values between .2 and 2.6 (increments of .4; total 7), two numbers specify the location of the arc centers and seven numbers specify the radii of the arcs for each of the four maneuver pairs. Thus, the total core requirement for this table lookup are 2600 words (65 x 4 + 65 x 4 x 9). For an arbitrary (γ, θ) pair, an interpolation program and a table lookup algorithm are used to determine the optimum maneuver pair and the corresponding terminal miss distance.

In order to illustrate the approximations used for implementation of the maneuver strategy, a typical maneuver diagram is shown in Fig. 6.8 for a specific (γ, θ) pair. This partitioning of the space into different regions by arcs meeting at the triple point T (where three out of the four possible strategies produce identical miss) was approximated by (dotted) straight-line segments meeting at T. The points U and V are the intersection of the $r_f = 2.6$ curve and the true dispersal line. The point T is defined by two numbers (Cartesian coordinates) and the slopes of lines TU and TV require two additional numbers.

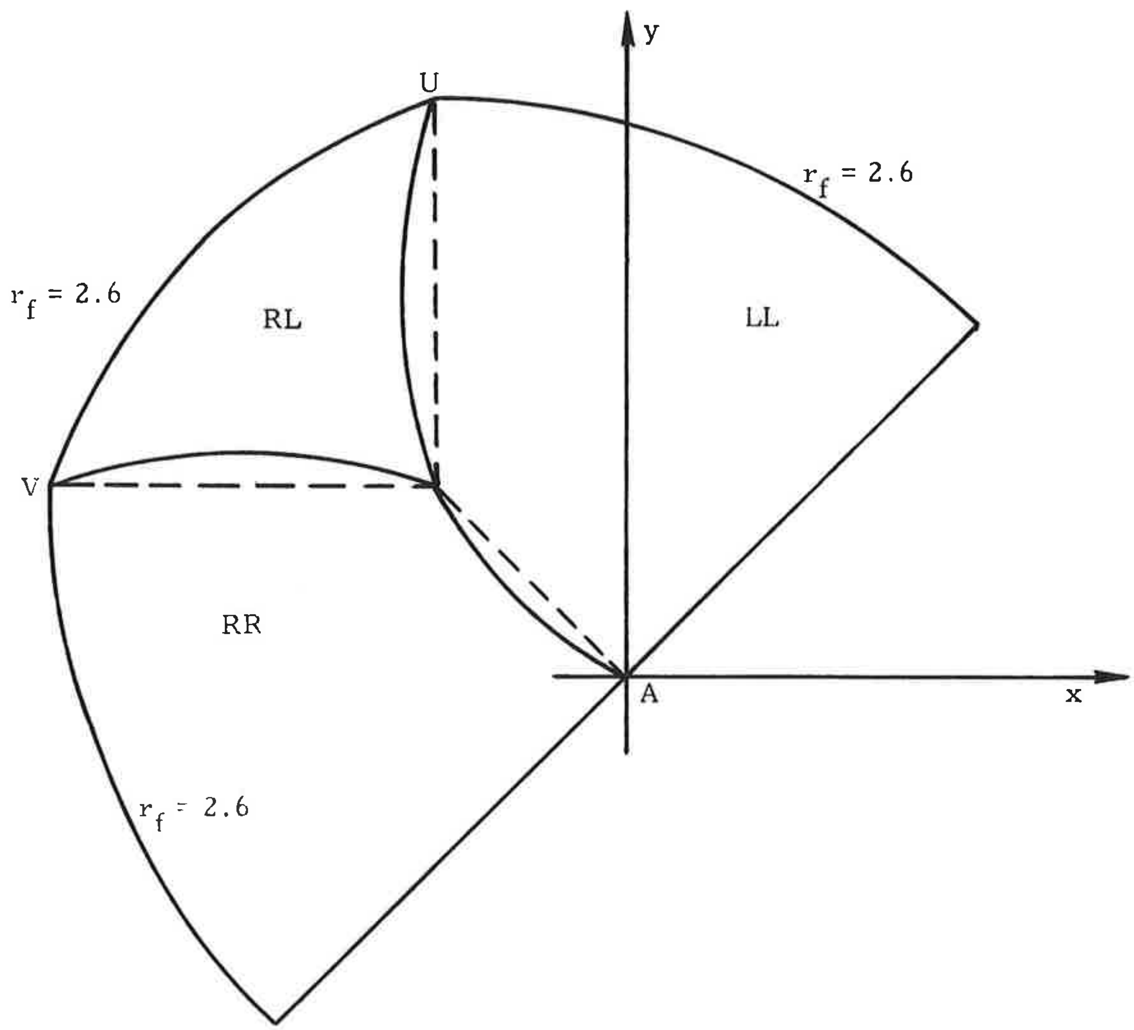

Figure 6.8 Approximation of the Optimal Maneuver Regions by Straight-Line Segments for a Given (γ, θ) Pair

It is possible to obtain polynomials as a function of the two variables γ and θ (multinomials) which fit these points over the range of interest, but this has not been done for the present study.

The algorithm determines the strategies assuming the origin of the maneuver space to be the location of the faster aircraft and then translates this result to reflect the situation as it exists for the aircraft under consideration. As a consequence, it is not necessary to store the maneuver charts in the coordinate system referenced to the slower aircraft.

The implementation of the miss distance contours entails curve fitting the actual miss distance loci from the charts by circular arcs having a common center and different radii. This procedure is repeated for each of the four possible strategies (RR/LL/RL/LR) in the appropriate region of interest of the maneuver charts. Thus, for a given (γ, θ) pair, the above set of numbers defines the necessary miss distance circular arc approximation.

As noted previously, multinomial curve fitting of this data can be undertaken to greatly reduce the core storage requirements. This procedure has the advantage of not requiring additional table lookup and interpolation algorithms to determine the miss distance r_f for an arbitrary (γ, θ) pair. Because there was no core space limitation, as far as the present study was concerned, multinomial curve fitting of the data was not attempted.

As an example of the fitting of circular arcs to the actual locus for the RL maneuver, Fig. 6.9 graphically depicts the approximation involved in fitting three loci simultaneously with one center and three radii. This curve fitting problem can be mathematically formulated as a least-squares fit to a set of circular arcs by defining a cost function

$$J = \sum_{j=1}^{m} \sum_{i=1}^{n} \{(x_{ij} - x_o)^2 + (y_{ij} - y_o)^2 - R_j^{\,2}\}^2 \tag{6.3}$$

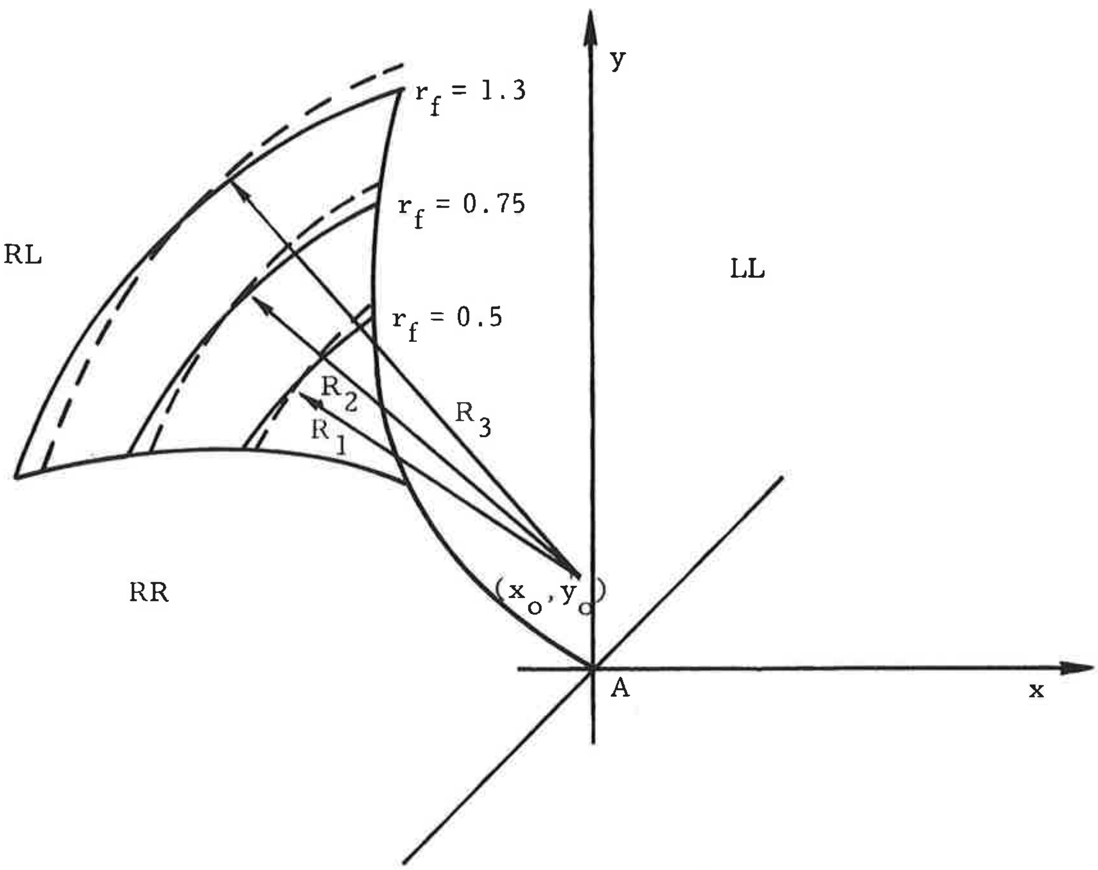

Figure 6.9 Approximation of the Constant Miss Distance r_f Loci

where m miss distance loci are to be fitted. Each locus is defined by a set of n points. The parameters x_o and y_o are the arc center coordinates and R_j is the radius to the jth arc. The problem is to find (x_o, y_o, R_j, j=1,...,m) such that J is minimized subject to the constraints $R_j \geq 0$.

6.3.2 Suboptimal Maneuver Algorithm

A major assumption leading to the suboptimality of the maneuver algorithm is that the curve fitting of miss distance is performed only for one part maneuver pairs. Although two part maneuvers can be initiated using a minimal amount of additional storage, the corresponding miss distance loci curve fitting is difficult. Consequently, although the optimal two part maneuver can be executed in a practical system, the gain that accrues in miss distance cannot be computed a priori at this time. Another major assumption of equal turn rates is imposed to reduce core requirements to a manageable level. It can be justified on the basis of conventional procedures in the terminal area. On the other hand, it is inefficient for aircraft pairs having a small speed ratio γ, i.e., widely differing speeds.

Granting these assumptions, the maneuver algorithm can be block diagrammed as in Figure 6.10. The first step is to determine time to minimum range T_{f_o} with no maneuver. Subsequent logic is activated only if this is less than a threshold time T_T (which is of the order of sixty seconds). Then minimum range r_{f_o} is determined. If this is less than acceptable range r_a, the maneuver command algorithm is activated.

The first step in the maneuver algorithm is to normalize the measured range in terms of the turning radius of the faster aircraft given by

$$R_A = V_A/\omega_A \tag{6.4}$$

where ω_A is the standard turn rate. Subsequently, the optimum turn direction pair is determined and used to evaluate the corresponding terminal miss r_f using the miss distance table lookup and interpolation program. This value of r_f is then continuously monitored as the aircraft range decreases, and it is compared to the acceptable miss r_a. When r_f falls below the threshold r_a, the maneuver commands are issued to both pilots.

Even after the maneuvers are initiated, the computer continues to cycle through the program to ensure that the desired minimum acceptable range r_a is going to be achieved. If it turns out that it is not, then the bank angle command is increased.

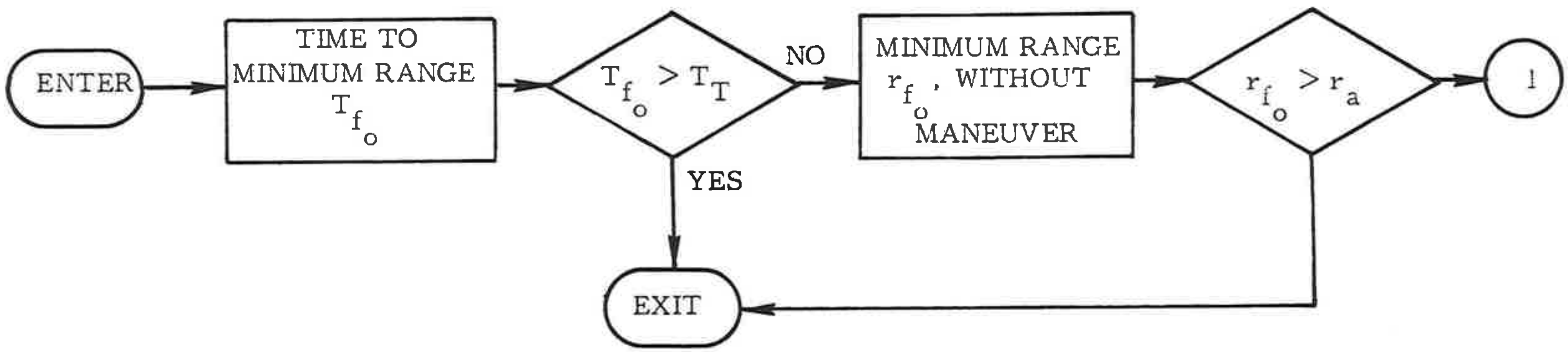

Figure 6.10(a) Maneuver Logic Block Diagram

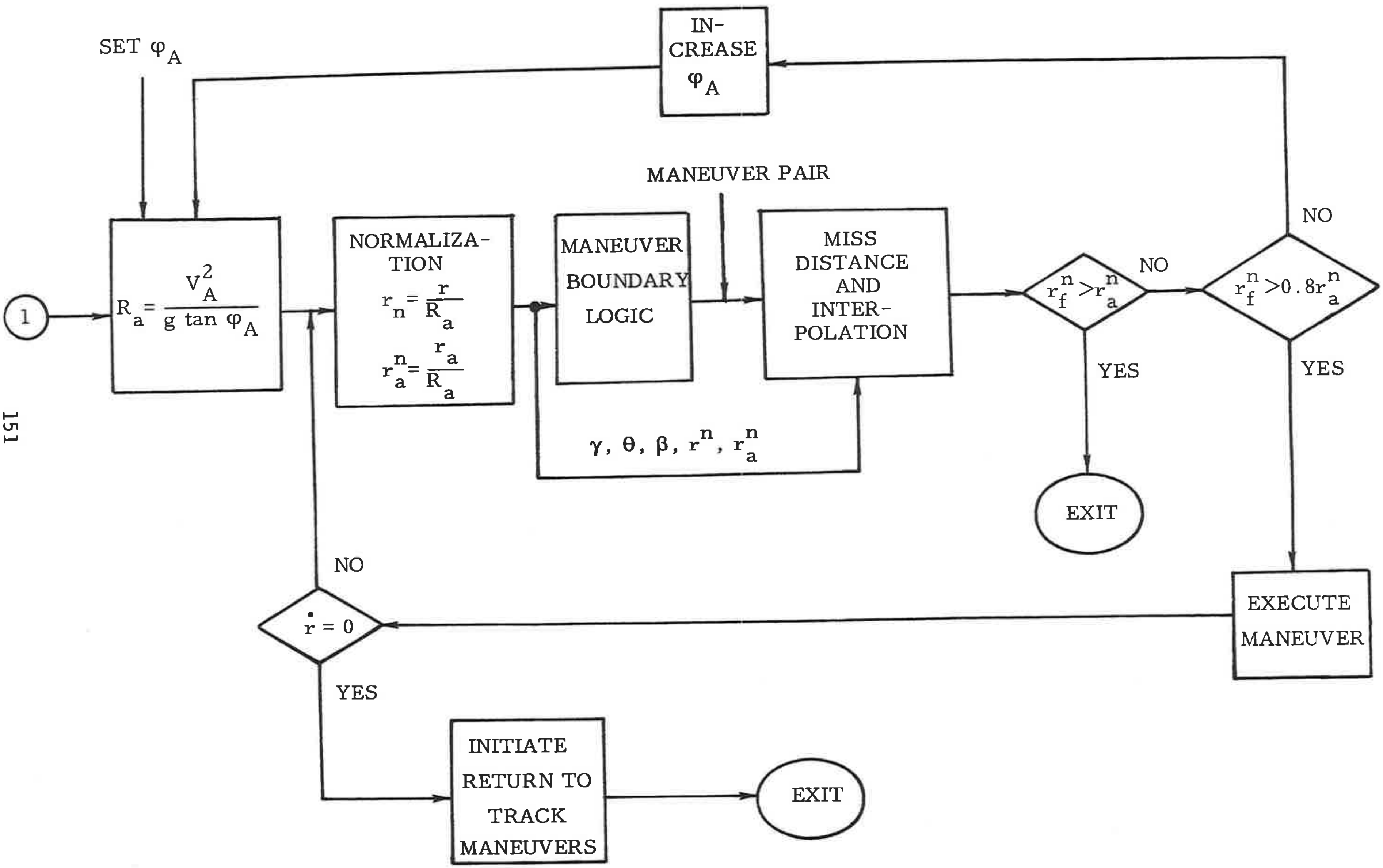

Figure 6.10(b) Maneuver Logic Block Diagram (Continued)

6.4 OTHER EQUIPMENT REQUIREMENTS

The previous sections considered the computer hardware/software requirements, estimation algorithms for heading and speed ratio, and maneuver logic algorithms. This section deals with other hardware requirements and summarizes what equipment is required in terms of sensors, computer, and display. Chapter VII is concerned with the effects of errors in this equipment.

The hardware items necessary for horizontal collision avoidance that are not considered in the previous sections include transponders (for exchanging information such as altitude, heading, velocity, turn rate, and aircraft identification), range and bearing sensors, gyros, and compasses. The main transponder requirement for data exchange is the ability to transmit digital data in a suitable encoded form for noise immunity. The receiver must have the necessary decoding logic and synchronization circuitry.

There are two methods currently considered for range measurement: interrogator-transponder [14] and time frequency. [16] These two techniques are described in Chapter II. Bearing measurement can be performed by infrared detectors, radar, radio signal triangulation, or interferometric techniques. The latter technique uses a multiple antenna (e.g., triad) and measures the electrical phase difference between the signals received at the different antennas. Turn rates can be measured with rate gyros or derived from the bank angle measured by a vertical gyro. A magnetic compass or directional gyro is used to measure the aircraft heading. Certain preprocessing is required before the range and bearing sensor data and the exchanged information is in a form usable for the maneuver algorithm.

In summary, the hardware and software requirements for a collision avoidance system with reasonable expansion capability are as given in Table 6.16.

TABLE 6.16

Summary of Hardware and Software Requirements for Horizontal CAS

REQUIREMENT	MECHANIZATION	REMARKS
Sensors	range - time frequency, interrogator-transponder bearing - interferometric or other methods	essential essential
Information exchange	altitude - static pressure heading - magnetic heading speed - pitot pressure turn rate - rate gyro	essential may be estimated may be estimated may be estimated
Interface	A/D converters, data buffers for data input to computer: range, bearing, altitude, static pressure, pitot pressure	essential
Computer hardware	16 bit digital computer, 8K core, 1 μsec clock	essential
Computer algorithms	1) range data preprocessing 2) bearing data preprocessing 3) altitude static pressure } data handling pitot pressure } 4) heading and speed ratio estimation 5) threat assessment altitude filtering time to minimum range filtering 6) horizontal maneuver generation 7) terminal miss monitoring 8) display message generation	essential
Display	Electromechanical or electronically programmable (graphic or alphanumeric)	essential

VII. EFFECT OF MEASUREMENT AND DYNAMIC ERRORS

To make the choice of parameters contained in a collision avoidance system's software requires that the several sources of error affecting the system's performance be identified and quantified. This must be followed by error analysis and sensitivity studies. Then it is necessary to adjust the software parameters so as to achieve the best system effectiveness in terms of adequate safety and tolerable false alarm rates and missed alarm probabilities. If acceptable performance cannot be achieved by parameter adjustment, the system must be redesigned to lower the error magnitudes. Often, there is a cost/benefit tradeoff.

The block diagram in Fig. 7.1 depicts a typical collision avoidance system (CAS) configuration. The sensors, CAS algorithm, and display requirements are summarized in Chapter VI. Error sources can be conveniently partitioned into dynamic and sensor errors. Dynamic errors are introduced into the system due to pilot reaction delay, servomechanism delay, aircraft response delay, computation delay, effects of winds, gusts, and turbulence, and modeling errors resulting from the use of approximate aircraft dynamics. All these errors can be effectively compensated for by introducing lead compensation into the algorithm and providing miss distance margin. On the other hand, sensor measurement errors (i.e., range, bearing, heading, and airspeed ratio) which are generally random in nature cannot be directly dealt with in this fashion. The effect of measurement errors on system effectiveness must first be analyzed via statistical techniques.

The software design parameters to be determined depend on the character and magnitude of the sensor and dynamic errors. For a given set of system errors, the objective is to select the design parameters (such as data update rate, acceptable miss distance, and lead time) to ensure that the corresponding false alarm and missed alarm probabilities are below acceptable thresholds.

Because actual design optimization is highly dependent on the specific system mechanization and the associated error sources and aircraft data, this was considered to be beyond the scope of the present study. As a more meaning-

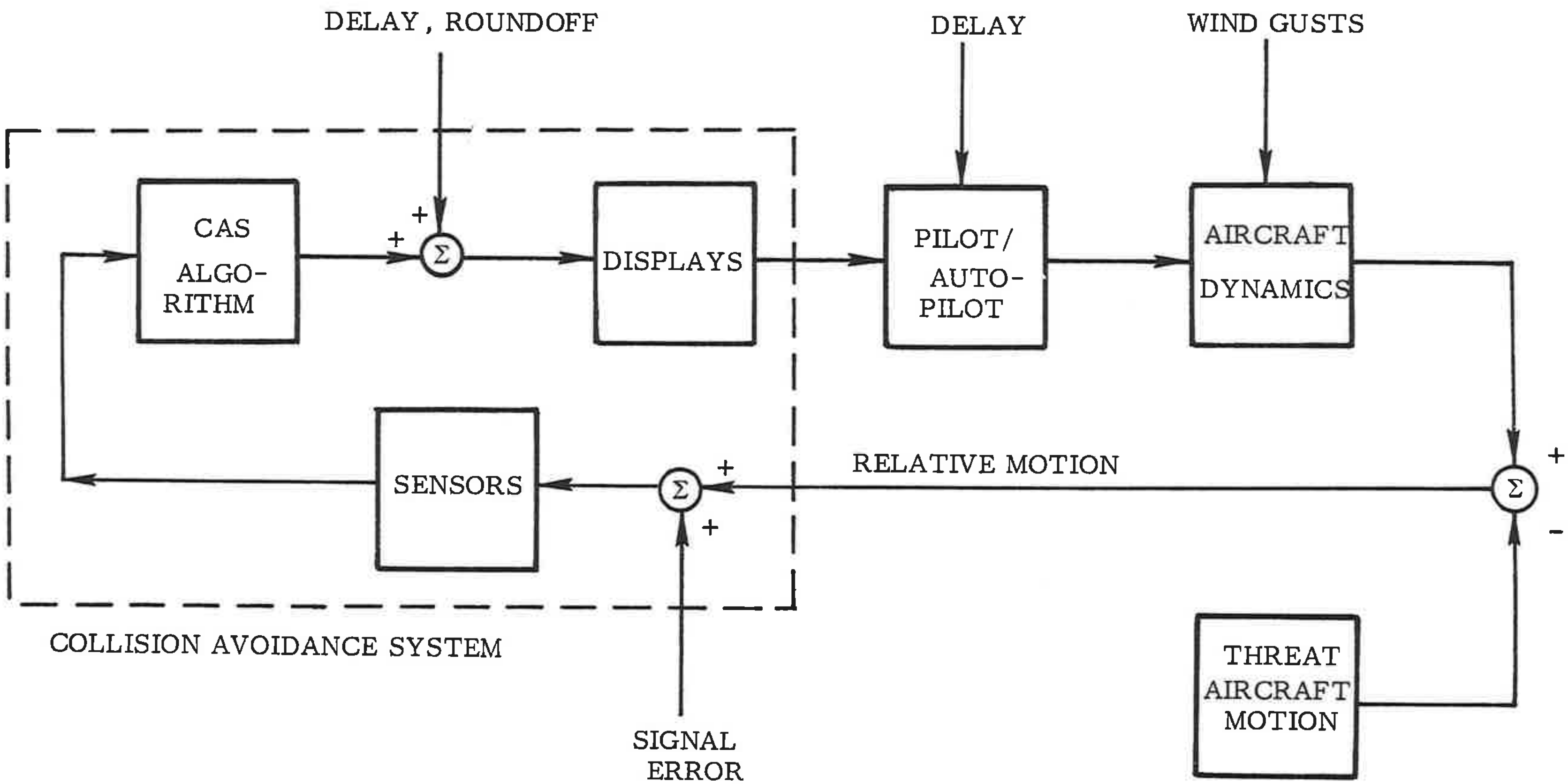

Figure 7.1 Block Diagram of a Typical CAS Configuration

ful alternative, general error analyses were conducted on models of typical horizontal collision avoidance systems. These analyses were used to derive general conclusions regarding the effect of measurement errors. The system models were based on the material presented in Section 6.3.

A simple worst-case error analysis was first performed for identical aircraft (equal speeds and turn rates). This analysis was used to determine the general effects of different types of errors. The worst-case analysis was also used to determine initial separation contours which approximate where maneuvers should begin in order to obtain an acceptable miss distance.

To obtain more information regarding the statistical distribution of miss distance resulting from measurement errors affecting the horizontal CAS's operation, a Monte Carlo error analysis was conducted. This was based on a detailed digital simulation of an encounter between two aircraft, each equipped with the horizontal CAS. Each pass through this simulation was affected by randomly generated errors. The Monte Carlo simulation program was exercised to generate false alarm and missed alarm ratios for prespecified encounter geometries, data update rates, lead time, and error statistics. Variations in the miss distance distribution were found as a function of the different error magnitudes. Attention was mainly directed to obtaining the above mentioned system effectiveness measures for several different speed ratios (γ), encounter geometries (θ), sensor errors (r, β, θ, γ), and acceptable miss distance r_a.

In the following sections, the models used for characterizing the system errors are first described. This is followed by discussions of the worst-case and Monte Carlo error analyses.

7.1 DYNAMIC AND MEASUREMENT SENSOR ERROR MODELS

The error sources resulting from dynamic effects and sensor mechanization were previously noted. This section is devoted to quantifying these errors and assessing their relative effect on performance.

7.1.1 Dynamic Error Sources and Models

The various sources of dynamic error that can be quantified are listed in Table 7.1. Some of the data was obtained from Ref. [34]. The symbol $N[\mu,\sigma^2]$ denotes a normal distribution with mean μ and standard deviation σ. Although the Monte Carlo simulation program has provisions to incorporate these delay distributions, for the purposes of the present study, a fixed lead time of 9 seconds was used to compensate for the delays.

TABLE 7.1

Dynamic Error Sources, Distributions, and Magnitudes

SOURCE	PARAMETER	DISTRIBUTION	COMMENTS
Aircraft Servo	T_S (secs)	$N[1, .25^2]$	Truncated so that $T_S > .1$
Roll out/Roll in	T_R (secs)	$N[4, 2^2]$	Truncated so that $T_R > 1$
Pilot Delay	T_p (secs)	$n_1, n_2 = N[0,1.5^2]$ $T_p = (n_1^2+n_2^2)^{\frac{1}{2}} + 1$	Rayleigh; truncated so that $T_p > 1$.
Computation Delay	T_C (sec)	impulse	1 second (nominal)
Data Update Rate	T_{SC} (sec)	impulse	1 second (nominal)

Other dynamic errors that must be considered are dispersion from a circular coordinated turn due to wind gusts and turbulence. References [91] and [92] provide useful numerical values for half turns executed by a fully automatic (simulation results) jet transport and a manually flown (flight test results) general aviation (GA) aircraft, respectively. On the basis of these results, the worst situation is that of a light GA aircraft in light to moderate turbulence. The corresponding quarter turn standard deviation from track was estimated to be 100 ft. This yields a three sigma correction factor (to be incorporated into the acceptable miss distance) for a GA/GA encounter to be about 450 ft. (three times the root-sum-square of 100 ft. for two aircraft). In reality, there are insufficient data available concerning each of the dynamic errors to make any valid conclusions about their quantitative effect on the resulting miss distance.

7.1.2 Measurement Sensor Errors and Models

As noted previously, the sensor errors to be considered are measurements of range, bearing, heading, and airspeed ratio. Range and bearing are determined by onboard sensors whereas heading and airspeed ratio can either be determined by information exchange or estimation.

Range can be determined by an interrogator-transponder scheme or the time frequency method. In either case, the causes of range error are range bin resolution, oscillator stability, data update rate, neglecting elevation angle between aircraft, antenna/receiver noise, and table lookup errors. Quoted accuracies for ranging systems have standard deviations between 15 ft. (stationkeeping applications) and 200 ft.[6,18]

Bearing can be determined by phase interferometric techniques using multiple antenna systems mounted above and below the aircraft. The major causes of bearing errors are antenna orientation error due to mounting misalignment, attitude errors from the navigation system, neglecting the elevation angle, antenna/receiver system noise and table lookup errors, transmitting antenna pattern, and heading of the threat aircraft. Quoted accuracies for bearing measurement systems have standard deviations of between 1.5^o to 10^o.[18,19]

When heading and speed ratio are estimated from range and bearing data, the quality of these measurements, in terms of their standard deviations, have a central effect on the quality of the estimates. Results relating these factors are detailed in Section 6.2 and Appendix E. On the other hand, when heading and speed are exchanged, the principal error source is digitization error due to A/D converters. Errors due to heading and speed measurement inaccuracies onboard the measuring/transmitting aircraft are relatively negligible.

For the purposes of the Monte Carlo simulation, the nominal distributions presented in Table 7.2 were assumed. It was assumed that these errors are random biases. It is emphasized that the correct error models are highly dependent on the actual mechanization. That is, an instrument's error will be normally made up of bias, noise, and quantization error effects with various magnitudes.

TABLE 7.2

Nominal Distributions of Measurement Errors

MEASUREMENT	ERROR DISTRIBUTION	UNITS
range	$N[0,\ 200^2]$	ft.
bearing	$N[0,\ 5^2]$	degrees
heading	$N[0,\ 5^2]$	degrees
speed ratio	$N[0,\ .05^2]$	dimensionless

7.2 WORST-CASE ANALYSIS FOR SMALL MEASUREMENT ERRORS

As a simple illustration of the effect of measurement errors in range and bearing on miss-distance, consider aircraft B to be moving in relative space along the straight dotted line depicted in Fig. 7.2. As aircraft B gets closer to A, the orientation and shape of the error ellipse (3σ) changes. The solid line arc in this figure indicates the nominal relative motion of B with respect to A when both aircraft maneuver. The dashed line arcs are the relative motion as a result of worst-case errors. The miss-distance with no maneuver, the desired miss-distance, and the limits of the resultant 3σ miss-distance distribution due to the measurement errors are indicated.

It was assumed for Fig. 7.2 that the aircraft were traveling along known nominal paths, and then the aircraft maneuvered based on measurements affected by the sensor errors. Based on the concept illustrated in this figure, a worst-case sensitivity analysis was conducted for identical aircraft. This analysis assumed that both aircraft make either right or left turns simultaneously. Then for given range, bearing, and heading sensor bias error maximim values, the worst possible combination of these errors was chosen such that r_f, the corresponding terminal miss (with maneuver), was minimized.

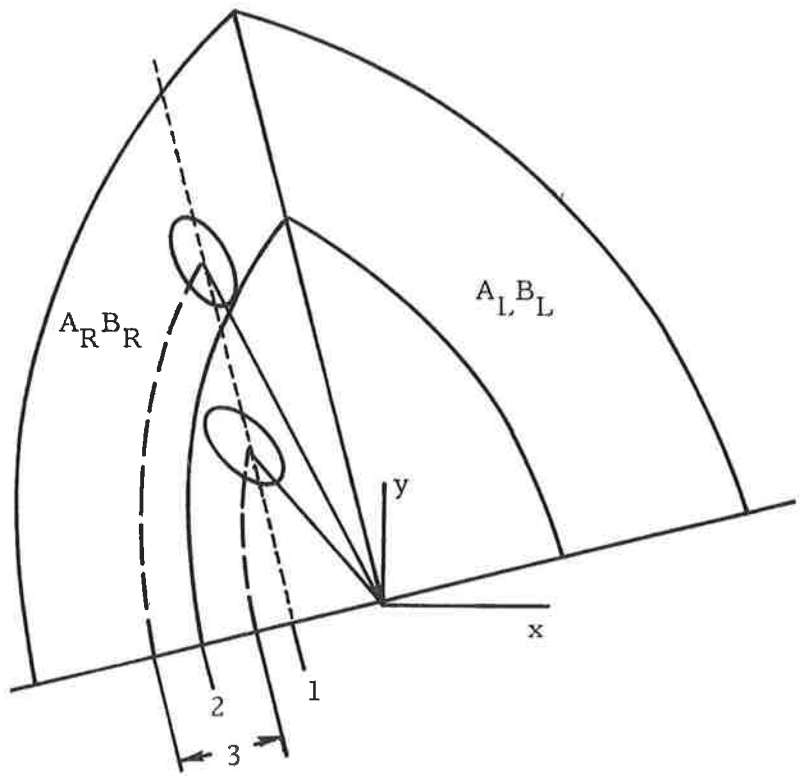

1. Miss distance with no maneuver.
2. Desired miss distance.
3. Distribution of miss distance due to range and bearing measurement errors.

Figure 7.2 Effect of Measurement Errors on Miss Distance

Figure 7.3 shows the miss distance variation as a function of range, bearing, and heading errors for a head-on collision geometry, and for three different closing airspeeds. It can be seen that as the speeds increase, the miss distance error increases, but its sensitivity to range error decreases. On the other hand, the sensitivity to bearing error increases dramatically, and sensitivity to heading error also increases as the speed of the encounter increases. Comparison with similar curves generated for other encounter geometries indicates that miss distance is most sensitive to sensor errors for the head-on collision geometry (Fig. 7.4). Moreover, sensitivity to bearing errors is approximately twice that due to heading errors.

$V = V_A = V_B = 160$ Knots

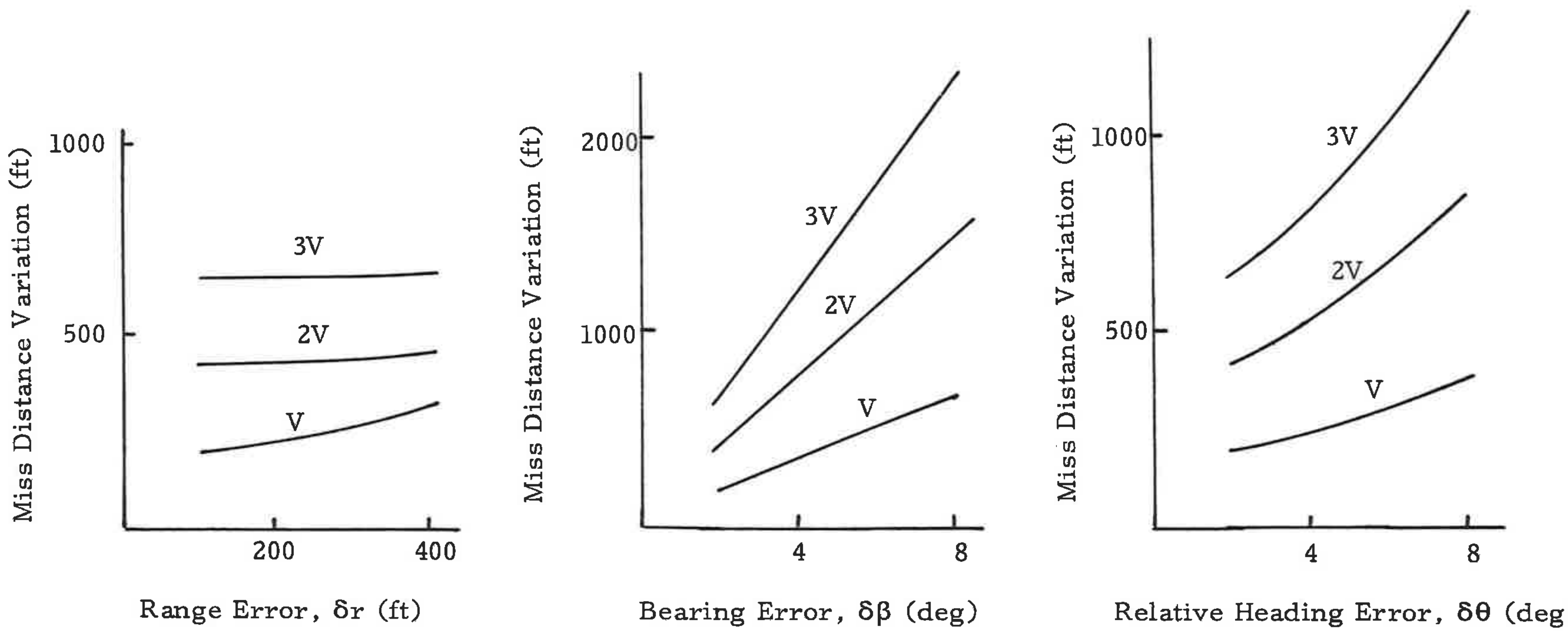

Figure 7.3 Sensitivity Curves of Miss Distance as a Function of Measurement Errors

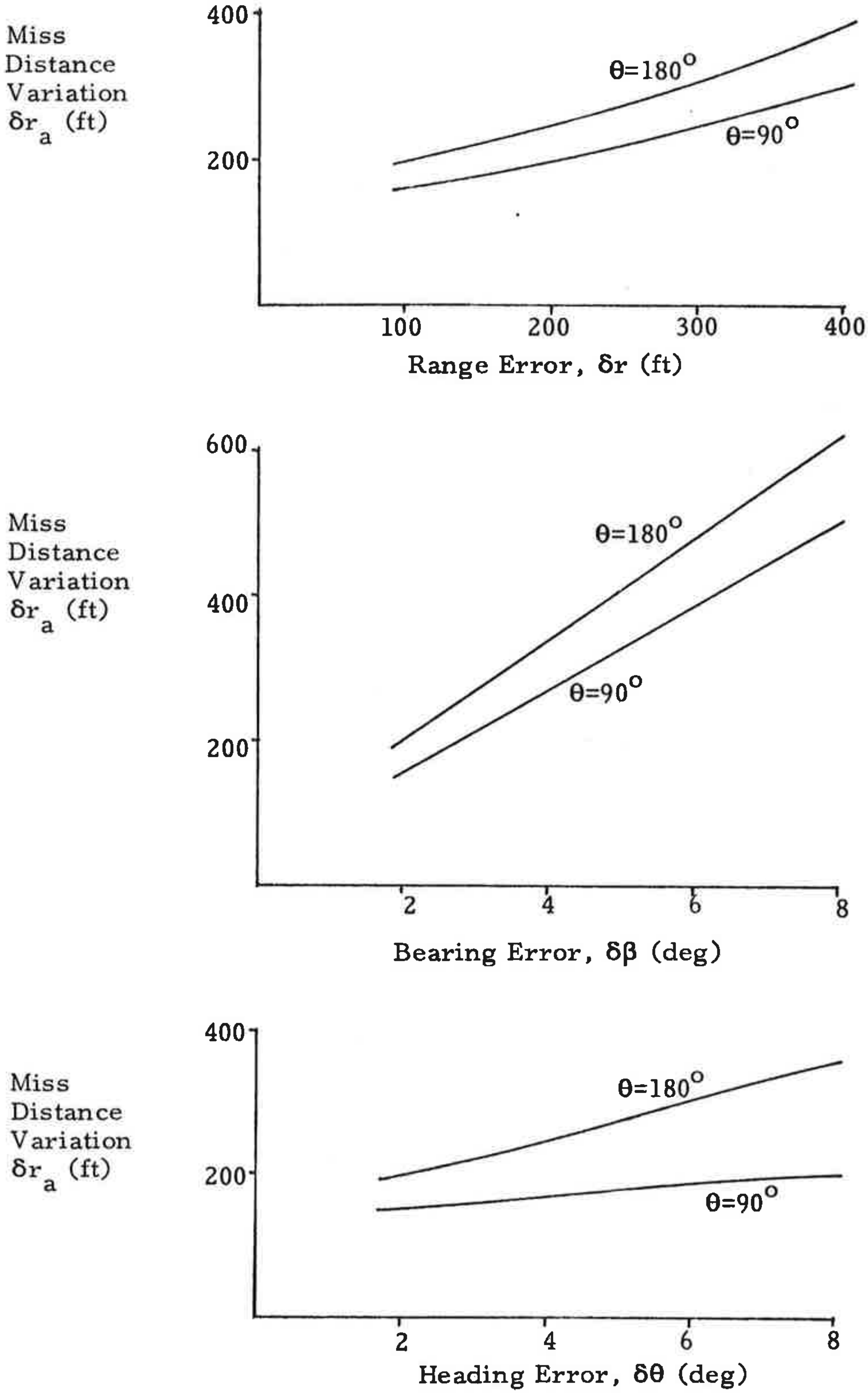

Figure 7.4 Error Analysis Results for Aircraft Initially on a Collision Course as a Function of Initial Relative Heading

Given the sensor bias errors, Figs. 7.3 and 7.4 can be used to set the acceptable miss-distance parameter in the maneuver algorithm to limit the number of missed alarms. Suppose the range, bearing, and heading sensor error biases are 200 ft., 5^{o}, and 5^{o}, respectively. The corresponding miss-distance variation can be read off the appropriate curves to be approximately 250 ft., 250 ft., and 275 ft., respectively. The resulting variations due to the presence of all three biases is given by the root-sum-square of the individual variations (this step implies an independence assumption that is generally not valid). Consequently, a standard deviation in miss-distance of about 450 ft. is obtained. Thus, there is a .01% probability of collision (5σ) if the acceptable miss-distance parameter is set at 2250 ft.; this number provided the basis for selecting a nominal value of acceptable miss-distance, r_a, as 2000 ft. in the Monte Carlo error analysis discussed in the next section.

When the expected sensor errors are large, the methods used in the analysis above can be applied to determine contours in relative space where maneuvers must begin (for given sensor errors) to achieve a safe miss-distance. The contours shown in Fig. 7.5 were determined by assuming that identical aircraft are on a collision course. When a threat aircraft crosses the appropriate contour (protection boundary), both aircraft must cooperatively turn right or left to achieve acceptable miss-distance. These curves are also useful in defining hazard regions as would be used for Pilot Warning Indicator systems.

7.3 MONTE CARLO ERROR ANALYSIS

The purpose of this section is to describe the digital computer simulation used to conduct Monte Carlo analysis of the horizontal CAS system and the results of the subsequent analysis. This analysis was used to obtain a statistical rather than worst-case characterization of errors which could occur in a mechanization of the horizontal CAS. The simulation is a variable-time increment simulation of encounters of two aircraft equipped with horizontal CAS's.

7.3.1 Computer Simulation

The computer simulation involves three basic components:

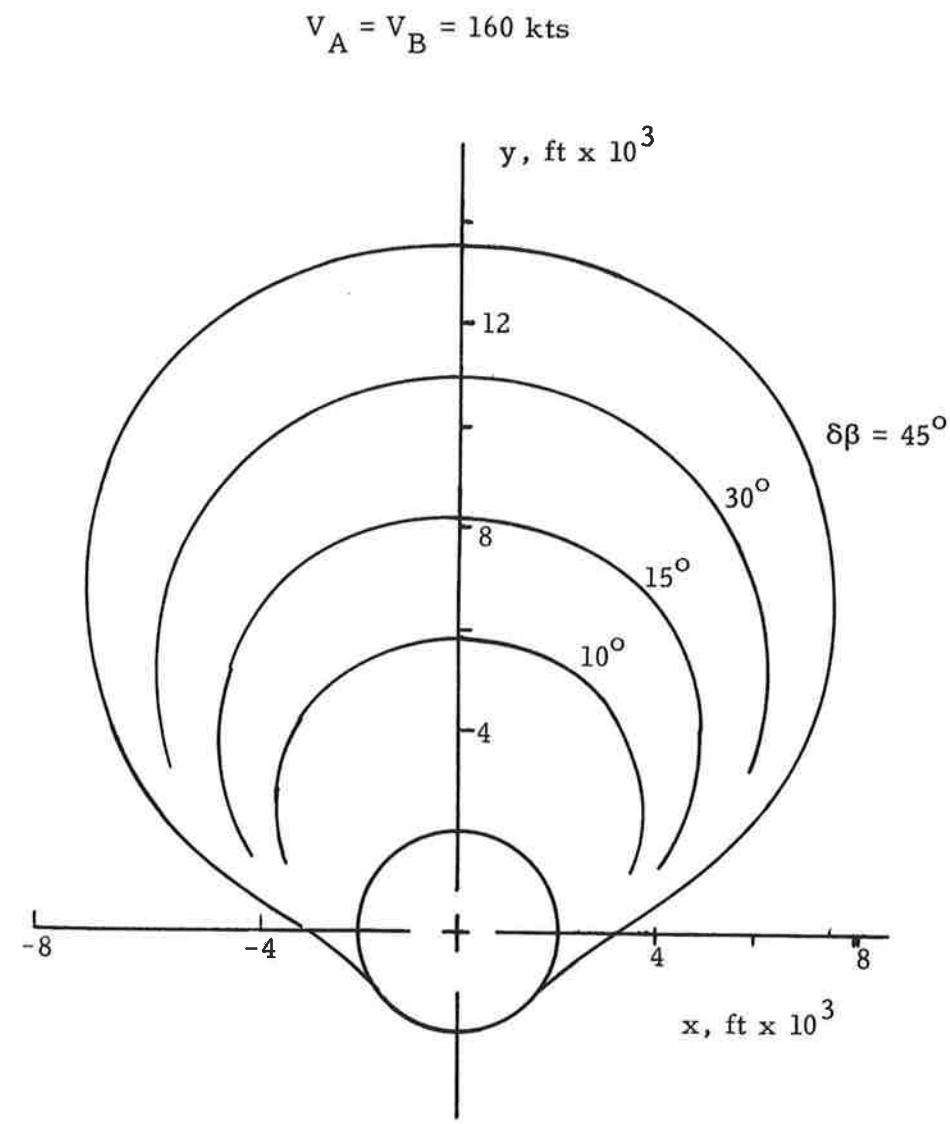

Figure 7.5 Initial Range Required for Acceptable Miss Distance with Variable Bearing Error

1. The maneuver logic described in Section 6.3;

2. The statistical distribution of aircraft in the airspace; and

3. The statistical characteristics of dynamic and sensor errors in the mechanized CAS.

The output of the simulation was the determination of performance measures, such as miss-distance distribution, missed alarm rate, false alarm rates, and collision probabilities. The purpose of the simulation study was not to propose or advocate how a horizontal CAS should be mechanized, but to indicate the kind of performance that could be expected from such a system for given sensor qualities.

A flow chart of the simulation is shown in Fig. 7.6. Given an initial relative heading, a pair of airspeeds, and a set of parameters specifying the sensor qualities, the program generates a random sample of aircraft encounters which begin at the given relative heading and involve pairs of aircraft at the given airspeeds.

The initial relative positions of the two aircraft (with a given initial relative heading) are chosen to be uniformly distributed along a line of initial positions which result in a no maneuver miss-distance between zero and a specified large number, r_{in}, as shown in Fig. 7.7. Thus, encounters for which there can be no collision threat (except in the case of extremely large sensor errors, or if incorrect maneuvers are initiated) are eliminated. The maneuvers based on erroneous measurements cause the resultant distribution of actual miss-distances to extend beyond r_{in}. However, this constraint is required in order to limit (to a reasonable level) the computation costs of obtaining a sample of sufficient size to enable the deduction of valid statistical inferences.

The maneuver logic algorithm discussed in Section 6.3 is incorporated with the additional feature of simulating two aircrafts' sensor errors and maneuver initiation decisions simultaneously. The actual maneuver decision and resulting terminal miss is determined by the aircraft that is first to sense that a maneuver is required to achieve an acceptable miss distance of at least r_a. It is assumed that the other aircraft would maneuver as if the first aircraft's resulting maneuver commands are transmitted and are correct.

Sensor errors in range, relative heading, bearing, and speed ratio were assumed to be zero mean normally distributed biases for the study. Other more general error models are possible. However, because biases are probably the

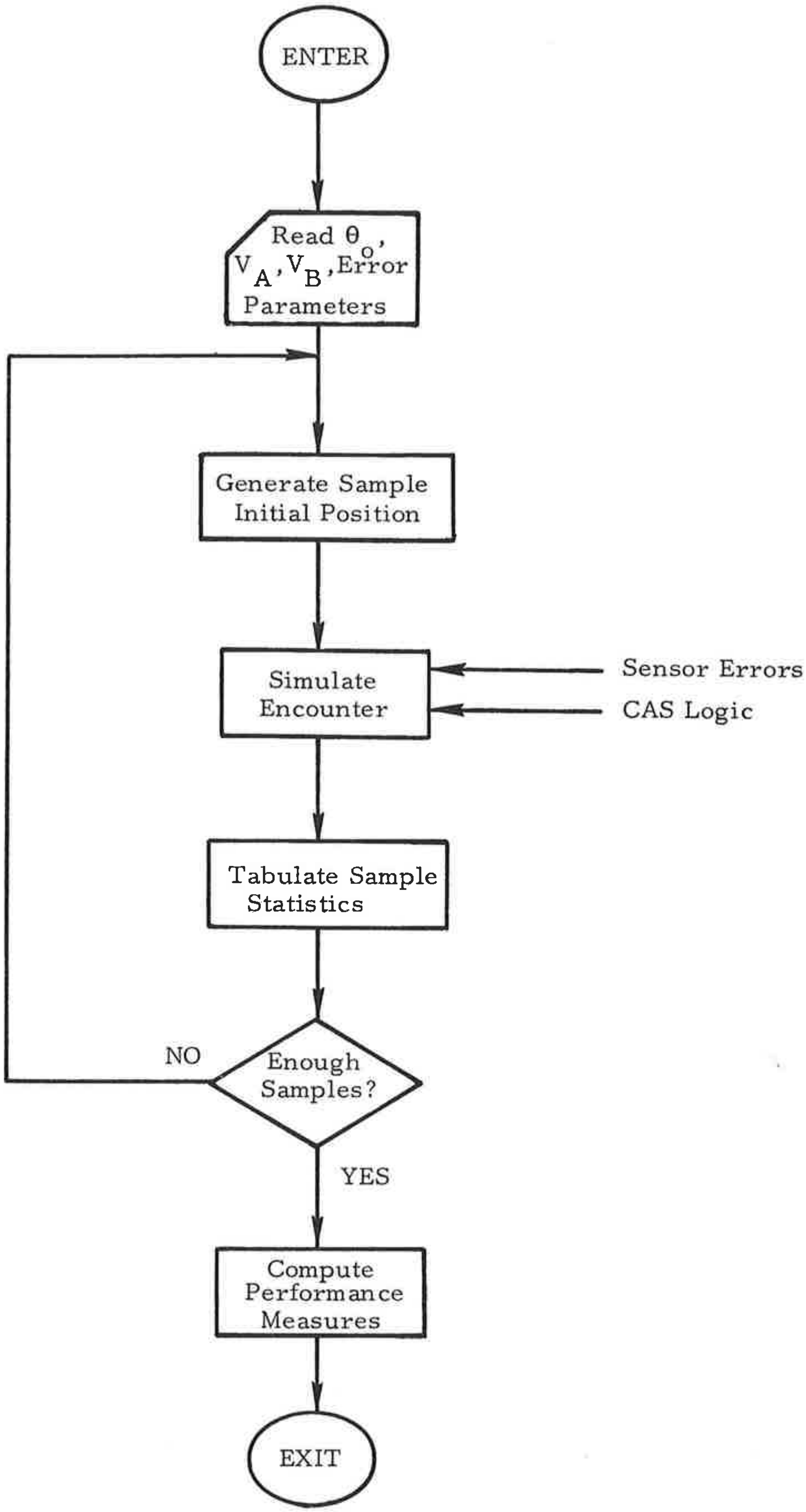

Figure 7.6 Flow Chart of Monte Carlo Simulation to Determine CAS Performance as a Function of Sensor Error Magnitudes

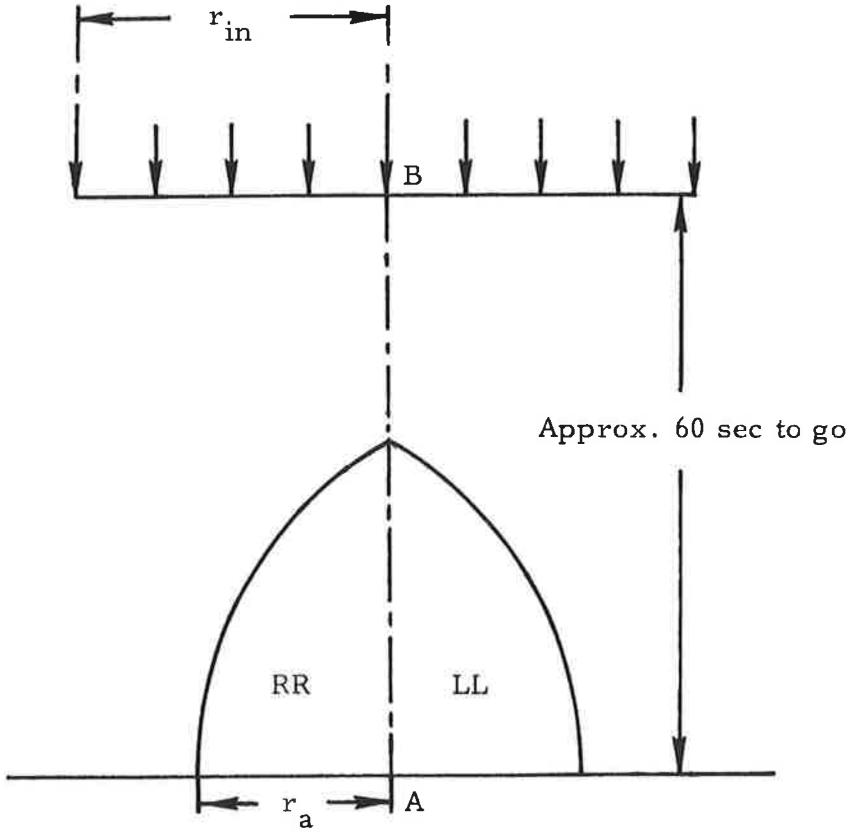

Figure 7.7 Initial Aircraft Encounter Distribution Generation for the Monte Carlo Error Analysis Simulation

dominant source of error from the point of view of the maneuver logic, the assumptions above are adequate for the preliminary investigation reported here. Time delays due to aircraft dynamics, pilot delay, and computer computations were treated as constants. However, there is an option in the simulation program so that the delays can be treated as random variables in future studies.

The output of the program is an estimate of the random distribution of the miss distance given the initial relative heading of the encountering aircraft. Other quantities tabulated include the miss distance as expected by the pilots, false alarm rate, missed alarm rate, and probability of collision, near-miss, acceptable miss, and excessive miss. These quantities are defined later.

Because the encounter simulation portion of the program is a variable time-increment simulation, the computation required to simulate a specific encounter is greatly reduced over that required by a fixed time-increment simulation. In other words, the simulation is an event-based simulation rather than a time-based simulation.

After each sample encounter has been simulated, the appropriate sample statistics are tabulated so that the performance measures can be computed after the entire ensemble has been collected. A technique for computing a consistent and asymptotically unbiased estimate of the probability density function for the miss-distance, given the heading angle, from a finite set of encounter simulations is described in Appendix F. For $\theta_o = 150^o$, $r_a = 2000$ ft, and N (number of samples) = 2000, the density function estimate $\hat{p}_N(r_f|\theta_o)$ is as shown in Fig. 7.8. For this example, the mean μ_{r_f} and standard deviation σ_{r_f} of the miss distance were computed to be 2116.6 ft and 457.8 ft, respectively.

This density function approach was used to select the number of encounters N for each of the simulation runs. The method also provided verification that computation of the various performance probabilities via the classical relative frequency approach was accurate enough, relative to the source of the data. For a more complete simulation study with more realistic conditions and constraints, the density function approach should be used to obtain the accuracy consistent with the realism of the data.

A tabulation of the raw data results of the Monte Carlo simulation may be found in Appendix G. The following sections are devoted to summarizing the principal results and conclusions of the error analysis.

7.3.2 Simulation Input and Output Parameters

Prior to carrying out a set of simulation runs to study the effect of several different system parameters, it was necessary to select appropriate values for some of the simulation parameters, select a set of baseline sensor error parameters, and define output performance parameters of interest. As noted in Section 7.2, the worst-case analysis data provide a basis for selecting a base-

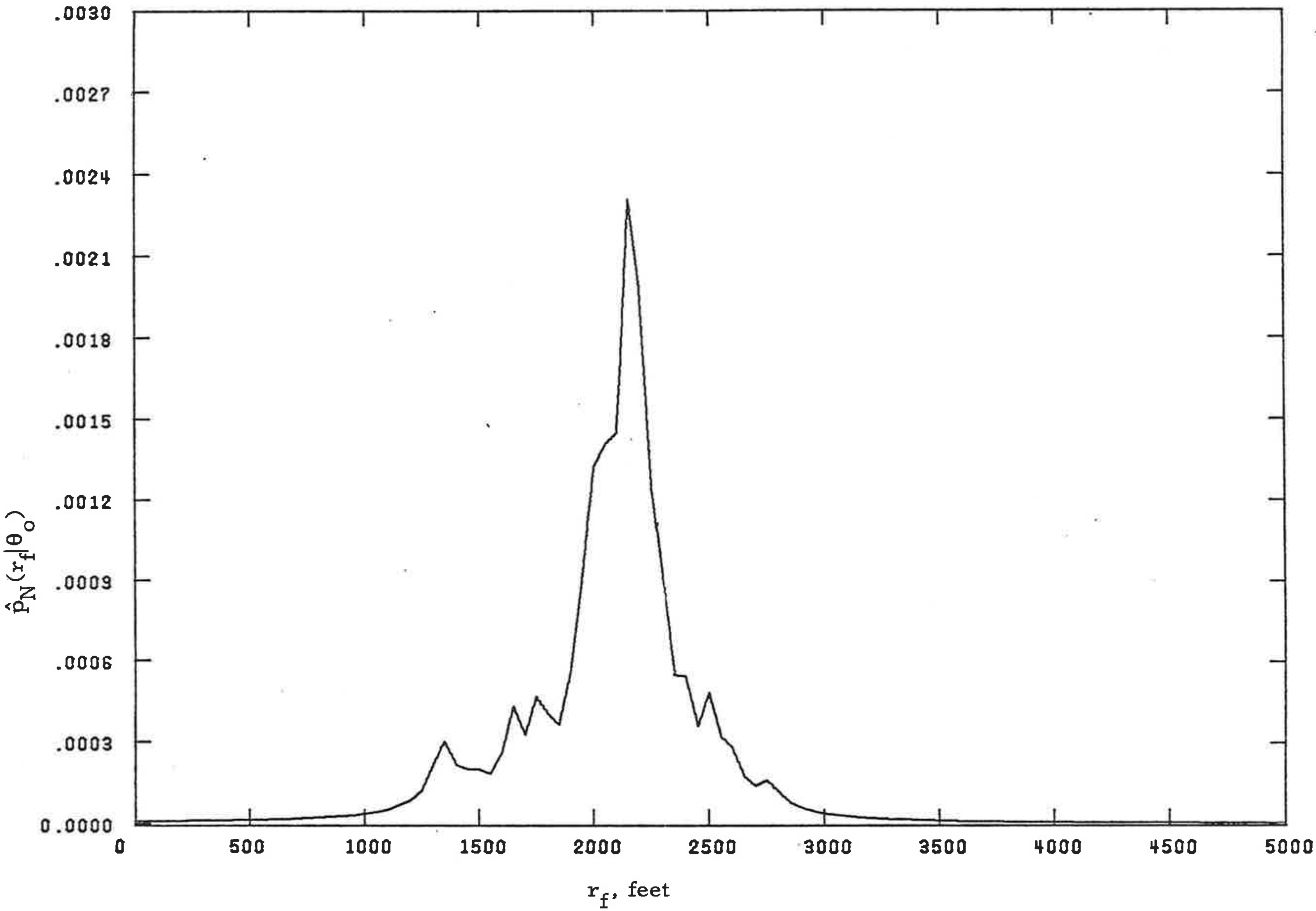

Figure 7.8 Conditional Density Function of Miss Distance r_f With $\theta_o = 150^o$, N = 2000, r_a = 2000 ft, V_A/V_B = 360/180, σ_r = 200 ft, $\sigma_\beta = 5^o$, $\sigma_\theta = 5^o$, $\sigma_\gamma = 0.05$

line value for the acceptable miss distance r_a as 2000 ft. The number of samples for each simulation run was fixed at 2000 for all runs, on the basis of a tradeoff between computation time and stationarity of the resulting miss-distance probability distribution, as shown in Appendix F. This also established the validity of using a relative frequency definition for computing false alarm rate, missed alarm rates, and other output performance parameters of interest.

On the basis of quoted sensor accuracies, the following sensor error standard deviations were selected for the baseline system: σ_r - 200 ft., $\sigma_\beta = 5^o$, $\sigma_\theta = 5^o$, and $\sigma_\gamma = .05$. The worst-case analysis, described in Section 7.2, indicated that the head-on or near head-on encounter geometry was the most susceptible to errors; therefore, the nominal value of initial relative heading θ_o was chosen to be 150^o. Assuming the encounter under investigation to be in the near terminal area, the current limit of 250 knots airspeed was used to arrive at $(V_A)_{max} = 425$ ft/sec. Also, a lower speed limit of approximately 100 knots was used, resulting in $(V_B)_{min} = 180$ ft/sec.

For the present study, dynamic error sources were assumed to be known deterministic quantities. To account for these dynamic error effects, a fixed lead time of 9 seconds was used in the algorithm. The two aircraft were assumed to be flying straight and level prior to detection. The distribution of aircraft B with respect to aircraft A is as shown in Fig. 7.7. When the range sensor error parameter σ_r and acceptable miss-distance r_a were varied from their nominal value, to study their effect on the performance parameters, r_{in} was set at 4000 ft. For all other parameter variations, r_{in} was set to $(r_a + 3\sigma_r)$.

It is noteworthy that the simulation assumes a cooperative encounter between two similarly equipped aircraft. Consequently, for each initial geometry that is randomly selected from the uniform distribution shown in Fig. 7.7, the sensor error distribution is sampled twice, and two passes are made through the maneuver logic algorithm described in Chapter VI. Furthermore, it is assumed that the aircraft that receives the alarm first, relays the cooperative strategy to the other aircraft and both aircraft initiate the proper maneuvers. The corresponding terminal miss is computed prior to making the next pass through the simulation (i.e., sampling the initial position distribution).

It is emphasized that in order to reduce the simulation time, once the simulated maneuver was initiated, the range between the two aircraft was not continually monitored (as would be the case in the real-world implementation). The algorithm simulated did not use the feature of taking corrective action (e.g., banking harder), if the acceptable miss-distance was seen to be unachievable, on the basis of range monitoring. More extensive studies using this simulation should certainly make use of this feature.

The output of the program is the miss-distance distribution in histogram form ranging from 0 to 4500 ft in steps of 300 ft. Additional results generated by the program in tabular form include the types of maneuvers ((RR/RL/LL/LR/OO), where RR means both aircraft turn right, etc.), the missed alarms, false alrm, and the incorrect/faulty maneuvers.

7.3.3 Simulation Results

In order to facilitate the generation of the above mentioned tabular forms, definitions of the various acronyms which are used are given in Table 7.3. For notational convenience, the conditioning of relevant parameters to compute the various probabilities is suppressed.

The effect of the encounter geometry (relative initial heading) on CAS performance is illustrated by the curves in Fig. 7.9. From Figs. 7.9(a) and (b), the missed alarm rates (MAR_C and MAR_{NM}) have a maximum value between 90^o and 150^o. Incorrect maneuver rate (near misses), IMR_{NM}, (Fig. 7.9(c)) is higher for θ_o greater than 90^o. The total incorrect maneuver rate, IMR_T, (Fig. 7.9(d)) has a peak at 90^o due to the differing maneuver strategies on either side of $\theta_o = 90^o$ (see Chapter VI). The false alarm rate, FAR, (Fig. 7.9(e)) curve shows an increase for initial headings greater than 90^o.

Tables 7.4-7.9 were derived based on variations to the nominal condition ($\theta = 150^o$). Table 7.4 shows the effect of increasing the speed ratio γ (i.e., $V_A = 425$ fps, $V_B = 375$ fps and 180 fps) and the effect of increasing the speed of the faster aircraft (i.e., $V_B = 180$ fps, $V_A = 360$ fps and 425 fps). As γ increases, the missed alarm rates and incorrect maneuver rates generally decrease.

TABLE 7.3

Definition of Terms for Monte Carlo Simulation Results

TERM	SYMBOL	DEFINITION
Collisions	C	Number of terminal misses between 0 and 300 ft.
Probability of collision	P{C}	Relative frequency of terminal misses between 0 and 300 ft., C/no. samples
Near-misses	NM	Number of terminal misses between 300 and 900 ft.
Probability of near-miss	P{NM}	Relative frequency of terminal misses between 300 and 900 ft., NM/no. samples
Collisions and near misses	C+NM	Number of terminal misses between 0 and 900 ft.
Probability of collision or near-miss	P{C+NM}	Relative frequency of terminal misses between 0 and 900 ft., C+NM/no. samples
Acceptable misses	AM	Number of terminal misses between 900 and 2700 ft. (3900 ft. when effects of changes in r_a and σ_r are studied)
Probability of acceptable miss	P{AM}	Relative frequency of terminal misses between 900 and 2700 ft. (3900 ft.), AM/no. samples
Excessive misses	EM	Number of terminal misses greater than 2700 ft. (3900 ft.)
Probability of excessive miss	P{EM}	Relative frequency of terminal misses greater than 2700 ft. (3900 ft.), EM/no. samples
Missed alarm rate (collisions)	MAR_C	Relative frequency of missed alarms which result in collisions for encounters which begin on collision courses
Missed alarm rate (near-misses)	MAR_{NM}	Relative frequency of missed alarms which result in collisions or near-misses for encounters which begin on collision or near-miss courses
Incorrect maneuver rate (near-misses)	IMR_{NM}	Ratio of incorrect maneuvers which result in collision or near-miss to total incorrect maneuvers
Incorrect maneuver rate (total)	IMR_T	Ratio of total incorrect maneuvers to maneuvers initiated in ensemble
False alarm rate	FAR	Relative frequency of alarms for encounters which begin with a terminal miss greater than r_a

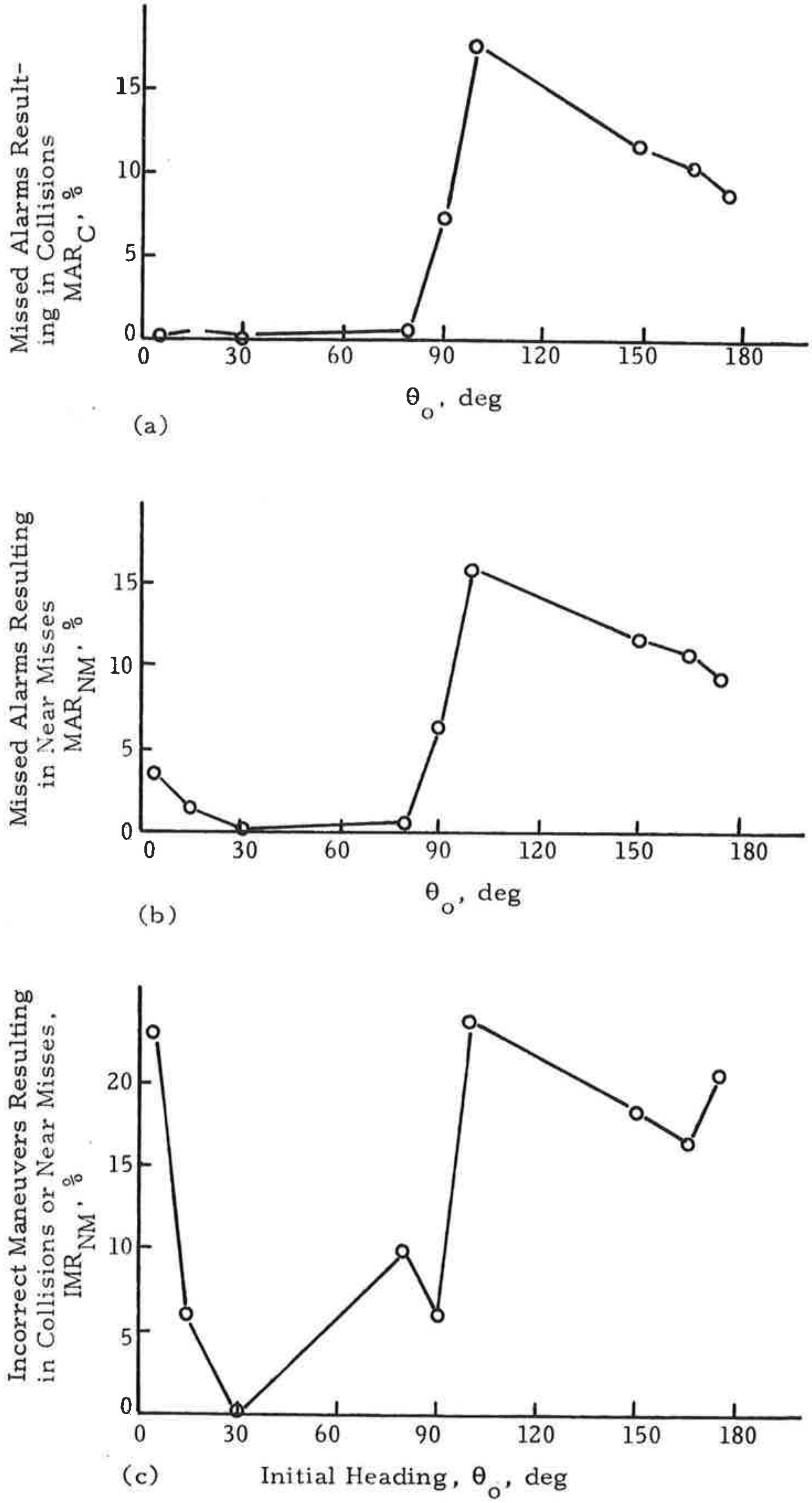

Figure 7.9 Effect of Encounter Geometry on CAS Performance Measures

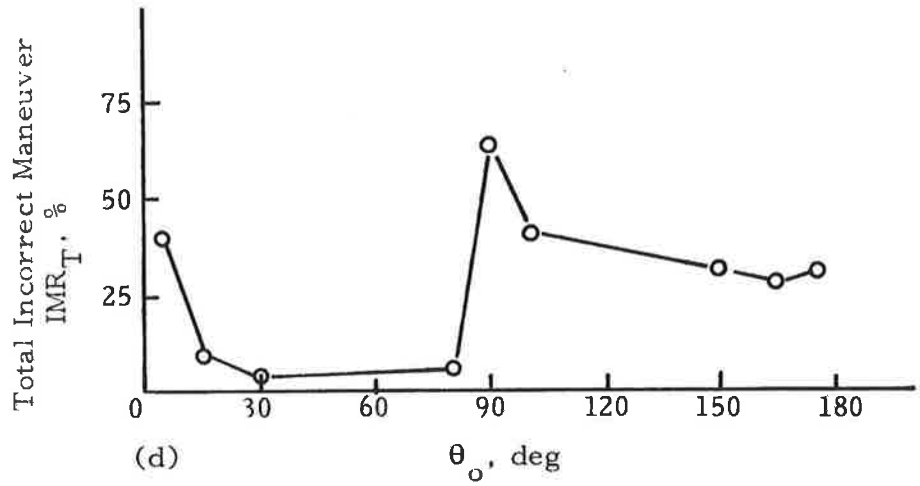

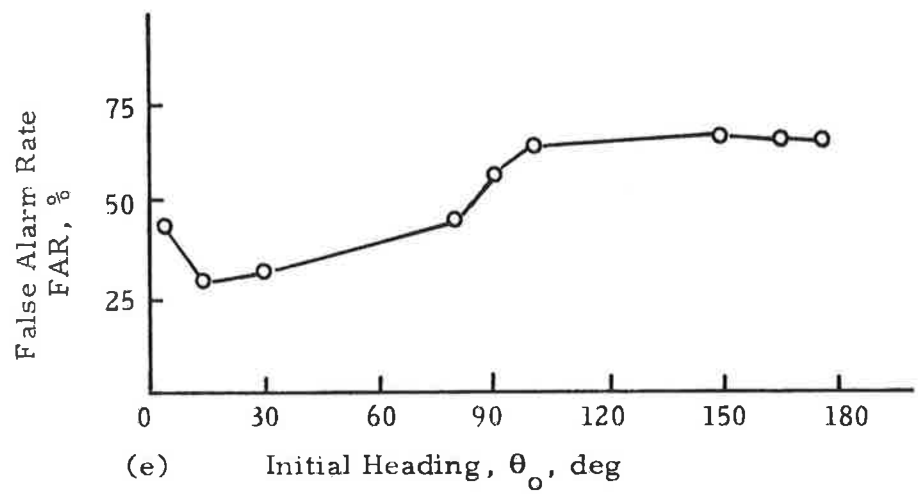

Figure 7.9 (Cont'd) Effect of Encounter Geometry on CAS Performance Measures

TABLE 7.4 Effect of Speed Changes on CAS Performance

P{C}	MAR_C	P{NM}	MAR_{NM}	P{C+NM}	IMR_{NM}	P{AM}	P{EM}	IMR_T	FAR	V_A/V_B
1.25	11.68	3.95	11.77	5.20	18.36	88.70	6.10	31.12	67.88	425/375
0.10	0.93	0.35	1.34	0.45	2.65	96.70	2.85	19.54	62.96	360/180
0.25	2.34	0.80	3.13	1.05	5.36	96.05	2.90	22.76	64.88	425/180

TABLE 7.5 Effect of Bearing Errors on CAS Performance

P{C}	MAR_C	P{NM}	MAR_{NM}	P{C+NM}	IMR_{NM}	P{AM}	P{EM}	IMR_T	FAR	σ_β (deg)
0.05	0.48	0.45	0.75	0.50	0.15	92.80	6.70	18.31	61.67	2.5
1.25	11.68	3.95	11.77	5.20	18.36	88.70	6.10	31.12	67.88	5.0
2.40	22.43	5.80	22.06	8.20	23.82	86.00	5.80	43.56	66.17	7.5

TABLE 7.6 Effect of Heading Errors on CAS Performance

P{C}	MAR_C	P{NM}	MAR_{NM}	P{C+NM}	IMR_{NM}	P{AM}	P{EM}	IMR_T	FAR	σ_β (deg)
0.95	8.88	2.45	9.09	3.40	13.88	92.75	3.85	28.02	67.02	2.5
1.25	11.68	3.95	11.77	5.20	18.36	88.70	6.10	31.12	67.88	5.0
1.55	13.55	5.65	14.90	7.20	20.78	84.65	8.15	37.37	65.52	7.5

TABLE 7.7 Effect of Range Errors on CAS Performance

P{C}	MAR_C	P{NM}	MAR_{NM}	P{C+NM}	IMR_{NM}	P{AM}	P{EM}	IMR_T	FAR	σ_r (feet)
0.85	13.39	3.55	8.20	4.40	17.66	67.70	27.90	25.25	46.51	100
0.85	13.39	3.75	8.20	4.60	18.37	93.30	2.10	25.04	46.61	200
0.90	51.97	4.60	12.22	5.50	20.55	66.40	28.10	24.55	46.51	400

TABLE 7.8 Effect of Speed Ratio Errors on CAS Performance

P{C}	MAR_C	P{NM}	MAR_{NM}	P{C+NM}	IMR_{NM}	P{AM}	P{EM}	IMR_T	FAR	σ_γ
1.25	11.68	3.95	11.77	5.20	18.36	88.70	6.10	31.12	67.88	0.05
1.15	10.75	4.45	11.77	5.60	19.73	88.80	5.60	31.22	67.88	0.075

TABLE 7.9 Effect of Changing Nominal Miss Distance r_a on CAS Performance

P{C}	MAR_C	P{NM}	MAR_{NM}	P{C+NM}	IMR_{NM}	P{AM}	P{EM}	IMR_T	FAR	r_a (feet)
0.85	13.39	3.75	8.20	4.60	18.37	93.30	2.10	25.04	46.61	2000
0.50	7.87	1.40	7.60	1.90	9.02	95.95	2.15	24.32	53.49	2400
0.25	3.94	0.75	4.61	1.00	5.38	94.15	4.85	22.66	60.00	2800
0.05	0.79	0.30	1.62	0.35	1.78	87.10	12.55	22.53	66.01	3200

Again, no conclusions can be drawn from the false alarm rate figures. However, from the data it appears that the missed alarm and incorrect maneuver rates increase largely as functions of increased airspeed V_A and V_B. This confirms the trends predicted by the worst-case analysis.

Table 7.5 shows the effect of bearing error magnitude on the CAS performance. As the standard deviation σ_β increases, the probability of a collision or a near-miss increases, while the probability of an acceptable miss or an excessive miss decreases. This is as one would expect. Also, as σ_β increases, the missed alarm rates and the incorrect maneuver rates increase, which are also expected. It is important to note that of the 2000 runs made, only 2.4% resulted in a collision for $\sigma_\beta = 7.5^\circ$. However, for the same error, 22.4% of those aircraft on collision courses ended up colliding due to missed alarms. The bearing error has to be reduced to 2.5° for a reasonable missed alarm (collision) rate.

The effect of increases in heading errors is shown in Table 7.6. As in the bearing error case, the probabilities of collision and near miss increase with increases in the standard deviation σ_θ. The probability of an acceptable miss decreases a rather small amount, while the probability of an excessive miss increases. The missed alarm rates and incorrect maneuver rates increase with σ_θ, but the variation is not as great as in the bearing error case.

The probabilities of collision and near miss for bearing and heading errors are shown in Figs. 7.10(a) and (b). As can be seen, the collision rate is four times as sensitive to bearing error as heading error. In fact, for bearing error less than 2.5°, the collision and near-miss rates are negligible, despite the presence of 5° heading errors, 200 ft range errors, and 5% speed ratio error.

Table 7.7 shows the effect of increasing range errors on the CAS performance. The probability of collision and near miss are relatively unaffected by increases in the standard deviation σ_r below 200 ft. The probability of acceptable miss and excessive miss exhibited wide variations which compensate for the other. This is due to the arbitrary definition of the boundary between

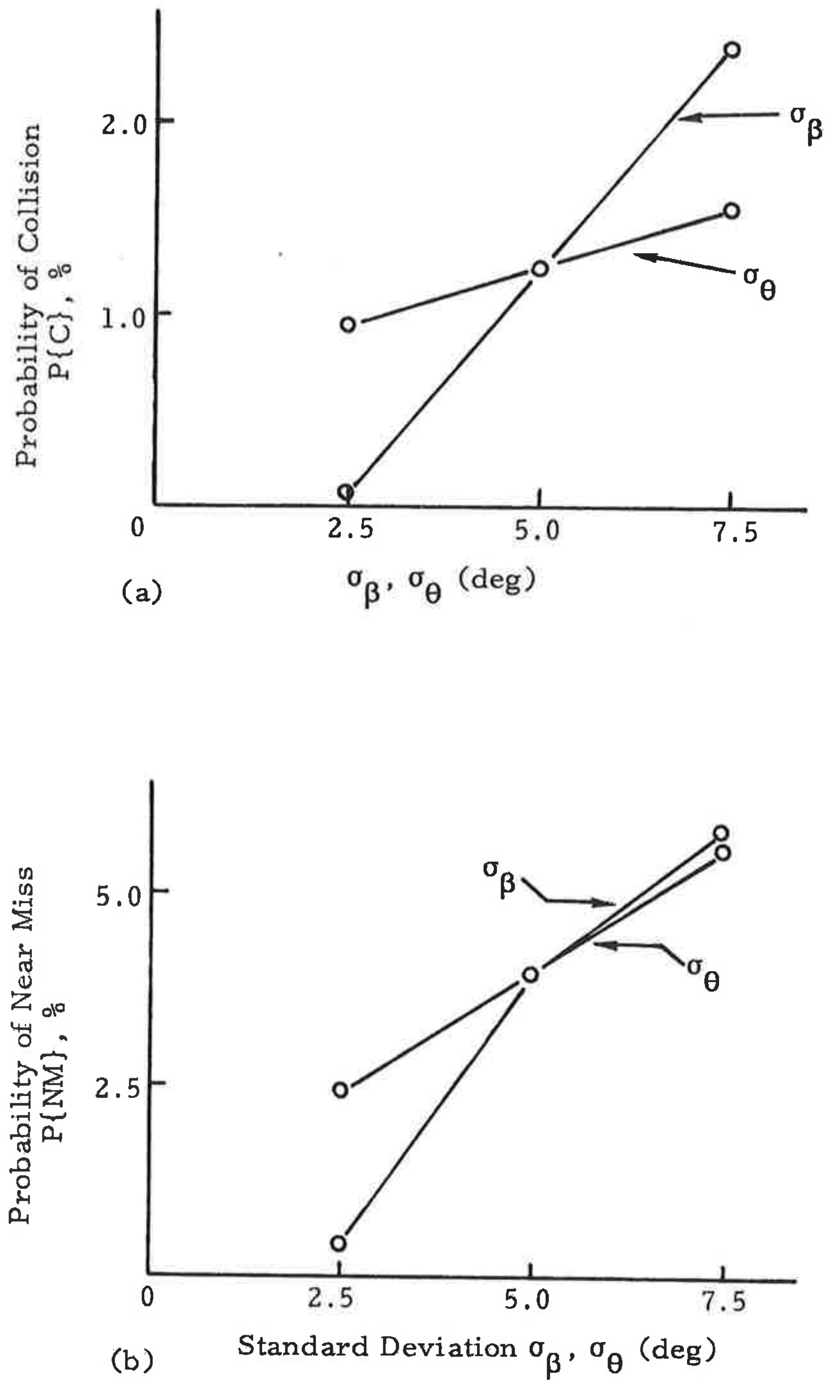

Figure 7.10 Variation of Miss Probabilities with Bearing and Heading Errors

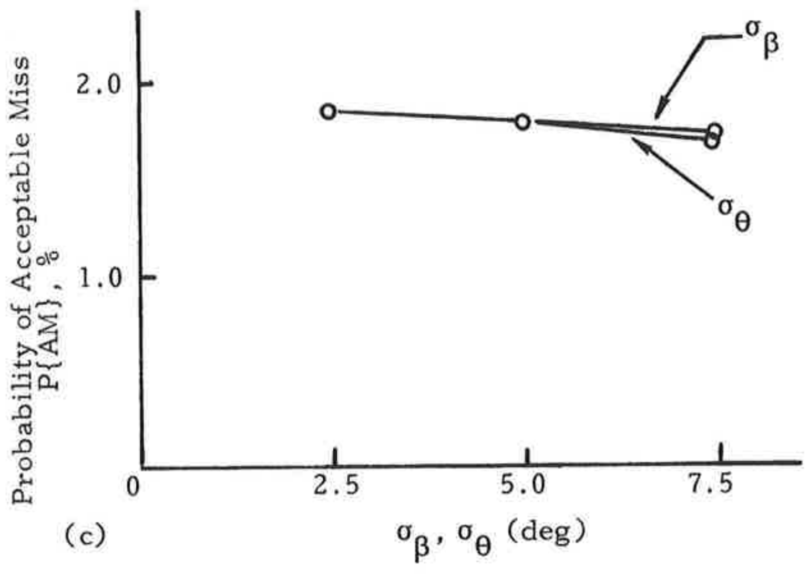

(c)

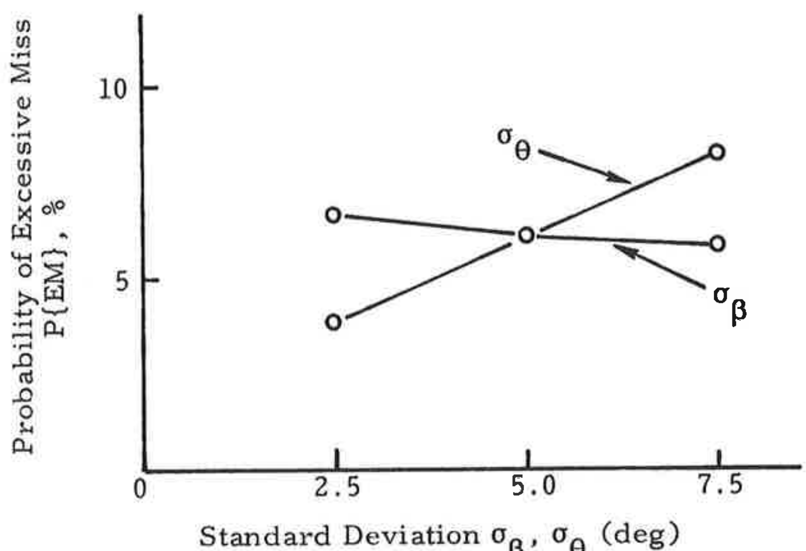

(d)

Figure 7.10 (Cont'd) Variation of Miss Probabilities with Bearing and Heading Errors the two categories of miss distance. A range error of 400 ft (1σ) increased the probability of collision substantially from 13% to 52%.

In Table 7.8, the effect of an increase in the speed ratio error is shown. The various performance measures are not significantly effected by changes in this parameter.

Table 7.9 shows the effect of increases in the desired miss distance r_a. As to be expected, the probabilities of a collision and a near-miss are decreased since the alarm region is increased by increases in r_a. The probability of an acceptable miss is relatively unaffected, while the probability of an excessive miss ($r_f > 3900$ ft) shows an increase with increase in r_a. The missed alarm rates and the incorrect maneuver rates show mild decreases and the false alarm rate has a slight increase as r_a increases. This is due to the increased alarm region. Clearly, the data in Table 7.9 demonstrates the importance of the parameter r_a and how it can be used to achieve required safety levels with fixed measurement errors.

Based upon the preceding simulation results, the performance of the hypothesized horizontal CAS is most affected by large range and bearing errors. The encounter geometries for which performance is worse is for encounters which are more nearly head-on ($\theta_o > 90^o$) rather than overtaking situations ($\theta_o < 90^o$). It appears that bearing error should be held to less than 2.5^o for reasonable collision rates in the terminal areas.

To be more precise in the conclusions requires a more detailed examination of error effects. More accurate models of the error characteristics are required, and the provision for monitoring the maneuvers after they have started should be utilized.

VIII. SUMMARY, CONCLUSIONS, AND RECOMMENDATIONS

In this chapter, the technical results obtained in this study are summarized. Specific conclusions are made regarding the merits of horizontal collision avoidance capability, and requirements for mechanizing such a system are presented. Finally, recommendations are made of further work which should be conducted to enable specifying in more detail the system requirements for preventing midair collisions.

8.1 SUMMARY OF TECHNICAL RESULTS

Chapter III presents the differential equations of motion describing an encounter between two aircraft. Based on the examination of the motion of a single aircraft, the approximate equations of relative motion between two encountering aircraft are derived. The result is four differential equations in which the constant parameters are the airspeed, available turn rate, and available dive/climb rates of each aircraft. These equations provide the basis for determining the appropriate maneuvers for collision avoidance.

Chapter IV is devoted to determining the best horizontal and combined horizontal/vertical maneuvers for avoiding the collision or near-miss situation. The "best" maneuvers are those which provide adequate miss-distance with minimum initial range, minimum deviation off the nominal flight path, and acceptable values of turn rate. These general maneuvers are obtained for conflicting aircraft with arbitrary initial conditions by first computing the maneuver strategies which provide maximum miss distance using fixed turn rate limits. The results are summarized in a series of compact maneuver charts. Then, the tradeoffs between the various criteria (miss distance, turn rate, initial range, and deviation off-track) are found. These sensitivity results can be used with the maneuver charts to evaluate the degree of safety that is potentially available from a horizontal collision avoidance system. The results can also be used to design a CAS maneuver command algorithm or to evaluate any existing CAS system command logic.

Chapter V compares horizontal maneuvers with vertical maneuvers and speed control for collision avoidance. Comparisons are made of initial range requirements, deviation off-track, and time lost from the nominal time slot due to each of the maneuvers. Specific conclusions made by previous examinations of horizontal collision avoidance are examined in detail.

The basic requirements for implementing a typical airborne collision avoidance system which provides horizontal commands are addressed in Chapter VI. This includes a discussion of the hardware and software requirements of the computer and of the sensors, display, interface equipment, and other system hardware. The feasibility of using digital filtering for estimating airspeed and relative heading of the threat aircraft from noisy range and bearing measurements is examined. These estimates are necessary to implement horizontal maneuvers if this information is not exchanged between aircraft.

A digital algorithm (suitable for an airborne computer) for computing the appropriate horizontal maneuvers based on relative position and velocity measurements is also presented in Chapter VI. This algorithm was utilized in the study to conduct system error analysis which is the subject of Chapter VII.

The effects of both dynamic errors and measurement errors on the collision avoidance system's ability to provide a safe miss distance are examined in Chapter VII. Dynamic errors include delays due to pilot reaction time, computation and sampling time, and aircraft transient response. Other dynamic errors are due to wind effects and incorrect values of system parameters in the airborne CAS computer logic. The basic measurement errors are the inaccuracies in the values of range, bearing, relative heading, and airspeed used by the collision avoidance system. The dynamic errors can be compensated for by increasing the initial range used to activate the system and the standard miss distance used to govern the maneuvers.

The effect of measurement errors is first examined by computing the sensitivity of miss distance to small values of the errors which are assumed to be random biases. A digital computer program which simulates an encounter between two arbitrary aircraft (developed for more detailed analysis of the measurement error effects and variations in airspeed ratio, standard miss distance, and the encounter geometry) is next presented. This simulation is used for conducting a Monte Carlo sensitivity analysis of various effects, when the measurement errors and actual encounter geometry are randomly generated. Statistical quantities such as false alarm rate, missed alarm rate, collision rate, incorrect maneuvers, and near miss probability are computed as functions of the various parameters. The data is useful for selecting software parameters and sensor accuracy requirements which provide the required balance between false alarms and safety from midair collisions.

To produce the results contained in this report, this study required the development and use of many digital computer programs. Major programs developed include:

1. Simulation of the relative motion of two aircraft in a conflict situation. Each aircraft's motion is governed by nonlinear, coupled differential equations, stability and control derivatives relevant to the aircraft, and pilot models which provide typical response. The program equations are described in Appendix A.

2, Program for solution of the horizontal maneuvers which provide maximum miss distance for any two aircraft with an arbitrary encounter geometry. The solutions are obtained by applying optimization theory as described in Appendix B.

3. Simulation of the use of the least-squares-smoothing filter and extended Kalman filter for estimating airspeed and relative heading from noisy range and bearing measurements. The principles of these filters are described in Appendix E.

4. Simulation of a midair encounter between two aircraft, each equipped with horizontal collision avoidance systems. The simulation models all dynamic and measurement errors and the utilization of typical maneuver command algorithms. More details are given in Chapter VII.

The horizontal maneuver algorithm developed in this study is suitable for application in an airborne or ground-based computer. It determines: (1) if maneuvers are required, based on estimates of the threat aircraft's relative position and velocity, (2) what maneuvers should be performed, (3) the time at which the maneuvers should begin in order to achieve a fixed miss distance with a specified turn rate, and (4) what miss distance is expected, based on monitoring the maneuver state.

8.2 CONCLUSIONS

The study was divided between analysis of appropriate horizontal collision avoidance maneuvers and study of airborne CAS mechanization requirements. Conclusions based on the maneuver analysis (Chapters III, IV, and V) are as follows:

1. To compute own aircraft's best horizontal maneuver for collision avoidance requires measurements or estimates of the threat aircraft's range, bearing, relative heading, and airspeed. Horizontal/vertical maneuvers require the additional measurement of relative altitude (or elevation angle). It is also necessary to know whether the threat aircraft has operating CAS equipment.

2. To achieve maximum miss distance, the faster aircraft should turn right or left at its maximum rate. The slower aircraft should turn at maximum rate, go straight, or turn at maximum rate followed by a straight-line maneuver. The correct maneuvers for each aircraft can be determined from maneuver charts derived in this study. The charts indicate the appropriate maneuvers which are based on the relative position and velocity of the aircraft, and their turn-rate ratio.

3. There exists an interdependency between miss distance, range at the beginning of the maneuvers, turn rates, and distance traveled off the nominal flight path. The relationship is complex, but certain general conclusions can be derived based on analysis of the encounter geometries:

a. The required deviation off-track decreases strongly as the required miss distance is decreased. Increased bank angle (turn rate) slightly decreases the deviation off-track for a fixed miss distance.

b. The initial range required to begin the maneuvers decreases strongly as the required miss distance decreases and the maximum bank angles increase.

These trends hold for all relative headings. Quantitative variations to the "tradeoff" curves relating these performance elements are important. They allow selection of system parameters which yield adequate midair safety, acceptable false alarm rates, and minimum interference with adjacent aircraft for a given CAS measurement accuracy.

4. The correct vertical portion of each maneuver can be determined independently of the horizontal maneuver. The total miss distance is found approximately at the time of closest approach of each aircraft's position projected in the horizontal plane.

5. Horizontal maneuvers, vertical maneuvers, and speed control each have points which favor their use. Horizontal maneuvers generally require less initial range to achieve reasonable values of miss distance. Vertical maneuvers require less deviation off-track and, therefore, less time loss than horizontal maneuvers. Speed control requires no deviation off the track and has a time loss comparable to the horizontal maneuver. However, this "longitudinal maneuver" requires a larger initial range and is not useful for head-on or tail-on encounters. An ideal system would be able to use all three methods of collision avoidance, with the choice governed by the encounter situation.

Conclusions based on the study of the mechanization requirements are as follows:

1. It is feasible to estimate airspeed and relative heading from noisy range and bearing measurements by use of a digital filter. The quality of these estimates is affected by the bearing and range measurement accuracy, type of measurement errors, sample rate, encounter geometry, and airspeed. Typical bearing errors tend to have a larger effect on the estimates than do range errors. A simple least-squares-smoothing filter typically estimates position to within 200 ft, airspeed to within 25 ft/sec, and relative heading to within 4° (all 1σ) for white noise range errors of 100 ft (1σ) and bearing errors of 3° (1σ). This filter requires less than 500 words of computer core.

2. A typical airborne CAS computer logic that commands horizontal maneuvers to achieve a fixed miss distance for an encounter between arbitrary aircraft turning at standard rates requires less than 3000 words of computer core. The logic is based on table lookup as governed by the appropriate maneuver charts.

3. The dynamic error sources which affect the horizontal CAS performance include delays due to the pilot's reaction, the roll transient time, servo-actuation, computation, and sample time. Other dynamic errors are due to wind gust effects and incorrect values of system parameters used by the CAS computer. Insufficient data exist to make valid quantitative conclusions concerning the effect of these errors.

4. The worst-case measurement error analysis showed that as the airspeeds increased, the miss-distance error also increased for given bearing, heading, and range measurement errors. The sensitivity of miss-distance error to bearing and heading error increases with speed increase. The bearing error effect on miss distance is significant and twice the amplitude of the relative heading error effect. The error effects are greatest for head-on encounters.

5. From the Monte Carlo measurement error analysis, the following conclusions can be made regarding the horizontal CAS performance :

   a. The missed alarm rate is greater for encounters close to head-on.

   b. The incorrect maneuver rate is greater for relative headings near 90^{o}.

   c. Both missed alarm and incorrect maneuver rates increase as the airspeeds of the two aircraft increase.

   d. For the nominal set of measurement errors considered (range error standard deviation $\sigma_r = 200$ ft; bearing error $\sigma_\beta = 5^{o}$; relative heading error $\sigma_\theta = 5^{o}$; and airspeed ratio error $\sigma_\gamma = 0.05$), the error producing the most effect was the bearing inaccuracy. Changing the bearing error standard deviation from 2.5^{o} to 7.5^{o} increased collision rate from less than 1% to 22%.

   e. The sensitivity of collision rate to relative heading error was 25% of that due to bearing error. This conclusion differs from that of worst-case analysis, although the trend is the same.

   f. The probability of collision and near-miss are relatively unaffected by range errors less than 200 ft (1σ). However, a range error of 400 ft (1σ) increased the probability of a collision substantially over the 200 ft case (13% to 52%).

   g. For the encounters considered, speed ratio errors have little effect on the distribution of miss distance.

   h. For fixed measurement error statistics, the adjustment of the desired miss distance r_a (which is used as a parameter by the collision avoidance system) is the key to obtaining acceptable collision and near-miss rates (measures of safety). For the nominal case considered, increasing r_a from 2000 ft to 3200 ft reduced the probability of a collision due to a missed alarm from 13.4% to 0.8%. However, increasing this parameter generally increases the spread in the miss distance distribution and implies that more airspace is required to maneuver.

8.3 RECOMMENDATIONS FOR FURTHER WORK

This study has determined the basic characteristics of a horizontal collision avoidance system and the fundamental effects of system errors. The establishment of a national standard for airborne collision avoidance requires further analysis, simulation, experimentation, and flight test to establish more precise conclusions. Based on the investigation and analysis results of this study, the following recommendations are offered concerning the need for further work :

1. A more complete design study should be made of the requirements for mechanizing an airborne CAS. This would include the hardware, computer software, and all interface and display requirements. Such a study would allow making a complete cost/benefit analysis of horizontal collision avoidance.

2. The Monte Carlo error analysis in this report is based on pessimistic error models. Models based on laboratory and flight data should be obtained and used to provide more precise evaluation of the effect of measurement errors on CAS performance. The assumptions used in constructing the simulation of the encounter between two aircraft should be thoroughly reviewed to insure that the results are realistic and compatible with candidate horizontal collision avoidance systems.

3. The pilot's reaction time to an alarm and his resulting steering errors are largely unknown. A simulator or flight test program

should be established which can obtain this information so that quantitative effects can be determined.

4. The digital filters for obtaining relative heading and airspeed estimates based on white noise models of the range and bearing errors look promising. These results should be extended to determine the effects of other types of errors and motion of the threat aircraft off a straight flight path. Improved filters should be considered.

5. Speed control results were only obtained for encounters with limited geometry and control capability. These results should be extended for various ranges of geometry and control. The feasibility and value of combining speed control with vertical or horizontal maneuvers should also be investigated.

6. The results of this report were limited to an encounter between two aircraft in unrestricted airspace. These results should be extended to include multiple aircraft encounters and to determine the effects of restricting the airspace in which maneuvers can be made.

7. The error analyses presented in this report were based on the assumption that the systems were mechanized in the aircraft. Similar analyses should be conducted for ground-based systems such as air traffic control (ATC) via the Discrete Address Beacon System (DABS).

8. The amount of airspace usage and false collision warning alarms affect the air traffic controller's task. The interaction between ATC and a general airborne collision avoidance system needs to be established as a function of the initial range, miss distance, and deviation off-track requirements, and the dynamic and measurement errors. This would aid in establishing system software parameters and measurement standards.

APPENDIX A

EQUATIONS OF MOTION FOR AN AIRCRAFT/PILOT SYSTEM

The equations which govern the motion of a rigid aircraft are required for modeling the dynamic response of the aircraft to representative control inputs. These inputs, on the other hand, are provided by the pilot or autopilot as functions of the errors in position, attitude, and their rates of change. The entire system can be conceptually modeled by the block diagram shown in Fig. A.1.

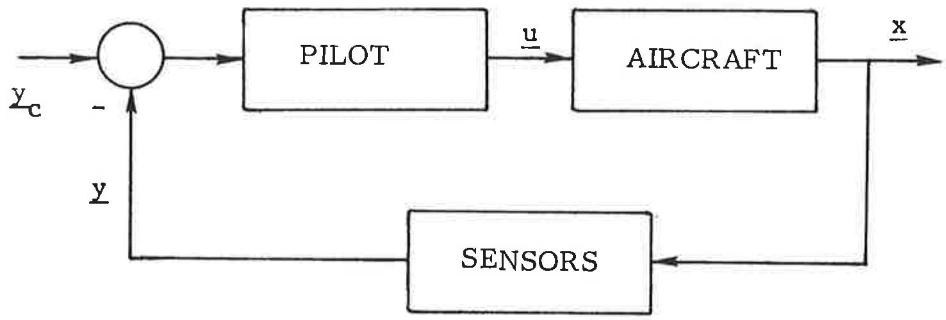

Figure A.1 Aircraft Control System

In this figure are shown the controls $\underline{u}$ of the pilot (e.g., throttle, elevator, rudder and aileron changes), the state of the aircraft $\underline{x}$ (e.g., altitude, altitude rate, heading, roll angle, etc.) and the output $\underline{y}$ (e.g., heading, velocity) which is to be controlled by the pilot/autopilot. The controls are typically changed only when an error is detected by the pilot, and a realistic model of the dynamic response can result only if realistic bounds are included in the pilot's dynamic response capabilities.

For short term transient response purposes, a set of earth-fixed axes can be considered as an inertial reference. Therefore, the position of the aircraft center of mass can be measured relative to these axes by the position vector (x, y, z). These can be conveniently defined in the north, east, and vertical directions, respectively, as measured from the initial location of the aircraft. The orientation of the aircraft axes relative to the earth axes is expressible by an orthogonal transformation, or equivalently by three Euler angles. The sequence of angles (ψ, θ, φ) shown in Fig. A.2 is conventional for aircraft applications, and these angles are defined as yaw, pitch and roll, respectively.

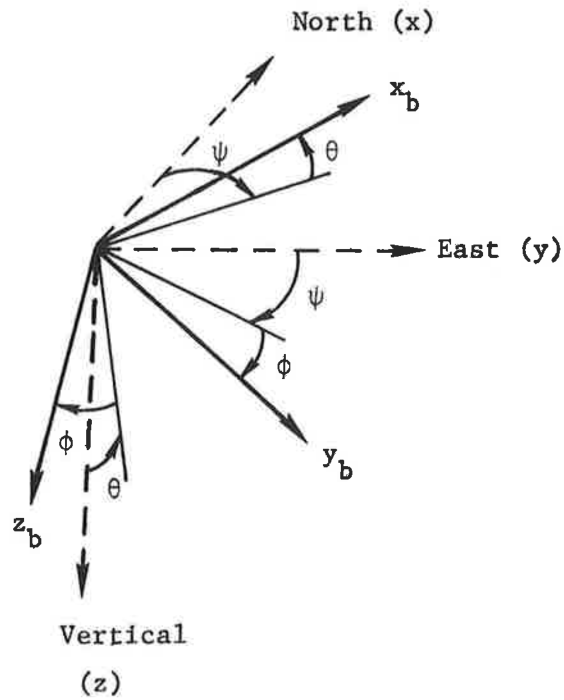

Figure A.2 Euler Angles ψ, θ, φ.

The body-Axis components of the aircraft linear velocity vector are $\underline{V} = (u, v, w)$, while the earth-axis equivalents in the north, east, and downward directions are*, respectively,

$$\dot{x} = uc\theta c\psi - v(c\varphi s\psi - s\varphi s\theta c\psi) + w(s\varphi s\psi + c\varphi s\theta c\psi)$$

$$\dot{y} = uc\theta s\psi + v(c\varphi c\psi + s\varphi s\theta s\psi) - w(s\varphi c\psi - c\varphi s\theta s\psi) \qquad (A.1)$$

$$\dot{z} = -us\theta + vs\varphi c\theta + wc\varphi c\theta$$

The body axis components of the angular velocity vector are $\underline{\omega} = (p,q,r)$, which are rates that would be measured by body mounted rate gyros. The Euler angle rates of change are along various non-orthogonal directions, as shown in

*Here, s and c are used to abbreviate "sine" and "cosine".

Fig. A.2. The equations relating these angular rates can be derived from this figure as

$$\begin{aligned}
\dot{\psi} &= (qs\varphi + rc\varphi)/c\theta \\
\dot{\theta} &= qc\varphi - rs\varphi \\
\dot{\varphi} &= p + (qs\varphi + rc\varphi) \tan \theta
\end{aligned} \tag{A.2}$$

The kinematic differential equations for the position and attitude of the aircraft thus have the highly nonlinear form given in Eqs. (A.1) and (A.2). Integration of these equations is possible only when the body axis components of linear and angular velocity are known, and this requires consideration of Newton's laws of motion.

Since the aerodynamic forces are most easily expressed in body axes, it is prefereable to write the translational and rotational forms of Newton's law in this rotating axis system. Use of the Coriolis law for differentiation in a rotating axis system then results in

$$\dot{m}(\underline{V} + \underline{\omega} \times \underline{V}) = \underline{F} \tag{A.3}$$

The scalar form of this equation is

$$\begin{aligned}
m(\dot{u} + qw - rv) &= F_x \\
m(\dot{v} + ru - pw) &= F_y \\
m(\dot{w} + pv - qu) &= F_z,
\end{aligned} \tag{A.4}$$

where F_x, F_y, F_z are body-axis components of the total force due to gravity, thrust, and aerodynamics. It is assumed that the mass (m) remains constant during the time interval of interest, so that the equations can be solved for the linear accelerations; i.e.,

$$\begin{aligned}
\dot{u} &= -qw + rv - gs\theta + \delta T/m + C_x \bar{q}S/m \\
\dot{v} &= -ru + pw + gs\varphi c\theta + C_y \bar{q}S/m \\
\dot{w} &= -pv + qu + gc\varphi c\theta + C_z \bar{q}S/m
\end{aligned} \tag{A.5}$$

Here it has been assumed that the thrust deviation from equilibrium δT is aligned with the body x-axis. Aerodynamic forces have been expressed as the products of coefficients C_x, C_y, C_z and the reference force $\bar{q}S$, where $\bar{q}$ is the dynamic pressure and S is the reference (wing) area of the aircraft.

The angular momentum of the rigid aircraft is expressed in terms of the inertia tensor of the aircraft. Assuming that the x-z plane is a plane of symmetry, the angular momentum is expressed in body axes by the product $\underline{H} = I\underline{\omega}$, where

$$I = \begin{bmatrix} I_x & 0 & -I_{xz} \\ 0 & I_y & 0 \\ -I_{xz} & 0 & I_z \end{bmatrix} \tag{A.6}$$

The applied torque is due to the thrust and aerodynamic forces, and this torque causes the angular momentum to change according to:

$$\dot{\underline{H}} + \underline{\omega} \times \underline{H} = \underline{M} \tag{A.7}$$

This has the following scalar form, when the inertia tensor is constant:

$$\begin{aligned} &I_x\dot{p} - I_{xz}\dot{r} + (I_z - I_y)qr - I_{xz}pq = C\,\bar{q}Sb \\ &I_y\dot{q} + (I_z - I_z)pr + I_{xz}(p^2 - r^2) = C_m\bar{q}Sc + \ell_T\delta T \\ &I_z\dot{r} - I_{xz}\dot{p} + (I_y - I_x)pq + I_{xz}qr = C_n\bar{q}Sb \end{aligned} \tag{A.8}$$

Here the moments have been expressed in standard form, as a product of a dimensionless coefficient and a reference moment. The lengths b and c are the span and reference chord of the wing. It has been assumed here that any moment due to the equilibrium thrust is balanced by an appropriate bias in the elevator setting. The angular velocities are then given by the solutions to the following equations:

$$\dot{p} = [\bar{q}Sb(I_z C_\ell + I_{xz} C_n) - (I_z^2 - I_z I_y + I_{xy}^2)qr$$

$$-I_{xz}(I_y - I_x - I_z)pq]/(I_x I_z - I_{xz}^2)$$

$$\dot{q} = [\ell_T \delta T + \bar{q}ScC_m - (I_x - I_z)pr - I_{xz}(p^2 - r^2)]/I_y \qquad \text{(A.9)}$$

$$\dot{r} = [\bar{q}Sb(I_x C_n + I_{xz} C_\ell) + (I_x^2 - I_x I_y + I_{xz}^2)pq$$

$$+ I_{xz}(I_y - I_x - I_z)pr]/(I_x I_z - I_{xz}^2)$$

The thrust contribution to the pitching moment equation is the product of the thrust variation (δT) and its moment arm (ℓ_T). The aerodynamic forces are functions of the angles of attack and sideslip, which are defined in terms of body axis velocity components as follows:

$$\alpha = \tan^{-1} (w/u)$$

$$\beta = \sin^{-1} (v/V) \qquad \text{(A.10)}$$

The coefficients C_x and C_z are usually expressed in terms of the lift and drag coefficients and a reference angle of attack, α_o, so that

$$C_x = C_L s\alpha_o - C_D \, c\alpha_o$$

$$C_z = -C_L c\alpha_o - C_D \, s\alpha_o \qquad \text{(A.11)}$$

The lift and drag coefficients are then typically expressed in the form of a Taylor series, involving the longitudinal variables (α, q) and control (δe):

$$C_L = C_{L_\alpha} \alpha + \frac{c}{2V} (C_{L_q} q + C_{L_{\dot{\alpha}}} \dot{\alpha}) + C_{L_{\delta e}} \delta e$$

$$C_D = C_{D_\alpha} \alpha + \frac{c}{2V} (C_{D_q} q + C_{D_{\dot{\alpha}}} \dot{\alpha}) + C_{D_{\delta e}} \delta e \qquad \text{(A.12a)}$$

Similarly, the side-force coefficient is written as

$$C_y = C_{y_\beta}\beta + \frac{b}{2V}(C_{y_r} r + C_{y_p} p) + C_{y_{\delta r}}\delta r + C_{y_{\delta a}}\delta a \qquad \text{(A.12b)}$$

where δr and δa are variations in the rudder and aileron deflections.

The moment coefficients about the body x, y and z axes are then typically expressed as:

$$C_\ell = C_{\ell_\beta}\beta + \frac{b}{2V}(C_{\ell_p} p + C_{\ell_r} r) + C_{\ell_{\delta a}}\delta a + C_{\ell_{\delta r}}\delta r$$

$$C_m = C_{m_\alpha}\alpha + \frac{c}{2V}(C_{m_q} q + C_{m_{\dot\alpha}}\dot\alpha) + C_{m_{\delta e}}\delta e \qquad \text{(A.13)}$$

$$C_n = C_{n_\beta}\beta + \frac{b}{2V}(C_{n_p} p + C_{n_r} r) + C_{n_{\delta a}}\delta a + C_{n_{\delta r}}\delta r$$

The equations of motion can then be solved for any variations in δa, δe, δr and δT, after substituting Eqs. (A.11) - (A.13) into Eq. (A.5) and Eq. (A.9). The resulting equations are "exact" only if the higher-ordered terms in the coefficients are negligible.

To complete the simulation of the pilot/aircraft system next requires that the control inputs be specified as "reasonable approximations" to a pilot's actual inputs.[93] Excellent results have been obtained in simulations for which the controls are linear functions of the errors. Suitable realism can be incorporated by adding a transport lag and a dead-zone to the transfer function representing the pilot dynamics.

Longitudinal pitch maneuvers have been found to be well modeled by using an elevator transfer function derived from:

$$\delta e = C_1(\theta_c - \theta) - C_1\hat{\theta},$$

where requirements on the gains can be established by an approximate root locus analysis.

A typical "lateral" maneuver such as a coordinated turn, requires specification of all controls as functions of the errors. This is because a coordinated turn about the vertical axis requires a steady pitch rate, as provided by an elevator deflection. The inertial cross-coupling may cause nonlinearities to have a large influence on the stability of the resulting motion, so that the control deflections are required to be resonable in magnitude. It has been found that good lateral motion results from deflecting the rudder in proportion to the sideslip angle,

$$\delta r = C_3 \beta .$$

Similarly, the heading angle or yaw rate can be used to generate an aileron deflection; i.e.,

$$\delta a = C_4(\psi_c - \psi) - C_5\dot{\psi}$$

In a typical steady turn maneuver, $C_3 = 0$ while the turn rate (i.e., roll angle) is being controlled. Near the end of such a maneuver, the heading itself is to be controlled, and C_4 is increased to an appropriate level, dependent upon the aircraft and flight condition in question.

When these feedback functions are used with the exact equations of motion, the aircraft/pilot system is complete. That is, the motion of the aircraft in response to a command maneuver is found by implementing the block diagram system which is shown in Fig. A.1. The pilot/aircraft system is then represented by a set of equations in a digital computer. When the desired maneuver is commanded, the resulting transient response of the relevant quantities can be found. For the purposes of this study, such maneuver simulations have the principal purpose of demonstrating that simpler equations accurately approximate the set which has been derived above.

Such a simplification can be obtained by implementing the following approximations:

1. The velocity is practically constant during a maneuver.

2. The time constant in roll is negligible, and any steady-turn flight condition can be immediately achieved.

3. The pitch dynamics are of negligible time duration, such that steady climb or dive conditions can also be immediately achieved.

The effect of these simplifications is to ignore the components of the motion which are of small amplitude and high frequency. The horizontal turn maneuver, in particular, can be formally approximated by combining Eqs. (A.2), (A.4) and (A.5) to obtain the steady-state force balances in the vertical and horizontal direction. Together, these imply the "coordinated turn" condition which relates the horizontal turn rate to the bank angle and velocity ($V \cong u$), i.e.,

$$\dot{\psi} \cong (g/V)\ \tan\ \varphi \cong (g/V)\varphi \tag{A.14}$$

A steady turn rate at constant velocity together imply a circular arc path of the aircraft in realistic space.

The vertical maneuver can be similarly approximated by ignoring the pitch dynamics and assuming that the steady climb condition can be immediately achieved. The thrust and elevator settings required for a given steady rate of climb or dive can be determined by implementing appropriate equilibrium conditions. That is, the longitudinal equations in Eqs. (A.1) - (A.5) can be simplified by linearizing and reducing to the steady-state condition.

The principal feature of the transient response is the time interval occurring between the initial condition (e.g., straight and level flight) and the final condition (e.g., a steady turn combined with a steady climb or dive). This time interval is typically in the range from 2 sec. to 6 sec.

When the relative motion of two aircraft is to be modeled according to these principles, a new coordinate system is defined, in which the position of aircraft B is given relative to axes fixed in aircraft A. The new coordinate system is a Cartesian set, with the relative y-axis aligned with the forward velocity of aircraft A. The relative x-axis is then directed along the right wing.*

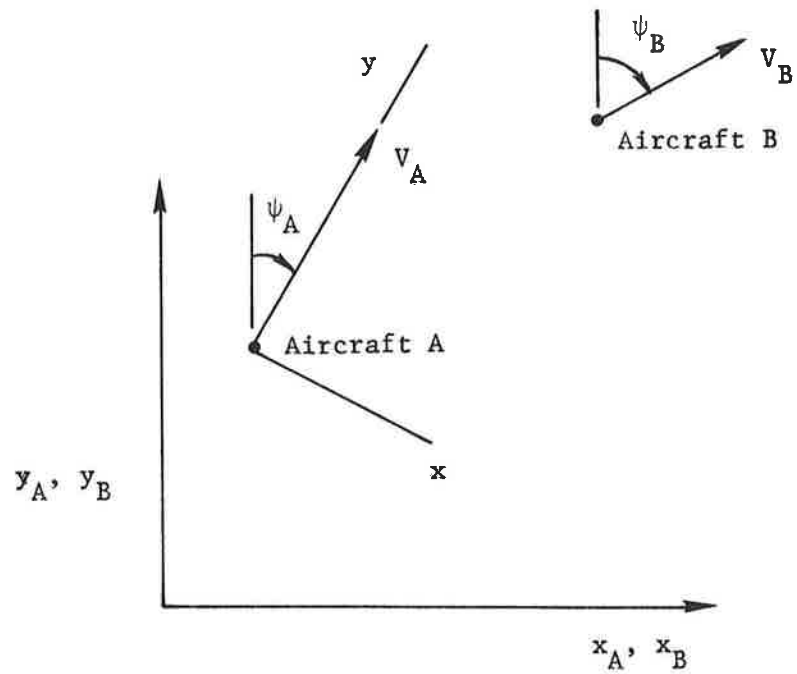

Figure A.3 Coordinates of Horizontal Position of Aircraft

The horizontal position of either aircraft is given by solving the kinematic differential equations implied by Fig. A.3.

$$\begin{aligned} \dot{x}_i &= V_i \sin \psi_i \\ & \qquad\qquad (i = A \text{ or } B) \qquad\qquad (A.15) \\ \dot{y}_i &= V_i \cos \psi_i \end{aligned}$$

while the vertical motion is simply expressed in terms of the rate of climb,

*Note that the dynamic equations of motion are written in "body axes", which are traditionally defined with the x-axis forward and the y-axis to the right.

$$\dot{z}_i = \delta_i \tag{A.16}$$

The heading angles are given in terms of the horizontal turn rate controls according to

$$\dot{\psi}_i = \omega_i \tag{A.17}$$

where each turn rate is bounded in magnitude;

$$|\omega_i| = \omega_{i_{max}}$$

As shown in Fig. A.3, the relative location of aircraft B is expressible by the transformation equations,

$$\begin{aligned}
x &= (x_B - x_A) \cos \psi_A - (y_B - y_A) \sin \psi_A \\
y &= (x_B - x_A) \sin \psi_A + (y_B - y_A) \cos \psi_A \\
\theta &= \psi_B - \psi_A \\
z &= z_B - z_A
\end{aligned} \tag{A.18}$$

Differentiation of both sides of Eq. (A.18) and substitution from Eqs. (A.15) - (A.17) yields the approximate equations of relative motion,

$$\begin{aligned}
\dot{x} &= -\omega_A y + V_B \sin \theta \\
\dot{y} &= -V_A + \omega_A x + V_B \cos \theta \\
\dot{\theta} &= -\omega_A + \omega_B \\
\dot{z} &= -\delta_A + \delta_B
\end{aligned} \tag{A.19}$$

These equations are used to determine the controls (ω_i, δ_i) in terms of the relative position and heading (x, y, z, θ) of the aircraft.

APPENDIX B

TURN AND CLIMB MANEUVERS TO MAXIMIZE MISS DISTANCE

When two aircraft encounter each other at the same altitude, the miss distance depends upon the turn-rate and climb-rate controls chosen by the two aircraft. In the simplest version of the horizontal collision avoidance problem, each aircraft is constrained to horizontal motion, and is controlled as to maximize the horizontal miss-distance. That is, no other performance criterion is considered to be relevant. More realistic and complete versions of the problem are considered in the body of this report. Similarly, the vertical collision avoidance problem is analyzed by choosing the rates of climb which maximize the vertical miss-distance.

In accordance with the stated assumptions, the horizontal maneuvers are first determined for two aircraft which encounter each other at the same altitude. The aircraft have constant velocities, and maneuver by choosing their horizontal turn rates, which are assumed to be variable between fixed positive (right turn) and negative (left turn) limits. Since, also by assumption, the aircraft are constrained to motion in the same plane, the approximate relative position of the aircraft is given by the solution to three first-order differential equations,*

$$
\begin{aligned}
\dot{x} &= -\omega_A y + V_B s\theta \\
\dot{y} &= -V_A + \omega_A x + V_B c\theta \\
\dot{\theta} &= -\omega_A + \omega_B ,
\end{aligned}
\tag{B.1}
$$

where the aircraft speeds and turn rates are V_A, V_B and ω_A, ω_B, respectively. These equations describe the variation of aircraft B's heading (θ) and position (x,y) relative to a set of axes fixed to the faster aircraft, A. The control ω_A multiplies the position components x and y, and the equations are, therefore, nonlinear.

*Sine and cosine functions are indicated by "s" and "c", respectively.

In order to minimize the number of sets of parameters in the problem, it is convenient to normalize the units of length and time. This is most easily accomplished by setting $V_A = 1$ and $\omega_A = 1$, where A is chosen as the faster aircraft. That is, since only the ratios of speeds and turn rates are relevant to the problem, the first two equations of relative motion can be divided through by V_A, and the angular equation divided by ω_A. The radius of A's minimum-turn circle is then equal to one, and the normalized form of Eq. (B.1) is:

$$\begin{aligned} \dot{x} &= -\sigma_A y + \gamma s\theta \\ \dot{y} &= -1 + \sigma_A x + \gamma c\theta \\ \dot{\theta} &= -\sigma_A + \omega\sigma_B \qquad |\sigma_i| \leq 1, \quad i = A \text{ or } B \end{aligned} \tag{B.2}$$

Here, the speed and maximum turn rate of the slower aircraft are γ and ω, respectively. It will be found that when B is more maneuverable, it is appropriate to let the unit of distance be B's turn radius. The maneuverability of aircraft B is here measured by the minimum turn radius (γ/ω), although the turn rate (ω) or the maximum magnitude of the normal acceleration $(\gamma\omega)$ could also have been used for this purpose. This normalization method allows a presentation of the maneuver regions in the case when the faster aircraft does not turn, in which case its minimum turn radius would be infinite.

The distance at minimum range is the quantity being maximized, and there exists such a unique payoff at every relative initial position and heading (x, y, θ). Since this payoff quantity $J(x, y, \theta) = r_f$ is a constant (which is, however, initially unknown), its total time derivative must equal zero. This time derivative is defined as the "Hamiltonian", and can be expressed[94,95] as a function of the vector gradient of the payoff, $\underline{\lambda}^T = \partial J/\partial \underline{x}$, as follows:

$$\frac{dJ}{dt} = \max_{\sigma_A, \sigma_B} H(x, y, \theta) = \underline{\lambda}^T \dot{\underline{x}} = \underline{\lambda}^T \underline{f}(x, y, \theta) = 0 \tag{B.3}$$

The second time-derivative of this quantity must also vanish, i.e.,

$$\frac{d^2J}{dt^2} = \frac{dH}{dt} = \dot{\underline{\lambda}}^T f + \underline{\lambda}^T \underline{f}_{\underline{x}} \dot{\underline{x}} = (\dot{\lambda}^T + \underline{\lambda}^T \underline{f}_{\underline{x}})\underline{f} = (\dot{\underline{\lambda}}^T + \underline{H}_{\underline{x}})\underline{f} = 0 \tag{B.4}$$

The "costate" or "influence" functions, therefore, must satisfy the following differential equations:

$$\dot{\lambda}_x = -\partial H/\partial x = -\sigma_A \lambda_y$$

$$\dot{\lambda}_y = -\partial H/\partial y = \sigma_A \lambda_x \qquad \text{(B.5)}$$

$$\dot{\lambda}_\theta = -\partial H/\partial \theta = -\gamma(\lambda_x c\theta - \lambda_y s\theta)$$

for which the boundary conditions are given by

$$\underline{\lambda}^T(t_f) = \partial J/\partial \underline{x}|_{t_f} = [x_f/r_f \quad y_f/r_f \quad 0] \ . \qquad \text{(B.6)}$$

These boundary conditions can be formally derived by examining the partial derivative of the payoff $J = r_f$, with respect to the state $\underline{x}^T = (x, y, \theta)$. That is, since $r_f^2 = x_f^2 + y_f^2$, the gradient $\partial J/\partial \underline{x}$ is aligned with the relative range vector at the time of minimum range.

The state (x,y,θ) and costate $(\lambda_x, \lambda_y, \lambda_\theta)$ are, therefore, coupled through the turn rates. A "two point boundary value problem"[94] results because the state is known at the initial time (t=0) while the costate is known at the unknown final time ($t=t_f$). To avoid the trial and error numerical method of solution, the necessary conditions are applied to find controls at the terminal time. Backwards integration of the equations of relative motion is then possible from any terminal condition. The result is a specification of the turn maneuvers for both aircraft, as a function of the relative position and heading.

The retrograde integration of these equations of motion is carried out for a certain specific miss-distance, r_f. It is then found that each family of retrograde paths (corresponding to a specific maneuver pair, e.g., $\sigma_A = 1$, $\sigma_B = -1$) intersects another family of paths (corresponding, say, to $\sigma_A = \sigma_B = -1$). The intersection of two such retrograde paths is called a "dispersal point", and for initial relative positions beginning at such a point, the maneuvers are not unique. Equally important is the fact that these dispersal points are not predicted by the theory, and must instead be found numerically.

Returning to the specifications of the turn maneuvers for aircraft A and B, the maximization operation in Eq. (B.3) yields the controls of the aircraft as

$$\sigma_A = -\mathrm{sgn}(\lambda_x y - \lambda_y x + \lambda_\theta) = -\mathrm{sgn}\ S_A$$
$$\sigma_B = \mathrm{sgn}\ \lambda_\theta \qquad (B.7)$$

According to Eq. (B.6), both of these arguments are zero when $t=t_f$. It is, therefore, necessary (as with applications of l'Hospital's rule) to examine the retrograde derivatives, so as to determine σ_A and σ_B <u>just before</u> $t=t_f$. Doing so, the terminal turn controls are found as

$$\sigma_A = \mathrm{sgn}(\dot{\lambda}_x y + \lambda_x \dot{y} - \dot{\lambda}_y x - \lambda_y \dot{x} + \dot{\lambda}_\theta)$$
$$= -\mathrm{sgn}\ \lambda_x(t_f) = -\mathrm{sgn}\ x_f = -\mathrm{sgn}\ \beta_f \qquad (B.8)$$

and

$$\sigma_B = -\mathrm{sgn}\ \dot{\lambda}_\theta$$
$$= \mathrm{sgn}\ (x_f c\theta_f - y_f s\theta_f) = -\mathrm{sgn}\ (\theta_f - \beta_f) \qquad (B.9)$$

where β_f is the terminal value of the relative bearing.

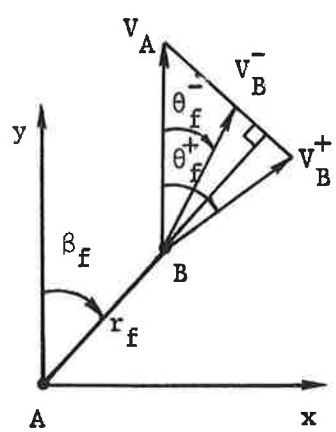

Figure B.1 Position and Headings at Minimum Range

Since the relative bearing and heading are both measured clockwise from the direction of A's velocity, these results show that at termination (when $\dot{r} = 0$), each aircraft must be turning away from the other. This is exactly as would be expected intuitively, and as shown in Fig. B.1, two terminal headings correspond to each terminal bearing. That is,

$$\dot{r}(t_f) = -c\beta_f + \gamma c(\theta_f - \beta_f) = 0 \quad ,$$

so that, in the notation of Fig. B.1,

$$\theta_f^- = \beta_f + \cos^{-1}\left(\frac{c\beta_f}{\gamma}\right)$$

and

$$\theta_f^+ = \beta_f + \cos^{-1}\left(\frac{c\beta_f}{\gamma}\right) \qquad \text{(B.10)}$$

The terminal controls (σ_A, σ_B) are given in Eqs. (B.8) and (B.9), and are used with a representative terminal condition (r_f, β_f, θ_f), to allow backward solutions of the equations of relative motion Eqs. (B.2) and the costate equations Eqs. (B.5). Together, these allow simultaneous computation of the switch functions in Eqs. (B.7).

The following general conclusions hold with respect to these optimal collision avoidance maneuvers:

1. The faster aircraft is always turning hard right or hard left, during the time interval in which $\dot{r} \leq 0$. That is, $S_A \neq 0$, and $\sigma_A = \pm 1$.

2. The slower aircraft may require a two-stage maneuver, typical of which is a hard turn, followed by a straight dash. That is, $\sigma_B = \pm 1$ or $\sigma_B = 0$, in that order.

The present version of the problem is of third order, and the three dimensional state space will be subdivided by various curved "exceptional" surfaces into a number of sub-volumes. One of the curved surfaces is a locus of trajectories for which the slower aircraft goes straight. This is termed a "universal" surface[74] and is pictorally represented in Fig. B.2(a). The terminology "singular arc" is also used to denote paths which correspond to zero argument of the signum function, and the universal surface is, therefore, simply a family of singular arcs.

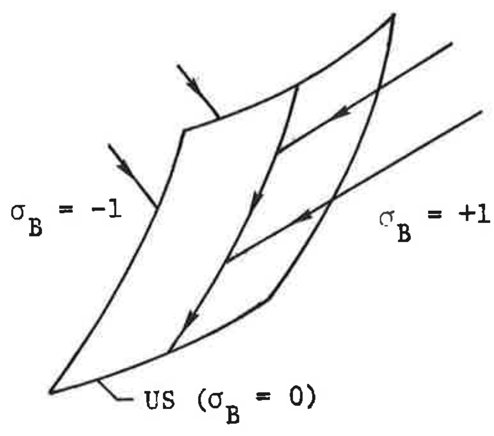

a) Universal Surface and Tributaries

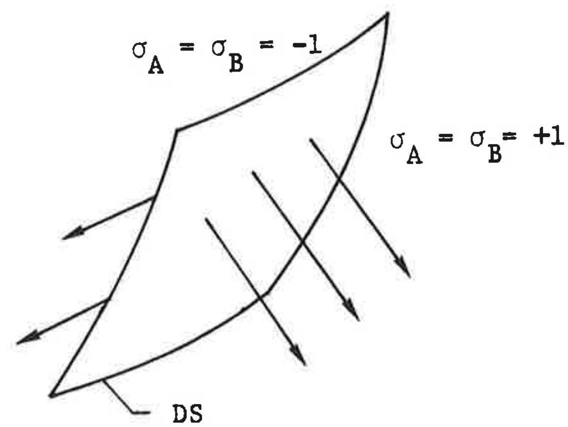

b) Dispersal Surface

Figure B.2 Exceptional Surfaces in Collision Avoidance

A second type of exceptional surface occurs where two retrograde optimal trajectories intersect. As discussed in Section 4.3, and as shown in Fig. B.2(b), these "dispersal surfaces" are loci of relative initial conditions for which either of two maneuver pairs leads to the same miss distance. When the state (x, y, θ) is initially on such a surface, optimality requires that it move away in either direction. Such loci are not specified by the necessary conditions, and must be found numerically. The strategies of either or both aircraft change for initial conditions across this type of surface. Consequently, a notational abbreviation of the following three forms of dispersal surface has been used here:

1. DS: dispersal surface across which maneuvers of both aircraft change.

2. ADS: dispersal surface across which only A's maneuver changes.

3. BDS: dispersal surface across which only B's maneuver changes.

Maneuvers in the vertical plane are also determined by using a simplified dynamic model of the relative motion. An appropriate model of this motion is one for which the controls of the aircraft are the rates of climb. These vertical velocities are bounded between upper and lower limits, which are typically known as a function of the aircraft flight condition.

The approximate equation of relative vertical motion has been given in Eq. (A.19), and this is seen to be formally uncoupled from the horizontal equations, i.e.,

$$\dot{z} = -\delta_A + \delta_B, \quad |\delta_i| \leq \delta_{i_{max}} \tag{B.11}$$

The performance criterion is the terminal miss distance, as before, and termination is again defined by the minimum range condition,

$$\psi(t_f) = \dot{r}(t_f) = (x/r)\dot{x} + (y/r)\dot{y} + (z/r)\dot{z}\big|_{t_f} = 0 \tag{B.12}$$

The optimum controls in this more general problem can be formally derived using the Hamiltonian function, according to which

$$\max_{\omega_i,\, \delta_i} H = \max_{\omega_i, \delta_i} (\lambda_x \dot{x} + \lambda_y \dot{y} + \gamma_\theta \dot{\theta} + \lambda_z \dot{z}) = 0 \tag{B.13}$$

The horizontal turn controls are then given as in Eq. (B.7), while the vertical climb-rate controls depend on λ_z. That is,

$$\begin{aligned} \delta_A &= -\delta_{A_{max}} \operatorname{sgn} \lambda_z \\ \delta_B &= \delta_{B_{max}} \operatorname{sgn} \lambda_z \, . \end{aligned} \tag{B.14}$$

3. Compute and draw the curves corresponding to the DS, the ADS and the BDS, by numerical solution of the relevant sets of simultaneous equations. [66]

It is found that at least one of these three dispersal curves exists at every relative heading. The intersections of the dispersal curves must be found numerically, and these intersections mark the ends of the dispersal curves involved. Each point on a dispersal curve is associated with two maneuver pairs (e.g., $A_R B_L$ and $A_L B_R$). Intersections of dispersal curves occur in one of the following forms:

1. When $0 < \theta < \cos^{-1} \gamma$, a special maneuver point occurs at the intersection of the ADS, the DS and the US, as in Fig. 4.2(a). For this initial relative position, the optimal maneuvers are either $A_R B_L$ or $A_L B_O$.

2. When $\cos^{-1} \gamma < \theta < \pi$, a triple maneuver point occurs at the intersection of three dispersal surfaces, as shown in Fig. 4.2(b). For this initial relative position, the optimal maneuvers are $A_R B_L$, $A_L B_L$ or $A_R B_R$, and all three sets of maneuvers yield the same miss-distance.

Maneuver charts are presented in the following pages for the combinations of speed ratios and turn-rate ratios described in Sec. 4.3.

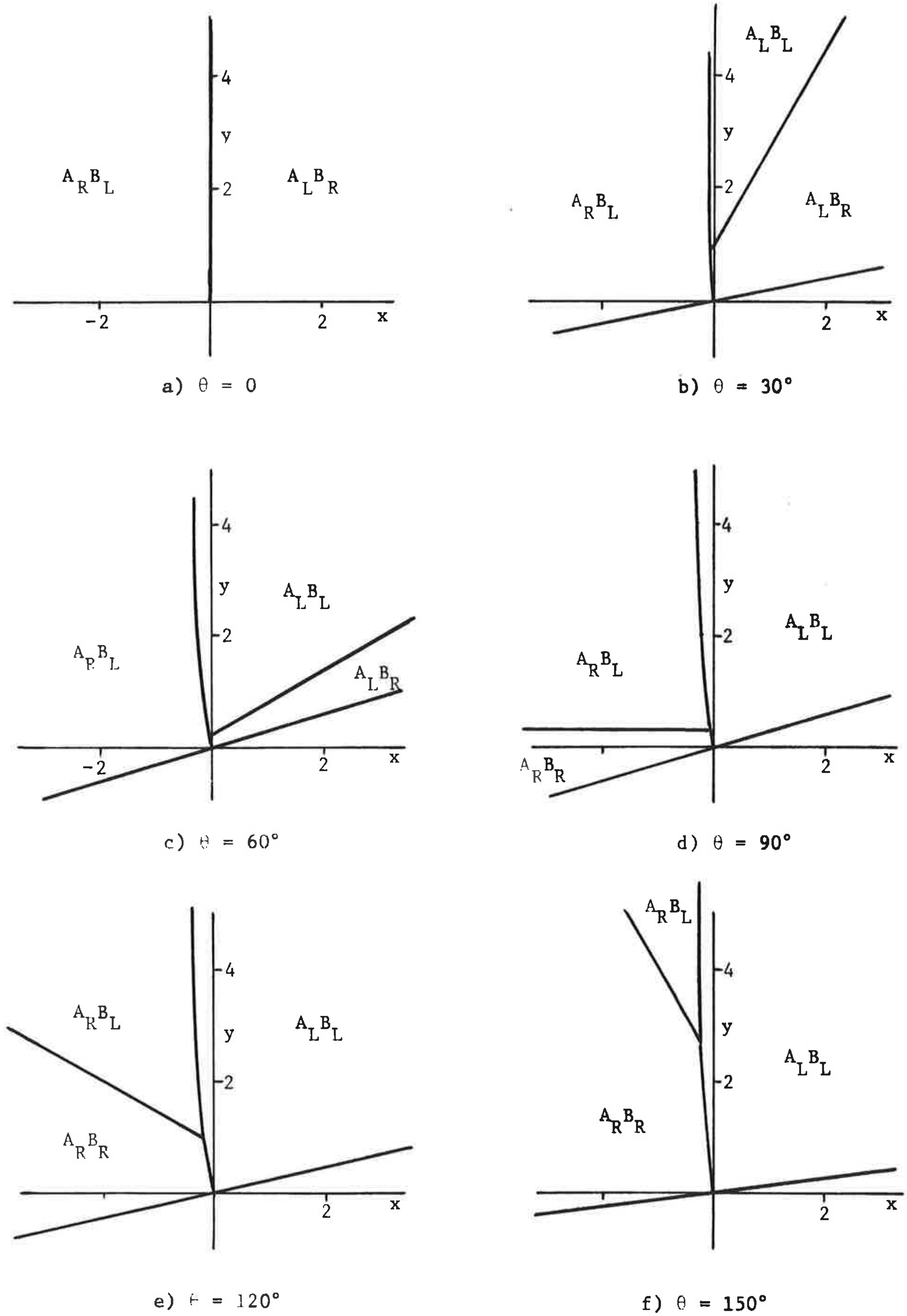

Figure C.1 $\gamma = .3$, $\omega = .1$

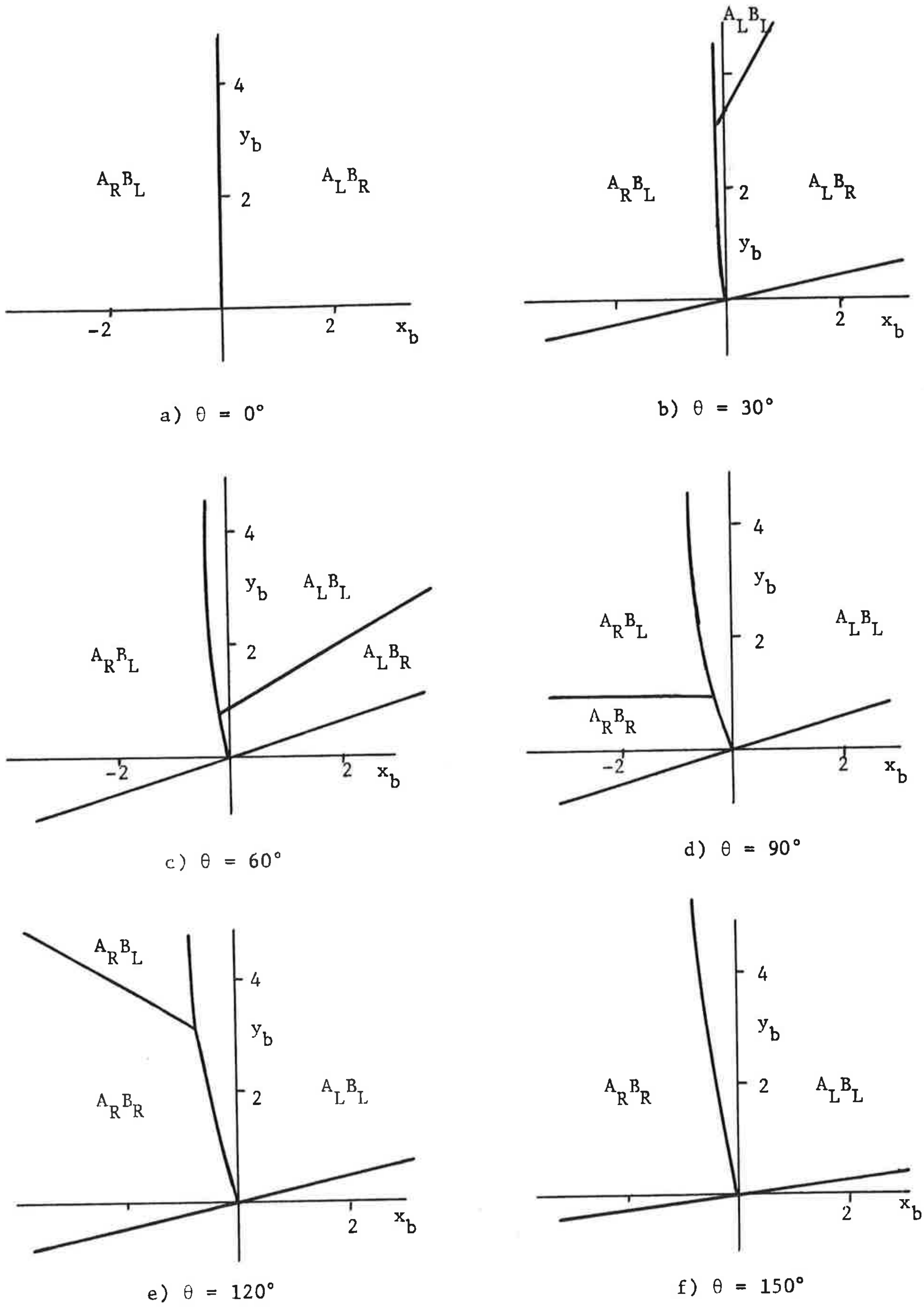

Figure C.2 $\gamma = .3$, $\omega = 1$.

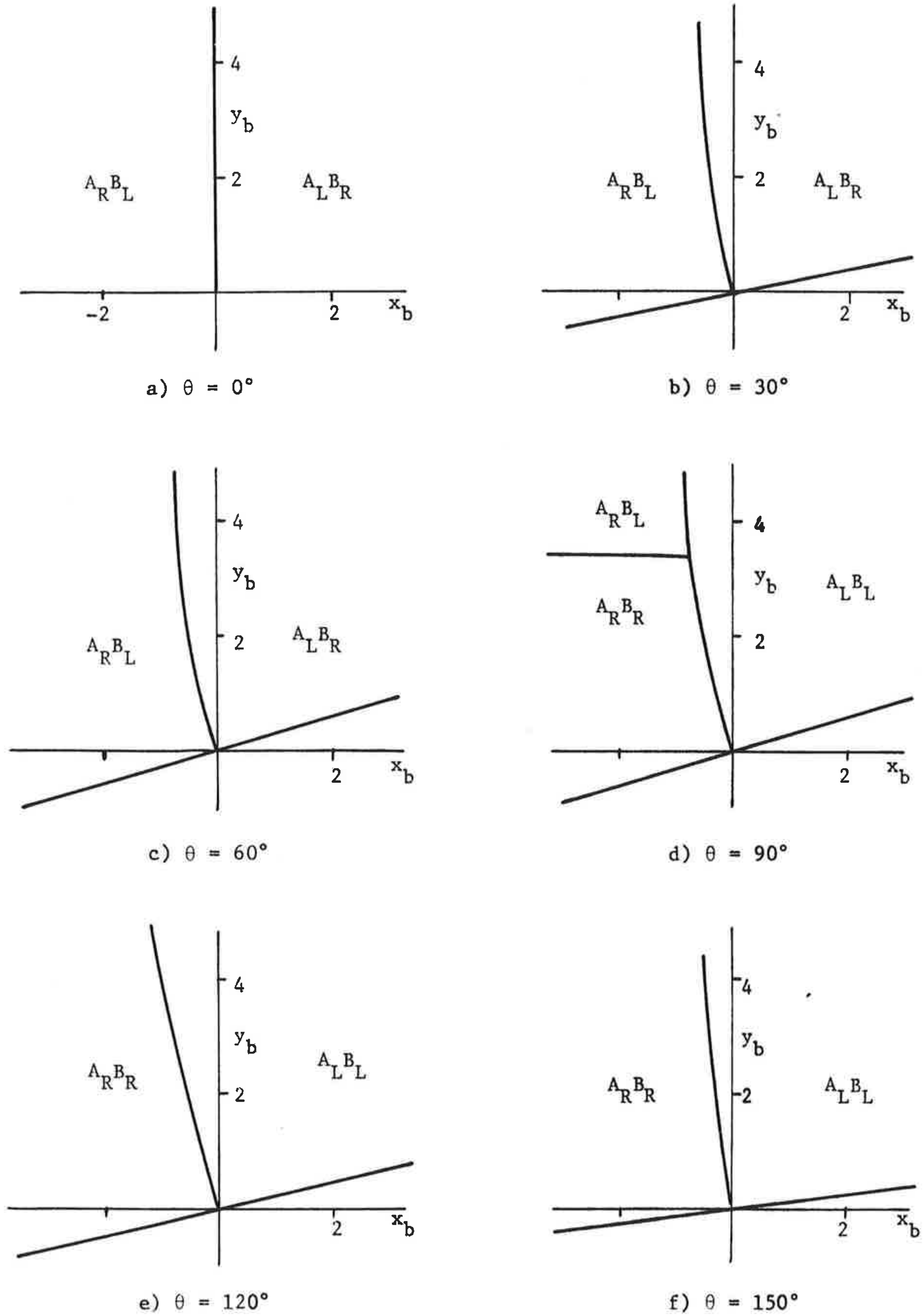

a) $\theta = 0°$

b) $\theta = 30°$

c) $\theta = 60°$

d) $\theta = 90°$

e) $\theta = 120°$

f) $\theta = 150°$

Figure C.3 $\gamma = .3$, $\omega = 10$.

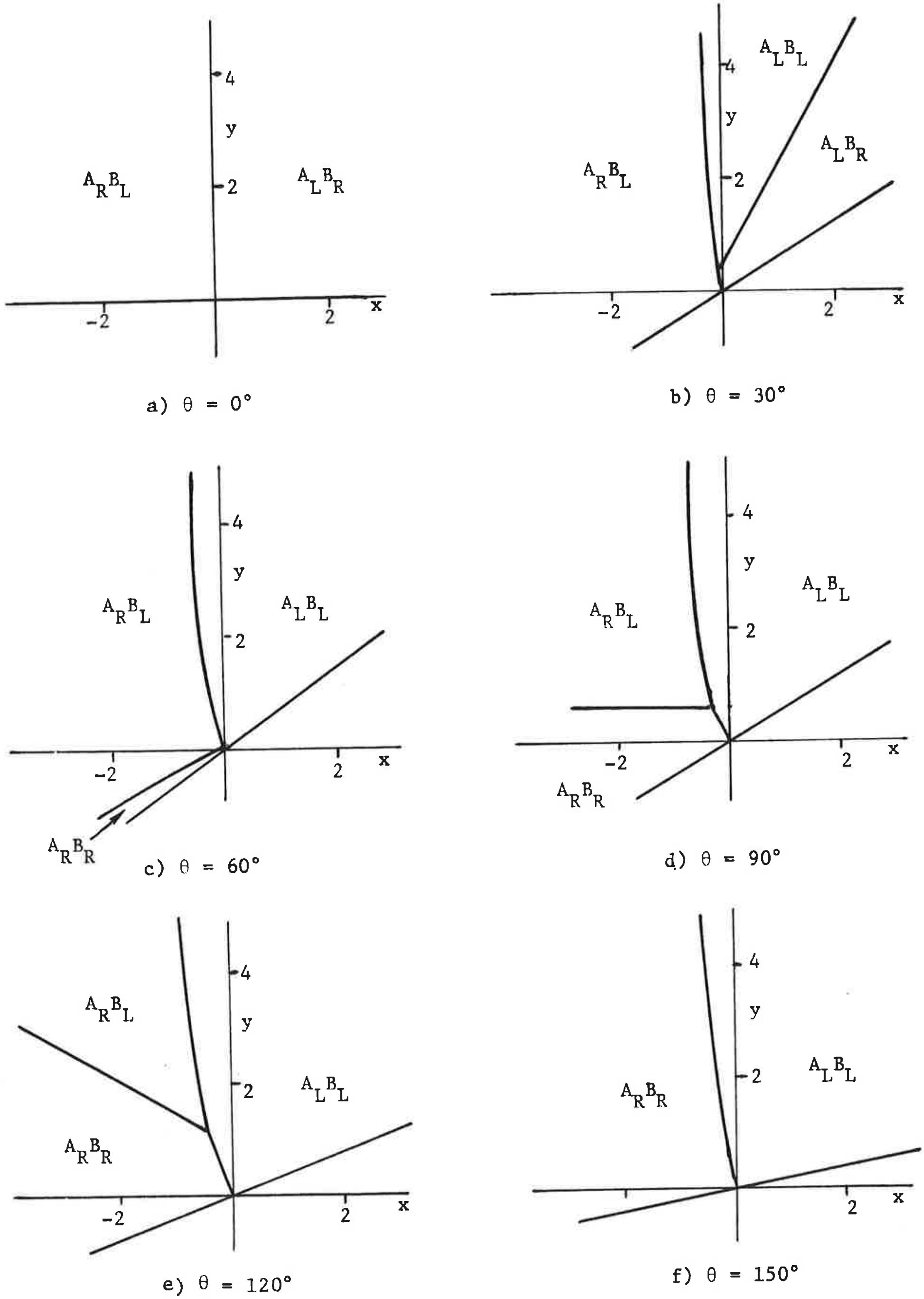

Figure C.4 $\gamma = .6, \omega = .1$

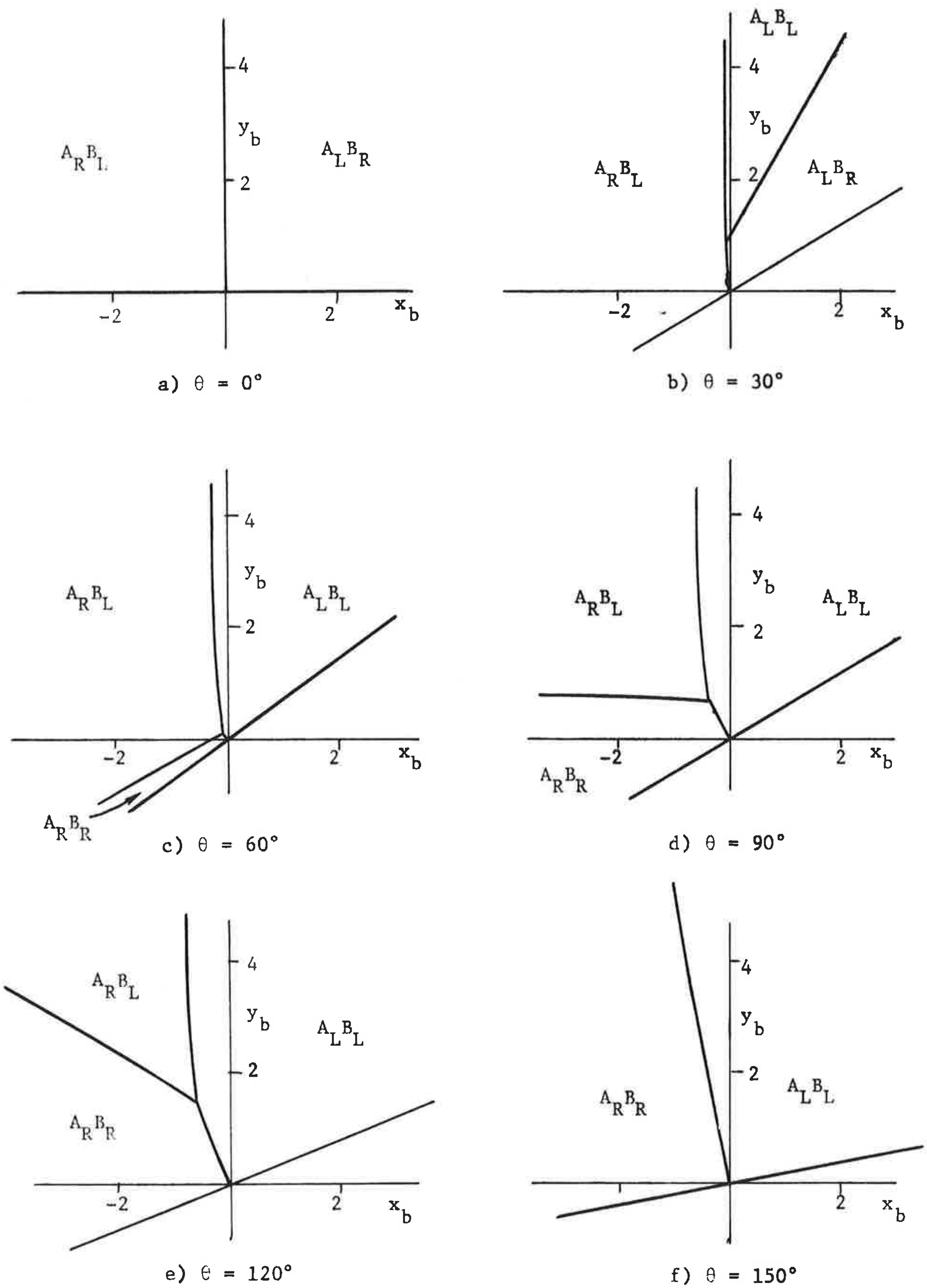

Figure C.5 $\gamma = .6$, $\omega = 1$.

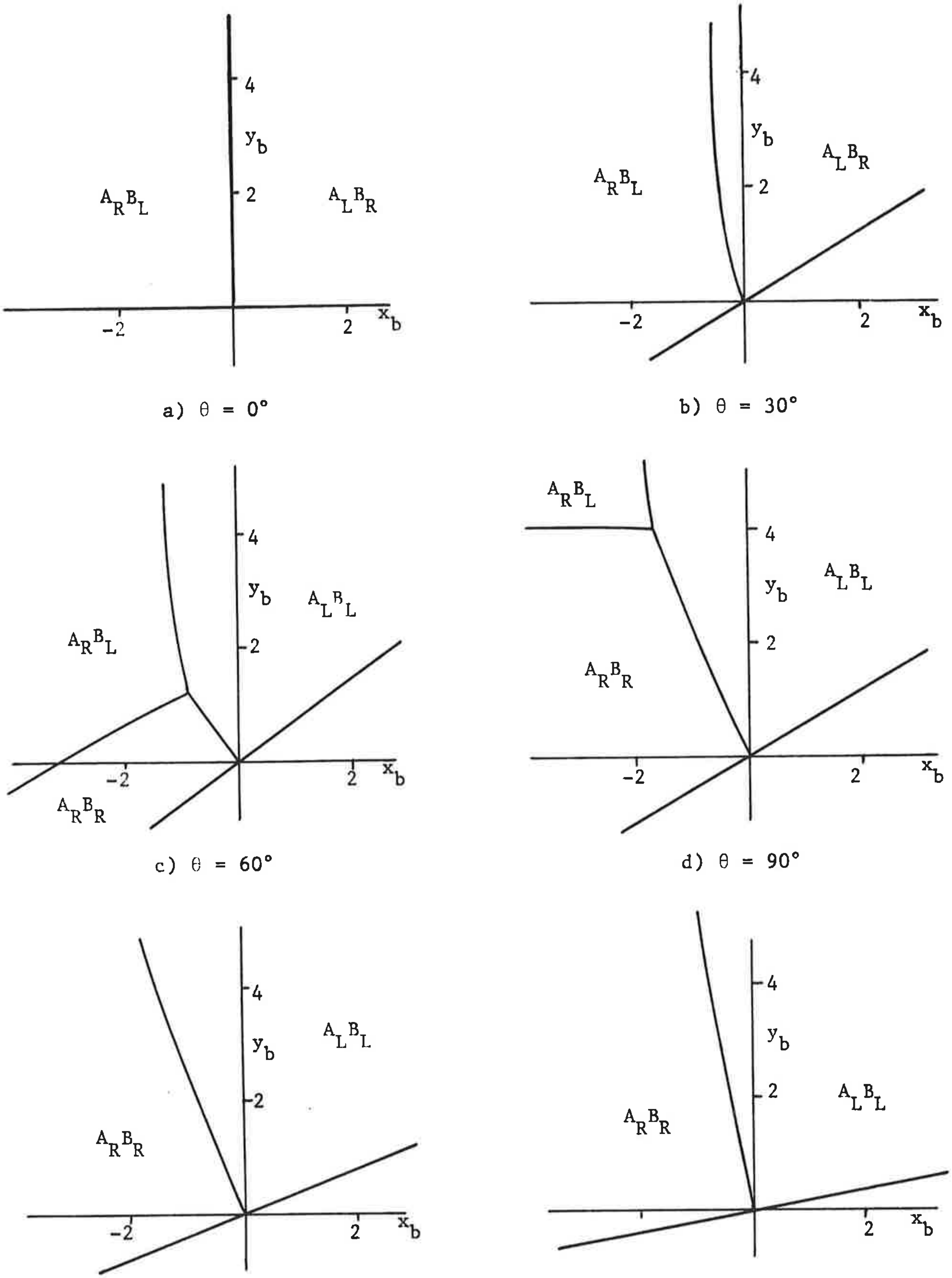

a) $\theta = 0°$ b) $\theta = 30°$

c) $\theta = 60°$ d) $\theta = 90°$

e) $\theta = 120°$ f) $\theta = 150°$

Figure C.6 $\gamma = .6,\ \omega = 10.$

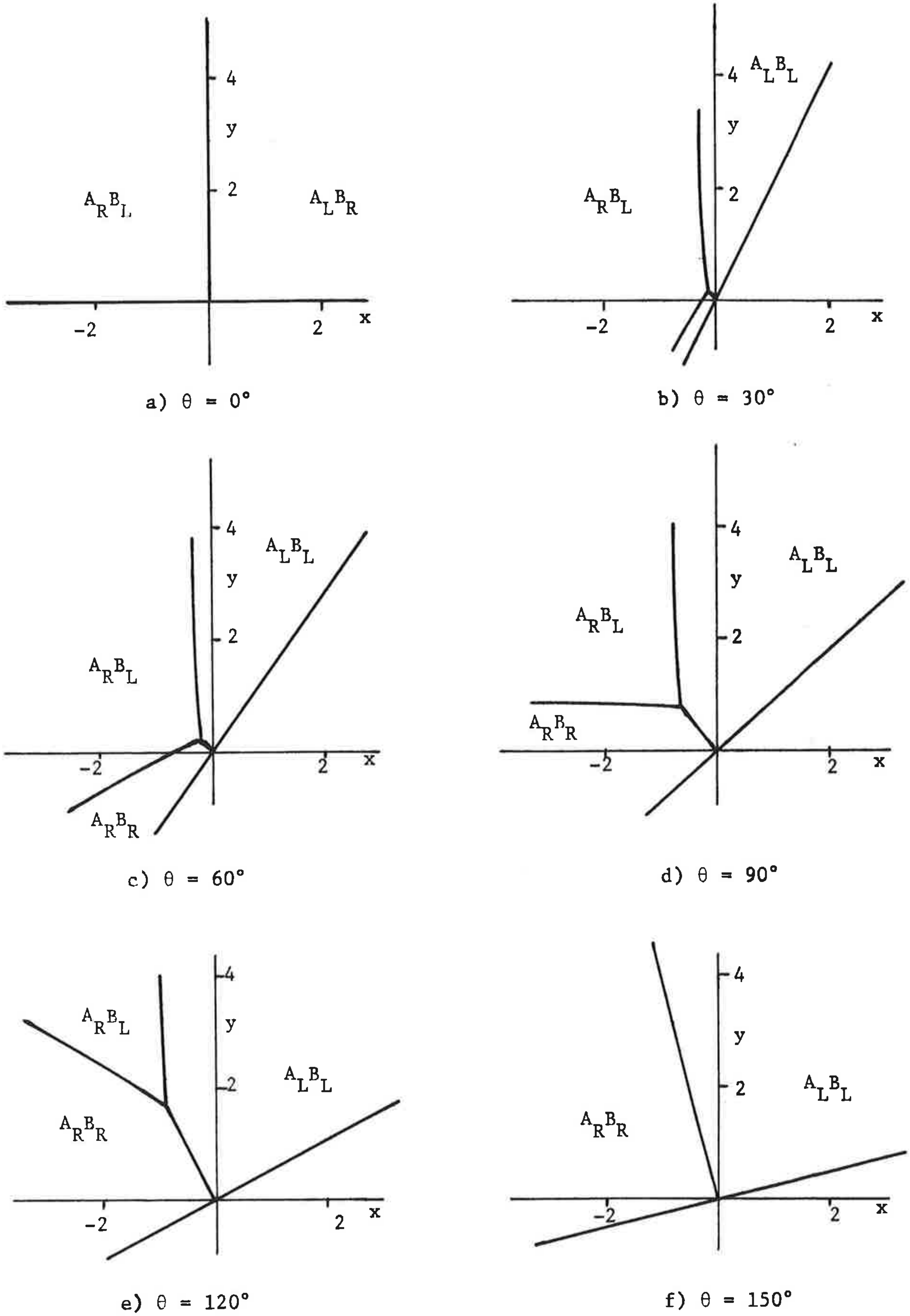

a) $\theta = 0°$

b) $\theta = 30°$

c) $\theta = 60°$

d) $\theta = 90°$

e) $\theta = 120°$

f) $\theta = 150°$

Figure C.7 $\gamma = .9$, $\omega = .1$

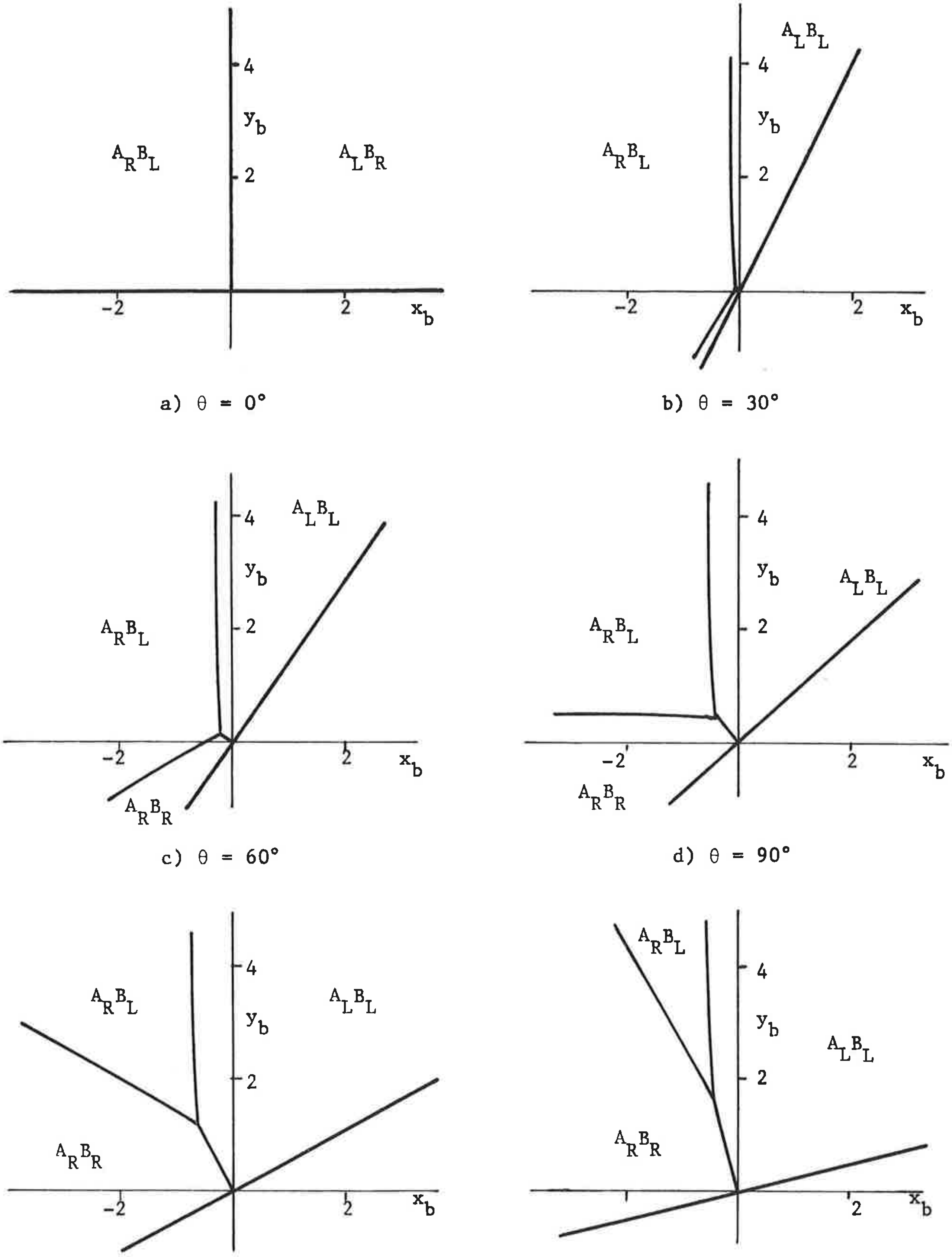

a) θ = 0°
b) θ = 30°
c) θ = 60°
d) θ = 90°
e) θ = 120°
f) θ = 150°

Figure C.8 $\gamma = .9$, $\omega = 1$.

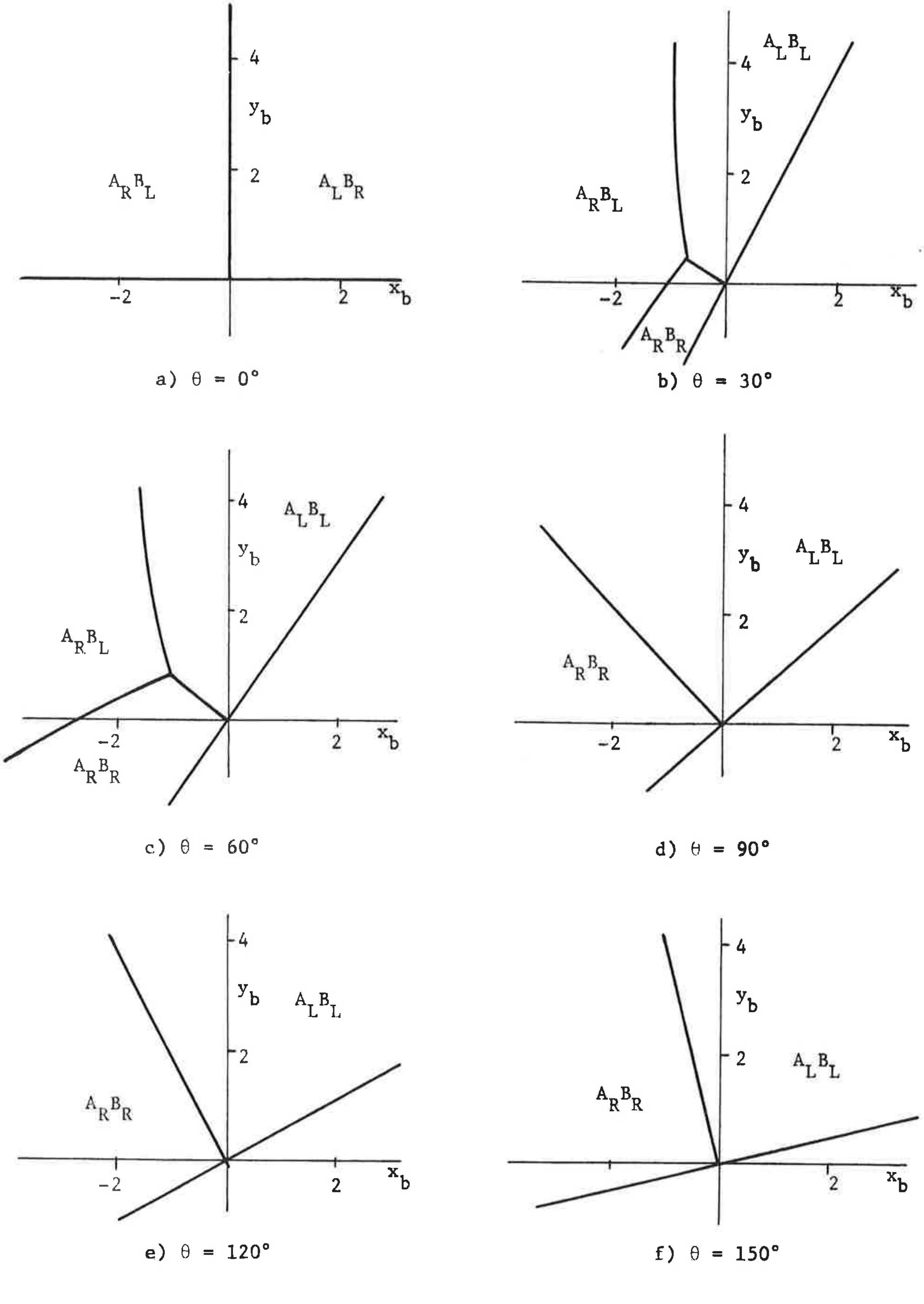

Figure C.9 $\gamma = .9, \ \omega = 10.$

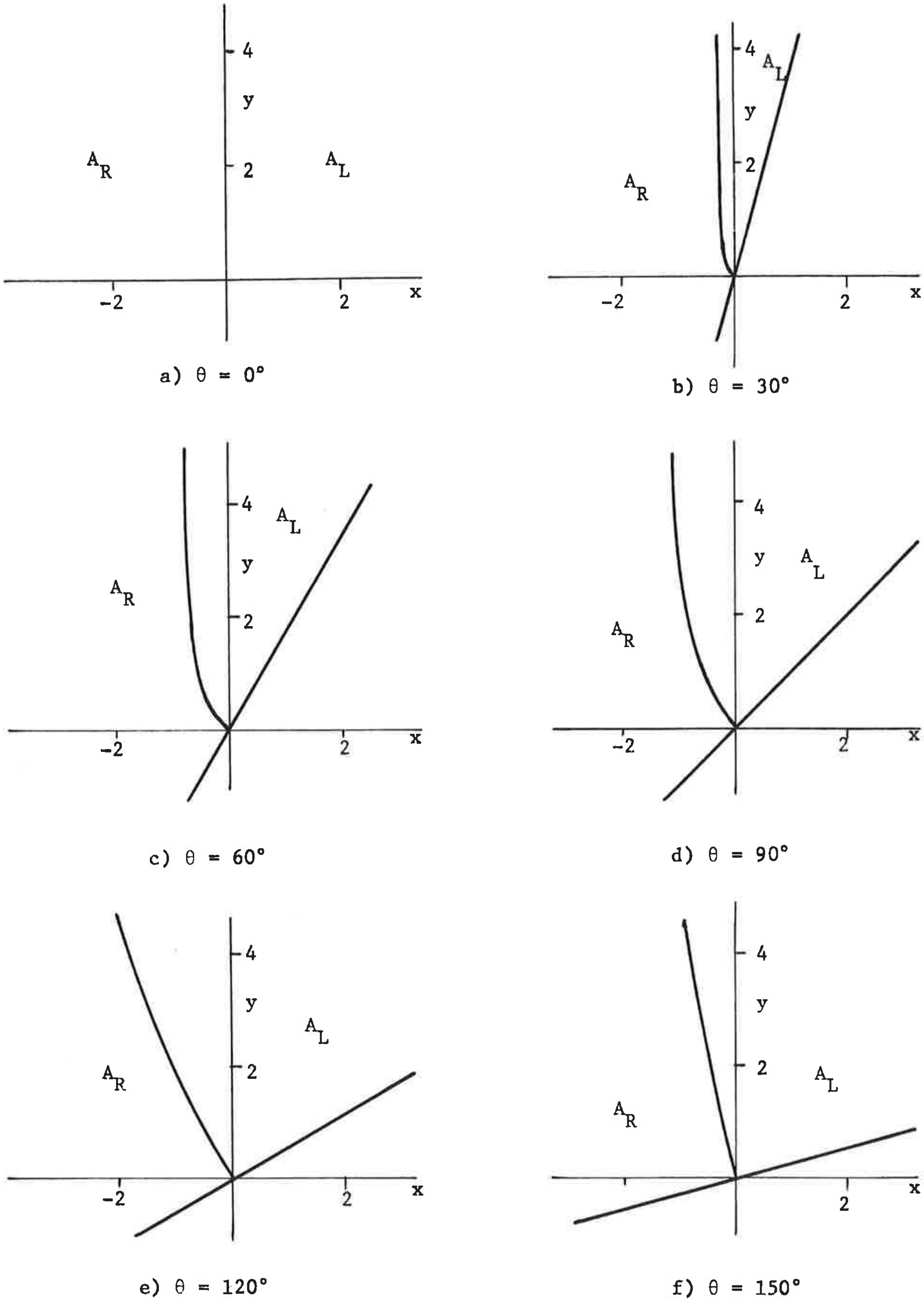

Figure C.10 γ = 1., ω = 0

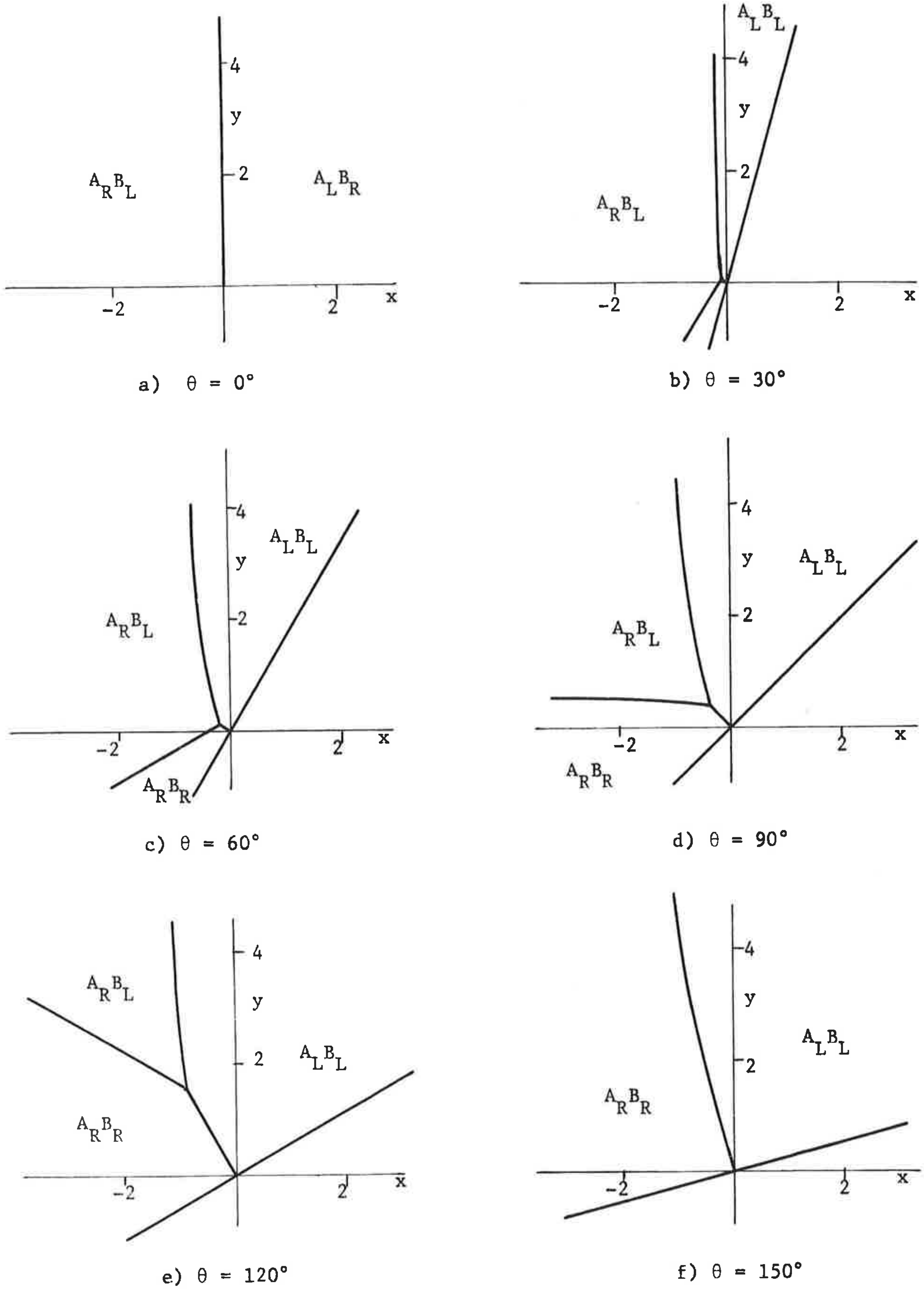

Figure C.11 $\gamma = 1.$, $\omega = .1$

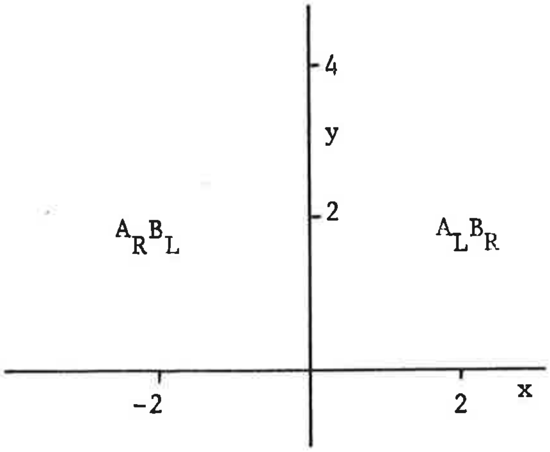

a) $\theta = 0°$

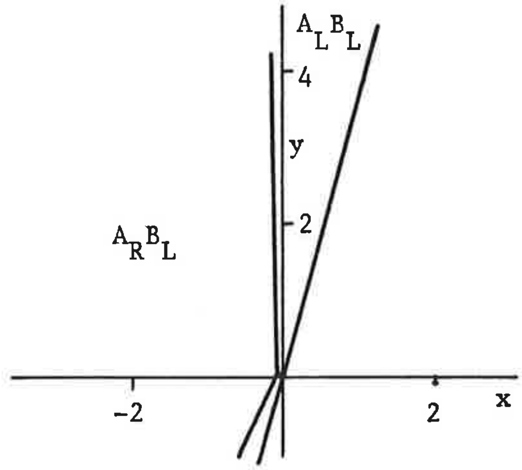

b) $\theta = 30°$

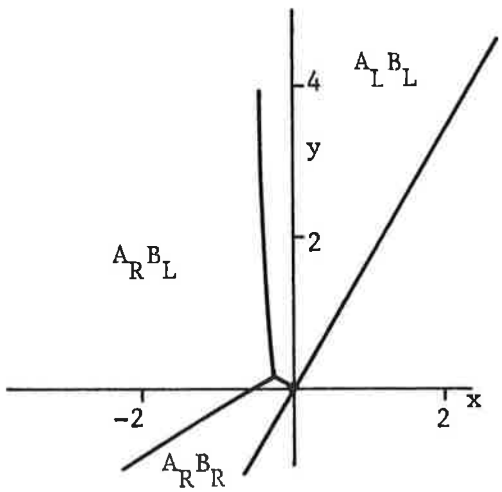

c) $\theta = 60°$

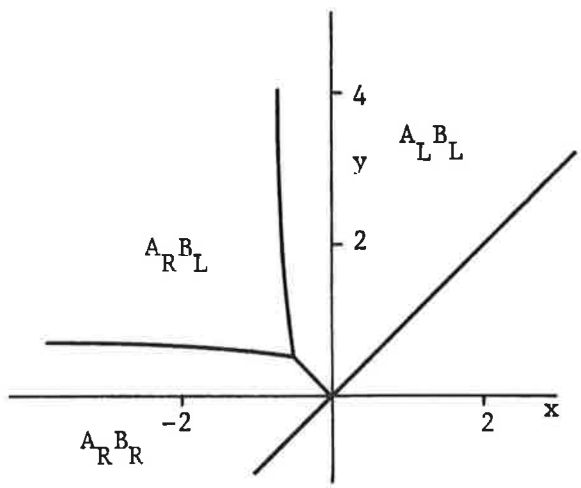

d) $\theta = 90°$

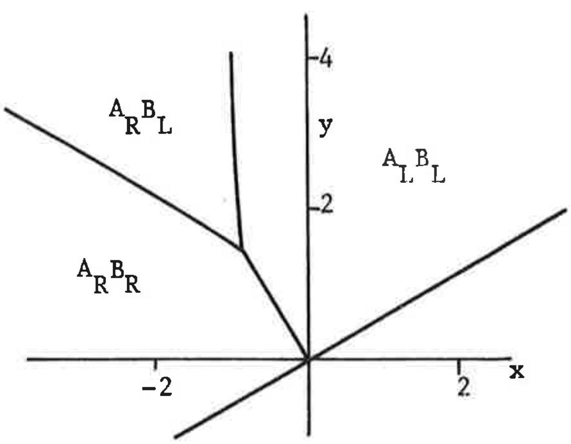

e) $\theta = 120°$

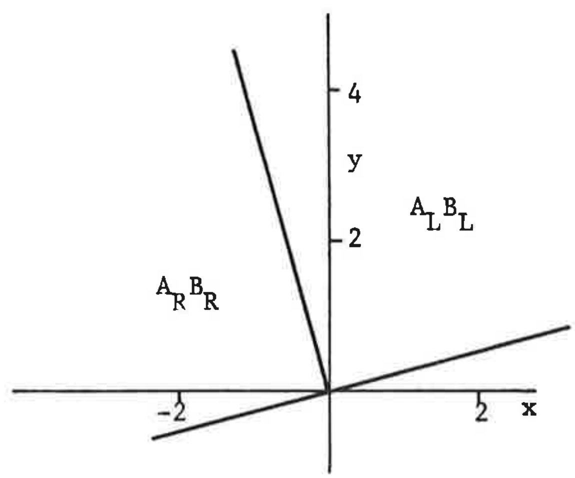

f) $\theta = 150°$

Figure C.12 $\gamma = 1$, $\omega = 1$

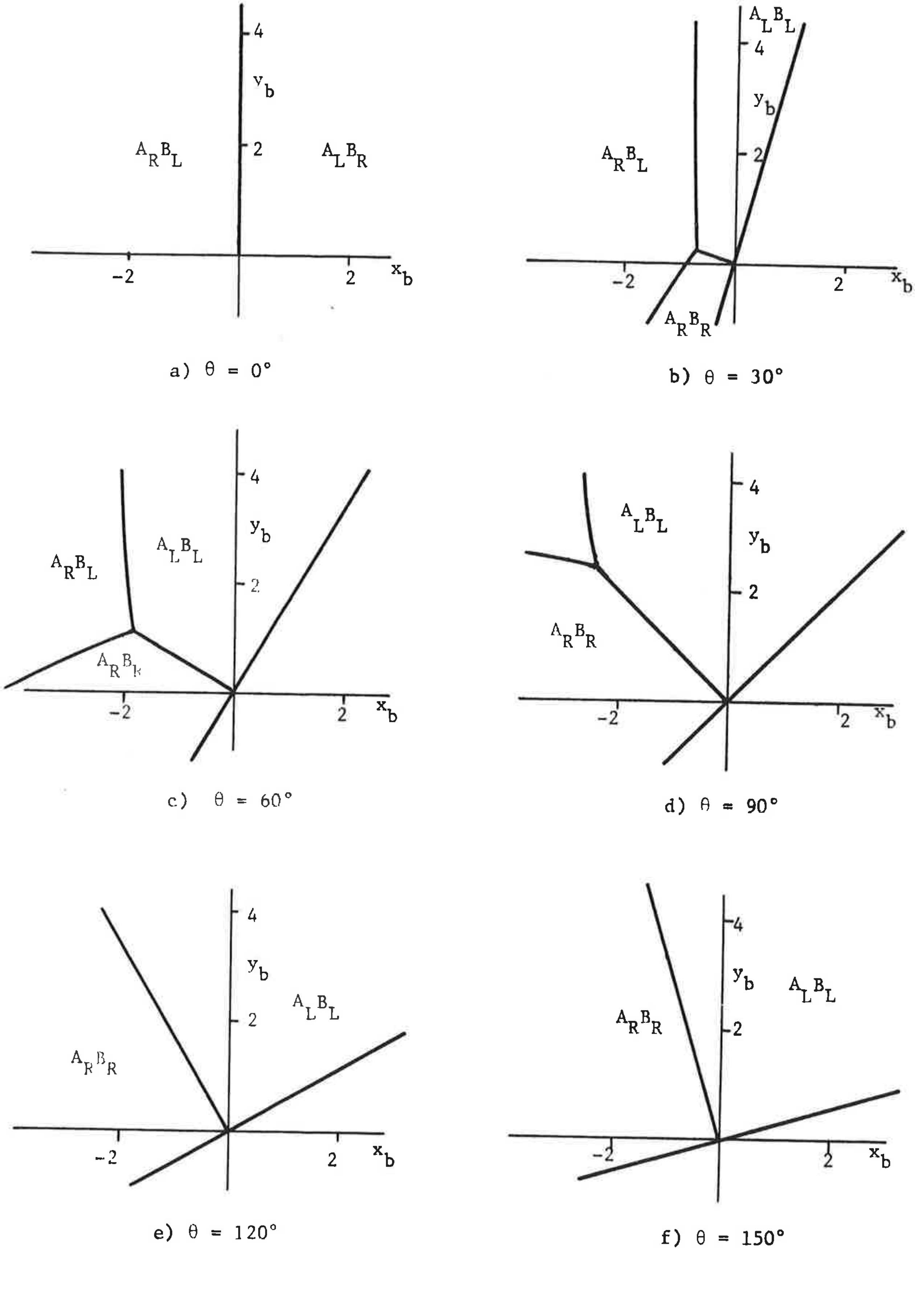

Figure C.13 $\gamma = 1$, $\omega = 10$

reduce speed by a specified amount while the other aircraft maintains speed.* The reduced speed is maintained for a specified time; then the original speed is resumed. No deviation from the flight path is required. Depending on the amount of time spent flying at reduced speed, the aircraft which reduced speed incurs an increased travel time, or a delay in arrival time. The procedure of reducing speed to avoid collision is referred to as a "delay maneuver" and the incremental change in travel time is referred to as the "time delay" associated with the maneuver. For certain combinations of aircraft speeds and intersection geometry, the time delay is negligible. Likewise, the "time-to-go", or the time at which the delay maneuver is initiated, is also acceptable. A direct comparison of delays indicates which aircraft should reduce speed.

Aircraft longitudinal dynamics are not considered in the analysis given below. Transients associated with deceleration commands can be accounted for by anticipating the need for a speed reduction by an appropriate amount of time.

D.2 INTERSECTION GEOMETRY

Let two aircraft flight paths intersect as shown in Fig. D.2, where $\overline{V}_A, \overline{V}_B$ denote the velocity vectors of aircraft A and B, respectively, and V_A, V_B are the initial aircraft speeds. Let the angle θ be the angle of intersection between the flight paths (the included angle between $\overline{V}_A$ and $\overline{V}_B$). Depending on the relative times of arrival of the aircraft at the intersection, the aircraft may or may not conflict while navigating their flight paths.

In a coordinate frame attached to aircraft A, the motion of aircraft B is defined by $\overline{V}_B - \overline{V}_A$. For fixed $\overline{V}_A$ and $\overline{V}_B$, the path of B relative to A is always parallel to the relative velocity vector, $\overline{V}_B - \overline{V}_A$, as shown in Fig. D.3. Moreover, all straight lines drawn parallel to $\overline{V}_B - \overline{V}_A$ define possible paths of B relative to A. The actual relative path seen by A depends on the boundary conditions for the aircraft time of arrival at the intersection.

*An alternate scheme in which one aircraft slows down while the other speeds up may be treated in the same manner as given here.

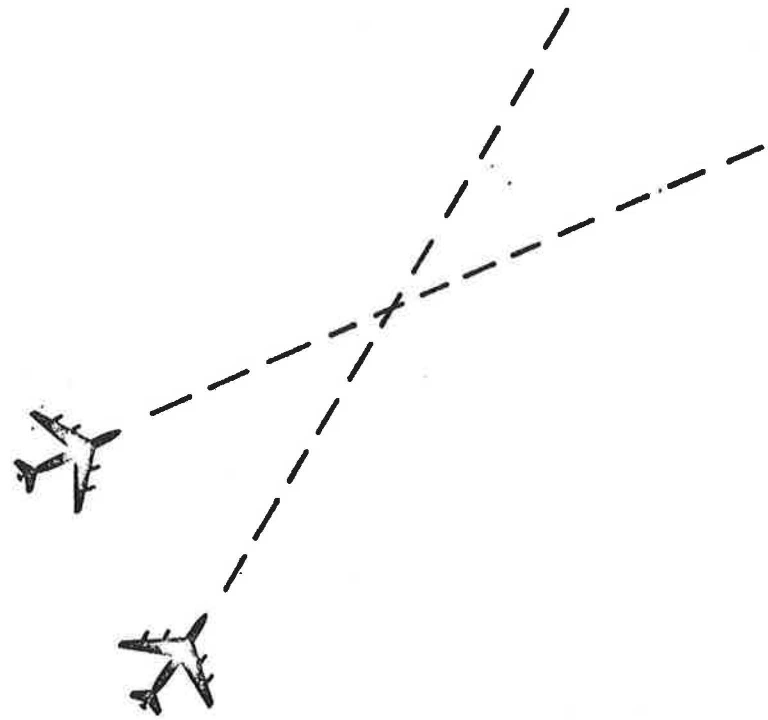

Figure D.1 Conflicting Flight Paths

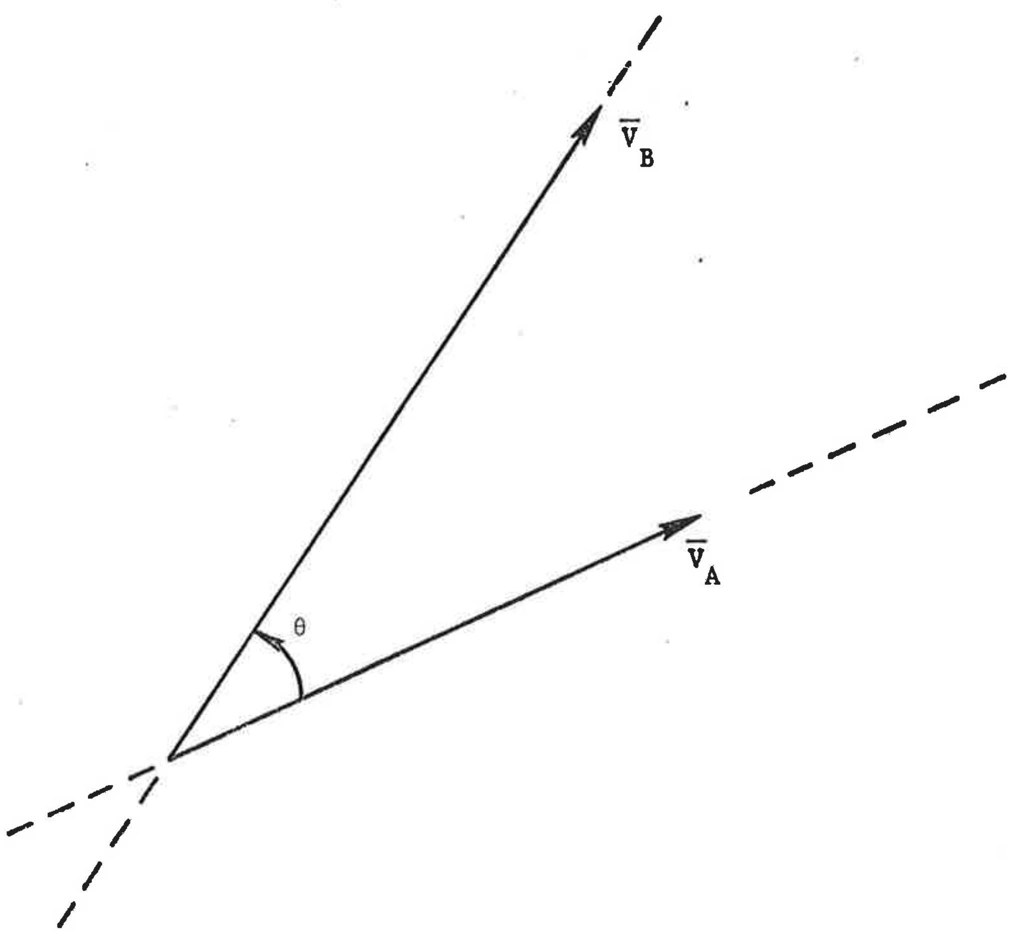

Figure D.2 Intersection Geometry

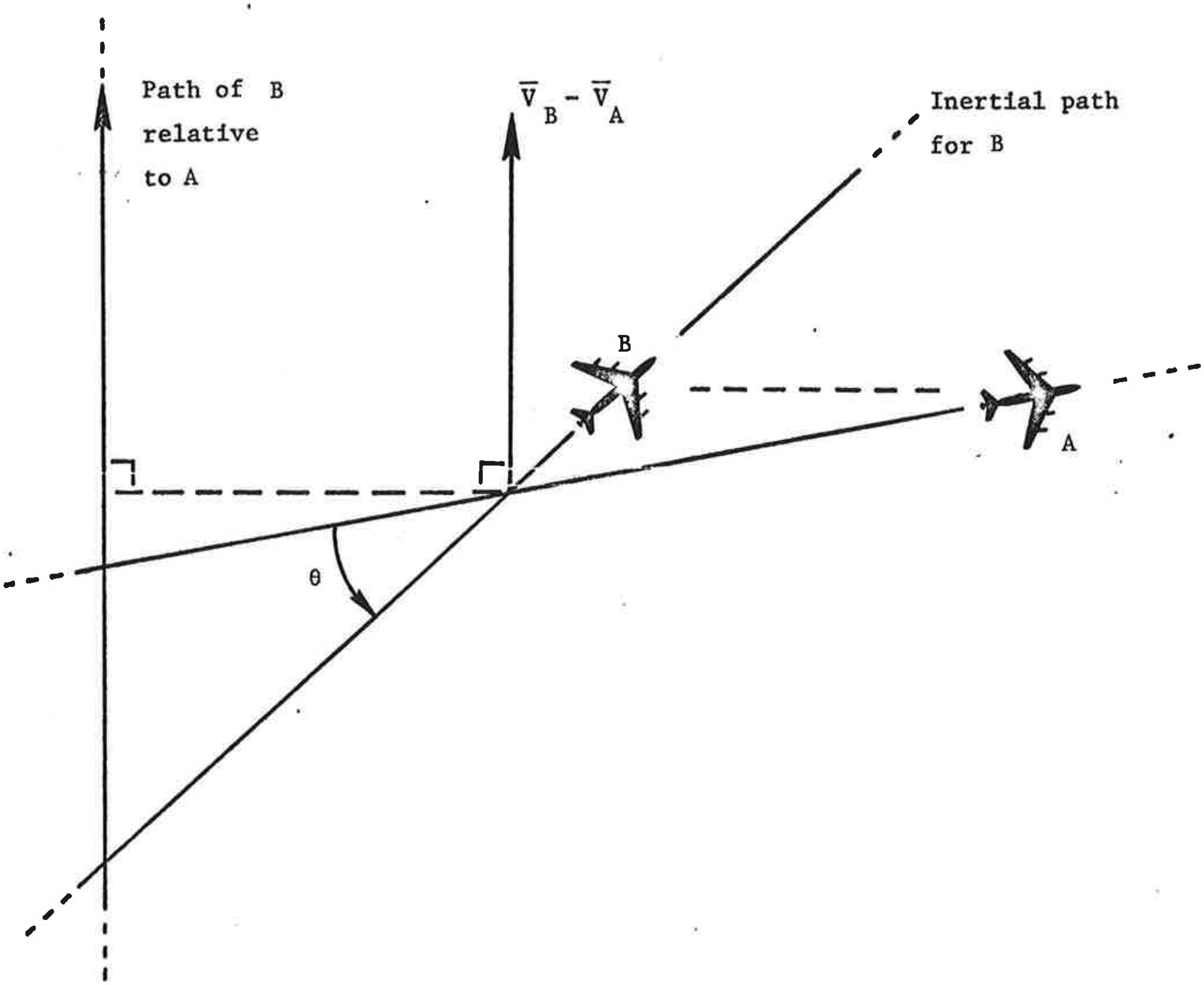

Figure D.5 Aircraft Positions for Minimal Separation

D.3 SPEED CONTROL FOR COLLISION AVOIDANCE

The property that the path of aircraft B relative to aircraft A passes through the circle of radius r_c if and only if the two aircraft attain a separation less than r_c at some time suggests a straightforward technique for collision avoidance. The technique involves changing V_B to KV_B at some time t_o where $K \leq 1$. As shown in Fig. D.6, this speed change effectively rotates and shortens the relative velocity vector. Consequently, if transients are neglected, the relative flight path becomes that shown in Fig. D.7, while the inertial tracks remain unchanged. The time for initiating the maneuver, t_o, is chosen so that the new relative path is tangent to the separation circle. At time t_1, aircraft B resumes speed. If transients are again neglected, the relative flight path becomes parallel to the relative flight path flown before the maneuver was initiated. The time t_1 is chosen so that the realigned relative path is tangent to the separation circle.

The net effect of the delay maneuver is to cause aircraft B to fly at reduced speed along the original flight path, thereby incurring an increased travel time, while avoiding a conflict with aircraft A. It is clear that the same effect is achieved when the speed reduction is initiated at any time $t \leq t_o$ and maintained for Δt seconds, with $\Delta t = t_1 - t_o$. The following section presents an algorithm for computing the time delay and the time-to-go in terms of the aircraft speeds and the intersection geometry.

D.4 SPEED CONTROL ALGORITHMS

With reference to Fig. D.7, the arrival time delay incurred by aircraft B can be obtained by first computing the time interval, $t_1 - t_o$, over which aircraft A flies at reduced speed. Then the distance flown at reduced speed during this interval is compared with the distance that could be flown at unreduced speed during the same time. Under the assumption that B returns to the original speed, the difference in distance divided by the original speed is the increased travel time induced by the use of speed control.

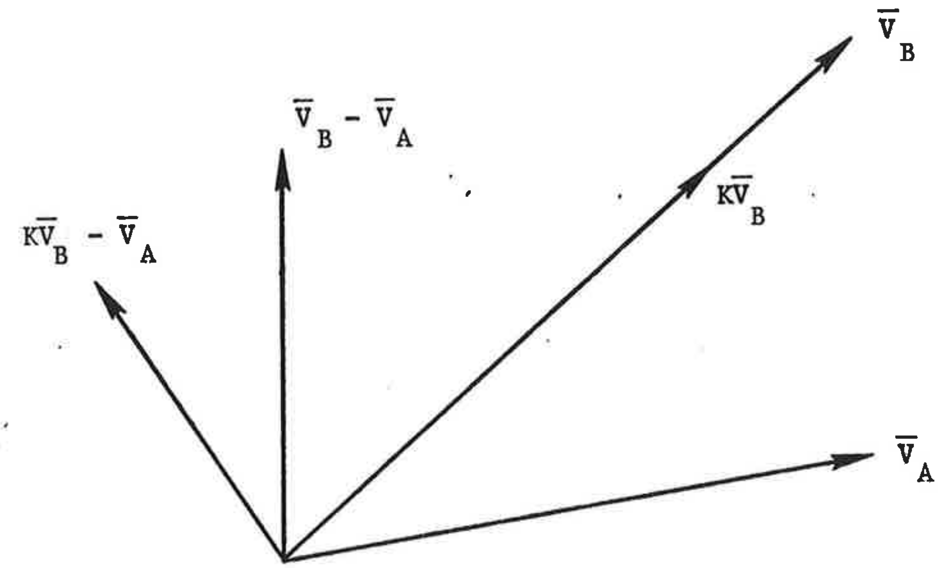

Figure D.6 Effect of Speed Reduction

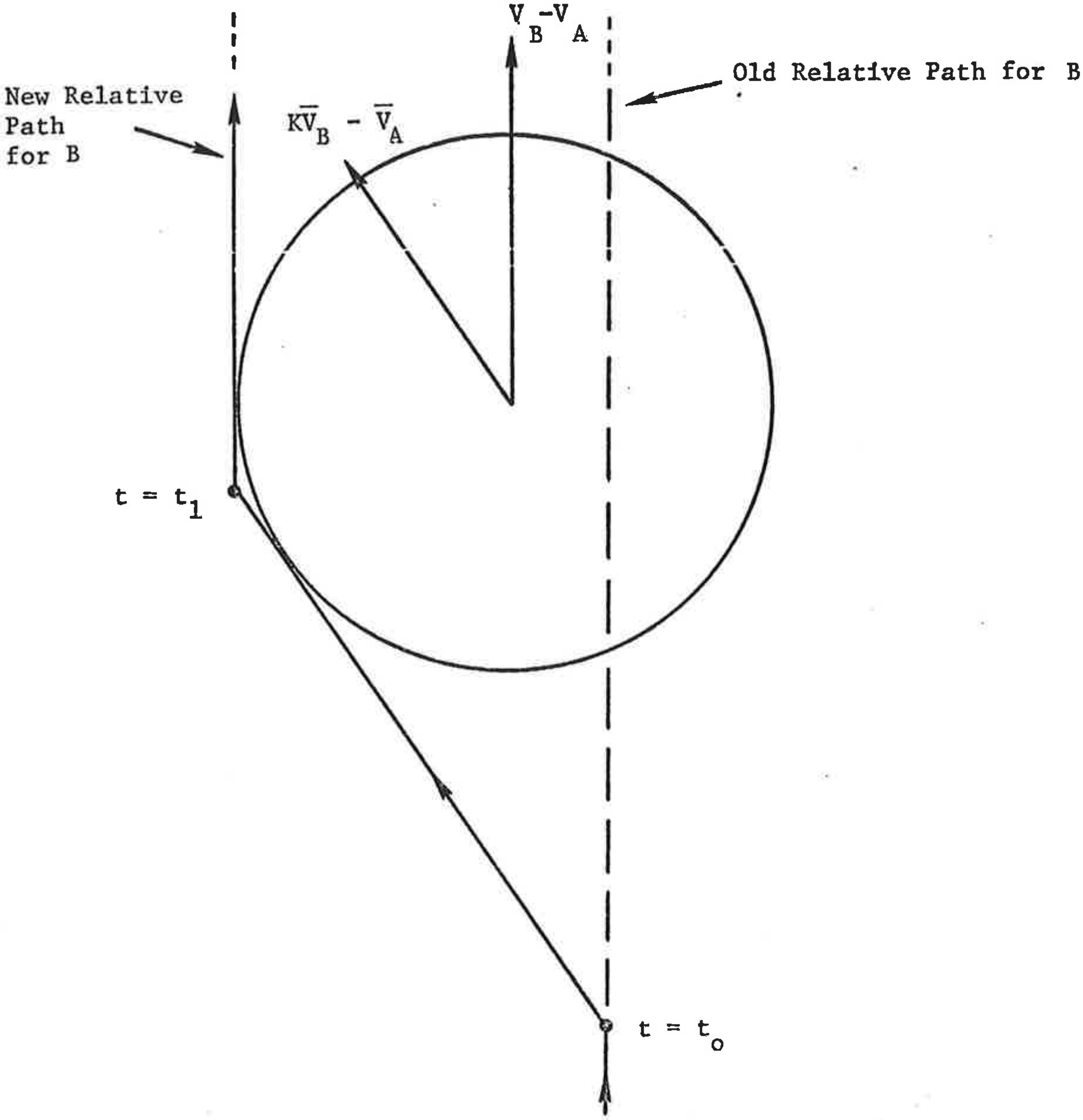

Figure D.7 Speed Control for Collision Avoidance

The geometry for computing the maneuver delay is shown in Figs. D.8 and D.9. Without loss of generality, aircraft A is taken as a reference, and the following quantities are defined:

θ = angle from $\overline{V}_A$ to $\overline{V}_B$

ξ_{AB} = angle from $\overline{V}_A$ to $\overline{V}_B - \overline{V}_A$

$\hat{\xi}_{AB}$ = angle from $\overline{V}_A$ to $K\overline{V}_B - \overline{V}_A$

$\Delta\xi$ = $\hat{\xi}_{AB} - \xi_{AB}$

ψ_{AB} = $\xi_{AB} - 90^o$

$\hat{\psi}_{AB}$ = $\hat{\xi}_{AB} - 90^o$

r_f = algebraic distance* from origin to the relative path $-r_c \leq r_f \leq r_c$

r_c = separation standard

d = length of relative path traveled at reduced relative speed

t_o = time to initiate speed reduction

t_1 = time to reduce speed

Δt_r = time at reduced speed

The assumption is made that only aircraft B will reduce speed. Thus, it can be shown that $\Delta\xi = \hat{\xi}_{AB} - \xi_{AB} \geq 0$ for $K \leq 1$.

---

*$|r_f|$ is commonly referred to as the miss distance. For $r_f < 0$, aircraft B passes behind aircraft A. For $r_f = 0$, the aircraft collide. For $r_f > 0$, aircraft B passes in front of aircraft A at the time of closest approach.

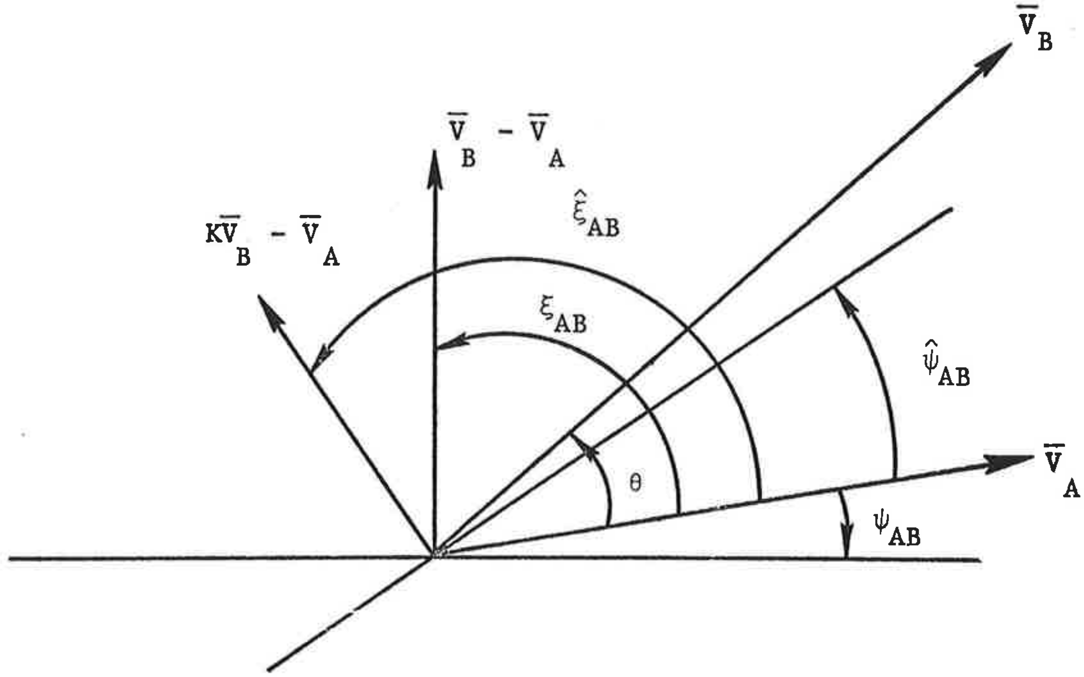

Figure D.8 Velocity Vector Relationships

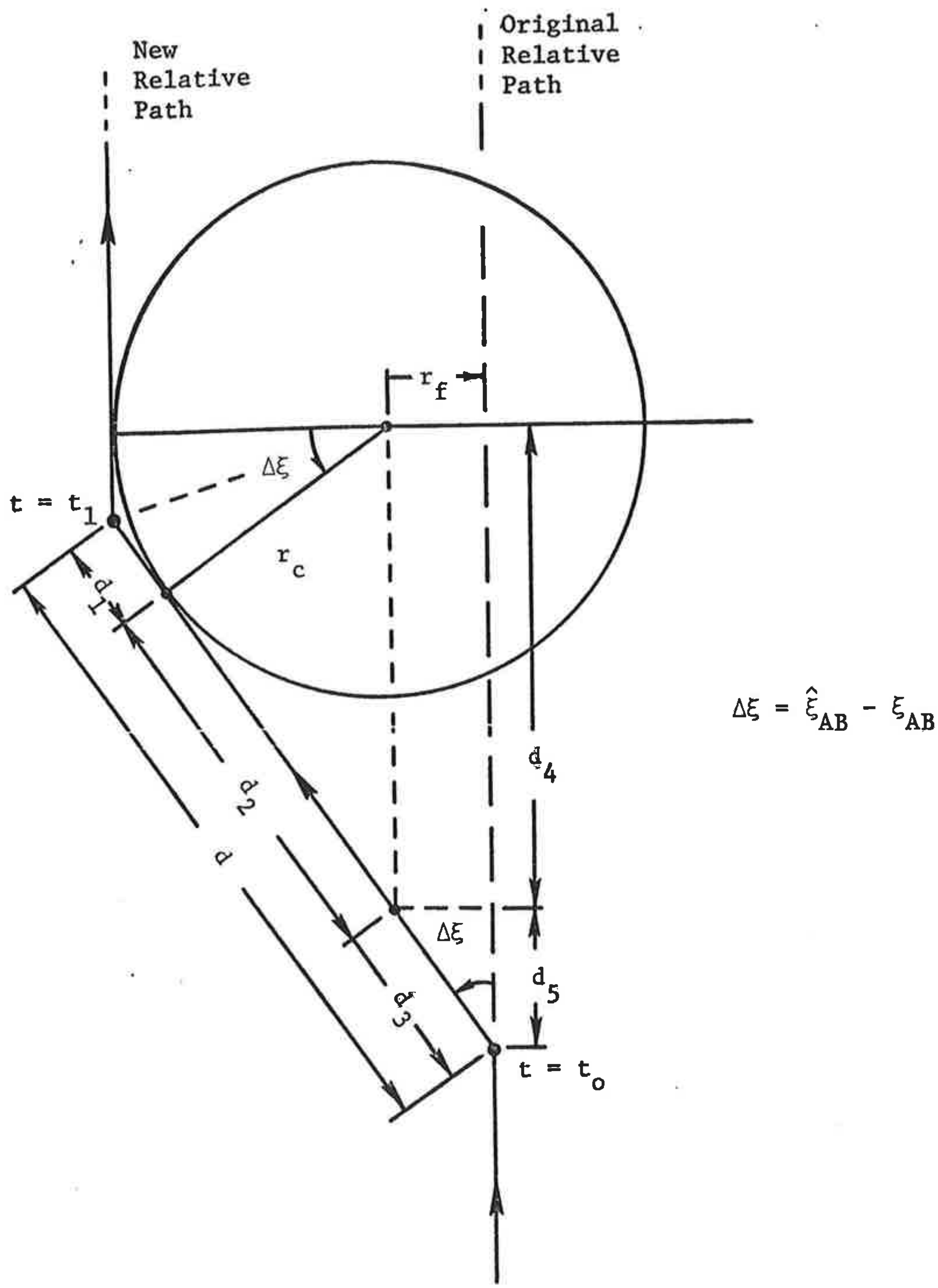

Figure D.9 Relative Path for Collision Avoidance

It is also true that:

$$\xi_{AB} = \cos^{-1}\left[\frac{V_B \cos\theta - V_A}{[V_A^2 + V_B^2 - 2V_AV_B \cos\theta]^{\frac{1}{2}}}\right]$$

$$\hat{\xi}_{AB} = \cos^{-1}\left[\frac{KV_B \cos\theta - V_A}{[V_A^2 + K^2V_B^2 - 2KV_AV_B \cos\theta]^{\frac{1}{2}}}\right]$$

An expression for the time delay is given by the following:

$$\Delta t_r = t_1 - t_o = \frac{d}{|K\overline{V}_B - \overline{V}_A|}$$

$$D_B = V_B \,\Delta t_r$$

$$\hat{D}_B = KV_B \,\Delta t_r$$

$$t_d = \frac{D_B - \hat{D}_B}{V_B}$$

The quantity t_d is the extra flight time required for aircraft B to make up the lost distance $D_B - \hat{D}_B$ after resuming speed. It follows that

$$t_d = [1 - K]\,\Delta t_r$$

and so

$$t_d = \frac{[1 - K]}{|K\overline{V}_B - \overline{V}_A|}\, d \quad ,$$

where

$$|K\bar{V}_B - \bar{V}_A| = [V_A^2 + K^2V_B^2 - 2KV_AV_B \cos\theta]^{\frac{1}{2}}$$

and

$$|\bar{V}_B - \bar{V}_A| = [V_A^2 + V_B^2 - 2V_AV_B \cos\theta]^{\frac{1}{2}}$$

It is necessary to obtain an expression for d in terms of the parameters specifying the conflict geometry. Figure D.9 depicts the situation for $r_c \geq r_f \geq 0$. It is easily verified that the expressions given below are also valid for $-r_c \leq r_f \leq 0$. The distance traveled at reduced relative speed on the relative path is given by

$$d = d_1 + d_2 + d_3$$

where

$$d_a = r_c \tan \frac{\Delta\xi}{2}$$

$$d_2 = r_c \operatorname{ctn} \Delta\xi$$

$$d_3 = r_f \csc \Delta\xi.$$

For $-r_c \leq r_f \leq r_c$ it follows that

$$d = [r_c + r_f] \csc \Delta\xi .$$

In preparation for computing the time-to-go, ℓ_o is defined to be the distance along the original relative path from the point of closest approach to the point at which the speed reduction is made. Then

$$\ell_o = d_4 + d_5 ,$$

with

$$d_4 = r_c \csc \Delta\xi$$

$$d_5 = r_f \operatorname{ctn} \Delta\xi,$$

and

$$\ell_o = [r_c + r_f \cos \Delta\xi] \csc \Delta\xi.$$

Letting t_d denote the arrival <u>time delay</u>, or the increased flight time associated with the speed reduction, it follows that:

$$t_d = \frac{[1 - K][r_c + r_f] \csc \Delta\xi}{|K\bar{V}_B - \bar{V}_A|},$$

for $K \leq 1$, $-r_c \leq r_f \leq r_c$. The time-to-go, t_g, is measured relative to the time of closest approach on the original relative path, and it is given by:

$$t_g = \frac{\ell_o}{|\bar{V}_B - \bar{V}_A|}$$

$$t_g \quad \frac{[r_c + r_f \cos \Delta\xi] \csc \Delta\xi}{|K\bar{V}_B - \bar{V}_A|}.$$

For collision avoidance, the speed reduction must be accomplished at least t_g units before the predicted point of closest approach is reached.

D.5 NORMALIZED SPEED CONTROL ALGORITHMS

For computational purposes, it is convenient to obtain nondimensional expressions for the time delay and the time-to-go. Let

$$\tau_d = \frac{V_A}{r_c} t_d$$

and $\{\underline{v}(t_i),\ i=0,1,2,\ldots\}$ is a sequence of independent zero-mean normally distributed random two-dimensional vectors with covariance matrix

$$R = \begin{bmatrix} \sigma_r^2 & 0 \\ 0 & \sigma_\beta^2 \end{bmatrix}.$$

The solution to Eq. (E.1) is of the form

$$\begin{aligned} x(t) &= p_1 + p_3 t \\ y(t) &= p_2 + (p_4 - V_A)t \end{aligned} \qquad \text{(E.3)}$$

where $t_o = 0$, $p_1 = x(t_o)$, $p_2 = y(t_o)$, $p_3 = V_B \sin\theta$, and $p_4 = V_B \cos\theta$. Note that Eq. (E.3) describes a line in the (x,y) plane. Given an estimate $\hat{\underline{p}}$ of $\underline{p}$, estimates of x, y, V_B and θ can be computed. The following procedure for doing this results in the least-squares smoothing (LSS) filter.

Suppose that the measurements of Eq. (E.2) are transformed from line-of-sight coordinates to Cartesian coordinates by

$$\begin{aligned} z_x(t_k) &= z_1(t_k) \sin z_2(t_k), \\ z_y(t_k) &= z_1(t_k) \cos z_2(t_k). \end{aligned} \qquad \text{(E.4)}$$

Now, given the data $\{(z_x(t_i),\ z_y(t_i)),\ i = 0,\ldots,k\}$ up to time t_k, the parameters $\underline{p}$ describing the line in Eq. (E.3) can be estimated by performing a least-square curve-fit of a line to the data.

To be more precise, the estimate $\hat{\underline{p}}_k$ is the value of $\underline{p}$ which minimizes the quadratic cost

$$J = \tfrac{1}{2} \sum_{i=0}^{k} \{[p_1 + p_3 t_i - z_x(t_i)]^2 + [p_2 + (p_4 - V_A)t_i - z_y(t_i)]^2\}. \qquad \text{(E.5)}$$

at the time N.

The solution to this minimization problem is given by the solution to the set of four linear equations

$$A_k \, \hat{\underline{p}}_k = \underline{c}_k \tag{E.6}$$

where

$$A_k = \begin{bmatrix} k+1 & 0 & \frac{1}{2}k(k+1)\Delta t & 0 \\ 0 & k+1 & 0 & \frac{1}{2}k(k+1)\Delta t \\ \frac{1}{2}k(k+1)\Delta t & 0 & \frac{1}{6}k(k+1)(2k+1)\Delta t^2 & 0 \\ 0 & \frac{1}{2}k(k+1)\Delta t & 0 & \frac{1}{6}k(k+1)(2k+1)\Delta t^2 \end{bmatrix},$$

$$\underline{c}_k = \begin{bmatrix} \sum_{i=0}^{k} z_x(t_i) \\ \frac{1}{2}k(k+1)\Delta t \, V_A + \sum_{i=0}^{k} z_y(t_i) \\ \sum_{i=0}^{k} t_i z_x(t_i) \\ \frac{1}{6}k(k+1)(2k+1)\Delta t^2 V_A + \sum_{i=0}^{k} t_i z_y(t_i) \end{bmatrix},$$

and Δt is the sampling period.

Note that for $k \neq 0$, A_k is positive definite and, hence, A_k^{-1} exists. Thus,

$$\hat{\underline{p}}_k = A_k^{-1} \, \underline{c}_k \tag{E.7}$$

Having $\hat{p}_k$, estimates of x, y, V_B and θ are obtained via the transformation

$$\begin{aligned}
\hat{x}(t_k) &= \hat{p}_{1k} + \hat{p}_{3k}t_k \\
\hat{y}(t_k) &= \hat{p}_{2k} + (\hat{p}_{4k} - V_A)t_k \\
\hat{V}_B(t_k) &= [\hat{p}_{3k}^2 + \hat{p}_{4k}^2]^{\frac{1}{2}} \\
\hat{\theta}(t_k) &= \tan^{-1}\left[\frac{\hat{p}_{3k}}{\hat{p}_{4k}}\right]
\end{aligned} \tag{E.8}$$

Due to the simple form of A_k, an analytical expression for A_k^{-1} can be easily derived. This eliminates the necessity of computing a matrix inverse at each step. If the LSS filter is to be used only as an initialization procedure for more complex filters, the computations need only be performed once, at the last step. If the filter is to be used alone, it is convenient to put $\underline{c}_k$ into the recursive form

$$\underline{c}_k = \underline{c}_{k-1}+(z_k(t_k),V_At_k+z_y(t_k),t_kz_x(t_k),V_At_k^2+t_kz_y(t_k))', \quad k=1,2,\ldots \tag{E.9}$$

with

$$\underline{c}_o = (z_x(0),\ z_y(0),\ 0,\ 0)'.$$

Note that the curve-fitting could have been done in the line-of-sight coordinates (r, β), but the transformation corresponding to Eq. (E.8) is much more complex and subject to numerical difficulties during actual computation.

As a "recursive" filter, the LSS filter operates in the following manner. After two sets of measurements have been accumulated, the linear Eq. (E.7) is evaluated followed by the nonlinear transformation of Eq. (E.8). As each new set of measurements is accumulated, the procedure is repeated.

The principal advantage of the LSS filter is its simplicity and low storage requirements. However, in its present form, it is not suitable when either of the aircraft maneuver sometime during the tracking period. There are modifications which can be made to improve the filter's performance under those conditions.

If Eqs. (E.1) and (E.2) are linearized about the most recent estimate of the state and the well-known linear theory is applied, the so-called extended Kalman (EK) filter results.[86] The EK filter algorithm is given by the following set of recursive equations.

One-step prediction:

$$\underline{\hat{x}}(t_{k+1}|t_k) = \underline{\hat{x}}(t_k|t_k) + \int_{t_k}^{t_{k+1}} \underline{f}(\underline{\hat{x}}(t|t_k))dt \; ; \tag{E.10}$$

$$P(t_{k+1}|t_k) = \Phi(t_{k+1},t_k;\underline{\hat{x}}(t_k|t_k)\; P(t_k|t_k)\Phi'(t_{k+1},t_k;\underline{\hat{x}}(t_k|t_k)); \tag{E.11}$$

Update at a measurement:

$$K(t_{k+1}) = P(t_{k+1}|t_k)h_{\underline{x}}(\underline{\hat{x}}(t_{k+1}|t_k))$$

$$\cdot\; [h_{\underline{x}}(\underline{\hat{x}}(t_{k+1}|t_k))\; P(t_{k+1}|t_k)\; h'_{\underline{x}}(\underline{\hat{x}}(t_{k+1}|t_k) + R]^{-1}; \tag{E.12}$$

$$\underline{\hat{x}}(t_{k+1}|t_{k+1}) = \underline{\hat{x}}(t_{k+1}|t_k) + K(t_{k+1})\; [\underline{z}(t_{k+1}) - \underline{h}(\underline{\hat{x}}(t_{k+1}|t_k))]; \tag{E.13}$$

$$P(t_{k+1}|t_{k+1}) = [I-K(t_{k+1})h_{\underline{x}}(\underline{\hat{x}}(t_{k+1}|t_k))]\; P(t_{k+1}|t_k)$$

$$\cdot\; [I-K(t_{k+1})h_{\underline{x}}(\underline{\hat{x}}(t_{k+1}|t_k))]' + K(t_{k+1})\; RK'(t_{k+1}). \tag{E.14}$$

The matrix Φ is the fundamental matrix associated with the solution of the linear differential equation

$$\dot{\delta}\underline{x} = f_{\underline{x}}(\underline{\hat{x}}(t_k|t_k)\; \delta\underline{x}$$

and is given by

$$\Phi(t_{k+1}, t_k; \underline{\hat{x}}(t_k|t_k)) = \begin{bmatrix} 1 & 0 & \Delta t \sin \hat{x}_4(t_k|t_k) & \Delta t\ \hat{x}_3(t_k|t_k) \cos \hat{x}_4(t_k|t_k) \\ 0 & 1 & \Delta t \cos \hat{x}_4(t_k|t_k) & -\Delta t\ \hat{x}_3(t_k|t_k) \sin \hat{x}_4(t_k|t_k) \\ 0 & 0 & 1 & 0 \\ 0 & 0 & 0 & 1 \end{bmatrix}$$

where $\Delta t = t_{k+1} - t_k$ is the sampling period.

In the linear case, the matrix $P(t_k|t_k)$ is the covariance matrix of the estimation error and is often used to assess the performance of the filter. In a nonlinear situation, such as this one, one must be careful in making such an interpretation. However, this matrix is a determining factor in how much weight is given new measurements through the gain matrix K. Hence, observation of its behavior as a function of time can often provide useful insights into the operation of the filter.

The EK filter operates in the following manner. Given an initial state estimate (say, from processing a set of measurements with the LSS filter) and an initial P-matrix, the state estimate and P-matrix are extrapolated ahead one sampling period, and a gain matrix is computed. When a new measurement has been obtained, the state estimate and P-matrix are updated, incorporating the new information contained in the most recent measurement. Then this process is repeated.

An appropriate initial P-matrix can be found experimentally during numerical studies or by calculation of the covariance of the error in the initial estimate. It was found most expedient for the purposes of this preliminary investigation to use the first alternative.

The system Eqs. (E.1) - (E.2) was simulated for a variety of initial conditions and parameter values. Estimates of the state were generated using the two filters, and the estimation error was computed. The general results of the simulation study are stated in Section 6.2.

In order to evaluate the performance of the filters, sample statistics were computed for each ensemble. The estimation error for the jth sample path is defined as $\underline{e}_k^j = \underline{x}^j(t_k) - \hat{\underline{x}}^j(t_k|t_k)$, and for a sample size of N, the sample mean and sample covariance matrix of the error are given by (k=0,1,2,...)

$$\underline{\mu}_k = \frac{1}{N} \sum_{j=1}^{N} \underline{e}_k^j, \tag{E.15}$$

$$\Sigma_k = \frac{1}{N} \sum_{j=1}^{N} (\underline{e}_k^j \, \underline{e}_k^{j\prime}) - \underline{\mu}_k \, \underline{\mu}_k^{\prime} \tag{E.16}$$

It can be shown[96] that the sample central moments are asymptotically (as $N \to \infty$) normally distributed and converge in probability to the true mean and covariance matrix of the error (i.e., they are consistent estimates of the true error mean and covariance). The sample mean of the error is a measure of the filter's biasedness; i.e., an indication of how much it will be in error "on the average". The sample variance of the error is a measure of the reliability to be expected of the filter. If the variance is large, the filter will be unreliable since the quality of its estimates will tend to be inconsistent from one encounter to the next.

APPENDIX F
PERFORMANCE STATISTICAL ANALYSIS

In Section 7.3, a Monte Carlo simulation was described which was used to perform an error analysis of a possible horizontal collision avoidance mechanization scheme.

The output of each run of the simulation is (in principle) an ensemble of independent identically distributed miss distances and various other statistics, which are described presently. Since the initial relative heading geometry (θ_o) is fixed deterministically and is an input to the program, the output distribution of miss distances is conditioned on θ_o. It is also implicitly conditioned on the values of the various parameters used to specify the error sources, time delays, etc. This point is emphasized because it has an important effect on how the results of the simulation are to be interpreted.

The purpose of this appendix is to describe the more important performance measures for a CAS relative to the task of assessing overall system effectiveness and performance in the presence of imperfect information and equipment errors. Also, how these measures are computed from experimental (simulation) data is explained.

Of primary importance as a measure of CAS effectiveness is the (conditional) distribution of the miss distance. Let $p(r_f|\theta_o)$ denote the conditional probability density function of the miss distance given an initial relative heading θ_o (suppressing for notational convenience the conditioning on other relevant parameters). Now suppose that one has N independent sample values of r_f from the distribution specified by $p(r_f|\theta_o)$. Then, using the kth-nearest neighbor method of Loftsgaarden and Quesenberry[97], a consistent and asymptotically unbiased estimate $\hat{p}_N(r_f|\theta_o)$ of $p(r_f|\theta_o)$ can be obtained.

Let k_N be some integer less than or equal to N such that

$$\lim_{N\to\infty} k_N = \infty,$$

$$\lim_{N\to\infty} \frac{k_N}{N} = 0.$$

Let $d_N(r_f)$ be the distance of the k_N-th closest sample value to r_f among the ensemble $\{r_{f1}, r_{f2}, \ldots, r_{fN}\}$. Then at every point of continuity of p,

$$\hat{p}_N(r_f|\theta_o) = k_N/2Nd_N(r_f) \quad . \tag{F.1}$$

In practice, the value of $k_N = \sqrt{N}$ is often used, which is the choice used in this study. The computational procedure is:

1. Collect the samples $\{r_{fi};\ i=1,2,\ldots,N\}$;
2. For each r_f and θ_o for which an estimate of $p(r_f|\theta_o)$ is desired, compute $d_N(r_f)$;
3. Compute $\hat{p}_N(r_f|\theta_o)$ for each such r_f and θ_o using Eq. (F.1).

Once having an estimate of the density function, a great deal of information can be extracted from it regarding the effectiveness of the CAS.

The conditional mean and variance of the miss distance can be computed via

$$\mu_{r_f} \cong \int_0^\infty r_f\ \hat{p}_N(r_f|\theta_o)\ dr_f \ , \tag{F.2}$$

$$\sigma^2_{r_f} \cong \int_0^\infty (r_f - \hat{\mu}_{r_f})^2\ \hat{p}_N(r_f|\theta_o)\ dr_f \ . \tag{F.3}$$

Computation of μ_{r_f} and σ_{r_f} as a function of the number of samples N, provides a basis for selecting a finite number for N, to perform the Monte Carlo simulation runs.

Several probabilities of interest can be computed. For example, if it is agreed that a collision takes place if $r_f \leq r_c$ (to account for the fact that aircraft are not point masses), then

$$P\{C|\theta_o\} = P\{\text{collision}|\theta_o\} \cong \int_0^{r_c} \hat{p}_N(r_f|\theta_o)\, dr_f. \tag{F.4}$$

A value of 300 feet was used in the present study for r_c.

If a near-miss is defined as a miss distance $r_c < r_f \leq r_{nm}$, then

$$P\{NM|\theta_o\} = P\{\text{Near-Miss}|\theta_o\} \cong \int_{r_c}^{r_{nm}} \hat{p}_N(r_f|\theta_o)\, dr_f\ . \tag{F.5}$$

A value of $r_{nm} = 900$ feet was used in this study.

Denoting a maximum acceptable miss distance by r_e,

$$P\{AM|\theta_o\} = P\{\text{Acceptable Miss}\ |\theta_o\} \cong \int_{r_{nm}}^{r_e} \hat{p}_N(r_f|\theta_o)\, dr_f \tag{F.6}$$

A value of $r_e = 2700$ feet was used in this study. Finally,

$$P\{EM|\theta_o\} = P\{\text{Excessive Miss}|\theta_o\} \cong \int_{r_e}^{\infty} \hat{p}_N(r_f|\theta_o)\, dr_f \tag{F.7}$$

Numerical integration is required to evaluate Eqs. (F.2) - (F.7).

Now, if an a priori distribution of the initial geometries of encounters is available (possibly from the Mid-Air Collision Report), then the unconditional distribution can be estimated. For example, if the values of possible θ_o's are restricted to a finite discrete set $\{\theta_{oi};\ i=1,2,\ldots,N_\theta\}$ with the corresponding probability masses $\{p_i;\ i=1,2,\ldots,N_\theta\}$, then

$$\hat{p}_N(r_f) = \sum_{i=1}^{N_\theta} \hat{p}_N(r_f | \theta_{oi}) \, p_i \quad . \tag{F.8}$$

Since digital calculations are anticipated, the restriction to a discrete set of θ_o's is not restrictive nor unrealistic.

Given $\hat{p}_N(r_f)$, Eqs. (F.2) - (F.7) can be repeated using $\hat{p}_N(r_f)$ in place of $\hat{p}_N(r_f|\theta_o)$ to get unconditional performance figures. Due to the lack of a reliable set of a priori probabilities for θ_o, this last step was not carried out in this study.

Other performance measures, which are of particular interest to pilots and air traffic controllers, are the probability of a missed alarm (missed alarm rate) and the probability of a false alarm (fasle alarm rate). The probability of a missed alarm can be estimated from the simulation data by computing the percentage of times no action was initiated when there was danger of a collision and action should have been initiated. Missed alarms can be further broken down into missed alarms which result in a collision, near miss, acceptable miss, and excessive miss. These probabilities can be similarly estimated as overall missed alarm rate. In an analogous manner, the false alarm rate can be estimated by computing the percentage of the occurrence of alarms and subsequent evasive action when there was no threat.

APPENDIX G
MONTE CARLO SIMULATION RESULTS

A tabulation of the raw data obtained from the Monte Carlo simulation study is presented in this appendix. The entries in each column were defined in Section 7.3.3. The numbers appearing here were normalized in appropriate fashion to obtain the probabilities presented in Section 7.3.3. The raw data is presented so that the interested reader may examine in more detail the way in which the various parameters affect the CAS performance. For all cases below, the number of samples in the ensemble is 2000.

Table G.1 Effect of Encounter Geometry

r_a = 2000 ft, σ_r = 200 ft, σ_β = 5°, σ_θ = 5°, σ_γ = 0.05, V_A = 425 fps,
V_B = 375 fps, r_{in} = 2600 ft.

C	MAR_C	NM	MAR_{NM}	C+NM	IMR_{NM}	AM	EM	IMR_T	FAR	θ, deg
8	0/197	125	22/655	133	133/575	1560	307	575/1474	204/472	5
1	1/204	8	8/662	9	9/151	1969	22	151/1547	136/469	15
0	0/214	0	0/671	0	0/52	1940	60	52/1631	150/467	30
6	1/190	41	2/647	47	10/102	1373	580	102/1697	217/474	80
30	15/208	99	41/664	129	91/1059	1095	776	1059/1662	267/468	90
46	38/214	131	106/671	177	156/655	1664	9	655/1561	298/467	100
25	25/214	79	79/671	104	94/512	1774	122	512/1645	317/467	150
22	22/214	63	70/671	85	77/461	1802	113	461/1655	310/467	165
32	19/214	74	63/671	106	105/510	1743	151	510/1666	313/467	175

Table G.2 Effect of Bearing Errors

$r_a = 2000$ ft, $\theta = 150°$, $\sigma_r = 200$ ft, $\sigma_\theta = 5°$, $\sigma_\gamma = 0.05$, $V_A = 425$ fps, $V_B = 375$ fps, $r_{in} = 2600$ ft.

C	MAR_C	NM	MAR_{NM}	C+NM	IMR_{NM}	AM	EM	IMR_T	FAR	σ_β, deg
1	1/214	9	5/671	10	5/318	1856	134	318/1737	288/467	2.5
25	25/214	79	79/671	104	94/512	1774	122	512/1645	317/467	5.0
48	48/214	116	148/671	164	157/659	1720	116	659/1513	309/467	7.5

Table G.3 Effect of Heading Errors

$r_a = 2000$ ft, $\theta = 150°$, $\sigma_r = 200$ ft, $\sigma_\beta = 5°$, $\sigma_\gamma = 0.05$, $V_A = 425$ fps, $V_B = 375$ fps, $r_{in} = 2600$ ft.

C	MAR_C	NM	MAR_{NM}	C+NM	IMR_{NM}	AM	EM	IMR_T	FAR	σ_θ, deg
19	19/214	49	61/671	68	65/468	1855	77	468/1670	313/467	2.5
25	25/214	79	79/671	104	94/512	1774	122	512/1645	317/467	5.0
31	29/214	113	100/671	144	123/592	1693	163	592/1584	306/467	7.5

Table G.4 Effect of Range Errors

$r_a = 2000$ ft, $\theta = 150°$, $\sigma_\beta = 5°$, $\sigma_\theta = 5°$, $\sigma_\gamma = 0.05$, $V_A = 425$ fps,
$V_B = 375$ fps, $r_{in} = 4000$ ft.

C	MAR_C	NM	MAR_{NM}	C+NM	IMR_{NM}	AM	EM	IMR_T	FAR	σ_r, feet
17	17/127	71	55/434	88	59/334	1354	558	334/1323	466/1002	100
17	17/127	75	55/434	92	61/332	1866	42	332/1326	467/1002	200
18	66/127	92	82/434	110	67/326	1328	562	326/1328	466/1002	400

Table G.5 Effect of Speed Ratio Errors

$r_a = 2000$ ft, $\theta = 150°$, $\sigma_r = 200$ ft, $\sigma_\beta = 5°$, $\sigma_\theta = 5°$, $V_A = 425$ fps,
$V_B = 375$ fps, $r_{in} = 2600$ ft.

C	MAR_C	NM	MAR_{NM}	C+NM	IMR_{NM}	AM	EM	IMR_T	FAR	σ_γ
25	25/214	79	79/671	104	94/512	1774	122	512/1645	317/467	0.05
23	23/214	89	79/671	112	101/512	1776	112	512/1640	317/467	0.075

Table G.6 Effect of Changes in r_a

$\theta = 150°$, $\sigma_r = 200$ ft, $\sigma_\beta = 5°$, $\sigma_\theta = 5°$, $\sigma_\gamma = 0.05$, $V_A = 425$ fps,
$V_B = 375$ fps, $r_{in} = 4000$ ft.

C	MAR_C	NM	MAR_{NM}	C+NM	IMR_{NM}	AM	EM	IMR_T	FAR	r_a, feet
17	17/127	75	55/434	92	61/332	1866	42	332/1326	467/1002	2000
10	10/127	28	33/434	38	33/366	1919	43	366/1505	422/789	2400
5	5/127	15	20/434	20	20/372	1883	97	372/1642	363/605	2800
1	1/127	6	7/434	7	7/394	1742	251	394/1749	270/409	3200

Table G.7 Effect of Changes in Speeds

$r_a = 2000$ ft, $\theta = 150°$, $\sigma_r = 200$ ft, $\sigma_\beta = 5°$, $\sigma_\theta = 5°$, $\sigma_\gamma = 0.05$, $r_{in} = 2600$ ft.

C	MAR_C	NM	MAR_{NM}	C+NM	IMR_{NM}	AM	EM	IMR_T	FAR	V_A/V_B
25	24/214	79	79/671	104	94/512	1774	122	512/1645	317/467	425/375
2	2/214	7	9/671	9	9/339	1934	57	339/1735	294/467	360/180
5	5/214	16	21/671	21	21/392	1921	58	392/1722	303/467	425/180

REFERENCES

1. J.H. Flanders, P.A. Grundy, and N.A. Carlson, "PWI Systems Survey", Report DOT-TSC-188-2, Department of Transportation, Transportation Systems Center, November, 1971.

2. D.E. Bulford, "Collision Avoidance - A Bibliography - 1955 - September 1968", FAA Report NA-68-54, Atlantic City, N.J., November 1968.

3. D.E. Bulford, "Collision Avoidance: An Annotated Bibliography", FAA Report NA-72-41, Atlantic City, N.J., August 1972.

4. F.C. White, "Airborne Collision Avoidance System Development - Introduction", IEEE Trans. on Aerospace and Electronic Systems, Vol. AES-4, No. 2, March 1968, pp. 234-237.

5. E.J. Koenke, "A Theory of Aircraft Collision Avoidance System Design and Evaluation" Report DOT-TSC-OST-71-4, Department of Transportation Systems Center, May 1971.

6. M.R. Bates, et al., "History of Time Frequency Technology", IEEE Trans. on Aerospace and Electronic Systems, Vol. AES-4, No. 2, March 1968, pp. 238-256.

7. P.J. Klass, "Anti-Collision: Systems Fight Anticipated", Aviation Week and Space Technology, Nov. 15, 1971, p. 29.

8. P.J. Klass, "Decision on Collision Avoidance Delayed for Joint Investigation", Aviation Week and Space Technology, Jan. 17, 1972, pp. 27-28.

9. P.J. Klass, "Two-Way CAS Models Simulated", Aviation Week and Space Technology, April 3, 1972, pp. 33-35.

10. P.G. Thomas, "Collision Avoidance", Space/Aeronautics, June 1967, pp. 82-91.

11. E.O. Frye and D.E. Killham, "Aircraft Collision Avoidance Systems", IEEE Spectrum, January 1966, pp. 72-80.

12. C.S. McKown and J.J. Morrone, "Prevention of Mid-Air Collisions", Sperry Engineering Review, Winter, 1963, pp. 8-14.

13. Anon., "Problems Confronting the Federal Aviation Administration in the Development of an Air Traffic Control System for the 1970's", Twenty-Ninth Report by the Committee on Government Operations, House Report 91-1303, Union Calendar No. 623, July 16, 1972.

14. Anon., "Aircraft Collision Avoidance Systems", Tenth Report by the Committee on Government Operations, House Report 92-919, Union Calendar No. 462, March 15, 1972.

15. E. Roessger, "A History of the Air Collision Problem", The Journal of Navigation, Vol. 11, No. 1, January 1958, pp. 14-27.

16. Anon., "Aircraft Collision Avoidance Systems", Hearing Before a Subcommittee of the Committee on Government Operations, House of Representatives, 92nd Congress, First Session, August 3, 1971.

17. K.E. Willis, et al., "Intermittent Positive Control", Proc. of the IEEE, Vol. 58, No. 3, March 1970, pp. 361-369.

18. J.L. Parsons, "SECANT - A Solution to the Problem of Mid-Air Collisions", SAE paper 720313, National Business Aircraft Meeting, March 1972.

19. R.J. Follen, et al., "Mid-Air Collisions - The Problem - A Solution", Document ASD-132, Honeywell Government and Aeronautical Systems Div., January 1971.

20. Anon., "Utilization of Time/Frequency in Collision Avoidance Systems", Minutes of Meeting Sponsored by DOT/FAA, August 1968 (AD631881).

21. R.M. Buck, "Time Frequency and the FAA", NAECON 1970 Convention Record, IEEE National Aerospace Electronics Conference, Dayton, Ohio, May 1970, pp. 355-362.

22. G.B. Litchford, "SSR Listen-In Feature for Proximity Warning", EASCON '68 Convention Record, IEEE Electronics and Aerospace Systems Convention, Washington, D.C., September 9, 1968.

23. M.J. Borrok, "EROS in Operation", Paper presented at Institute of Navigation Air Meeting on Collision Avoidance, Dayton, Ohio, Feb. 23, 1967.

24. AWARE - Aircraft Warning Avoidance Radar Equipment, Technical Brochure published by Cygned, Inc., Salem, New Hampshire, 1971.

25. Anon., "FAA Plans Test of Low Cost Proximity Warning Unit", Aviation Week and Space Technology, September 20, 1971, pp. 82-83.

26. J.S. Morrel, "The Mathematics of Collision Avoidance in the Air", The Journal of Navigation, Vol. 11, No. 1, January 1958, pp. 13-28.

27. J.S. Morrel, "Fundamental Physics of the Aircraft Collision Problem", Bendix TM 465 1016 39, June 1956.

28. B.W. Russell, "Characteristics of Airborne Anti-Collision Devices and Their Role in Air Traffic Control", WADC TR 59-209, May 1959 (AD 214388).

29. E.S. Calvert, "Maneuvers to Ensure the Avoidance of Collision", The Journal of Navigation, Vol. 14, No. 3, June 1961, pp. 366-378.

30. J.M. Holt and R.M. Anderson, "Analysis of Warning Times for Collision Avoidance Systems", IEEE Trans. on Aerospace and Electronic Systems, Vol. AES-4, No. 2, March 1968, pp. 305-314.

31. Anon., "Potential of Airborne Collision Prevention Devices", Report of Proc. of the FAA Collision Prevention Advisory Group Symposium, FAA System Research and Development Service, Washington, D.C., July 12, 1962, (AD 415918).

32. B.V. Dinerman and K. Burkard, "Evaluation of a Ground-Bounce Ranging/ Altitude Exchanging Collision Avoidance System Technique", Report RD-64-5, FAA Systems Research and Development Service, Washington, D.C., October 1963, (AD 431914).

33. J.M. Holt and G.R. Marner, "Computer/Simulation Study of Air Derived Separation Assurance Systems in Multiple Aircraft Environment", Collins Radio Company Final Report, No. RD-69-31, FAA Systems Research and Development Service, Washington, D.C., October 1969, (AD 697942).

34. F.D. Watson, et al., "Evaluation of Threat Logic for the Air Transport Association Airborne Collision Avoidance Systems", MDC-E0016, McDonnell Douglas Corp., March 1970.

35. R.A. Horn, "Development of Airborne Time/Frequency Range/Altitude Monitor", National Company, Inc., Melrose, Massachusetts, Report RD-68-39, June 1968 (AD 680254).

36. A.S.L. Nagy, "Operational Analysis of Time-Frequency Collision Avoidance Systems", Boeing Document D6-19535, Renton, Washington, March 1968, (AD 668163).

37. Anon., "Analysis of an Advanced Time-Frequency National Airspace System Concept, Volume III - Systems Analysis", Autonetics Div. of North American Aviation Corporation, Report RD-69-32, III, August 1969 (AD 695437).

38. Anon., "Flight Test and Evaluation of Airborne Collision Avoidance System", Vol., I, Martin-Marietta Corp., Baltimore, July 1968, (AD 705530).

39. J.M. Holt and G.R. Marner, "Separation Theory in Air Traffic Control System Design", Proc. of the IEEE, Vol. 58, No. 3, March 1970, pp. 369-376.

40. Anon., "Airborne Collision Avoidance System - Statement of Airline Policy and Technical Description of the System", ANTC Report 117, issued by Air Transport Association of America, June 1967; Revised and corrected, March 1972.

41. W.G. Shear, "Elements of the ATA Collision Avoidance System", IEEE Trans. on Aerospace and Electronic Systems, Vol. AES-4, No. 2, March 1968, pp. 295-304.

42. R.E. Perkinson, "CAS Message Format", IEEE Trans. on Aerospace and Electronic Systems, Vol. AES-4, No. 2, March 1968, pp. 273-277.

43. R.L. Jaycox, "Collision Avoidance System Synchronization", IEEE Trans. on Aerospace and Electronic Systems, Vol. AES-4, No. 2, March 1968, pp. 257-264.

44. Anon., "Air Transport Time/Frequency Collision Avoidance System", ARINC Characteristic No. 587, Aeronautical Radio, Inc., September 1970.

45. J. Breckman, "SECANT - An Anti-Collision System for Airplanes", Status Report, Defense Electronic Products, RCA, Camden, New Jersey, April 1970.

46. Anon., "SECANT Concepts-Status-Plans", RCA Document describing Vertical Escape Collision Avoidance System, March 1972.

47. Anon., "Navy Flight Experiment of Secant Transponder Correlation Ranging Equipment, NADC-72112-AE, January 1972.

48. Anon., "Analysis of the Traffic Handling Capability of the Secant System", Report MDC M0008, McDonnell Douglas Electronics Co., February 7, 1972.

49. P.J. Klass, "Army Plans Proximity Warning Test", Aviation Week and Space Technology, August 4, 1969.

50. Anon., "Aircraft Collision Avoidance System (ACAS)", Vol. I, Final Report on Phase II, Instrument Systems Corp., Huntington, New York, July 1970.

51. H.A. Augenblick, "Collision Avoidance System for General Aviation", Proc. Flight Safety Foundation Annual Business Aircraft Meeting, May 13, 1968.

52. R.T. Daly, "An Optical Radar Pilot Warning Indicator", Proc. of the IEEE, Vol. 58, No. 3, pp. 456-461, March 1970.

53. Anon., "Genave Proximity Warning Indicator - Pilot Information Manual", General Aviation Electronics, Indianapolis, Indiana.

54. A.G. Afward, "A Proposed Low Cost Pilot Proximity Warning Device for Aircraft", 1969 NAECON Proceedings, May 19, 1969, Dayton, Ohio, pp. 325-331.

55. C.H. Leigh and A.S. Richardson, "Performance Analysis of an Infrared Pilot-Warning Indicator System", Proc. of the IEEE, Vol. 58, No. 3, March 1970, pp. 462-469.

56. Anon., "AWARE - Aircraft Warning Avoidance Radar Equipment: A Non-Cooperative PWI", paper presented before the FAA Planning and Review Conf., Washington, D.C., April 1970.

57. S.H. Hollingdale, "The Mathematics of Collision Avoidance in Two Dimensions", The Journal of Navigation, Vol. 14, No. 3, July 1961, pp. 243-261.

58. E.S. Calvert, "A Comparison of Two Systems for Avoiding Collision", The Journal of Navigation, Vol. 14, No. 4, October 1961, pp. 379-401.

59. J.S. Morrel, "The Physics of Collision at Sea", The Journal of Navigation, Vol. 14, No. 2, April 1961, pp. 163-184.

60. E.O. Anderson, et al., "Relative Movement and the Collision Problem", The Journal of Navigation, Vol. 10, No. 2, 1957, pp. 184-204.

61. D.H. Sadler, "The Mathematics of Collision Avoidance at Sea", The Journal of Navigation, Vol. 10, No. 4, 1957, pp. 306-319.

62. P. Gaudillere, "Visual and Electronic Methods of Avoiding Collision", The Journal of Navigation, Vol. 11, No. 1, January 1958, pp. 40-55.

63. P.A. Thompson, "Revised Rules for Preventing Collisions at Sea", The Journal of Navigation, Vol. 23, No. 1, January 1970, pp. 81-86.

64. Anon., "Revision of the Collision Regulations", The Journal of Navigation, Vol. 23, No. 4, October 1970, pp. 443, 455.

65. E.S. Calvert, "The Use of Aircrew-Interpreted Devices for Preventing Collision in the Air", The Journal of Navigation, Vol. 1., No. 4, October 1958, pp. 327-343.

66. A.W. Merz, "Optimal Aircraft Collision Avoidance", 1973 Joint Automatic Control Conference Proceedings, Ohio State University, Columbis, Ohio, June 1973, pp. 449-454.

67. A.W. Merz, "Optimal Evasive Maneuvers in Maritime Collision Avoidance", The Journal of the Institute of Navigation, Vol. 20, No. 2, 1973.

68. J.S. Morrel, "Physical Aspects of Collision Avoidance", IRE Trans. on Aero. and Nav. Electronics, June 1957, pp. 75-81.

69. V.W. Bolie, "Analysis of Lateral Turns to Avoid Collisions", Collins Engineering Report CER-704, Collins Radio, Inc., Cedar Rapids, Iowa.

70. A.G. Corbet, "Collision Avoidance at Sea", The Journal of Navigation, Vol. 25, 1972, p. 520.

71. E.S. Calvert, "Collision Avoidance in a Traffic System", The Journal of Navigation, Vol. 26, 1973, p. 137.

72. Anon., "Model 172 and Skyhawk, Owner's Manual", Cessna Aircraft Publication, 1973.

73. F.C. Hall, Boeing Aircraft Co., Renton, Washington, Personal Communication, February 10, 1973.

74. R. Isaacs, Differential Games, Wiley and Sons, Inc., New York, 1965.

75. Anon., "Federal Aviation Regulations", Vol. VI, Part 91.70, November 1970.

76. C.R. Souza and M.D. Ciletti, "Locally Optimum Games and Vehicular Collision", Tech. Report EE-6512, Department of Electrical Engineering, University of Notre Dame, September 1965.

77. Anon., "Eight Bit Parallel Central Processor Unit - User's Manual", Intel Corp., March 1973.

78. Anon., "Microprogrammable Arithmetic Processor System - Detailed Descriptions and Capabilities", National Semiconductor, May 1972.

79. Anon., "Naked Mini LSI/Alpha LSI Programming Reference Manual", Computer Automation, Inc., April 1973.

80. Anon., "Spaceborne Digital Computer Systems", NASA SP-8070, March 1971.

81. Anon., "Programmer's Reference Manual for the Model 960A Computer", Texas Instruments, April 1972.

83. K. Springarn and H.L. Weidemann, "Linear Regression Filtering and Prediction for Tracking Maneuvering Aircraft Targets", IEEE Trans. Aerospace and Electronic Systems, Vol. AES-8, No. 6, Nov. 1972, pp, 800-810.

84. J.W. Andrews and G. Prado, "The Influence of Surveillance System Parameters on Automated Conflict Detection and Resolution", Project Report ATC-15, Lincoln Laboratory, MIT, Cambridge, Massachusetts, November 29, 1972.

85. R.E. Kalman, "A New Approach to Linear Filtering and Prediction Problems", Trans. ASME, Ser. D: J. Basic Engr., Vol. 82, 1960, pp. 35-45.

86. A.H. Jazwinski, Stochastic Processes and Filtering Theory, New York: Academic Press, 1970.

87. G.J. Bierman, "A Comparison of Discrete Linear Filtering Algorithms", IEEE Trans. Aerospace and Electronic Systems, Vol. AES-9, No. 1, 1973, pp. 28-37.

88. R.A. Singer, "Estimating Optimal Tracking Filter Performance for Manned Maneuvering Targets", IEEE Trans. Aerospace and Electronic Systems, Vol. AES-6, No. 4, July 1970, pp. 473-483.

89. R.L.T. Hampton and J.R. Cooke, "Unsupervised Tracking of Maneuvering Vehicles", IEEE Trans. Aerospace and Electronic Systems, Vol. AES-9, No. 2, March 1973, pp. 197-207.

90. R.J. McAulay and E. Denlinger, "A Decision-Directed Adaptive Tracker", IEEE Trans. Aerospace and Electronic Systems, Vol. AES-9, No. 2, March 1973, pp. 229-236.

91. H.Q. Lee, et al., "Guidance and Control Techniques for Automated Air Traffic Control", Journal of Aircraft, Vol. 9, No. 7, July 1972.

92. S. Gee, et al., "A Flight Evaluation of Curved Landing Approaches", STOL Technology Conference, NASA Ames, July 1972.

93. W. Taylor, Advanced Engineering Department, United Airlines, San Francisco, California, Private Communication, June 1972.

94. A.E. Bryson and Y.C. Ho, Applied Optimal Control, Blaisdell Publishing Company, 1969.

95. R. Isaacs, "Theory of Collisions Between Moving Craft", Hughes Aircraft Company, SRSM 1-189, 1958.

96. H. Cramer, Mathematical Methods of Statistics, Princeton, New Jersey: Princeton University Press, 1946.

97. D.O. Loftsgaarden and C.P. Quesenberry, "A Nonparametric Estimate of a Multivariate Density Function", Ann. Math. Stat., Vol. 36, 1965, p. 358, (Abstract).